Experimental and Theoretical Studies of Silylenes, Silicenium Ions, and Organometallic Reactive Intermediates

Thesis by
Seung Koo Shin

In Partial Fulfillment of the Requirements
for the Degree of
Doctor of Philosophy

California Institute of Technology
Pasadena, California
1989
(Submitted May 25, 1989)

For my parents,

Soon-Ah Lee and Chul-Mo Shin

and

for my wife,

Hye Joo

Acknowledgments

There have been a large number of people who have made my graduate stay at Caltech more pleasant and who have also contributed to the research presented in this thesis. I am greatly indebted to my research advisor, Jack Beauchamp, for all of his help, both from the standpoint of financial support as well as his friendship, encouragement, and delightful stream of ideas throughout the years. Bill Goddard, who played a large role in getting me interested in theoretical calculations, also deserves my thanks for allowing me to work on theoretical problems associated with my experimental research. I would also like to thank my other committee members, Henry Weinberg and Daniel Weitekamp, for their time and effort.

Past and present members of both the Beauchamp and Goddard groups have been good friends. They have provided fellowship as well as expertise in their various areas of work. Jung Goo Lee, Mark Brusich, Emily Carter, Dave Smith, Terry Coley, and Jean-Marc Langlois deserve thanks for all of the discussions either dealing with chemistry or computers or both. Maureen Hanratty, Heon Kang, and Gary Kruppa introduced me to the ion cyclotron spectroscopy, ion beam spectroscopy, and photoelectron spectroscopy. They, along with Maggie Tolbert, Bruce Schilling, Dave Dearden, Bob Sweeny, Srihari Murthy, Ching-Hwa Kiang, Ed Fowles, Martin Schär, and especially Karl Irikura, always kept things interesting both in the lab and the office. Karl Irikura deserves special thanks for his friendship through the years.

I would also like to thank other members of the Caltech community, especially Joon Won Park and Jim Hanson for their invaluable assistance. Thanks also to Tom Dunn, Tony Stark, Terrence Yeh, Roger Tang, and Mihai Azimioara for their timeless help.

Lastly, I thank my parents and the rest of my family for their love and support throughout my life and also my wife, Hye Joo. Thank you very much for all of your love, encouragement, and support. Thanks God.

Abstract

Fourier transform ion cyclotron resonance spectroscopy has been used to investigate thermochemistry and relative stabilities of silylenes, silaethylene, and silicenium ions in the gas phase. Proton affinities of silylene, methylsilylene and silaethylene have been derived from studies of kinetics and thermochemistry of proton transfer from the corresponding silicenium ions to a series of n-donor bases with well-established gas-phase base strengths. Values of proton affinities combined with the known heats of formation of the corresponding silicenium ions yield heats of formation of silylene, methylsilylene, and silaethylene. Experimental results for the relative stability between methylsilylene and silaethylene are corroborated by *ab initio* generalized valence bond (GVB)-configuration interaction (CI) calculations which indicate that silaethylene is more stable than methylsilylene. Hydride affinities of the methyl-substituted silicenium ions have been precisely determined from examination of kinetics and equilibria of hydride-transfer reactions of methyl-substituted silanes with various hydrocarbons having well-established gas-phase hydride affinities. The result shows that the silicenium ions are significantly more stable than the corresponding carbonium ions in the gas phase with H^- as a reference base.

Photoelectron spectroscopy and mass spectrometry have been employed to identify the gas-phase reactive intermediate in the chlorosilane chemical vapor deposition under the heterogeneous flash vacuum pyrolytic condition. The result indicates that dichlorosilylene and hydrogen chloride are the major gas-phase products and monochlorosilylene is not an abundant gas-phase intermediate.

The *ab initio* theoretical methods have been used to calculate the equlibrium geometries and singlet-triplet splittings of chlorine- and fluorine-substituted silylenes and methylenes. The GVB-dissociation consistent CI (DCCI) method has been developed to accurately predict singlet-triplet energy gaps within 1 kcal/mol error.

Finally, we have employed Fourier transform ion cyclotron resonance spectroscopy combined with a line tunable CW CO_2 laser to isolate the coordinatively

unsaturated organometallic intermediates and examine structures, reactivities, and spectroscopic properties of the isolated intermediates for the methyl-migratory decarbonylation reaction and ligand displacement reaction. The results show that the CF_3 group is an ideal infrared chromophore to investigate the infrared photochemistry of organometallic complexes, $L_nM–CF_3$, structures, and reaction mechanisms of their coordinatively unsaturated intermediates containing metal-bonded CF_3 groups. The infrared multiphoton dissociation spectra of the isolated intermediates containing metal-bonded CF_3 group are presented.

Table of Contents

Introduction

The thermochemical properties of the reactive molecule silylene are of fundametal interest in organosilicon chemistry and also of importance in understanding the process of silicon chemical vapor depostion (CVD)[1]. Although the heat of formation of silylene has been studied experimentally, there was considerable discrepancy among the various published values. For example, the previously accepted value of ΔH°_{f298} (SiH_2) = 58 kcal/mol based on pyrolysis measurements of silane species[2] was considerably lower than the *ab initio* theoretical result of 68.1 kcal/mol obtained at MP4/6-31G** level by Ho et al.[3].

To more firmly define an experimental value for the heat of formation of silylene, we have used the technique of Fourier transform ion cyclotron resonance (FT-ICR) spectroscopy to examine proton-transfer reactions of SiH_3^+ with a series of n-donor bases having known gas-phase basicities as described in Chapter I.[4] The experimental proton affinity of 201 $\pm$ 3 kcal/mol for silylene combined with heats of formation of SiH_3^+ and H^+ yields the heat of formation of silylene. The heat of formation of SiH_3^+ can be obtained from the heat of formation and ionization potential of the SiH_3 radical. A value of 46.4 kcal/mol for the heat of formation of SiH_3 by Walsh[2] combined with the reported ionization potential of 8.14 eV from photoelectron spectroscopic studies by Dyke et al.[5] yields $\Delta H_{f298}(SiH_3^+)$ = 234.1 kcal/mol. This value leads to $\Delta H_{f298}(SiH_2)$ = 69 $\pm$ 3 kcal/mol.

After our recommendation of the revision of the heat of formation of silylene, various experimental techniques have been used to evaluate the heat of formation of silylene. The reported values are 69.0$\pm$2 kcal/mol from the endothermicities of reactions of silicon ion with silane by Boo and Armentrout[6], 65.4 or 68.4 kcal/mol from photoionization mass spectrometric studies of silane by Berkowitz *et al.*[7], 65.3 $\pm$ 1.5 kcal/mol from reanalyses of silane pyrolysis data by Walsh and co-workers[8], 65.1 kcal/mol from kinetic studies of reactions of silylene with hydrogen by Jasinski and Chu[9], and 65.4 $\pm$ 1.6 kcal/mol from spectroscopic studies of production of Si($^1D_2$)

from electronically excited SiH_2 by Steinfeld and co-workers[10]. Our recommended value appears to be slightly higher than the kinetically derived values. However, adopting the ionization potential of 8.01 eV for SiH_3 by Berkowitz *et al.*[7] results in $\Delta H_{f298}(SiH_2) = 66 \pm 3$ kcal/mol which is in excellent agreement with other values. The recommended heat of formation of SiH_2 is 65.3 ± 1.5 kcal/mol which is 7.3 kcal/mol higher than the previously accepted value of 58 kcal/mol.

This revision of $\Delta H_{f298}(SiH_2)$ requires some changes in the *estimated* thermochemistry of processes involving silylene. Since heats of formation of methyl-substituted silylenes have been estimated from that of silylene by assuming a constant methyl substituent effect of 16 kcal/mol,[2] it is necessary to revise heats of formation of methylsilylenes from 42 to 49.3 kcal/mol. Also, the relative stability between methylsilylene and its isomer silaethylene has been the subject of extensive theoretical study, ever since dimethylsilaethylene was first suggested as a reactive intermediate in the pyrolysis of 1,1-dimethylsilacyclobutane[11]. Previously suggested values of heats of formation of silaethylene (39 ± 5 kcal/mol) and methylsilylene (42 kcal/mol) yield a 3-kcal/mol difference, in agreement with some previous theoretical calculations ($\Delta E = -6.8$ to 3.5 kcal/mol). However, the revision of the heat of formation of methylsilylene results in the stability difference of 10.3 kcal/mol, which is substantially larger than what appears to be the "best" theoretical calculations.

To resolve some of the apparent conflicts and firmly define the values of the heats of formation of silaethylene and methylsilylene, we have studied the kinetics and thermochemistry of the proton- and deuteron-transfer reactions of $CH_3SiD_2^+$ with various n-donor bases of well-established gas-phase basicities using FT-ICR spectroscopy as presented in Chapter II.[12] Transfer of carbon-bound proton from $CH_3SiD_2^+$ to the base yields silaethylene, and transfer of the silicon-bound deuteron produces methylsilylene as the neutral products. An examination of the deprotonation energetics of the methylsilicenium ion, $CH_3SiD_2^+$, shows that silaethylene is 10 ± 3 kcal/mol more stable than methylsilylene, as expected, and yields the pro-

ton affinities of 205 ± 3 and 215 ± 4 kcal/mol for silaethylene and methylsilylene, respectively. These results are corroborated by *ab initio* generalized valence bond (GVB)-configuration interaction (CI) calculations which indicate that silaethylene is more stable than methylsilylene by 11.6 kcal/mol, in good agreement with the experimental difference (10 ± 3 kcal/mol).

In order to derive heats of formation of silaethylene and methylsilylene, evaluation of the heat of formation of the methylsilicenium ion is required. Since there have been no reliable experimental values for the heat of formation of methylsilicenium ion, we have examined kinetics and equilibria of hydride-transfer reactions of methylsilicenium ion with cyclopentane as described in Chapter III.[13] The derived value of $\Delta H_{f298}(CH_3SiH_2^+)$ = 204 ± 1 kcal/mol from hydride-transfer equilibria measurements leads to heats of formation of 43 ± 3 kcal/mol and 53 ± 4 kcal/mol for silaethylene and methylsilylene, respectively. The value for the heat of formation of silaethylene is slightly higher than the previously acepted value of 39±5 kcal/mol (with a reduced uncertainty), but that of methylsilylene is somewhat higher than the most recent estimate of 43.9 kcal/mol by Walsh[14]. The recent kinetic studies of methylsilane pyrolysis[15] yielded the heat of formation of 51.9 kcal/mol for methylsilylene which is in agreement with our experimental value.

Recently, Schaefer and Gordon[16] reexamined the relative stability between silaethylene and methylsilylene with large basis sets and a variety of methods for the inclusion of electron correlation effects and reported their "best" theoretical energy difference of about 4 kcal/mol which is in direct constrast to our experimental and theoretical result[12] of about 10 kcal/mol. Their theoretical estimate indirectly support a value of ΔH°_{f298} (CH_3SiH) = 43.9 kcal/mol by Walsh[14].

Since the major discrepancy is in the heat of formation of methylsilylene, we have employed *ab initio* GVB-dissociation consistent CI (DCCI) methods to calculate the bond dissociation energies of HSi–H and HSi–CH_3 bonds.[17] The DCCI yields D_{298} (HSi–H) = 76.0 kcal/mol in excellent agreement with the derived value of 76.8 kcal/mol from known heats of formation of 65.3, 90, and 52.1 kcal/mol for

SiH_2, SiH, and H, respectively. The value of 43.9 kcal/mol for the heat of formation of CH_3SiH leads to $D(HSi-CH_3)$ = 80.9 kcal/mol from known heats of formation of 90 and 34.8 kcal/mol for SiH and CH_3, respectively. This value is 4 kcal/mol higher than the HSi–H bond energy. In general, the silicon-carbon bond is slightly weaker than the silicon-hydrogen bond (e.g. $D(H_3Si-H)$ = 90.3 kcal/mol and $D(H_3Si-CH_3)$ = 88.2 kcal/mol).[2] The calculated value for $D_{298}(HSi-CH_3)$ using the DCCI method is 71.2 kcal/mol which is significantly smaller than the estimated value of 80.9 kcal/mol from ΔH°_{f298} (CH_3SiH) = 43.9 kcal/mol[14]. However, the DCCI result for $D_{298}(HSi-CH_3)$ = 71.2 kcal/mol is in remarkable agreement with the derived value of 71.8 kcal/mol from the heat of formation of 53 kcal/mol for CH_3SiH[12].

The DCCI result directly supports the higher value of the heat of formation for methylsilylene and indirectly corroborates our previous experimental and theoretical results[12] for the relative stability between silaethylene and methylsilylene. In light of this result, it is obvious that theoretical methods employed by Schaefer and Gordon[16] are inaccurate in balancing the relative stability between structural isomers due to unbalanced levels of electron correlation for both silaethylene and methylsilylene.

Carbonium ions are well-established reactive intermediates and their properties have been extensively studied both in solution[18] and in the gas phase[19]. In contrast, exhaustive experimental attempts to generate even detectable concentrations of silicenium ions (R_3Si^+) in solution, under conditions where analogous carbonium ions are long-lived, have been unsuccessful.[20] However, the recent progress[21] in the solvolytic generation of silicenium ions calls for a reconsideration of silicenium ions as viable intermediates and draws attention to the relative stabilities of carbonium and silicenium ions both in solution and in the gas phase.

Fourier transform ion cyclotron resonance spectroscopy has been used to examine kinetics and equilibria of hydride-transfer reactions of methyl substituted silanes with various hydrocarbons having well established gas-phase hydride affinities as described in Chpter III[13]. The hydride affinities of the silicenium ions have

been precisely determined. The result shows that the silicenium ions are significantly more stable than the corresponding carbonium ions in the gas phase with H^- as a reference base. A quantitative comparison of the relative stabilities between the silicenium ions and their carbon analogues in the gas phase with those in solution leads to a conclusion that the silicenium ions are considerably less stable than the analogous carbonium ions in CH_2Cl_2 solution with both Cl^- and F^- as reference bases, and the hydride affinity differences between the silicenium ions and the analogous carbonium ions are greatly attenuated in solution.

The importance of chemical vapor deposition (CVD) to the electronics industry has led to a number of attempts to measure the concentrations and identities of the reactive species in CVD systems.[1] In spite of the extensive studies performed on chlorosilane CVD systems, some controversy remains as to the relative concentration of monochlorosilylene (SiHCl) and dichlorosilylene ($SiCl_2$) in these systems. Dichlorosilylene has been previously accepted as the dominant silicon containing species in the vapor phase under CVD conditions between 1000 °C and 1200 °C and considered to be formed homogeneously in the gas phase above the hot susceptor. However, in a most recent study, Ho and Breiland[22] detected the laser-induced fluorescence spectrum of monochlorosilylene in a CVD reactor under both atmospheric pressure (AP) and low pressure (LP) conditions. Ho and Breiland also asserted that the fluorescence previously used in profiling the concentration of dichlorosilylene in an APCVD reactor[23] was due to monochlorosilylene and not dichlorosilylene. In contrast, a recent study by Sausa and Ronn[24] on the infrared multiphoton dissociation (IRMPD) of SiH_2Cl_2 showed that dichlorosilylene and hydrogen molecule were the only product observed in the homogeneous gas phase decomposition of dichlorosilane.

In order to determine the relative importance of intermediates such as SiHCl and $SiCl_2$ in CVD systems using the chlorosilanes as source gases, we have employed photoelectron spectroscopy and mass spectrometry in Chapter IV[25]. Dichlorosilylene and hydrogen chloride are the major gas phase products in the heterogeneous

decomposition of dichlorosilane and trichlorosilane on silicon surfaces above 600° C and 800° C, respectively. This result, combined with results of the detection of dichlorosilylene on the homogeneous IRMPD of dichlorosilane[24], indicates that monochlorosilylene may not be an abundant gas phase intermediate in both homogeneous and heterogeneous CVD systems using dichlorosilane as a source gas.

Chapters V and VI presents an excursion into theoretical studies of singlet-triplet energy gaps (ΔE_{ST}) of chlorine- and fluorine-substituted methylenes and silylenes. The diverse chemical properties of methylenes and silylenes are strongly dependent upon the spin multiplicities of their low-lying electronic states and the interstate energy gaps. The energetics of these low-lying electronic states are prerequisite to understanding the chemistry of methylenes and silylenes.

The parent molecules CH_2 and SiH_2 have been extensively studied, and their singlet-triplet energy gaps have been determined from experiments[26] and corroborated by theoretical calculations[27]. In contrast, there are only a few experimental data for the singlet-triplet energy gaps for the chlorine and fluorine substituted methylenes and silylenes. The most recent photoelectron spectroscopic studies of the halocarbene anions yielded singlet-triplet splittings of the halocarbenes.[28] However, the previous theoretical estimates are not accurate enough to pinpoint the correct experimental singlet-triplet splittings from several possible values resulting from the uncertain contribution of the hot bands. For example, Lineberger and coworkers[28] reported three possible triplet excitation energies of 14.7 ± 0.2, 11.4 ± 0.3, and 8.1 ± 0.4 kcal/mol for CHF and suggested that 11.4 kcal/mol is the most likely (with 14.7 due to a hot band). They also provide triplet excitation energies of $(11.4 \pm 0.3) - n(2.5 \pm 0.2)$ kcal/mol for CHCl, with the constraint $(0 \leq n \leq 4)$ of a singlet ground state for CHCl.

We have employed the relatively simple GVB-DCCI method, starting with GVB wavefunctions and emphasizing correlation consistency between the singlet and triplet states. Values of the singlet-triplet splittings for CH_2, CF_2, SiH_2, and SiF_2 are in excellent agreement with available expreimental results [theory

(T_e): −10.0, 57.1, 21.4, and 76.6 kcal/mol; experiment (T_e): −9.215[26a], 56.7[29], 20.7[26b], 76.2[30] kcal/mol]. We expect the predictions for the other cases CHF(14.5), SiHF(41.3), CHCl(6.0), CCl_2(20.5), SiHCl(35.8), and $SiCl_2$(55.2) to be equally accurate. The remarkable accuracy of the DCCI method allows us to unambiguously pinpoint the correct experimental singlet-triplet energy gaps of 14.7 ± 0.2 kcal/mol for CHF and 6.4 ± 0.7 kcal/mol for CHCl.

Again, the result shows that the GVB-DCCI is a powerful method to resolve the experimental uncertainties and the conflicts between experiments and unbalanced levels of theoretical calculations.

Organometallic migration reactions have been studied extensively in recent years.[31] Many kinetic and stereochemical studies of alkyl to acyl migratory-insertion reactions have been reported. Considerable attention has been directed to determine whether these reactions proceed by CO insertion or alkyl-migration,[32] but information on the reverse alkyl-migration step from the acyl intermediate to the alkyl complex has been rarely studied. To provide fundamental undertandings of these complex organometallic reaction mechanisms, it is prerequisite to devise methods to isolate the coordinatively unsaturated intermediate, identify the structures, and examine the reaction kinetics in the absence of solvent effects. However, there has been no report of kinetic studies of methyl-migration reactions in the gas phase. In chapters VII and VIII, we employ Fourier transform ion cyclotron resonance spectroscopy to isolate the coordinatively unsaturated intermediates and examine structures, reactivities, and spectroscopic properties of the isolated intermediates for the trifluoromethyl-migratory decarbonylation reaction and ligand displacement reaction.

The trifluoromethyl-migration reaction involving decarbonylation from the trifluoroacetylmanganese tetracarbonyl anion to the trifluoromethylmanganese tetracarbonyl anion is studied in Chapter VII. The dissociative electron attachment of trifluoroacetylmanganese pentacarbonyl produces $Mn(CO)_5CF_3^-$ and

$Mn(CO)_4CF_3^-$ ions. $Mn(CO)_5CF_3^-$ slowly decomposes to yield $Mn(CO)_4CF_3^-$ with loss of CO. In order to identify the structures of these two ions, we have employed infrared multiphoton dissociation in conjuction with collision-induced dissociation and kinetics of ligand displacement reactions. $Mn(CO)_4CF_3^-$ ion derived from the dissociative electron attachment of a different precursor, trifluoromethylmanganese pentacarbonyl, is also used to confirm the identity of the trifluoromethyl-migration product ion.

Spectroscopy of molecular ions has been of great experimental interest in recent years.[33] Various techniques have been employed to obtain information about the structures, vibrational and electronic spectra, and photodissociation dynamics of molecular ions.[34] Recent developments in high-resolution infrared spectroscopy made it possible to study the individual vibration-rotation levels of relatively simple ions such as HD^+, HeH^+, CH^+, and H_3^+. However, there have been only a few experimental observation of infrared spectra of organometallic ions in the gas phase.

In Chapter VIII, an infrared multiphoton dissociation spectrum of $CF_3Mn(CO)_3(NO)^-$ resulted from ligand displacement reaction of $CF_3Mn(CO)_4^-$ with NO has been presented in the CO_2 laser wavelength range. The trifluoromethyl group in the anion shows two absorption maxima at 1045 and 980 cm^{-1}. The peak at 1045 is assigned as a C–F stretch of A_1-type symmetry and the peak at 980 cm^{-1} is ascribed to a C–F stretch of E-type symmetry. It is quite interesting to observe that the symmetric C–F stretching mode changes little in frequency from 1063 cm^{-1} for $CF_3Mn(CO)_5$ to 1046 cm^{-1} for $CF_3Mn(CO)_3(NO)^-$, while the C–F stretching frequency of E-type symmetry decreases from 1043 cm^{-1} for the 18 e^- neutral precursor to 980 cm^{-1} for the 18 e^- anion. Comparison with the infrared multiphoton dissociation spectrum of $CF_3Mn(CO)_4^-$ ion reveals that the degenerate C–F stretch of E-type symmetry increases from 945 cm^{-1} for the 17 e^- $CF_3Mn(CO)_4^-$ to 980 cm^{-1} for the 18 e^- $CF_3Mn(CO)_3(NO)^-$, whereas the symmetric C–F stretching bands overlap with each other quite well within experimental uncertainties.

Variations of the electron density and hybridization in the σ donor orbital of the CF_3 ligand due to the different d orbital splittings of the complexes may be responsible for the distinctive C–F stretching frequencies observed in $CF_3Mn(CO)_5$ (18 e^-), $CF_3Mn(CO)_4^-$ (17 e^-), and $CF_3Mn(CO)_3(NO)^-$ (18 e^-).

The CF_3 group is an ideal infrared chromophore to investigate the infrared photochemistry of organometallic complexes, $L_nM–CF_3$, structures, and reaction mechanisms of their coordinatively unsaturated intermediates containing metal bonded CF_3 groups. The C–F stretching frequency shift, which is sensitive to the net charge of the complex and ligand substituents, may be useful to differentiate the structures of intermediates.

References and Notes

(1) Jasinski, J. M.; Meyerson, B. S.; Scott, B. A. *Ann. Rev. Phys. Chem.* **1987**, *38*, 109.

(2) (a) Walsh, R. *Acc. Chem. Res.* **1981**, *14*, 246. (b) Walsh, R. *J. Phys. Chem.* **1986**, *90*, 389.

(3) Ho, P.; Coltrin, M. E.; Binkley, J. S.; Melius, C. F. *J. Phys. Chem.* **1985**, *89*, 4647.

(4) Shin, S. K.; Beauchamp, J. L. *J. Phys. Chem.* **1986**, *90*, 1507.

(5) Dyke, J. M.; Jonathan, N.; Morris, A.; Ridha, A.; Winter, M. J. *Chem. Phys.* **1983**, *81*, 481.

(6) Boo, B. H.; Armentrout, P. B. *J. Am. Chem. Soc.* **1987**, *109*, 3549.

(7) Berkowitz, J.; Greene, J. P.; Cho, H.; Ruscic, B. *J. Chem. Phys.* **1987**, *86*, 1235.

(8) Frey, H. M.; Walsh, R.; Watts, I. M. *J. Chem. Soc. Chem. Commun.* **1986**, 1189.

(9) Jasinski, J. M.; Chu, J. O. *J. Chem. Phys.* **1988**, *88*, 1678.

(10) Van Zoeren, C. M.; Thoman, J. W. Jr.; Steinfeld, J. I.; Rainbird, M. W. *J. Phys. Chem.* **1988**, *92*, 9.

(11) (a) Nametkin, N. S.; Vdovin, V. M.; Gusel'nikov, L. E.; Zav'yalov, V. I. *Izv. Akad. Nauk SSSR, Ser Khim.* **1966**, 584. (b) Flowers, M. C.; Gusel'nikov, L. E. *J. Chem. Soc. B* **1968**, *419*, 1396.

(12) Shin, S. K.; Irikura, K. K.; Beauchamp, J. L.; Goddard, W. A., III *J. Am. Chem. Soc.* **1988**, *110*, 24.

(13) Shin, S. K.; Beauchamp, J. L. *J. Am. Chem. Soc.* **1989**, *111*, 900.

(14) (b) Walsh, R. *Organometallic* **1988**, *7*, 75.

(15) Neudorfl, P.; Lown, E. M.; Safarik, I.; Jodhan, A.; Strausz, O. P. *J. Am. Chem. Soc.* **1987**, *109*, 5780, and earlier references therein.

(16) Grev, R. S.; Scuseria, G. E.; Scheiner, A. C.; Schaefer, H. F. III; Gordon, M.

S. *J. Am. Chem. Soc.* **1988**, *110*, 7337.

(17) Shin, S. K.; Goddard, W. A. III; Beauchamp, J. L. unpublished results, manuscript in preparation.

(18) *Carbonium Ions*; Olah, G. A.; Schleyer, P. v. R. Eds.; Wiley-Interscience: New York, 1976.

(19) *Gas Phase Ion Chemistry*; Bowers, M. T. Ed.; Academic Press: New York, 1979; vols. 1 and 2, 1984; vol. 3.

(20) (a) Sommer, L. H. *Stereochemistry, Mechanisms, and Silicon*; McGraw-Hill: New York, 1965 and earlier references therein. (b) Corriu, R. J. P; Henner, M. *J. Organomet. Chem.* **1974**, *74*, 1, and references therein. (c) Bickart, P.; Llort, F. M.; Mislow, K. *ibid.* **1976**, *116*, C1. (d) Cowley, A. H.; Cushner, M. C.; Riley, P. E. *J. Am. Chem. Soc.* **1980**, *102*, 624, and references therein.

(21) (a) Lambert, J. B.; Schulz, W. J. Jr.; McConnell, J. A.; Schilf, W. *J. Am. Chem. Soc.* **1988**, *110*, 2201. and earlier references therein. (b) Robinson, L. R.; Burns, G. T.; Barton, T. J. *J. Am. Chem. Soc.* **1985**, *107*, 3935. (c) Eaborn, C.; Lickiss, P. D.; Najim, S. T.; Romanelli, M. N. *J. Chem. Soc., Chem. Commun.* **1985**, 1754. (d) Apeloig, Y.; Stanger, A. *J. Am. Chem. Soc.* **1987**, *109*, 272. (e) Chojnowski, J.; Fortuniak, W.; Stańczyk, W. *J. Am. Chem. Soc.* **1987**, *109*, 7776. (f) Chen, Y.-L.; Barton, T. J. *Organometallics* **1987**, *6*, 2590. (g) Prakash, G. K. S.; Keyaniyan, S.; Aniszfeld, R.; Heiliger, L.; Olah, G. A.; Stevens, R. C.; Choi, H.-K.; Bau, R. *J. Am. Chem. Soc.* **1987**, *109*, 5123.

(22) (a) Ho, P.; Breiland, W. G. *Appl. Phys. Lett.* **1983**, *43*, 125. (b) Breiland, W. G.; Ho, P.; Coltrin, M. E. *J. Appl. Phys.* **1986**, *60*, 1505.

(23) (a) Sedgwick, T. O.; Smith, J. E. *Thin Solid Films* **1977**, *40*, 1. (b) Nishzawa, J. *J. Cryst. Growth* **1982**, *56*, 273. and earlier references therein.

(24) Sausa, R. C.; Ronn, A. M. *Chem. Phys.* **1985**, *96*, 183.

(25) Kruppa, G. H.; Shin, S. K.; Beauchamp, J. L. *J. Phys. Chem.* submitted for publication.

(26) (a) Jensen, P.; Bunker, P. R. *J. Chem. Phys.* **1988**, *89*, 1327 and earlier references therein. (b) Berkowitz, J.; Greene, J. P.; Cho, H.; Ruscic, B. *J. Chem. Phys.* **1987**, *86*, 1235.

(27) (a) Shavitt, I. *Tetrahedron*, **1985**, *41*, 1531; (b) Goddard, W. A. III *Science*, **1985**, *227*, 917; (c) Schaefer, H. F. III *Science*, **1986**, *231*, 1100; (d) Bauschlicher, C. W. Jr.; Langhoff, S. R. *J. Chem. Phys.* **1987**, *87*, 387 and earlier references therein.

(28) Murray, K. K.; Leopold, D. G.; Miller, T. M.; Lineberger, W. C. *J. Chem. Phys.* **1988**, *89*, 5442.

(29) (a) Koda, S. *Chem. Phys. Lett.* **1978**, *55*, 353; (b) Koda, S. *Chem Phys.* **1986**, *66*, 383.

(30) Rao, D. R. *J. Mol. Spectry* **1970**, *34*, 284.

(31) (a) Collman, J. P.; Hegedus, L. S. *Principles and Applications of Organotransition Metal Chemistry*; University Science Books: Mill Valley; 1980, Chapter 5. (b) Collman, J. P.; Hegedus, L. S.; Norton, J. R.; Finke, R. G. *Principles and Applications of Organotransition Metal Chemistry*; University Science Books: Mill Valley; 1987, Chapter 6.

(32) Basolo, F.; Pearson, R. G. *Mechanisms of Inorganic Reactions*; 2nd Ed; Wiley: New York; 1967, pp 578-609.

(33) *Molecular Ions: Spectroscopy, Structure, and Chemistry* Miller, T. A.; Bondybey, V. E. Ed; North-Holland Publishing: Amsterdam; 1983, 231.

(34) *Molecular Photodissociation Dynamics* Ashfold, M. N. R.; Baggott, J. E. Ed; The Royal Society of Chemistry: London; 1987.

Chapter I

Proton Affinity and Heat of Formation of Silylene

Reprinted from The Journal of Physical Chemistry, 1986, 90, 1507

Proton Affinity and Heat of Formation of Silylene

Seung Koo Shin and J. L. Beauchamp*

The Arthur Amos Noyes Laboratory of Chemical Physics,† California Institute of Technology, Pasadena, California 91125 *(Received: February 25, 1986)*

Using the techniques of Fourier transform ion cyclotron resonance spectroscopy, we determined the proton affinity of silylene to be 201 ± 3 kcal·mol^{-1} from a study of the kinetics and thermochemistry of proton transfer from SiH_3^+ to a series of n-donor bases with well-established gas-phase base strengths. This value leads to $\Delta H_f°_{298}(SiH_2)$ = 69 ± 3 kcal·mol^{-1}, which is 11 kcal·mol^{-1} higher than the previously accepted value (Walsh, R. *Acc. Chem. Res.* **1981**, *14*, 246–252), but in excellent agreement with the recent theoretically recommended value of 68.1 kcal·mol^{-1} (Ho, P.; Coltrin, M. E.; Binkely, J. S.; Melius, C.F. *J. Phys. Chem.* **1985**, *89*, 4647–4654).

The thermochemical properties of the reactive molecule silylene are of fundamental interest in organometallic chemistry and also of importance in understanding the process of silicon chemical vapor deposition (CVD).[1] Although the heat of formation of silylene has been studied experimentally, there is considerable discrepancy among the various published values. For example, the value of $\Delta H_f°_{298}$ (SiH_2) = 58 kcal·mol^{-1} recommended by Walsh[2] (based on pyrolysis measurements of silane species)[3] is considerably below the more questionable value of 81 kcal·mol^{-1} obtained from the mass spectrometric study of silylarsine by Saalfeld and McDowell.[4] However, the higher value is supported by arguments offered by Robertson et al.[5] in their recent studies of silane pyrolysis. Ho et al.[6] obtained a heat of formation of SiH_2 of 68.1 kcal·mol^{-1} by ab initio calculation at the MP4/6-31G** level. This is corroborated by the value of 67.9 kcal·mol^{-1} estimated from the most recent theoretical calculation (MP4SPTQ/6-31G* level) reported by Luke et al.[7]

To more firmly define an experimental value for the heat of formation of silylene, we have used the techniques of Fourier transform ion cyclotron resonance spectroscopy[8] to examine proton-transfer reactions of SiH_3^+ (reaction 1) with a series of

$$SiH_3^+ + B \rightarrow SiH_2 + BH^+ \quad (1)$$

n-donor bases B with known gas-phase basicities[9,10] (proton affinities). The proton affinity of SiH_2 determined in this fashion yields $\Delta H_f°(SiH_2)$ with the use of eq 2. This experimental

$$\Delta H_f°(SiH_2) = PA(SiH_2) + \Delta H_f°(SiH_3^+) - \Delta H_f°(H^+) \quad (2)$$

methodology has successfully yielded heats of formation of halocarbenes[11] and other reactive molecules[12] in previous studies.

Silane ionized by electron impact with an electron energy of 14 eV provides a convenient source of SiH_3^+ ions. The most abundant primary ions are SiH_2^+ and SiH_3^+,[13] the former being converted to the latter by reaction 3 (k = 6.2 × 10^{-10} cm^3·molecule^{-1}·s^{-1}).[14] The symmetrical hydride-transfer reaction of

$$SiH_2^+ + SiH_4 \rightarrow SiH_3^+ + SiH_3 \quad (3)$$

SiH_3^+ with silane is also very fast.[14] The silyl cation reacts very slowly with silane to yield $Si_2H_5^+$.[15] Various oxygen-, nitrogen-, and sulfur-containing n-donor bases were chosen as neutral reactants, covering a range of base strengths and expected reactivities. The Fourier transform ICR spectrometer used in these studies comprises a 1-in. cubic cell[16] in a 15-in. electromagnet (operated typically at 1 T) with an Ionspec FTMS-2000 data system. Pressures were measured with a Schulz-Phelps ion gauge calibrated against an MKS Baratron (Model 390 HA-0001) capacitance manometer. Experiments were carried out with 1:1 SiH_4–B mixtures with a total pressure in the range (1–2) × 10^{-6} torr and an electron energy of 14 eV. Although other reactions are noted below, this study focused on the proton-transfer reaction of SiH_3^+ with the neutral bases. Ion ejection pulses were used to remove all ions except SiH_3^+ from the ICR cell shortly after the electron beam pulse.[17] The results are summarized in Table I.

As reported by Lampe et al.,[18] SiH_3^+ reacts sequentially with D_2O to yield a protonated silanone (H_2SiOD^+), $HSi(OD)_2^+$, and $Si(OD)_3^+$. The primary reaction products with CD_3OD are $H_2SiOCD_3^+$, H_2SiOD^+, and a deuteride-transfer product CD_3OD^+. The protonated silanone was also observed as a major product in the reaction of SiH_3^+ with CH_3CHO and $(CD_3)_2CO$. In the reaction of SiH_3^+ with aliphatic nitriles, the formation of $RCNSiH^+$ (R = CH_3, c-C_3H_5) is predominant, with hydrogen being eliminated from the silicon center.[19] SiH_3^+ reacts with CH_3OCH_3 exclusively via a hydride-transfer reaction. Hydride

† Contribution No. 7377.

(1) (a) Hirose, M. *Semiconductors and Semimetals*, Pankove, J. I., Ed.; Academic Press: Orlando, 1984; Vol. 21A, Chapter 6. (b) Viswanathan, R.; Thompson, D. L.; Raff, L. M. *J. Chem. Phys.* 1984, *80*, 4230–4240.

(2) (a) Walsh, R. *Acc. Chem. Res.* **1981**, *14*, 246–252. (b) Walsh, R. *J. Phys. Chem.* **1986**, *90*, 389–394.

(3) (a) Purnell, J. H.; Walsh, R. *Proc. R. Soc. London, Ser. A* **1971**, *293*, 543–561. (b) Bowrey, M.; Purnell, J. H. *Proc. R. Soc. London, Ser. A* **1971**, *321*, 341–359. (c) John, P.; Purnell, J. H. *J. Chem. Soc., Faraday Trans. 1* **1973**, *69*, 1455–1461. (d) Vanderwielen, A. J.; Ring, M. A.; O'Neal, H. E. *J. Am. Chem. Soc.* **1975**, *97*, 993–998.

(4) Saalfeld, F. E.; McDowell, M. V. *Inorg. Chem.* **1967**, *6*, 96–98.

(5) Robertson, R.; Hills, D.; Gallagher, A. *Chem. Phys. Lett.* **1984**, *103*, 397–404.

(6) Ho, P.; Coltrin, M. E.; Binkley, J. S.; Melius, C. F. *J. Phys. Chem.* **1985**, *89*, 4647–4654.

(7) The reaction enthalpy at 0 K for SiH_4 + $CH_2(^3B_1)$ → CH_4 + $SiH_2(^1A_1)$ is estimated to be −51.9 kcal·mol^{-1} from Luke, B. T.; Pople, J. A.; Krogh-Jespersen, M.-B.; Apeloig, Y.; Chandrasekhar, J.; Schleyer, P. v. R. *J. Am. Chem. Soc.* **1986**, *108*, 260–269. It is assumed that the enthalpy of this reaction at 298 K is nearly the same as that at O K by an ideal gas approximation. This value of the enthalpy of reaction and the heat of formation of silane (8.2 kcal·mol^{-1}; ref 2), methane (−17.9 kcal·mol^{-1}; Pedley, J. B.; Rylance, J. Sussex N. P. L. *Computer Analyzed Thermochemical Data: Organic and Organometallic Compounds*; University of Sussex: Sussex, England, 1977) and methylene (93.7 kcal·mol^{-1}; Rosenstock, H. M.; Draxl, K.; Steiner, B. W.; Herron, J. T. *J. Phys. Chem. Ref. Data Suppl.* 1977, 6.) leads to $\Delta H_f°_{298}(SiH_2)$ = 67.9 kcal·mol^{-1}.

(8) Marshall, A. G. *Acc. Chem. Res.* **1985**, *18*, 316–322, and references contained therein.

(9) (a) Kebarle, P. *Annu. Rev. Phys. Chem.* **1977**, *28*, 445–476. (b) Wolf, J. F.; Staley, R. H.; Koppel, I.; Taagepera, M.; McIver, R. T. Jr., Beauchamp, J. L.; Taft, R. W. *J. Am. Chem. Soc.* **1977**, *99*, 5417–5429. (c) Taft, R. W. *Prog. Phys. Org. Chem.* **1983**, *14*, 247–350.

(10) Lias, S. G.; Liebman, J. F.; Levin, R. D. *J. Phys. Chem. Ref. Data* **1984**, *13*, 695–808.

(11) (a) Vogt, J.; Beauchamp, J. L. *J. Am. Chem. Soc.* **1975**, *97*, 6682–6685. (b) Lias, S. G.; Karpas, Z.; Liebman, J. F. *J. Am. Chem. Soc.* **1985**, *107*, 6089–6096, and references contained therein.

(12) (a) Meot-Ner, M. *J. Am. Chem. Soc.* **1982**, *104*, 5–10. (b) Pau, C. F.; Pietro, W. J.; Hehre, W. J. *J. Am. Chem. Soc.* **1983**, *105*, 16–18.

(13) Potzinger, P.; Lampe, F. W. *J. Phys. Chem.* **1969**, *73*, 3912–3917.

(14) Henis, J. M. S.; Stewart, G. W.; Tripodi, M. K.; Gaspar, P. P. *J. Chem. Phys.* **1972**, *57*, 389–398.

(15) We obtain a reaction rate constant for SiH_3^+ + SiH_4 → $Si_2H_5^+$ + H_2 of 0.58 × 10^{-10} cm^3·molecule^{-1}·s^{-1}.

(16) Comisarow, M. B. *Int. J. Mass. Spectrom. Ion Phys.* **1981**, *37*, 251–257.

(17) Cody, R. B.; Burnier, R. C.; Freiser, B. S. *Anal. Chem.* **1982**, *54*, 96–101.

(18) Cheng, T. M. H.; Lampe, F. W. *J. Phys. Chem.* **1973**, *77*, 2841–2846.

(19) The reaction of SiH_3^+ with CD_3CN shows that SiH_3^+ + CD_3CN → CD_3CNSiH^+ + H_2.

0022-3654/86/2090-1507$01.50/0

TABLE I: Observed Reactions and Rate Constants for the Reactions

$SiH_3^+ + B \rightarrow$ products

B	PA[a]	products	prod distr[b]	k_{total}[c]	k_{ADO}[d]
D_2O	166.5[e]	$H_2SiOD^+ + HD$	1.0	2.1 ± 0.2	19.7
CD_3OD	181.9[e]	$H_2SiOCD_3^+ + HD$	0.44	6.4 ± 0.7	16.5
		$CD_2OD^+ + SiH_3D$	0.38		
		$H_2SiOD^+ + CD_3H$	0.18		
CH_3CHO	186.6	$H_2SiOH^+ + C_2H_4$	1.0	9.9 ± 0.8	21.4
CH_3CN	188.4	$CH_3CNSiH^+ + H_2$	>0.99	15.5 ± 1.5	29.3
$(CH_3)_2O$	192.1	$CH_3OCH_2^+ + SiH_4$	1.00	5.4 ± 0.5	14.7
c-C_3H_5CN	195.4	$C_3H_5CNSiH^+ + H_2$	0.65	22.8 ± 2.2	22.8
		$C_3H_5SiH_2^+ + HCN$	0.22		
		$C_3H_5^+ + SiH_3CN$	0.13		
$(CD_3)_2CO$	196.7[e]	$H_2SiOD^+ + C_3H_6$	0.80	20.7 ± 1.1	21.5
		$CD_3CO^+ + SiH_3CD_3$	0.20		
$(C_2D_5)_2O$	200.2[e]	$C_2D_5OC_2D_4^+ + SiH_3D$	[f]	15.2 ± 1.6	15.3
		$C_2D_5OCD_2^+ + SiH_3CD_3$			
		$C_2D_5OSiH_2^+ + CD_3CD_2H$			
		$C_2D_5OH_2^+ + HSiCD_2CD_3$			
$(CH_3)_2S$	200.6	$CH_3SCH_2^+ + SiH_4$	0.86	17.2 ± 1.5	15.8
		$HSSiH_3^+ + C_2H_5$	0.14		
$(C_2H_5)_2CO$	201.4	$(C_2H_5)_2COH^+ + SiH_2$	0.56	14.4 ± 1.3	20.3
		$H_2SiOH^+ + C_4H_{10}$	0.24		
		$(C_2H_5)_2COSiH_3^+$	0.20		
$(n\text{-}Pr)_2O$	202.3	$(C_3H_7)_2OH^+ + SiH_2$	0.42	15.0 ± 1.4	17.5
		$C_3H_7^+ + H_3SiOC_3H_7$	0.44		
		$C_3H_7OC_3H_6^+ + SiH_3D$	0.07		
		$C_3H_7OH_2^+ + HSiC_3H_7$	0.07		
NH_3	204	$NH_4^+ + SiH_2$	0.74	6.0 ± 0.5	17.6
		$H_2SiNH_2^+ + H_2$	0.26		

[a] All proton affinity values from ref 10. In units of kcal·mol^{-1}. [b] Product distribution normalized to unity for reactant ions. [c] In units of 10^{-10} cm^3·molecule^{-1}·s^{-1}. [d] Ion–polar molecule collision rate constant obtained by using the average-dipole-orientation theory: Su, T.; Bowers, M. T. *Int. J. Mass Spectrom. Ion Phys.* **1973**, *12*, 347–416. [e] Proton affinity of the deuterated molecule is slightly lower. [f] The reaction sequence is too complicated to get a product distribution. Double resonance experiments indicate that nearly all of the secondary product ions undergo proton transfer to the neutral diethyl ether.

transfer and more complex processes occur in the reaction with $C_2D_5OC_2D_5$. With $(CH_3)_2S$, hydride-transfer is also a dominant reaction channel. Although a small amount of $(CH_3)_2SH^+$ is observed in this system, ion ejection experiments confirm that it results from a complex sequence of reactions and it is not a direct proton-transfer product involving SiH_3^+. The above molecules all have proton affinities below 200.6 ± 3 kcal·mol^{-1}.[20] With stronger bases, proton transfer is an important reaction channel. For example, the predominant reaction (~56% of the product distribution) of SiH_3^+ with 3-pentanone is a proton transfer, with a rate constant of 8.0×10^{-10} cm^3·molecule^{-1} s^{-1}. In the case of $(n\text{-}Pr)_2O$ and NH_3, proton transfer also occurs predominantly.

There are several factors[21] contributing to the uncertainty in deriving of a value of $\Delta H_f°(SiH_2)$ from these experiments. These include (i) the near impossibility of pinpointing from such experiments (in which other fast reactions compete with proton transfer) the precise transition point at which proton transfer from SiH_3^+ is thermoneutral; (2) the difficulties associated with the assignment of absolute values to the proton affinity scale,[10] and (3) the uncertainties in the heat of formation of SiH_3^+.[22] The results shown in Figure 1 strongly suggest that $PA((CH_3)_2S) < PA(SiH_2) < PA((C_2H_5)_2CO)$. Using a value of 204 ± 3 kcal·mol^{-1} for $PA(NH_3)$ leads to a value for $PA(SiH_2)$ of 201 ± 3 kcal·mol^{-1}. Using a value of 234.1 kcal·mol^{-1} for $\Delta H_f°(SiH_3^+)$[22] and 365.7 kcal·mol^{-1} for $\Delta H_f°(H^+)$[23] in eq 2 yields $\Delta H_f°(SiH_2)$ = 69 ± 3 kcal·mol^{-1}. This is 11 kcal·mol^{-1} higher than the previously accepted value (58 kcal·mol^{-1}),[2] but in good agreement with the recent theoretical value (68.1 kcal·mol^{-1}) recommended by Ho et al.[6] With this value and $\Delta H_f°_{298}(SiH_4)$ = 8.2 kcal·mol^{-1},[2,6] the enthalpy of the decomposition reaction 4 is 60.8 ±

$$SiH_4 \rightarrow SiH_2 + H_2 \quad (4)$$

3 kcal·mol^{-1} at 298 K, which is close to the activation energy (59.5 kcal·mol^{-1}) for silane pyrolysis obtained by Newman et al.[24] This

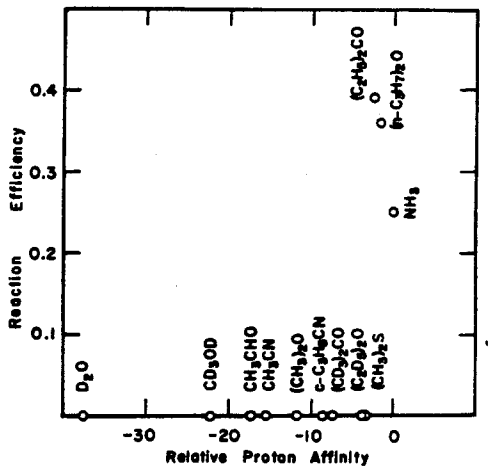

Figure 1. Variation with base strength of the reaction efficiency (defined as the ratio of the rate constant to the calculated collision rate) for proton transfer from SiH_3^+ to various n-donor bases. Base strengths (proton affinities) are given relative to NH_3 [$PA(NH_3)$ = 204 ± 3 kcal·mol^{-1}].

(20) $PA((CH_3)_2S)$ = 200.6 ± 3 kcal·mol^{-1}.; with $\Delta H_f°_{298}(SiH_2)$ = 58 kcal·mol^{-1}, the expected proton affinity of silylene is 189.6 kcal·mol^{-1}.

(21) Ausloos, P.; Lias, S. G. *J. Am. Chem. Soc.* **1978**, *100*, 4594–4595.

(22) $\Delta H_f°_{298}(SiH_3)$ = 46.4 kcal·mol^{-1} (ref 2), $IP_a(SiH_3)$ = 8.14 eV (Dyke, J. M.; Jonathan, N.; Morris, A.; Ridha, A.; Winter, M. J. *Chem. Phys.* **1983**, *81*, 481–488. This corresponds to $\Delta H_f°_{298}(SiH_3^+)$ = 234.1 kcal·mol^{-1}, which is in good agreement with unpublished results of the photoionization mass spectrometric studies of Coderman and Beauchamp (235.1 kcal·mol^{-1}) (Corderman, R. R. Ph.D. Thesis, California Institute of Technology, 1977) and the recent photoionization study of Ding et al. (237.1 ± 0.6 kcal·mol^{-1}) (ref 25).

(23) $\Delta H_f°_{298}(H)$ = 52.103 kcal·mol^{-1} and IP(H) = 13.598 eV from Moore, C.E. *Natl. Stand. Ref. Data Ser., Natl. Bur. Stand.* **1970**, *No.* 34.

(24) Newman, C. G.; O'Neal, H. E.; Ring, M. A.; Leska, F.; Shipley, N. *Int. J. Chem. Kinet.* **1979**, *11*, 1167–1182.

result strongly favors silylene chemistry, as opposed to silyl radical chemistry, as the primary decomposition reaction in silane pyrolysis. Using a similar approach, Hehre et al.[12] have determined the proton affinity of dimethylsilylene to be 232 kcal·mol^{-1}. The effect of methyl substitution (31 kcal·mol^{-1}) is close to that observed in comparing H_2S to $(CH_3)_2S$ (30.4 kcal·mol^{-1}). Combining the known heat of formation[25] $\Delta H_f°_{298}(SiH_2^+)$ = 276.3 kcal·mol^{-1} with the heat of formation of SiH_2 derived in this study yields an adiabatic ionization potential of 8.99 eV for SiH_2. This is in excellent agreement with the value 8.98 eV predicted by ab initio calculation at the MRD-CI level.[26]

The results of the present study signal another triumph for high-quality ab initio calculations as a reliable approach to predicting the thermochemical properties of reaction intermediates. With the necessary blessing granted by experimental certification, some changes in the estimated thermochemistry of processes involving silylene are recommended. Related studies of substituted silylenes are in progress in our laboratory.

Acknowledgment. We acknowledge the support of the National Science Foundation under Grant CHE-8407857.

(25) Ding, A.; Cassidy, R. A.; Cordis, L. S.; Lampe, F. W. *J. Chem. Phys.* **1985**, *83*, 3426–3432.

(26) Bruna, P. J., unpublished results cited in ref 25.

Chapter II

Thermochemistry of Silaethylene and Methylsilylene from Experiment and Theory

Reprinted from the Journal of the American Chemical Society, 1988, *110*, 24.

Thermochemistry of Silaethylene and Methylsilylene from Experiment and Theory

Seung Koo Shin, Karl K. Irikura, J. L. Beauchamp,* and William A. Goddard, III

Contribution No. 7595 from the Arthur Amos Noyes Laboratory of Chemical Physics, California Institute of Technology, Pasadena, California 91125. *Received June 15, 1987*

Abstract: Fourier transform ion cyclotron resonance spectroscopy has been used to examine the deprotonation energetics of the methylsilyl cation, $CH_3SiD_2^+$, to yield silaethylene and methylsilylene proton affinities of 205 ± 3 and 215 ± 4 kcal/mol, respectively. These values, combined with the known heat of formation of methylsilyl cation, yield $\Delta H_f^\circ{}_{298}(CH_2SiH_2) = 43 \pm 3$ kcal/mol and $\Delta H_f^\circ{}_{298}(CH_3SiH) = 53 \pm 4$ kcal/mol. These results are corroborated by ab initio generalized valence bond–configuration interaction calculations which indicate that silaethylene is more stable than methylsilylene by 11.6 kcal/mol, in excellent agreement with the experimental difference (10 ± 3 kcal/mol). The adiabatic ionization potential of methylsilylene is calculated to be 8.22 eV, which is lower than the value of 8.85 eV determined for silaethylene using photoelectron spectroscopy.

The reactivities, structures, and thermochemistry of Si–C double-bonded compounds,[1] silaethylenes, and divalent silicon compounds, silylenes,[2] have been the subject of extensive study, ever since dimethylsilaethylene was first suggested as a reactive intermediate in the pyrolysis of 1,1-dimethylsilacyclobutane.[3] Silaethylene (**1**) and its isomer methylsilylene (**2**) have been

isolated in an argon matrix[4] and spectroscopically characterized.[5,6] The interconversion of these two reactive species has been examined to elucidate the isomerization energetics.[5,7] However, no experimental determinations of the heats of formation of these

Table I. Theoretical Predictions of the Relative Stabilities of Silaethylene and Methylsilylene

year	method[a]	$\Delta E(SiHCH_3 - SiH_2CH_2)$ (kcal/mol)	ref
1978	CI/STO-3G//HF/STO-4G	−6.8	*b*
1980	MP2/6-31G*//HF/4-31G	2.1	*c*
1980	CI/DZ+d//HF/DZ	−0.4	*d*
1981	CI(pseudo-pot)/DZ+d	3.5	*e*
1982	CI/DZ+P//HF/DZ+P + Davidson correction	1.7	*f*
1982	CEPA/extended (p+d) //HF/extended (d)	0.6	*g*
1984	CI/6-31G*//HF/6-31G* + Davidson correction	−3.4	*h*
1987	CC-CI/VDZ+P//MP2/6-31G** + zero-point-energy correction	11.6	*i*

[a] Calculational level for total energy/basis sets//calculational level for geometry optimization/basis sets; for example, CI/STO-3G//HF/STO-4G represents the CI level energy calculation with STO-3G basis sets and the HF/STO-4G optimized geometry. For details, see references. [b] Reference a. [c] Reference 8b. [d] Reference 8c. [e] Reference 8d. [f] Reference 1d. [g] Reference 8e. [h] Reference 8f. [i] This work.

However, no experimental determinations of the heats of formation of these

(1) For recent reviews, see: (a) Raabe, G.; Michl, J. *Chem. Rev.* **1985**, *85*, 419. (b) Bertrand, G.; Trinquier, G.; Mazerolles, P. *J. Organomet. Chem. Libr.* **1981**, *12*, 1. (c) Gusel'nikov, L. E.; Nametkin, N. S. *Chem. Rev.* **1979**, *79*, 529. (d) Schaefer, H. F., III *Acc. Chem. Res.* **1982**, *15*, 283.

(2) Gaspar, P. P. In *Reactive Intermediates*; Jones, M., Moss, R. A., Eds.; Wiley: New York, 1985; Vol. 3, Chapter 9 and earlier volumes.

(3) (a) Nametkin, N. S.; Vdovin, V. M.; Gusel'nikov, L. E.; Zav'yalov, V. I. *Izv. Akad. Nauk SSSR, Ser. Khim.* **1966**, 584. (b) Flowers, M. C.; Gusel'nikov, L. E. *J. Chem. Soc. B* **1968**, 419.

(4) Maier, G.; Mihm, G.; Reisenauer, H. P. *Chem. Ber.* **1984**, *117*, 2351.

(5) (a) Maier, G.; Mihm, G.; Reisenauer, H. P.; Littman, D. *Chem. Ber.* **1984**, *117*, 2369. (b) Rosmus, P.; Bock, H.; Solouki, B.; Maier, G.; Mihm, G. *Angew. Chem., Int. Ed. Engl.* **1981**, *20*, 598.

(6) Auner, N.; Grobe, J. *Z. Anorg. Allg. Chem.* **1979**, *459*, 15.

0002-7863/88/1510-0024$01.50/0

Scheme I

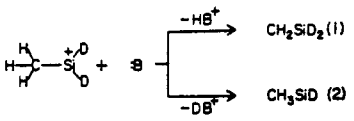

reactive isomers have been reported. There have been numerous theoretical studies[8] of the relative stabilities of silaethylene and methylsilylene, resulting in values of $\Delta E = E(2) - E(1)$ which range from −6.8 to 3.5 kcal/mol (note that a positive value of this quantity indicates that **1** is more stable than **2**).

Herein, we report the deprotonation energetics of methylsilyl cation using Fourier transform mass spectrometry to estimate the heats of formation of silaethylene and methylsilylene. Our previously reported[9] results for silylene using this experimental methodology are in excellent agreement with both a theoretical recommendation[10] and the recent experiments of Berkowitz et al.[11] and Boo et al.[12] The current consensus is that the heat of formation of silylene is 69 ± 3 kcal/mol. This revision in the heat of formation of silylene from the previously accepted value[13] of 58 kcal/mol leads to some changes in the *estimated* heats of formation of methyl-substituted silylenes.[14]

Previously suggested values[13] of heats of formation of silaethylene (39 ± 5 kcal/mol) and methylsilylene (42 kcal/mol)[14] yield a 3-kcal/mol differences, in agreement with some previous theoretical calculations (ΔE = −6.8 to 3.5 kcal/mol), as indicated in Table I. For example, an MP2 calculation by Gordon[8b] leads to ΔE = 2.1 kcal/mol. Schaefer's[8d] CI calculation with Davidson's correction yields 1.7 kcal/mol and a CI calculation by Malrieu[8d] leads to 3.5 kcal/mol. On the other hand, the most recent CI (Nagase[8f]) leads to −3.4 kcal/mol and CEPA[8e] leads to 0.6 kcal/mol. *However, the recent revision[14] of the heat of formation of methylsilylene (53 kcal/mol) leads to ΔE = 14.6 kcal/mol,* which is substantially larger than what appear to be the "best" theoretical calculations.

To resolve some of the conflicts apparent in the results discussed above and more firmly define the values of the heats of formation of silaethylene and methylsilylene, we have studied the kinetics and thermochemistry of the proton- and deuteron-transfer reactions of $CH_3SiD_2^+$ with various n-donor bases of well-established gas-phase basicities.[15,16] Using this methodology, Hehre and co-workers[17] have previously studied the onsets of proton and deuteron abstraction from $(CH_3)_2SiD^+$ by various n-donor bases and found that the proton transfer has the lower threshold than the deuteron transfer. As shown in Scheme I, transfer of the carbon-bound proton from $CH_3SiD_2^+$ to the base yields silaethylene, and transfer of the silicon bound deuteron produces methylsilylene as the neutral products. The proton affinities of silaethylene and methylsilylene determined in this fashion yield the heats of formation of the two isomers with the use of eq 1.

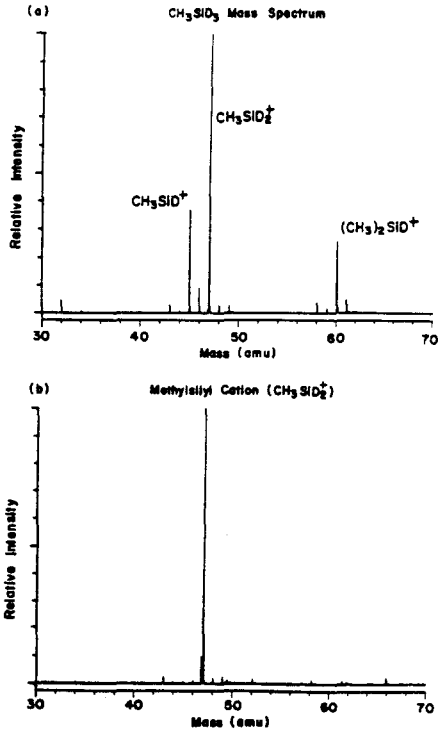

Figure 1. (a) Mass spectrum of CH_3SiD_3 with 15-eV electron energy at 1.2×10^{-6} torr and 30-ms delay before ion detection. (b) Mass spectrum of $CH_3SiD_2^+$ shortly after a series of ion ejection pulses. Even though the ion ejections are incomplete because of the use of low rf levels to avoid excitation of the isolated reactant ion, the conditions suffice for an examination of the deprotonation kinetics.

$$\Delta H_f^\circ{}_{298}(CH_2SiD_2 \text{ or } CH_3SiD) = PA(CH_2SiD_2 \text{ or } CH_3SiD) + \Delta H_f^\circ{}_{298}(CH_3SiD_2^+) - \Delta H_f^\circ{}_{298}(H^+ \text{ or } D^+) \quad (1)$$

In addition, we have performed ab initio calculations to reexamine the relative stabilities of the two isomers and to estimate the rotational barrier in silaethylene.

Experimental Section

Experimental techniques associated with ICR spectroscopy,[18] and in particular Fourier transform mass spectrometry,[19] have been previously described in detail. Experiments were performed with an Ion Spec-2000 Fourier transform mass spectrometer equipped with a 1-in. cubic trapping cell[20] built by Bio-Med Tech[21] situated between the poles of a Varian 15-in. electromagnet maintained at 1 T. Chemicals were obtained commercially in high purity and used as supplied except for multiple freeze–pump–thaw cycles to remove noncondensable gases. CH_3SiD_3 and CH_3SiH_3 were prepared by reducing CH_3SiCl_3 with $LiAlD_4$ and $LiAlH_4$.[22] Pressures were measured with a Schulz-Phelps ion gauge[23] cali-

(7) Davidson, I. M. T.; Ijadi-Maghsoodi, S.; Barton, T. J.; Tillman, N. *J. Chem. Soc., Chem. Commun.* **1984**, 478.

(8) (a) Gordon, M. S. *Chem. Phys. Lett.* **1978**, *54*, 9. (b) Gordon, M. S. *Ibid.* **1980**, *76*, 163. (c) Goddard, J. D.; Yoshioka, Y.; Schaefer, H. F., III *J. Am. Chem. Soc.* **1980**, *102*, 7644. (d) Trinquier, G.; Malrieu, J.-P. *Ibid.* **1981**, *103*, 6313. (e) Köhler, H. J.; Lischka, H. *Ibid.* **1982**, *104*, 5884. (f) Nagase, S.; Kudo, T. *J. Chem. Soc., Chem. Commun.* **1984**, 141. (g) Nagase, S.; Kudo, T.; Ito, K. In *Applied Quantum Chemistry*; Smith, V. H., Jr., Ed; D. Reidel: Boston, 1986; pp 249–267.

(9) Shin, S. K.; Beauchamp, J. L. *J. Phys. Chem.* **1986**, *90*, 1507.

(10) Ho, P.; Coltrin, M. E.; Binkley, J. S.; Melius, C. F. *J. Phys. Chem.* **1985**, *89*, 4647.

(11) Berkowitz, J.; Greene, J. P.; Cho, H.; Ruščić, B. *J. Chem. Phys.* **1987**, *86*, 1235.

(12) Boo, B. H.; Armentrout, P. B. *J. Am. Chem. Soc.* **1987**, *109*, 3549.

(13) Walsh, R. *Acc. Chem. Res.* **1981**, *14*, 246.

(14) Assuming a methyl substituent effect of 16 kcal/mol (ref 13) leads to predicted heats of formation of methylsilylene and dimethylsilylene of 53 and 37 kcal/mol, respectively. These values are based on a revised value of 69 kcal/mol for $\Delta H_f^\circ{}_{298}(SiH_2)$, compared with a previously accepted value of 58 kcal/mol (ref 13).

(15) (a) Kebarle, P. *Annu. Rev. Phys. Chem.* **1977**, *28*, 445. (b) Wolf, J. F.; Staley, R. H.; Koppel, I.; Taagepera, M.; McIver, R. T., Jr.; Beauchamp, J. L.; Taft, R. W. *J. Am. Chem. Soc.* **1977**, *99*, 5417. (c) Taft, R. W. *Prog. Phys. Org. Chem.* **1983**, *14*, 247.

(16) Lias, S. G.; Liebman, J. F.; Levin, R. D. *J. Phys. Chem. Ref. Data* **1984**, *13*, 695.

(17) Pau, C. F.; Pietro, W. J.; Hehre, W. J. *J. Am. Chem. Soc.* **1983**, *105*, 16.

(18) (a) Beauchamp, J. L. *Annu. Rev. Phys. Chem.* **1971**, *22*, 527. (b) Lehman, T. A.; Bursey, M. M. *Ion Cyclotron Resonance Spectrometry*; Wiley: New York, 1976.

(19) (a) Comisarow, M. B.; Marshall, A. G. *Chem. Phys. Lett.* **1974**, *25*, 282. (b) Ledford, E. B., Jr.; Gharderi, S.; White, R. L.; Spencer, R. B.; Kulkarni, P. S.; Wilkins, C. L.; Gross, M. L. *Anal. Chem.* **1980**, *52*, 463. (c) Marshall, A. G. *Acc. Chem. Res.* **1985**, *18*, 316 and references contained therein.

(20) Comisarow, M. B. *Int. J. Mass. Spectrom. Ion Phys.* **1981**, *37*, 251.

(21) Bio-Med Tech, 2001 E. Galbreth, Pasadena, CA 91104.

(22) Gaspar, P. P.; Levy, C. A.; Adair, G. M. *Inorg. Chem.* **1970**, *9*, 1272.

(23) Schulz, G. J.; Phelps, A. V. *Rev. Sci. Instrum.* **1957**, *28*, 1051.

Table II. Observed Reactions and Rate Constants for the Reactions $CH_3SiD_2^+ + B \rightarrow$ Products

B	PA[a]	products	prod distr[b]	k_{total}[c]	k_{ADO}[d]
$(CH_3)_2S$	200.6	$CH_3SCH_2^+ + CH_3SiD_2H$	1.0	11.2	19.3
NH_3	204.0	$CH_3SiDNH_2^+ + HD$	1.0	5.4	18.3
CH_3CONH_2	206.2	$CH_3CONH_3^+ + CH_2SiD_2$	0.75	18.7	18.5
		$CH_3SiDNH_2^+ + CH_3COD$	0.15		
		$CH_3SiDNHCOCH_3^+ + HD$	0.05		
		$CH_3SiD_2NH_2COCH_3^+$	0.05		
$C_6H_5NH_2$	210.5	$C_6H_5^+ + CH_3SiD_2NH_2$	0.40	26.2	18.1
		$C_6H_5NH_3^+ + CH_2SiD_2$	0.20		
		$CH_3SiDNHC_6H_5^+ + HD$	0.20		
		$CH_3SiD_2NH_2C_6H_5^+$	0.20		
CH_3NH_2	214.1	$CH_3NH_3^+ + CH_2SiD_2$	0.30	12.0	15.9
		$CH_2NH_2^+ + CH_3SiD_2H$	0.30		
		$CH_3SiDNHCH_3^+ + HD$	0.30		
		$CH_3SiDNH_2^+ + CH_3D$	0.05		
		$CH_3SiD_2NH_2CH_3^+$	0.05		
$C_6H_5CH_2NH_2$	216.8	$C_6H_5CH_2^+ + CH_3SiD_2NH_2$	0.55	2.8	17.8
		$C_6H_5CH_2NH_3^+ + CH_2SiD_2$	0.30		
		$C_6H_5CHNH_2^+ + CH_3SiD_2H$	0.10		
		$C_6H_5CH_2NH_2D^+ + SiDCH_3$	0.05[e]		
$C_2H_5NH_2$	217.0	$C_2H_5NH_3^+ + CH_2SiD_2$	0.40	16.0	15.6
		$C_2H_4NH_2^+ + CH_3SiD_2H$	0.20		
		$CH_3SiDNHC_2H_5^+ + HD$	0.20		
		$C_2H_5NH_2D^+ + SiDCH_3$	0.14[e]		
		$CH_3SiDNH_2^+ + C_2H_5D$	0.03		
		$CH_3SiD_2NH_2C_2H_5^+$	0.03		
$(CH_3)_2NH$	220.6	$(CH_3)(CH_2)NH^+ + CH_3SiD_2H$	0.55	20.5	14.7
		$(CH_3)_2NH_2^+ + CH_2SiD_2$	0.20		
		$(CH_3)_2NHD^+ + SiDCH_3$	0.20[e]		
		$(CH_3)_2NSiDCH_3^+ + HD$	0.05		

[a] All proton affinity values from ref 16. In units of kcal/mol. [b] Product distribution normalized to unity for reactant ion. [c] In units of 10^{-10} cm^3 molecule^{-1} s^{-1}. [d] Ion-polar molecule collision rate constant obtained by using the average-dipole-orientation theory: Su, T.; Bowers, M. T. *Int. J. Mass Spectrom. Ion Phys.* **1973**, *12*, 347. [e] Corrected for ^{13}C natural abundance.

brated against an MKS Baratron (Model 390 HA-0001) capacitance manometer. The principal errors in the rate constants (estimated to be ±20%) arise from uncertainties in pressure measurements.[24] Approximately 1:1 mixtures of methylsilane and base were used with a total pressure in the range $1 \sim 5 \times 10^{-6}$ torr. Ionization was by electron impact at 15 eV.

Although other reactions are noted below, this study focused on the proton- and deuteron-transfer reactions of $CH_3SiD_2^+$ with the neutral bases. Methylsilane ionized by electron impact is a convenient source of $CH_3SiD_2^+$ ions.[25,26] The most abundant primary ion is CH_3SiD^+, which is converted to $CH_3SiD_2^+$ by reaction 2 with a rate constant of 5.3×10^{-10} cm^3 molecule^{-1} s^{-1}.

$$CH_3SiD^+ + CH_3SiD_3 \rightarrow CH_3SiD_2^+ + CH_3SiD_2 \quad (2)$$

Ion ejection pulses were used to remove all ions except $CH_3SiD_2^+$ from the ICR cell shortly after the electron beam pulse.[27] We used as low rf levels as possible to avoid thermal excitation of the reactant ion. Figure 1 shows a spectrum of $CH_3SiD_2^+$ ion just after a series of ejection pulses. The temporal variations of reactant and product ion abundances were recorded and used to calculate rate constants directly. As an example, Figure 2 shows the temporal variations of the reactant $CH_3SiD_2^+$ ion and the product $CH_3CONH_3^+$ ion in the reaction involving carbon-bound proton transfer from methylsilyl cation to acetamide.

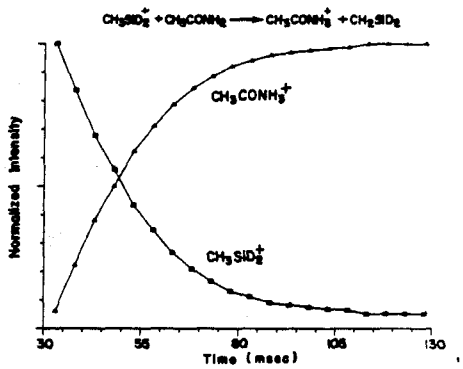

Figure 2. Temporal variation of methylsilyl cation and protonated acetamide ion in the proton-transfer reaction from methylsilyl cation to acetamide; $P(CH_3SiD_3) = 1.2 \times 10^{-6}$ torr, $P(CH_3CONH_2) = 9.5 \times 10^{-7}$ torr, and 15 eV electron energy.

Results and Discussion

Reactions of Methylsilyl Cation. Product distributions and rate constants for the reaction of $CH_3SiD_2^+$ with various n-donor bases are summarized in Table II. $CH_3SiD_2^+$ reacts with CH_3SiD_3 to yield $CH_3SiD_2^+$ by symmetrical deuteride transfer[28] with a rate constant of 6.4×10^{-10} cm^3 molecule^{-1} s^{-1} and $(CH_3)_2SiD^+$ with a rate constant of 1.6×10^{-10} cm^3 molecule^{-1} s^{-1}. The major reaction with $(CH_3)_2S$ yields the hydride transfer product $CH_3SCH_2^+$. In the reaction of $CH_3SiD_2^+$ with NH_3, the formation of $CH_3SiDNH_2^+$ with loss of HD is predominant, in contrast to the facile proton-transfer reaction[9] of SiH_3^+ with NH_3.[29] With CH_3CONH_2, the dominant reaction is H^+ transfer from $CH_3SiD_2^+$ to yield silaethylene as the neutral product ($k = 1.4 \times 10^{-10}$ cm^3 molecule^{-1} s^{-1}). There is no evidence that hydrogen and deuterium scrambling occurs either in the formation of the reactant ion or during the course of the reaction with acetamide.[30] Proton transfer in addition to more complex processes are observed with $C_6H_5NH_2$ as the neutral base. In the case of CH_3NH_2, proton-transfer, hydride-transfer, and Si–N

(24) Blint, R. J.; McMahon, T. B.; Beauchamp, J. L. *J. Am. Chem. Soc.* **1974**, *96*, 1269.
(25) Potzinger, P.; Lampe, F. W. *J. Phys. Chem.* **1970**, *74*, 587.
(26) Mayer et al. have reported the rate constants of $9.9 \pm 2 \times 10^{-10}$ and $2.9 \pm 0.7 \times 10^{-10}$ cm^3 molecule^{-1} s^{-1}, for the reaction 1 and the symmetric hydride transfer reaction of $CH_3SiH_2^+$ with CH_3SiH_3, respectively: Mayer, T. M.; Lampe, F. W. *J. Phys. Chem.* **1974**, *78*, 2422.
(27) Cody, R. B.; Burnier, R. C.; Freiser, B. S. *Anal. Chem.* **1982**, *54*, 96.
(28) Mayer, T. M.; Lampe, F. W. *J. Phys. Chem.* **1974**, *78*, 2429.
(29) In the reaction of SiH_3^+ with NH_3 (ref 9), the formation of $H_2SiNH_2^+$ with loss of H_2 is a minor reaction channel. This suggests that when proton transfer from a silicon center to an n-donor base is exothermic, it will be more facile than competing condensation reactions and may possibly occur in a direct process.
(30) If scrambling occurs in the $CH_3SiD_2^+$ ion, the ratio of BD^+ to BH^+ could be 0.4 instead of 0.0 at the onset of proton-transfer reaction

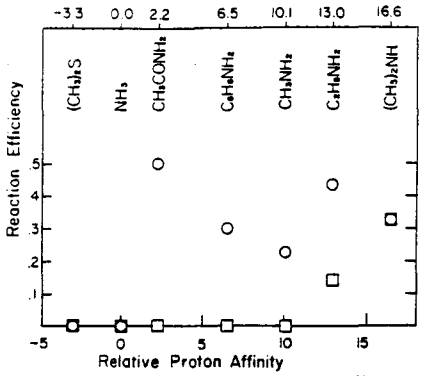

Figure 3. Variation with base strength of the reaction efficiency (defined as the ratio of the rate constant to the calculated collision rate) for proton and deuteron transfer from $CH_3SiD_2^+$ to various n-donor bases: O, proton transfer; □, deuteron transfer. Base strengths (proton affinities) are given relative to NH_3 [$PA(NH_3)$ = 204 ± 3 kcal/mol].

bond-formation processes are all important channels. Although a small amount of $CH_3NH_2D^+$ is observed in this system, double resonance experiments indicate that it is not a direct silicon-bound deuteron-transfer product involving $CH_3SiD_2^+$ but rather a higher order product of a complex sequence of reactions. $CH_3SiD_2^+$ undergoes proton, deuteron, hydride transfer, and more complex sequences of reactions with $C_6H_5CH_2NH_2$. The predominant reaction of $CH_3SiD_2^+$ with $C_2H_5NH_2$ is proton transfer (k = 6.4 × 10^{-10} cm^3 $molecule^{-1}$ s^{-1}), but ion ejection experiments confirm that direct deuteron transfer also occurs (k = 2.2 × 10^{-10} cm^3 $molecule^{-1}$ s^{-1}). In addition, hydride transfer and Si–N bond formation processes occur in this system. In the reaction of $CH_3SiD_2^+$ with $(CH_3)_2NH$, the ratio of the reaction efficiency of deuteron transfer to proton transfer increases by a factor of 3 relative to $C_2H_5NH_2$. Hydride transfer from $(CH_3)_2NH$ to $CH_3SiD_2^+$ is dominant and Si–N bond formation processes are also observed.

Proton Affinity and Heat of Formation. Several factors[31] in these experiments contribute to the uncertainty in derived heats of formation of silaethylene and methylsilylene. These include (i) the near impossibility of pinpointing (in the presence of fast, competing reactions) the precise base strength for which proton or deuteron transfer from $CH_3SiD_2^+$ is thermoneutral, (ii) the difficulties associated with the assignment of absolute values to the proton affinity scale,[16] and (iii) the uncertainty in the heat of formation of the $CH_3SiD_2^+$ ion.[32]

The results shown in Figure 3 strongly suggest that $PA(NH_3)$ < $PA(CH_2SiD_2)$ < $PA(CH_3CONH_2)$ and $PA(CH_3NH_2)$ < $PA(CH_3SiD)$ < $PA(C_2H_5NH_2)$. These values indicate that silaethylene is 10 ± 3 kcal/mol more stable than methylsilylene. Choosing a value of 204 ± 3 kcal/mol for $PA(NH_3)$[16] leads to values for $PA(CH_2SiD_2)$ and $PA(CH_3SiD)$ of 205 ± 3 and 215 ± 4 kcal/mol, respectively. Using a value of 204 ± 1 kcal/mol for $\Delta H_f°_{298}(CH_3SiD_2^+)$[32] and 365.7 kcal/mol for $\Delta H_f°_{298}(H^+)$[33] in eq 1 yields $\Delta H_f°_{298}(CH_2SiD_2)$ = 43 ± 3 kcal/mol, and $\Delta H_f°_{298}(CH_3SiD)$ = 53 ± 4 kcal/mol. The value for the heat of formation of silaethylene is slightly higher than the previously accepted value[13] (with a reduced uncertainty), but that of methylsilylene is somewhat higher than the previous estimate of 42 kcal/mol.[14] The heat of formation of dimethylsilylene may be estimated by assuming a constant CH_3 for H replacement energy

(31) Ausloos, P.; Lias, S. G. *J. Am. Chem. Soc.* **1978**, *100*, 4594.

(32) We use $\Delta H_f°_{298}(CH_3SiD_2^+)$ = 204 ± 1 kcal/mol determined from the kinetics and equilibrium studies of the hydride transfer reaction: c-$C_5H_9^+$ + CH_3SiH_3 ⇌ c-C_5H_{10} + $CH_3SiH_2^+$ (Shin, S. K.; Beauchamp, J. L., manuscript in preparation). This is significantly lower than the previous value of 213 ± 3 kcal/mol determined by Potzinger and Lampe using electron impact ionization (ref 25).

(33) $\Delta H_f°_{298}(H)$ = 52.1 kcal/mol and IP(H) = 13.598 eV from: Moore, C. E. *Natl. Stand. Ref. Data Ser., Natl. Bur. Stand.* **1970**, No. 34. We used the stationary electron convention (ref 16).

Table III. Thermochemical Data Used in Text (kcal/mol)

molecule	$\Delta H_f°_{298}$	ref	molecule	$\Delta H_f°_{298}$	ref
SiH_4	8.2	*a*	SiH_2Me_2	−23	*a*
SiH_3	47.6	*b*	$SiHMe_2$	14.3	*a*
SiH_2	69 ± 3	*c*	$SiMe_2$	26 ± 2, 37 ± 6	*d, e*
SiH_3Me	−7	*a*	$SiMe_4$	−55.4	*a*
SiH_2Me	30.5	*a*	$CH_3SiH_2^+$	204 ± 1	*f*
SiHMe	53 ± 4	*g*	SiH_2CH_2	43 ± 3	*g*

[a] Reference 13. [b] We use the average values of 46.4, 47.9, and 48.5 kcal/mol for $\Delta H_f°_{298}(SiH_3)$. The value of 46.4 kcal/mol is derived from $D(H_3Si–H)$ = 90.3 kcal/mol (ref 13). The value of 47.9 kcal/mol is derived from $D(H_3Si–H)$ = 91.8 kcal/mol, which is estimated from the gas-phase acidity, $D(H_3Si^––H^+)$ = 372.2 kcal/mol (Bartmess, J. E. In *Sturcture/Reactivity and Thermochemistry of Ions* (NATO ASI Series); Ausloos, P., Lias, S. G., Eds; D. Reidel: Dordrecht, 1987; pp 367–380), combined with $EA(SiH_3)$ = 33.2 kcal/mol (Reed, K. J.; Brauman, J. I. *J. Chem. Phys.* **1974**, *61*, 4380) and $\Delta H_f°_{298}(H^+)$ = 365.7 kcal/mol (ref 33). The value of 48.5 kcal/mol is taken from ref 12 and yields $D(H_3Si–H)$ = 92.4 kcal/mol. [c] References 9, 10, 11, and 12. [d] Reference 42. [e] Derived; see text. [f] Reference 32. [g] This work.

Table IV. Adiabatic Ionization Potentials for Silylenes

molecule	$\Delta H_f°_{298}(M)$ (kcal/mol)	$\Delta H_f°_{298}(M^+)$ (kcal/mol)	IP(M) (eV)
SiH_2	69 ± 3[a]	274.1[b]	8.89, 9.02[c]
SiHMe	53 ± 4[a]	242.6[b]	8.22
$SiMe_2$	37 ± 6[a]	211.3[b]	7.56

[a] See Table III. [b] The photoionization mass spectrometric study of Corderman and Beauchamp (Corderman, R. R. Ph.D. Thesis, California Institute of Technology, Pasadena, CA, 1977). [c] Reference 11.

Scheme II

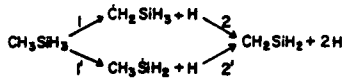

in silylenes.[34] Assuming a methyl-substituent effect of 16 ± 5 kcal/mol, which is the difference between the heats of formation of silylene (69 ± 3 kcal/mol) and methylsilylene (53 ± 4 kcal/mol), yields a heat of formation of 37 ± 6 kcal/mol for dimethylsilylene, which is significantly higher than Walsh's recent estimate[35] of 26 ± 2 kcal/mol. These results are summarized in Table III.

Using the above heats of formation of silylenes, combined with the known heats of formation of their molecular ions in Table IV, leads to the adiabatic ionization potentials of 8.89, 8.22, and 7.56 eV for SiH_2, $SiHCH_3$, and $Si(CH_3)_2$, respectively. The calculated adiabatic ionization potential of 8.22 eV for methylsilylene is 0.63 eV lower than the experimental value of 8.85 eV determined for silaethylene using photoelectron spectroscopy by Bock and coworkers.[5b] The value for the ionization potential of silaethylene, combined with its heat of formation, yields 247 ± 4 kcal/mol for the heat of formation of silaethylene molecular ion, which is only slightly higher than that (242.6 kcal/mol) of methylsilylene molecular ion. Interestingly, CH_3SiD^+ is the most abundant primary ion produced by the electron impact ionization of CH_3SiD_3 with 15 eV electron energy, even though the heat of formation of $CH_2SiD_2^+$ is only slightly higher than that of CH_3SiD^+. The absence of the $CH_2SiD_2^+$ ion may be attributed either to a higher activation energy for 1,2-hydrogen loss or to a kinetic shift or to both. It is well known that the analogous $C_2H_4^+$ ion formation from ethane occurs with an excess energy of 0.22 eV.[36]

The strength of the π-bond energy of silaethylene is an important index of its reactivity. A useful definition of the π-bond

(34) The methyl substituent effect of 16 kcal/mol is identical with the previous estimate (ref 13) based on the heats of formation of SiH_4 and $SiMe_4$.

(35) Baggott, J. E.; Blitz, M. A.; Frey, H. M.; Lightfoot, P. D.; Walsh, R. *Chem. Phys. Lett.* **1987**, *135*, 39.

(36) (a) Chupka, W. A.; Berkowitz, J. *J. Chem. Phys.* **1967**, *47*, 2921. (b) Stockbauer, R. *Ibid.* **1973**, *58*, 3800.

Table V. Calculated Energy Differences between $^1A_1$ SiH_2CH_2 and $^1A'$ $SiHCH_3$[a]

level	$^1A_1$ SiH_2CH_2 total energy[b] (hartrees)	$^1A_1$ SiH_2CH_2 CI lowering[c] (kcal/mol)	$^1A'$ $SiHCH_3$ total energy[b] (hartrees)	$^1A'$ $SiHCH_3$ CI lowering[c] (kcal/mol)	ΔE($SiHCH_3$ - SiH_2CH_2) (kcal/mol)
HF	-328.977 24 (1/1)	0.0	-328.984 01 (1/1)	0.0	-4.2
GVB(2/4)-PP	-329.012 85 (4/4)	-22.3	-329.014 67 (4/4)	-19.2	-1.1
GVB-RCI(4)	-329.024 12 (9/10)	-29.4	-329.014 67 (6/6)	-19.2	5.9
RCI(4)*D_π	-329.034 23 (813/1033)	-35.8	-329.030 87 (1421/1837)	-29.4	2.1
RCI(4)*D_σ	-329.038 10 (853/1093)	-38.2	-329.025 71 (979/979)	-26.2	7.8
RCI(4)*[D_σ+D_π]	-329.048 05 (1657/2116)	-44.4	-329.041 50 (2394/2810)	-36.1	4.1
RCI(4)*D_{GVB}	-329.057 99 (2233/3268)	-50.7	-329.048 02 (3902/5750)	-40.2	6.3
RCI(4)*S_{val}	-329.058 49 (657/1154)	-51.0	-329.037 74 (776/994)	-33.7	13.0
RCI(4)*[D_π+S_{val}]	-329.064 82 (1425/2129)	-55.0	-329.050 95 (2075/2671)	-42.0	8.7
RCI(4)*[D_σ+S_{val}]	-329.068 79 (1405/2109)	-57.4	-329.048 44 (1647/1865)	-40.4	12.8
DC-CI[d]	-329.074 91 (2173/3084)	-61.3	-329.061 44 (2946/3542)	-48.6	8.5
CC-CI[e]	-329.084 41 (2749/4236)	-67.2	-329.067 80 (4454/6482)	-52.6	10.4
zero-point-energy[f] (kcal/mol)	26.8		28.0		1.2

[a] See calculational details. [b] 1 hartree = 627.5096 kcal/mol. The number of spatial configurations/spin eigenfunctions associated with each calculation is given in parentheses under each total energy. [c] The CI lowering is the relative energy of CI calculation with respect to the HF level. [d] RCI(4)*[D_σ + D_π + S_{val}]. [e] RCI(4)*[D_{GVB}+S_{val}]. [f] Zero-point vibrational energies were calculated analytically at HF/6-31G** level with MP2/6-31G** optimized geometries and used without any corrections.

energy for silaethylene is the change in the bond strength of a C–H or Si–H bond, when the vicinal Si–H or C–H bond is broken.[37] From Scheme II, we see that D_1(C–H) + D_2(Si–H) = $D_{1'}$(Si–H) + $D_{2'}$(C–H), so that D_π(silaethylene) = D_1(C–H) - $D_{2'}$(C–H) = $D_{1'}$(Si–H) - D_2(Si–H). D_1(C–H) may be taken as 99 ± 2 kcal/mol,[38] and $D_{2'}$(C–H) is estimated to be 65 ± 3 kcal/mol using the values of heats of formation in Table III. These values of D_1(C–H) and $D_{2'}$(C–H) yield a π-bond energy of 34 ± 4 kcal/mol for silaethylene, compared with the value of 64.3 kcal/mol for ethylene.[39] This π-bond energy is less than the recent estimate[40a] of 41 ± 5 kcal/mol for D_π(dimethylsilaethylene).[40]

The stabilities of the divalent silylenes are associated with the Si lone-pair orbital containing substantial s character in the singlet ground state.[13] This divalent state stabilization energy (DSSE) may be operationally defined[13,40a] as the difference between the first and second dissociation energies, which is equal to the exothermicity of the disproportionation reaction:

$$2SiXYH \rightarrow SiXYH_2 + SiXY \quad (3)$$

$$\Delta H = \Delta H_f^\circ{}_{298}(SiXYH_2) + \Delta H_f^\circ{}_{298}(SiXY) - 2\Delta H_f^\circ{}_{298}(SiXYH) = -[D(XYHSi\text{–}H) - D(XYSi\text{–}H)] = -DSSE(SiXY)$$

The DSSE values for SiH_2, $SiHCH_3$, and $Si(CH_3)_2$ are estimated to be 18 ± 3, 15 ± 4, and 15 ± 6 kcal/mol, respectively, from the heats of formation in Table III. These are significantly less than the previous estimates of 26 kcal/mol for SiH_2[40a] and 28 kcal/mol for $Si(CH_3)_2$.[35]

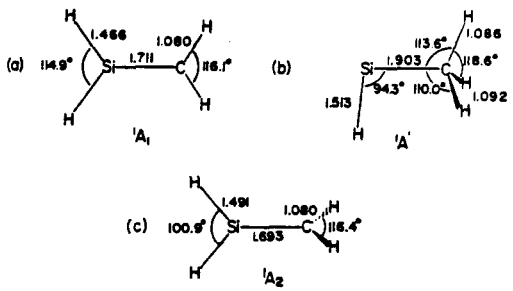

Figure 4. Optimum geometries at the MP2/6-31G** level for (a) silaethylene, (b) methylsilylene, and (c) 90° twisted silaethylene.

Theoretical Calculations

Geometry and Bonding. The calculated optimum geometries for CH_2SiH_2 ($^1A_1$), CH_3SiH ($^1A'$), and 90° twisted CH_2SiH_2 ($^1A_2$) are shown in Figure 4. The geometries for the ground-state silaethylene and methylsilylene compare well with the previous theoretical results. The Si=C bond length of 1.711 Å for silaethylene is in close agreement with a recent experimental value of 1.702 Å for $(Me)_2Si{=}C(SiMe_3)(SiMe)(t\text{-}Bu)_2$ by Wiberg and co-workers.[41] The lone pair on the Si is probably responsible for the Si–C bond length of 1.903 Å for methylsilylene being 0.036 Å longer than the prototype Si–C single bond length of 1.867 Å for SiH_3–CH_3.[42]

The generalized valence bond (GVB)[43] one-electron orbitals for the Si–C σ and π bonds in silaethylene, and for the Si–C σ

(37) Benson, S. W. *Thermochemical Kinetics*, 2nd ed.; Wiley: New York, 1976; p 67.

(38) $D(SiH_3CH_2\text{–}H)$ is estimated from $D(Me_3SiCH_2\text{–}H)$ = 99.2 kcal/mol (ref 13), $D(Me_3CCH_2\text{–}H)$ = 99.7 kcal/mol (ref 13), and $D(MeCH_2\text{–}H)$ = 100.6 kcal/mol (see ref 39).

(39) $\Delta H_f^\circ{}_{298}(C_2H_6)$ = -20.2 kcal/mol, $\Delta H_f^\circ{}_{298}(C_2H_4)$ = 12.5 kcal/mol (Wagman, D. D.; Schumm, R. H.; Bailey, S. M.; Churney, K. L.; Nuttall, R. L. *J. Phys. Chem. Ref. Data* **1982**, *11*, Suppl. 2), and $\Delta H_f^\circ{}_{298}(C_2H_3)$ = 28.3 kcal/mol (Doering, W. v. E. *Proc. Natl. Acad. Sci. U.S.A.* **1981**, *78*, 5279) yield $D(C_2H_5\text{–}H)$ = 100.6 kcal/mol and $D(C_2H_4\text{–}H)$ = 36.3 kcal/mol. These values give D_π(ethylene) = 64.3 kcal/mol.

(40) (a) Walsh, R. *J. Phys. Chem.* **1986**, *90*, 389. (b) Gusel'nikov, L. E.; Nametkin, N. S. *J. Organomet. Chem.* **1979**, *169*, 155.

(41) Wiberg, N.; Wagner, G.; Müller, G. *Angew. Chem., Int. Ed. Engl.* **1985**, *24*, 229.

(42) Kilb, R. W.; Pierce, L. *J. Chem. Phys.* **1957**, *27*, 108.

(43) Bobrowicz, F. W.; Goddard, W. A., III In *Modern Theoretical Chemistry: Methods of Electronic Structure Theory*; Schaefer, H. F., III, Ed.; Plenum Press: New York, 1977; Vol. 3, Chapter 4.

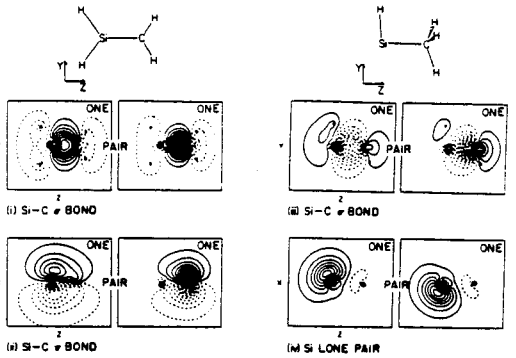

Figure 5. GVB orbitals for silaethylene (i and ii) and for methylsilylene (iii and iv): (i) Si–C σ bond; (ii) Si–C π bond; (iii) Si–C σ bond; (iv) Si lone-pair orbitals. Contours reflect regions of constant amplitude ranging from −1.0 to 1.0 au, with increments of 0.03 au.

and Si lone pair in methylsilylene, are shown in Figure 5. The nature of the Si=C bond in silaethylene is similar to that of the C=C bond in ethylene.[44] The Si–C σ and π bond pairs of silaethylene have overlaps of 0.85 and 0.61, respectively, which are close to the C–C σ and π overlaps of 0.88 and 0.65 in ethylene.[44] The overlaps are slightly lower in silaethylene than in ethylene due to the greater size of the Si 3p orbital relative to C 2p orbital [R(Si=C) = 1.711 Å vs. R(C=C) = 1.34 Å[45]]. The Si–C bond pair of methylsilylene has an overlap of 0.83, which is slightly lower than that of silaethylene because of the longer bond, and the Si lone pair has an overlap of 0.67 which is typical for lone pairs in SiH_2 ($^1A_1$) (0.67)[46] and CH_2 ($^1A_1$) (0.66).[46]

Relative Stabilities of Silaethylene and Methylsilylene and Rotational Barrier in Silaethylene. The energies of silaethylene and methylsilylene at various levels of theory are summarized in Table V. As electron correlation is included, ΔE changes from −4.2 kcal/mol (HF) to 10.4 kcal/mol (CC-CI). The subtle difference between HF and GVB(2/4)-PP (ΔE = −1.1 kcal/mol) is the higher correlation error in the HF Si–C π bond (because of the low overlap) with a differential correlation of 3.1 kcal/mol. Going from GVB(2/4)-PP to GVB-RCI(4) includes the additional spin coupling (more important for **1**) and also includes interpair correlations in the double bond leading to a differential effect of 7.0 kcal/mol and ΔE = 5.9 kcal/mol. Going to full correlation-consistent CI (CC-CI) leads to an additional differential of 4.5 kcal/mol (favoring the state with the largest correlation effect) and ΔE = 10.4 kcal/mol.

We calculate a zero-point-energy difference of 1.2 kcal/mol, in favor of silaethylene, leading to ΔE = 11.6 kcal/mol. This energy difference is significantly greater than the previous values but is in excellent agreement with our experimental result of 10 ± 3 kcal/mol.

The rotational barrier in silaethylene is calculated at various levels from the energy difference between the ground state $^1A_1$ CH_2SiH_2 and the 90° twisted biradical state $^1A_2$ $\dot{C}H_2\dot{S}iH_2$ (summarized in Table VI). The highest dissociation-consistent CI (DC-CI),[47] after correcting for the calculated zero-point-energy difference of −2.0 kcal/mol, yields the adiabatic rotational barrier of 59.9 kcal/mol, compared with the experimental value of 65 kcal/mol for ethylene.[48]

Table VI. Rotational Barrier in Silaethylene (kcal/mol)[a]

level	total energy (h)[b] $^1A_1$ SiH_2CH_2	total energy (h)[b] $^1A_2$ SiH_2CH_2	rotational barrier
HF	−328.977 24 (1/1)	−328.914 92 (1/1)	39.1
GVB(2/4)-PP	−329.012 85 (4/4)	−328.925 15 (2/2)	55.1
GVB-RCI(4)	−329.024 12 (9/10)	−328.927 16 (3/4)	61.0
RCI(4)*S_{val}	−329.058 49 (657/1154)	−328.965 42 (249/606)	58.4
RCI(4)*[D_σ+D_π]	−329.048 05 (1657/2116)	−328.943 06 (289/520)	65.8
DC-CI[c]	−329.074 91 (2173/3084)	−328.976 34 (503/1058)	61.9
zero-point-energy[d] (kcal/mol)	26.8	24.8	−2.0

[a] See calculational details. [b] 1 h = 1 hartree = 627.5096 kcal/mol. The number of spatial configurations/spin eigenfunctions associated with each calculation is given in parentheses under each total energy. [c] RCI(4)*[D_σ+D_π+S_{val}]. [d] Zero-point vibrational energies were calculated analytically at HF/6-31G** level with MP2/6-31G** optimized geometries and used without any corrections.

Summary

It is experimentally found that silaethylene is more stable than methylsilylene by 10 ± 3 kcal/mol. The correlation-consistent CI calculation, starting from the GVB(2/4) descriptions of the two isomers, yields an energy difference of 11.6 kcal/mol in favor of silaethylene. The effects of both electron correlation and zero-point-energy differences favor silaethylene. This result and our previously reported result for the parent silylene suggest that the lone-pair stabilization effects in (methyl-substituted) silylenes are significantly smaller than the previous expectations. The estimated π-bond energy and the calculated rotational barrier in silaethylene are 34 ± 4 and 59.9 kcal/mol, respectively, compared with the experimental values of 64.3 and 65 kcal/mol in ethylene, respectively. An experimental exploration of cis–trans isomerization in silaethylene is desired in order to determine the rotational barrier.

Calculational Details

Geometries and Vibrational Frequencies. The equilibrium geometries and harmonic vibrational frequencies were calculated using the GAUSSIAN 82 program.[49] All geometrical parameters were optimized at the MP2/6-31G** level (second-order Møller–Plesset perturbation theory[50] using the 6-31G** basis set[51]). MP2 theory incorporates the second-order perturbation corrections involving up to double excitations from the Hartree–Fock reference wave function. The 6-31G** basis set is of the split-valence quality and contains polarization functions on the hydrogen atoms as well as on the heavy atoms (Si and C). This level of theory has been shown to provide accurate equilibrium geometries.[52] Harmonic vibrational frequencies were calculated analytically at the HF/6-31G** level (Hartree–Fock theory[53] using the 6-31G** basis set) using the MP2/6-31G** geometries. These frequencies provide zero-point-energy corrections for de-

(44) (a) Carter, E. A.; Goddard, W. A., III *J. Am. Chem. Soc.* **1986**, *108*, 2180. (b) Carter, E. A.; Goddard, W. A., III *J. Phys. Chem.* **1984**, *88*, 1485.
(45) Harmony, M. D.; Laurie, V. W.; Kuczkowski, R. L.; Schwendeman, R. H.; Ramsay, D. A.; Lovas, F. J.; Lafferty, W. J.; Maki, A. G. *J. Phys. Chem. Ref. Data* **1979**, *8*, 676.
(46) The overlaps of lone pairs in SiH_2 ($^1A_1$) and CH_2 ($^1A_1$) were obtained at GVB(1/2) level with VDZ + P basis sets and MP2/6-31G** optimized geometries.
(47) Bair, R. A.; Goddard, W. A., III, submitted for publication in *J. Phys. Chem.* Bair, R. A. Ph.D. Thesis, California Institute of Technology, Pasadena, Calif., 1981.
(48) Douglas, J. E.; Rabinovitch, B. S.; Loony, F. S. *J. Chem. Phys.* **1955**, *23*, 315.
(49) Binkley, J. S.; Frisch, M. J.; Defrees, D. J.; Krishnan, R.; Whiteside, R. A.; Seeger, R.; Schlegel, H. B.; Pople, J. A. GAUSSIAN 82, Carnegie-Mellon University, Pittsburgh, PA.
(50) (a) Pople, J. A.; Binkley, J. S.; Seeger, R. *Int. J. Quantum Chem., Quantum Chem. Symp.* **1976**, No. 10, 1. (b) Pople, J. A.; Krishnan, R.; Schlegel, H. B.; Binkley, J. S. *Int. J. Quantum Chem.* **1978**, *14*, 545.
(51) (a) Hariharan, P. C.; Pople, J. A. *Theor. Chim. Acta* **1973**, *28*, 213. (b) Francl, M. M.; Pietro, W. J.; Hehre, W. J.; Binkley, J. S.; Gordon, M. S.; Defrees, D. J.; Pople, J. A. *J. Chem. Phys.* **1982**, *77*, 3654.
(52) (a) Defrees, D. J.; Levi, B. A.; Pollack, S. K.; Hehre, W. J.; Binkley, J. S.; Pople, J. A. *J. Am. Chem. Soc.* **1979**, *101*, 4085. (b) Simandiras, E. D.; Handy, N. C.; Amos, R. D. *Chem. Phys. Lett.* **1987**, *133*, 324.
(53) (a) Roothaan, C. C. J. *Rev. Mod. Phys.* **1951**, *23*, 69. (b) Pople, J. A.; Nesbet, R. K. *J. Chem. Phys.* **1954**, *22*, 571.

termining relative stabilities and the rotational barrier in silaethylene.

GVB Wave Functions. The energies of the ground state of silaethylene and methylsilylene were calculated by using various levels of the generalized valence bond (GVB) plus configuration interaction (CI) method.[43,47]

For the $^1A_1$ state of silaethylene, the GVB(2/4) wave function corresponds to correlating the Si–C σ and Si–C π bonds, each with the natural orbitals, leading to four natural orbitals for the two correlation pairs.

For the $^1A'$ state of methylsilylene, the GVB(2/4) wave function correlates the Si–C σ bond with a second natural orbital and the Si nonbonding orbital with an empty Si $3p_x$ orbital.

For both cases, all other orbitals are doubly occupied and calculated self-consistently. To relax the simple valence bond (perfect pairing) spin coupling restriction, we allow all configurations arising from distributing the two electrons of each GVB pair between its two natural orbitals. This leads to the GVB-RCI(4) wave function which allows all spin couplings. To include various higher order correlation effects (beyond GVB), we use correlation-consistent CI (CC-CI), in which we start with GVB pairs of each RCI and allow all single and double excitations to all GVB, valence, and virtual orbitals [denoted as RCI(4)*D_{GVB}]. Since the correlated wave function may want orbitals with slightly different shapes, we also allow all single excitations from the valence orbitals of the GVB-RCI(4) configurations to all GVB, valence, and virtual orbitals. Thus the full CC-CI wave function is RCI(4)*[D_{GVB}+S_{val}].

Calculations carried out for the rotational barrier in silaethylene are such that the wave function at the equilibrium geometry of the Si=C double-bonded CH_2SiH_2 ($^1A_1$) dissociates correctly to the 90° twisted Si—C single-bonded $\dot{C}H_2\dot{S}iH_2$ ($^1A_2$), retaining the same level of electron correlation. In addition, we allow the 90° twisted singlet biradical state to relax to its equilibrium geometry, thus obtaining the adiabatic rotational barrier.

The GVB(2/4), GVB-RCI(4), and RCI(4)*S_{val} wave functions for CH_2SiH_2 ($^1A_1$) dissociate correctly to the GVB(1/2) (which corresponds to correlating the Si–C σ bond with its natural orbital), GVB-RCI(2), and RCI(2)*S_{val} wave functions for $\dot{C}H_2\dot{S}iH_2$ ($^1A_2$), respectively. The RCI(4)*[D_σ+D_π] wave function dissociates to RCI(2)*[D_σ+S_{open}] (single excitation from singlet open-shell orbitals in the RCI wave function to all virtual orbitals in addition to all single and double excitations from σ GVB pair of each RCI to all GVB, valence, and virtual orbitals) wave functions. The full DC-CI [designated as RCI(4)*[D_σ+D_π+S_{val}]] wave function dissociates to RCI(2)*[D_σ+S_{val}] wave function.

GVB Basis Sets. All atoms were described with valence double-ζ (VDZ) basis sets[54] which may be described as Si(11s7p/4s3p), C(9s5p/3s2p), and H(4s/2s). In addition, one set of p-polarization functions (exponent α = 1.0) was added to the H basis set. Sets of d-polarization functions centered on Si (α = 0.42) and C (α = 0.62) (exponents optimized for CH_2SiH_2 at the HF level) were added to the valence double-ζ basis sets for Si and C.

Acknowledgment. S. K. S. thanks Dr. J.-G. Lee and Mr. M. J. Brusich for helpful theoretical discussions. We acknowledge the support of the National Science Foundation under Grants CHE84-07857(J.L.B.) and CHE83-18041(W.A.G.).

Registry No. 1, 51067-84-6; **2**, 55544-30-4; CH_3SiD_3, 1066-43-9; $(CH_3)_2S$, 75-18-3; NH_3, 7664-41-7; CH_3CONH_2, 60-35-5; $C_6H_5NH_2$, 62-53-3; CH_3NH_2, 74-89-5; $C_6H_5CH_2NH_2$, 100-46-9; $C_2H_5NH_2$, 75-04-7; $(CH_3)_2NH$, 124-40-3; SiH_2, 13825-90-6; $SiMe_2$, 6376-86-9.

(54) (a) Huzinaga, S. *J. Chem. Phys.* **1965**, *42*, 1293. (b) Huzinaga, S.; Sakai, Y. *Ibid.* **1969**, *50*, 1371. (c) Dunning, T. H. *Ibid.* **1970**, *53*, 2823. (d) Dunning, T. H.; Hay, P. J. In ref 43, Vol. 3, Chapter 1.

Chapter III

Precise Determination of Stabilities of Primary, Secondary, and Tertiary Silicenium Ions from Kinetics and Equilibria of Hydride-Transfer Reactions in the Gas Phase. A Quantitative Comparison of the Stabilities of Silicenium and Carbonium Ions in the Gas Phase

Reprinted from the Journal of the American Chemical Society, 1989, *111*, 900.

Precise Determination of Stabilities of Primary, Secondary, and Tertiary Silicenium Ions from Kinetics and Equilibria of Hydride-Transfer Reactions in the Gas Phase. A Quantitative Comparison of the Stabilities of Silicenium and Carbonium Ions in the Gas Phase

Seung Koo Shin and J. L. Beauchamp*

Contribution No. 7785 from the Arthur Amos Noyes Laboratory of Chemical Physics, California Institute of Technology, Pasadena, California 91125. *Received June 13, 1988*

Abstract: Fourier transform ion cyclotron resonance spectroscopy has been used to examine kinetics and equilibria of hydride-transfer reactions of methyl-substituted silanes with various hydrocarbons having well-established gas-phase hydride affinities. The derived hydride affinities, $D(R_3Si^+-H^-)$, for the silicenium ions $SiMeH_2^+$, $SiMe_2H^+$, and $SiMe_3^+$ are 245.9, 230.1, and 220.5 kcal/mol, respectively, to be compared with the values of 270.5, 251.5, and 233.6 kcal/mol for the corresponding carbonium ions. This indicates that the silicenium ions are significantly more stable than the corresponding carbonium ions in the gas phase with H^- as a reference base.

Carbonium ions are well-established reactive intermediates and their properties have been extensively studied both in solution[1] and in the gas phase.[2] In contrast, exhaustive experimental attempts to generate even detectable concentrations of silicenium ions (R_3Si^+) in solution, under conditions where analogous carbonium ions are long-lived, have been unsuccessful.[3] The factors responsible for the apparently exceedingly low stability of silicenium ions in solution as compared with their carbon analogues have been debated as the "silicenium ion question".[3b] Much of the progress in this field is fairly recent. Lambert et al.[4] reported preparation of two persistent silicenium ions (i.e., $(i\text{-PrS})_2Si^+$ and Ph_3Si^+) by the Corey method[5] involving hydride transfer from the silane to the trityl cation (Ph_3C^+). Barton and co-workers[6] proposed cyclopropylsilicenium ions as possible reaction intermediates in reactions of a variety of (chloromethyl)vinylsilanes with $AlCl_3$. Eaborn et al.[7] provided evidence for the formation of methoxy-bridged silicon-containing cations in the alcoholysis of organosilicon halides and the detection of methyl-bridged species. Evidence has been presented by Apeloig et al.[8] for the solvolytic generation of the silicenium ion via 1,2-methyl migration in a solvolytically produced α-silyl carbonium ion. The transient formation of silicenium ions, which may be modified by interactions with solvent, has been suggested by Chojnowski et al.[9] in the hydride-transfer reaction of organosilyl hydrides with carbonium ions having various complex counterions in CH_2Cl_2. The synthesis of cyclic silyl ethers from acyclic precursors has been accomplished by Chen and Barton[10] via catalytic, in situ, formation of transient silicenium ions. Most recently, Lambert et al.[11] demonstrated that the ionic triphenylsilyl perchlorate form is favored at low concentrations in polar solvents of low nucleophilicity but that association occurs at the high concentrations, which had been used by Prakash et al.[12] in their ^{29}Si and ^{35}Cl NMR spectroscopic study of triphenylsilyl perchlorate. This recent progress in the solvolytic generation of silicenium ions calls for a reconsideration of silicenium ions as viable reaction intermediates and draws attention to the relative stabilities of carbonium and silicenium ions both in solution and in the gas phase.

Studies of the positive ion chemistry of methylsilanes utilizing ion cyclotron resonance techniques[13] have provided information regarding the relative stabilities of methyl-substituted silicenium ions in the absence of complicating solvation phenomena.[14,15] The ion stability order (determined by the energetics of binding H^- as a reference base), $CH_3^+ < CMeH_2^+ < SiH_3^+ < CMe_2H^+ < SiMeH_2^+ < CMe_3^+ < SiMe_2H^+ < SiMe_3^+$, has been determined from investigations of hydride-, chloride-, and fluoride-exchange reactions between substituted carbonium and silicenium ions[14,15] and from photoionization mass spectrometric studies of silanes in our laboratory.[16] Results obtained through bracketing techniques are less reliable and precise than those obtained through equilibria measurements because of numerous possible complications.[17] Also, the interpretation of photoionization thresholds requires detailed considerations of both the dynamics and energetics of photofragmentation processes to obtain accurate heats

(1) *Carbonium Ions*; Olah, G. A.; Schleyer, P. v. R., Eds.; Wiley-Interscience: New York, 1976.
(2) *Gas Phase Ion Chemistry*; Bowers, M. T., Ed.; Academic Press: New York, 1979; Vols. 1 and 2; 1984; Vol. 3.
(3) (a) Sommer, L. H. *Stereochemistry, Mechanisms, and Silicon*; McGraw-Hill: New York, 1965, and earlier references therein. (b) Corriu, R. J. P.; Henner, M. *J. Organomet. Chem.* **1974**, *74*, 1, and references therein. (c) Bickart, P.; Llort, F. M.; Mislow, K. *Ibid.* **1976**, *116*, C1. (d) Cowley, A. H.; Cushner, M. C.; Riley, P. E. *J. Am. Chem. Soc.* **1980**, *102*, 624, and references therein.
(4) (a) Lambert, J. B.; McConnell, J. A.; Schulz, W. J., Jr. *J. Am. Chem. Soc.* **1986**, *108*, 2482. (b) Lambert, J. B.; Schulz, W. J., Jr. *Ibid.* **1983**, *105*, 1671.
(5) Corey, J. Y. *J. Am. Chem. Soc.* **1975**, *97*, 3237.
(6) Robinson, L. R.; Burns, G. T.; Barton, T. J. *J. Am. Chem. Soc.* **1985**, *107*, 3935.
(7) (a) Eaborn, C.; Lickiss, P. D.; Najim, S. T.; Romanelli, M. N. *J. Chem. Soc., Chem. Commun.* **1985**, 1754. (b) Dhaher, S. M.; Eaborn, C.; Smith, J. D. *J. Chem. Soc., Chem. Commun.* **1987**, 1183, and earlier references therein.
(8) Apeloig, Y.; Stanger, A. *J. Am. Chem. Soc.* **1987**, *109*, 272.
(9) Chojnowski, J.; Fortuniak, W.; Stańczyk, W. *J. Am. Chem. Soc.* **1987**, *109*, 7776.
(10) Chen, Y.-L.; Barton, T. J. *Organometallics* **1987**, *6*, 2590.
(11) Lambert, J. B.; Schulz, W. J., Jr.; McConnell, J. A.; Schilf, W. *J. Am. Chem. Soc.* **1988**, *110*, 2201.
(12) Prakash, G. K. S.; Keyaniyan, S.; Aniszfeld, R.; Heiliger, L.; Olah, G. A.; Stevens, R. C.; Choi, H.-K.; Bau, R. *J. Am. Chem. Soc.* **1987**, *109*, 5123.
(13) For reviews of ion cyclotron resonance spectroscopy, see: (a) Beauchamp, J. L. *Annu. Rev. Phys. Chem.* **1971**, *22*, 527. (b) Lehman, T. A.; Bursey, M. M. *Ion Cyclotron Resonance Spectrometry*; Wiley: New York, 1976. (c) Marshall, A. G. *Acc. Chem. Res.* **1985**, *18*, 316, and references therein.
(14) (a) Murphy, M. K. Ph.D. Thesis, California Institute of Technology, Pasadena, CA, 1977. (b) Corderman, R. R.; Murphy, M. K.; Beauchamp, J. L., unpublished results. Corderman, R. R. Ph.D. Thesis, California Institute of Technology, Pasadena, CA, 1977.
(15) Eyler, J. R.; Silverman, G.; Battiste, M. A. *Organometallics* **1982**, *1*, 477.
(16) Corderman, R. R.; Shin, S. K.; Beauchamp, J. L., to be submitted for publication in *J. Am. Chem. Soc.* In addition, the silylene cation (e.g. SiR_2^+, R = H and CH_3) stability order was included.
(17) Lias, S. G.; Liebman, J. F.; Levin, R. D. *J. Phys. Chem. Ref Data* **1984**, *13*, 695.

0002-7863/89/1511-0900$01.50/0

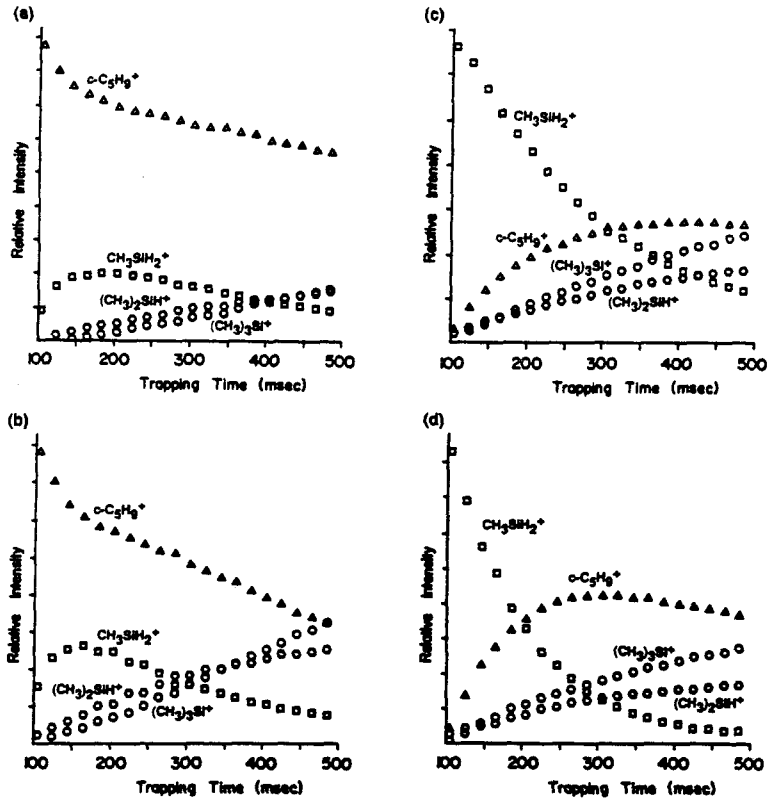

Figure 1. Temporal variations of reactant and product ion abundances starting with either the c-$C_5H_9^+$ ion (a,b) or the $CH_3SiH_2^+$ ion (c,d) in the hydride-transfer reaction 2 and the subsequent side reactions: (a) P(c-C_5H_{10}) = 2.0×10^{-7} Torr and $P(CH_3SiH_3) = 3.1 \times 10^{-7}$ Torr; (b) P(c-C_5H_{10}) = 2.0×10^{-7} Torr and $P(CH_3SiH_3) = 6.2 \times 10^{-7}$ Torr; (c) P(c-C_5H_{10}) = 2.0×10^{-7} Torr and $P(CH_3SiH_3) = 3.1 \times 10^{-7}$ Torr; (d) P(c-C_5H_{10}) = 4.0×10^{-7} Torr and $P(CH_3SiH_3) = 3.1 \times 10^{-7}$ Torr.

of formation of the fragments ions.[18,19] Measurement of ion–molecule reaction equilibria is a proven experimental methodology for the determination of accurate thermochemical properties of various carbonium ions.[20,21] In particular, hydride-transfer equilibria[20] directly provide precise *relative* hydride affinities. Reference hydride affinity values are provided by accurate heats of formation available for numerous carbonium ions, obtained from the known heats of formation and ionization potentials of the corresponding radicals, in addition to the well-established homolytic C–H bond dissociation energies of the corresponding alkanes.[23]

Fourier transform ion cyclotron resonance spectroscopy[13c] has been used in the present work to examine kinetics and equilibria of hydride-transfer reactions of methylsilanes with various hydrocarbons having well-established gas-phase hydride affinities.[22] Hydride affinities of primary, secondary, and tertiary silicenium ions obtained from these experiments permit a precise determination of gas-phase stabilities of the silicenium ions. These values serve to compare the stabilities of silicenium and carbonium ions in the gas phase. The derived heats of formation for the silicenium ions combined with heats of formation for silylenes[24] allow estimation of proton affinities for silylenes and silaethylenes,[24,25] which can be compared with their carbon analogues.[17]

Because of the interest in thermal decomposition processes of silanes, we discuss several pyrolysis mechanisms in the Appendix, using reaction enthalpies estimated from heats of formation of silanes, silylenes, and silaethylenes, and the available Arrhenius parameters for various thermal decomposition processes.

Experimental Section

Experimental techniques associated with ICR spectroscopy,[13] and in particular Fourier transform ion cyclotron resonance spectroscopy,[13c] have been previously described in detail. Experiments were performed with an Ion Spec FT-ICR data system in conjunction with a 1-in. cubic trapping cell[26] built by Bio-Med Tech[27] situated between the poles of a Varian 15-in. electromagnet maintained at 2 T. Where available, chemicals were obtained commercially in high purity and used as supplied except for multiple freeze–pump–thaw cycles to remove noncondensable gases. CH_3SiH_3 was prepared by reducing CH_3SiCl_3 with $LiAlH_4$.[28] Pressures were measured with a Schulz–Phelps ion gauge[29] calibrated

(18) Rosenstock, H. M.; Draxl, K.; Steiner, B. W.; Herron, J. T. *J. Phys. Chem. Ref. Data* **1977**, *6*, Supplement 1.
(19) (a) Chupka, W. A.; Berkowitz, J. *J. Chem. Phys.* **1967**, *47*, 2921. (b) Chupka, W. A. *Ibid.* **1971**, *54*, 1936. (c) Chupka, W. A. *Ibid.* **1959**, *30*, 191. (d) Rosenstock, H. M.; Larkins, J. T.; Walker, J. A. *Int. J. Mass Spectrom. Ion Phys.* **1973**, *11*, 309.
(20) (a) Aue, D. H.; Bowers, M. T. *Gas Phase Ion Chemistry*; Bowers, M. T., Ed.; Academic Press: New York, 1979; Chapter 9. (b) McMahon, T. B.; Kebarle, P. *J. Am. Chem. Soc.* **1985**, *107*, 2612. (c) McMahon, T. B.; Blint, R. J.; Ridge, D. P.; Beauchamp, J. L. *Ibid.* **1972**, *94*, 8934. (d) Blint, R. J.; McMahon, T. J.; Beauchamp, J. L. *Ibid.* **1974**, *96*, 1269.
(21) (a) Sharma, R. B.; Sen Sharma, D. K.; Hiraoka, K.; Kebarle, P. *J. Am. Chem. Soc.* **1985**, *107*, 3747, and references therein. (b) Sen Sharma, D. K.; Meza de Höjer, S.; Kebarle, P. *Ibid.* **1985**, *107*, 3757. (c) Solomon, J. J.; Field, F. H. *Ibid.* **1976**, *98*, 1567. (d) Meot-Ner, M. *Gas Phase Ion Chemistry*; Bowers, M. T., Ed.; Academic Press: New York, 1979; Chapter 6.
(22) See Table II and discussion section.
(23) See Table III.
(24) (a) Shin, S. K.; Beauchamp, J. L. *J. Phys. Chem.* **1986**, *90*, 1507. (b) Shin, S. K.; Irikura, K. K.; Beauchamp, J. L.; Goddard, W. A., III *J. Am. Chem. Soc.* **1988**, *110*, 24.
(25) (a) Pau, C. F.; Pietro, W. J.; Hehre, W. J. *J. Am. Chem. Soc.* **1983**, *105*, 16. (b) Pietro, W. J.; Pollack, S. K.; Hehre, W. J. *Ibid.* **1979**, *101*, 7126.
(26) Comisarow, M. B. *Int. J. Mass. Spectrom. Ion Phys.* **1981**, *37*, 251.
(27) Bio-Med Tech, 2001 E. Galbreth, Pasadena, CA 91104.
(28) Gaspar, P. P.; Levy, C. A.; Adair, G. M. *Inorg. Chem.* **1970**, *9*, 1272.

Table I. Thermochemical Data from Kinetics and Equilibira of Hydride-Transfer Reactions: $R^+ + (CH_3)_nSiH_{4-n} \rightleftharpoons (CH_3)_nSiH_{3-n}^+ + RH$

R^+	$(CH_3)_nSiH_{3-n}^+$	k_f[a]	k_r[a]	K	$\Delta G_{298}°$, kcal/mol	$\Delta S°$, eu	$\Delta H°$, kcal/mol
c-$C_5H_9^+$	$CH_3SiH_2^+$	1.4	5.4	0.28	0.8	−0.6	0.6
t-$C_4H_9^+$	$(CH_3)_2SiH^+$	6.0	0.036	167	−3.0	1.4	−2.6
p-$CH_3C_6H_4CH_2^+$	$(CH_3)_2SiH^+$	2.6	1.1	2.4	−0.5	0.8	−0.3
$C_6H_5C(CH_3)_2^+$	$(CH_3)_3Si^+$	0.41	0.56	0.74	0.2	3.0	1.1

[a] Units 10^{-10} cm^3 molecule^{-1} s^{-1}.

against an MKS Baratron (Model 390 HA-0001) capacitance manometer. The principal errors in the rate constants (estimated to be ±20%) arise from uncertainties in pressure measurements.[30] Mixtures of methylsilanes and hydrocarbons were used with a total pressure in the range $1-5 \times 10^{-6}$ Torr. Ionization was by electron impact at 15–25 eV. The reaction temperature in the ICR cell is assumed to be 298 K.

Although other reactions are noted below, this study focused on the hydride-transfer equilibria between methylsilanes and various hydrocarbons. Methylsilanes ionized by electron impact are convenient sources of silicenium ions.[24,31,32] Various carbonium ions are generated by either electron impact ionization or hydride-transfer reactions.

Ion ejection pulses were used to remove all species except selected silicenium or carbonium ions from the ICR cell.[33] Translational excitation of the reactant ion was minimized by using the lowest possible radio frequency fields. The temporal variations of reactant and product ion abundances starting from either the carbonium ion R^+ or the silicenium ion $(CH_3)_nSiH_{3-n}^+$ ion (n = 1–3) in the hydride-transfer reaction 1 were recorded and used to calculate forward and reverse rate constants

$$R^+ + (CH_3)_nSiH_{4-n} \rightleftharpoons (CH_3)_nSiH_{3-n}^+ + RH \quad (1)$$

and equilibrium constant therefrom. The occurrence of side reactions consuming the reactant or product ions in the reaction mixtures used for the measurements of hydride-transfer equilibria is unavoidable and complicates the measurements. However, the reaction rate constants from the separate forward and reverse hydride-transfer reactions made it possible to calculate the precise equilibrium constants. For example, the temporal variations of reactant and product ion abundances in the hydride-transfer reaction of c-$C_5H_9^+$ with methylsilane (forward process 2) and $CH_3SiH_2^+$ with cyclopentane (the reverse of process 2) are shown

$$\text{c-}C_5H_9^+ + CH_3SiH_3 \rightleftharpoons CH_3SiH_2^+ + \text{c-}C_5H_{10} \quad (2)$$

$$CH_3SiH_2^+ + CH_3SiH_3 \rightarrow (CH_3)_2SiH^+ + SiH_4 \quad (3)$$

in Figure 1 with the subsequent reaction products. Since the partial pressures of the reactant neutrals are kept constant during the experiment, we used the general solution for the first-order series and parallel reaction schemes to analyze the experimental data.[34]

Results and Discussion

Reactions. Reaction rates and equilibrium constants for the hydride-transfer process 1 are summarized in Table I with other thermochemical properties.

$CH_3SiH_2^+$ reacts with cyclopentane to yield c-$C_5H_9^+$ with a rate constant of 5.4×10^{-10} cm^3 molecule^{-1} s^{-1} and undergoes sequential reactions with CH_3SiH_3 to produce $(CH_3)_2SiH^+$ and $(CH_3)_3Si^+$. c-$C_5H_9^+$ generated from the hydride-transfer reaction of $C_7H_7^+$ with cyclopentane reacts with CH_3SiH_3 via exclusive hydride transfer with a rate constant of 1.4×10^{-10} cm^3 molecule^{-1} s^{-1}.

The reactions of $(CH_3)_2SiH^+$ in the 1:10 $(CH_3)_2SiH_2$–isobutane mixtures produce t-$C_4H_9^+$ and $(CH_3)_3Si^+$ with rate constants of 3.6×10^{-12} and 2.0×10^{-10} cm^3 molecule^{-1} s^{-1}, respectively. The reverse reaction of t-$C_4H_9^+$ with $(CH_3)_2SiH_2$ is exclusively via hydride transfer with a rate constant of 6.0×10^{-10} cm^3 molecule^{-1} s^{-1}. Since the hydride-transfer reaction of t-$C_4H_9^+$ with $(CH_3)_2SiH_2$ is estimated to be exothermic by 2.6 kcal/mol,[35] p-$CH_3C_6H_4CH_2^+$, the hydride affinity of which is 3.2 kcal/mol lower than that of t-$C_4H_9^+$,[35] is used to observe the near-thermoneutral hydride-transfer reaction with $(CH_3)_2SiH_2$. In the reactions of $(CH_3)_2SiH^+$ with p-xylene–$(CH_3)_2SiH_2$ mixtures, the desired hydride-transfer product p-$CH_3C_6H_4CH_2^+$ ($k = 1.1 \times 10^{-10}$ cm^3 molecule^{-1} s^{-1}) and $(CH_3)_3Si^+$ were observed. $(CH_3)_3Si^+$ reacted further to yield a p-xylene–$Si(CH_3)_3^+$ adduct. The predominant reaction of p-$CH_3C_6H_4CH_2^+$, generated from the electron impact ionization of p-xylene, with $(CH_3)_2SiH_2$ is hydride transfer ($k = 2.6 \times 10^{-10}$ cm^3 molecule^{-1} s^{-1}).

Finally, $(CH_3)_3Si^+$ reacts with cumene to give rise to a hydride-transfer product $C_6H_5C(CH_3)_2^+$ ($k = 5.6 \times 10^{-11}$ cm^3 molecule^{-1} s^{-1}) and a cumene–$Si(CH_3)_3^+$ adduct. The occurrence of hydride transfer is predominant ($k = 4.1 \times 10^{-11}$ cm^3 molecule^{-1} s^{-1}) in the reaction of $C_6H_5C(CH_3)_2^+$, isolated after long reaction time delay from the $(CH_3)_3Si^+$–cumene reaction products, with $(CH_3)_3SiH$. This hydride-transfer reaction was confirmed by the reaction of $C_6H_5C(CH_3)_2^+$, generated from the electron impact ionization of $C_6H_5C(CH_3)_3$, with $(CH_3)_3SiH$. In the reactions of silicenium ions with the substituted benzenes, there are no indications of problems associated with either the electron-transfer or the proton transfer reactions, which are known to complicate hydride-transfer equilibria measurements in studies of the corresponding carbonium ions.[21a]

Hydride Affinities and Heats of Formation of Silicenium Ions. Equilibrium constants for the hydride-transfer reactions are obtained from the calculated forward and reverse rate constants. The $\Delta G_{298}°$ values given in Table I for the hydride-transfer reactions are derived from equilibrium constants and estimated to have uncertainties of less than 0.5 kcal/mol arising from errors in the rate constants. Using the $\Delta S°$ values estimated on the basis of symmetry numbers[36] leads to the $\Delta H°$ values given in Table I. For the reaction 2 of c-$C_5H_9^+$ with CH_3SiH_3, the $\Delta S°$ value is estimated by combining the experimental $\Delta S°$ value for the reaction 4[21a] with the evaluated $\Delta S°$ value for the reaction 5 based on symmetry numbers (σ). For the substituted benzyl ions, apart

$$\text{c-}C_5H_9^+ + C_3H_8 \rightleftharpoons s\text{-}C_3H_7^+ + \text{c-}C_5H_{10} \quad \Delta S° = -1.4 \quad (4)$$

$$\underset{\sigma = 18}{s\text{-}C_3H_7^+} + \underset{9}{CH_3SiH_3} \rightleftharpoons \underset{6}{CH_3SiH_2^+} + \underset{18}{C_3H_8} \quad \Delta S° = R \ln (^3/_2) \quad (5)$$
$$\underset{0.8}{}$$

$$\text{c-}C_5H_9^+ + CH_3SiH_3 \rightleftharpoons CH_3SiH_2^+ + \text{c-}C_5H_{10} \quad \Delta S° = -0.6\text{(eu)} \quad (2)$$

from symmetry numbers, it is also assumed that a loss of entropy due to restricted internal rotations in the benzyl cation is 3 eu.[21a] Uncertainties of the $\Delta H°$ values coming from those of the $\Delta G°$ values and $\Delta S°$ estimates, which may be in error by as much as 3 eu,[21a] are expected to be ~1 kcal/mol.

The hydride affinities for methyl-substituted silicenium ions are derived from the $\Delta H°$ values in Table I and the hydride affinities for the reference hydrocarbons with aid of relationship 6 for the reaction 1. The reaction of p-$CH_3C_6H_4CH_2^+$ with

$$D(Me_nSiH_{3-n}^+\text{–}H^-) = D(R^+\text{–}H^-) + \Delta H°(1) \quad (6)$$

$(CH_3)_2SiH_2$ provides the $\Delta H°$ value used to calculate the hydride affinity of $(CH_3)_2SiH^+$. The hydride affinity of 245.3 kcal/mol for c-$C_5H_9^+$ is obtained by combining the hydride affinity of s-$C_3H_7^+$ in Table II with the $\Delta H°$ value of −6.2 kcal/mol for the hydride-transfer reaction of s-$C_3H_7^+$ with cyclopentane,[21a] with an estimated error of ±1 kcal/mol. The value of 230.4 kcal/mol for D(p-$CH_3C_6H_4CH_2^+$–H^-) is calculated by adding the relative chloride affinity[21a] of −6.5 kcal/mol for p-$CH_3C_6H_4CH_2^+$ with

(29) Schulz, G. J.; Phelps, A. V. *Rev. Sci. Instrum.* **1957**, *28*, 1051.
(30) Blint, R. J.; McMahon, T. B.; Beauchamp, J. L. *J. Am. Chem. Soc.* **1974**, *96*, 1269.
(31) (a) Potzinger, P.; Lampe, F. W. *J. Phys. Chem.* **1970**, *74*, 587. (b) Mayer, T. M.; Lampe, F. W. *Ibid.* **1974**, *78*, 2422, 2429.
(32) Litzow, M. R.; Spalding, T. R. *Mass Spectrometry of Inorganic and Organometallic Compounds*; Elsevier: Amsterdam, The Netherlands, 1973.
(33) Cody, R. B.; Burnier, R. C.; Freiser, B. S. *Anal. Chem.* **1982**, *54*, 96.
(34) Frost, A. A.; Pearson, R. G. *Kinetics and Mechanism*; 2nd ed.; Wiley: New York, 1961.
(35) See Table II.
(36) Benson, S. W. *Thermochemical Kinetics*, 2nd ed.; Wiley: New York, 1976; p 47.

Table II. Hydride Affinities and Heats of Formation Used in Text

R	$D(R^+-H^-)$,[a] kcal/mol	$\Delta H_f°_{298}(RH)$,[b] kcal/mol	$\Delta H_f°_{298}(R^+)$, kcal/mol
SiH_3	261.4[c]	8.2	234.9[c]
C_2H_5	270.5[d]	-20.24	215.6[d]
s-C_3H_7	251.5[d]	-24.83	192.0[d]
CH_3SiH_2	245.9[e]	-7.0	204 ± 1[e]
c-C_5H_9	245.3[f]	-18.44	191.9[g]
$C_6H_5CH_2$	236.9[h]	11.99	214.2[i]
t-C_4H_9	233.6[d]	-32.41	166.5[d]
p-$CH_3C_6H_4CH_2$	230.4[f]	4.31	200.0[g]
$(CH_3)_2SiH$	230.1[e]	-23.0	172 ± 2[e]
$(CH_3)_3Si$	220.5[e]	-39.0	147 ± 3[e]
$C_6H_5C(CH_3)_2$	219.4[f]	0.96	185.7[f]

[a] Accuracy of hydride affinities estimated as ±1 kcal/mol except ±2 kcal/mol for p-$CH_3C_6H_4CH_2^+$ and $(CH_3)_2SiH^+$ and ±3 kcal/mol for $C_6H_5C(CH_3)_2^+$ and $(CH_3)_3Si^+$. [b] Heats of formation for hydrocarbons from Cox and Pilcher[48] and those for methylsilanes from Walsh.[46] [c] Reference 16. [d] See Table III. [e] This work. [f] See text. [g] $\Delta H_f°_{298}(R^+) = D(R^+-H^-) + \Delta H_f°_{298}(RH) - \Delta H_f°_{298}(H^-)$; $\Delta H_f°_{298}(H^-) = 34.7$ kcal/mol. [h] From $\Delta H_f°_{298}(C_6H_5CH_2^+)$. [i] Derived from the $\Delta H°$ value of -0.5 kcal/mol for the chloride-transfer reaction of t-$C_4H_9^+$ with $C_6H_5CH_2Cl$ and heats of formation for t-$C_4H_9^+$ in Table II, C_4H_9Cl, and $C_6H_5CH_2Cl$ from Cox and Pilcher.[48]

respect to $C_6H_5CH_2^+$ to the hydride affinity of 236.9 kcal/mol for $C_6H_5CH_2^+$, assuming equality of the relative chloride and hydride affinities of $C_6H_5CH_2^+$ and p-$CH_3C_6H_4CH_2^+$,[37] and may be in error by 2 kcal/mol mainly due to uncertainties in this assumption. The hydride affinity for $C_6H_5C(CH_3)_2^+$ is evaluated from heats of formation of $C_6H_5C(CH_3)_2^+$ and cumene in Table II. Values of 207.0 and 27.0 kcal/mol for the proton affinity[17] and the heat of formation[38] of 2-methylstyrene, respectively, lead to a value of 185.7 kcal/mol for $\Delta H_f°_{298}(C_6H_5C(CH_3)_2^+)$. The calculated hydride affinity for $C_6H_5C(CH_3)_2^+$ is 219.4 kcal/mol and has an error estimate of ±3 kcal/mol due to uncertainties in the absolute proton affinity scales.[17]

The derived hydride affinities for the silicenium ions $SiMeH_2^+$, $SiMe_2H^+$, and $SiMe_3^+$ are 245.9, 230.1, and 220.5 kcal/mol, respectively, and listed in Table II. These values are significantly lower than the hydride affinities of 270.5, 251.5, and 233.6 kcal/mol in Table III for the analogous carbonium ions $C_2H_5^+$, s-$C_3H_7^+$, and t-$C_4H_9^+$, respectively, which indicates that *the silicenium ions are much more stable than the corresponding carbonium ions in the gas phase when H^- is used as a reference base.* Heats of formation for the silicenium ions in Table II are calculated from hydride affinities of silicenium ions and heats of formation of methylsilanes in Table II. The calculated heats of formation for silicenium ions are 204 ± 1, 172 ± 2, and 147 ± 3 kcal/mol for $SiMeH_2^+$, $SiMe_2H^+$, and $SiMe_3^+$, respectively. The heat of formation of $SiMe_3^+$ is in excellent agreement with a value of 145.0 kcal/mol derived from the photoionization mass spectrometric study of trimethylsilane in our laboratory[16] but slightly lower than the reported value of 150.5 kcal/mol estimated from the unimolecular decomposition of the $SiMe_3Br^+$ molecular ion using the photoelectron–photoion coincidence technique by Szepes and Baer.[39] Uncertainties of the derived hydride affinities and heats of formation for the silicenium ions mainly arise from those of reference hydride affinities for the corresponding carbonium ions used in the hydride-transfer equilibria measurements.

A Quantitative Comparison of the Stabilities of Silicenium and Carbonium Ions in the Gas Phase. A comparison of hydride affinities derived in this study for silicenium ions (Table II) with literature data for the analogous carbonium ions (Table III) is shown in Figure 2. Consider the hydride affinity data for the carbonium ions in Table III. In the series CH_3^+, $CMeH_2^+$, CMe_2H^+, and CMe_3^+, successive replacements of H in CH_3^+ by

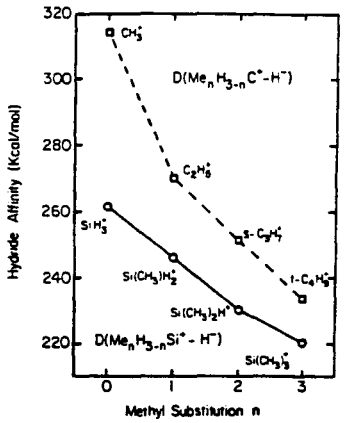

Figure 2. Hydride affinities of carbonium ions and silicenium ions.

a methyl group decrease the hydride affinity by 44.2, 19.0, and 17.9 kcal/mol, following in order. Since the incremental decrease in hydride affinity (ΔHA) directly reflects the difference between $D(R_2C^+-CH_3) - D(R_2HC-CH_3)$ (where R = H, CH_3) and $D(R_2C^+-H) - D(R_2HC-H)$,[40] this ΔHA is an index of an extra stabilization of the carbonium ions by methyl substitution. This extra stabilization effected by successive methyl substitution appears to be consistently smaller for silicenium ions than carbonium ions, presumably due to poorer spatial overlap of occupied substituent orbitals with an empty Si^+ 3p orbital relative to C^+ 2p orbital because of the greater size of Si 3p orbital and the longer Si–C bond. For example, the introduction of a first CH_3 on CH_3^+ in place of H decreases $D(C_2H_5^+-H^-)$ 44.2 kcal/mol below $D(CH_3^+-H^-)$ as compared with the 15.5 kcal/mol decrease in going from SiH_3^+ to $CH_3SiH_2^+$. This difference in methyl substituent effect between $C_2H_5^+$ and $CH_3SiH_2^+$ may result from extensive σ(C–H) participation[41] in $C_2H_5^+$, which favors a fully delocalized, two-electron, three-center nonclassical hydrogen-bridged ion. On the other hand, the C–H bonding electrons in $CH_3SiH_2^+$ are less effectively available to the empty Si^+ 3p orbital and favor a classical methylsilicenium ion. Both the nonclassical hydrogen-bridged $C_2H_5^+$[42] and the classical $CH_3SiH_2^+$[43] are found to lie at minima on their respective potential energy surfaces from theoretical calculations.

Comparison of Proton Affinities of Silylene and Silaethylene with Their Carbon Analogues. The proton affinities of 201 ± 3, 215 ± 4, and 205 ± 3 kcal/mol for SiH_2, $SiHCH_3$, and $H_2C{=}SiH_2$, respectively, have been determined from the deprotonation energetics of SiH_3^+ and $CH_3SiD_2^+$ using Fourier transform ion cyclotron resonance spectroscopy[21] and used to calculate heats of formation of silylenes. Assuming a constant CH_3 for H replacement energy of 16 kcal/mol in silylenes yields a heat of formation of 37 kcal/mol for $Si(CH_3)_2$, which is significantly higher than Walsh's recent estimate[44] of 26 ± 2 kcal/mol. The experimental value of 232 ± 3 kcal/mol for $PA(Si(CH_3)_2)$ by Hehre and co-workers[25a] supports the higher value of the heat of formation for $Si(CH_3)_2$, which leads to the proton affinity of 231 kcal/mol from heats of formation data in Table IV using eq 7.

$$PA(R) = \Delta H_f°_{298}(R) + \Delta H_f°_{298}(H^+) - \Delta H_f°_{298}(RH^+) \quad (7)$$

The proton affinities for silaethylenes are derived from heats of

(37) Hayashibara, K.; Kruppa, G. H.; Beauchamp, J. L. *J. Am. Chem. Soc.* **1986**, *108*, 5441.
(38) Benson, S. W.; Cruickshank, F. R.; Golden, D. M.; Haugen, G. R.; O'Neal, H. E.; Rodgers, A. S.; Shaw, R.; Walsh, R. *Chem. Rev.* **1969**, *69*, 279.
(39) Szepes, L.; Baer, T. *J. Am. Chem. Soc.* **1984**, *106*, 273.

(40) $D(R_2C^+-CH_3) - D(R_2HC-CH_3) - (D(R_2C^+-H) - D(R_2HC-H)) = \Delta H_f°_{298}(R_2(CH_3)CH) - \Delta H_f°_{298}(R_2(CH_3)C^+) - (\Delta H_f°_{298}(R_2CH_2) - \Delta H_f°_{298}(R_2HC^+)) = D(R_2HC^+-H^-) - D(R_2(CH_3)C^+-H^-) = \Delta HA$.
(41) Lowry, T. H.; Richardson, K. S. *Mechanism and Theory in Organic Chemistry*; Harper & Row: New York, 1981.
(42) (a) Lischka, H.; Köhler, H. J. *J. Am. Chem. Soc.* **1978**, *100*, 5297. (b) Raghavachari, K.; Whiteside, R. A.; Pople, J. A.; Schleyer, P. v. R. *Ibid.* **1981**, *103*, 5649.
(43) Hopkinson, A. C.; Lien, M. H. *J. Org. Chem.* **1981**, *46*, 998.
(44) (a) Baggott, J. E.; Blitz, M. A.; Frey, H. M.; Lightfoot, P. D.; Walsh, R. *Chem. Phys. Lett.* **1987**, *135*, 39. (b) Walsh, R. *Organometallics* **1988**, *7*, 75.

Table III. Thermochemical Data for Alkanes Used in Text

molecule (R)	$\Delta H_f°_{298}$(RH),[a] kcal/mol	$\Delta H_f°_{298}$(R), kcal/mol	D(R-H),[b] kcal/mol	IP(R), eV	$\Delta H_f°_{298}(R^+)$,[c] kcal/mol	$D(R^+-H^-)$,[d] kcal/mol
CH_3	-17.89	34.8[e]	104.8	9.842(S)[f]	261.8	314.4
$C(CH_3)H_2$	-20.24	28.4[g]	100.6	8.12[g]	215.6[i]	270.5
$C(CH_3)_2H$	-24.83	22.3[j]	99.2	7.36(PE)[k]	192.0	251.5
$C(CH_3)_3$	-32.41	12.0[l]	96.5	6.70(PE)[k]	166.5	233.6

[a] Reference 48. [b] $D(R-H) = \Delta H_f°_{298}(R) + \Delta H_f°_{298}(H) - \Delta H_f°_{298}(RH)$. [c] $\Delta H_f°_{298}(R^+) = \Delta H_f°_{298}(R) + IP(R)$. [d] $D(R^+-H^-) = \Delta H_f°_{298}(R^+) + \Delta H_f°_{298}(H^-) - \Delta H_f°_{298}(RH)$. [e] Wagman, D. D.; Evans, W. H.; Parker, V. B.; Schumm, R. H.; Halow, I.; Bailey, S. M.; Churney, K. L.; Nuttall, R. L. *J. Phys. Chem. Ref. Data* **1982**, *11*, supplement 2. [f] Herzberg, G.; Shoosmith, J. *Can. J. Phys.* **1956**, *34*, 523; S stands for spectroscopic measurement. [g] Brouard, M.; Lightfoot, P. D.; Pilling, M. J. *J. Phys. Chem.* **1986**, *90*, 445. [h] $IP(C_2H_5) = \Delta H_f°_{298}(C_2H_5^+) - \Delta H_f°_{298}(C_2H_5)$. The previously reported values for $IP(C_2H_5)$ are 8.39 eV detd. from Ne I photoelectron spectrum of ethyl radical generated by the pyrolysis of *n*-propyl nitrite (Houle, F. A.; Beauchamp, J. L. *J. Am. Chem. Soc.* **1979**, *101*, 4067) and 8.26 eV measured from He I photoelectron spectrum of ethyl radical produced by the reaction of fluorine atoms with ethane (Dyke, J. M.; Ellis, A. R.; Keddar, N.; Morris, A. *J. Phys. Chem.* **1984**, *88*, 2565). [i] Reference 17. [j] Tsang, W. *J. Am. Chem. Soc.* **1985**, *107*, 2872. [k] Houle, F. A.; Beauchamp, J. L. *J. Am. Chem. Soc.* **1979**, *101*, 4067. [l] Average value of $\Delta H_f°_{298}(t\text{-}C_4H_9) = 12.4$ (ref *j*) and 11.6 kcal/mol: Russell, J. J.; Seetula, J. A.; Timonen, R. S.; Gutman, D.; Nava, D. F. *J. Am. Chem. Soc.* **1988**, *110*, 3084.

Table IV. Proton Affinities of Silylenes, Silaethylenes, and Their Carbon Analogues

M	$\Delta H_f°_{298}$(M), kcal/mol	$\Delta H_f°_{298}(MH^+)$,[a] kcal/mol	PA(M), kcal/mol	R	$\Delta H_f°_{298}$(R), kcal/mol	$\Delta H_f°_{298}(RH^+)$,[b] kcal/mol	PA(R),[c] kcal/mol
SiH_2	69 ± 3[d-f]	234.9[b]	201 ± 3[d]	CH_2	93.4[g]	262.1	197.0
$SiHCH_3$	53 ± 4[e]	204 ± 1	215 ± 3[e]	$CHCH_3$	85.8[h]	215.6	235.9
$Si(CH_3)_2$	37 ± 6[e]	172 ± 2	231[e]	$C(CH_3)_2$	76.6[h]	192.0	250.3
$H_2C{=}SiH_2$	43 ± 4[e]	204 ± 1	205 ± 3[e]	$H_2C{=}CH_2$	12.5[i]	215.6	162.6
$H_2C{=}SiHCH_3$	27[h]	172 ± 2	221[e]	$H_2C{=}CHCH_3$	4.9[i]	192.0	178.6
$H_2C{=}Si(CH_3)_2$	11[h]	147 ± 3	230[e]	$H_2C{=}C(CH_3)_2$	-4.3[i]	166.9	194.5

[a] This work. [b] See Table III. [c] $PA(R) = \Delta H_f°_{298}(R) + \Delta H_f°_{298}(H^+) - \Delta H_f°_{298}(RH^+)$; $\Delta H_f°_{298}(H^+) = 365.7$ kcal/mol.[17] [d] Shin and Beauchamp.[24a] [e] Shin et al.[24b] [f] $\Delta H_f°_{298}(SiH_2) = 69.0 \pm 2$ kcal/mol (Boo, B. H.; Armentrout, P. B. *J. Am. Chem. Soc.* **1987**, *109*, 3549), 65.4 or 68.4 kcal/mol (Berkowitz et al.[14]), 65.3 ± 1.5 kcal/mol,[44b] 64.6 kcal/mol (Jasinski, J. M.; Chu, J. O. *J. Chem. Phys.* **1988**, *88*, 1678), and 65.4 ± 1.6 kcal/mol (Van Zoeren, C. M.; Thoman, J. W., Jr.; Steinfeld, J. I.; Rainbird, M. W. *J. Phys. Chem.* **1988**, *92*, 9. [g] Wagman, D. D.; Evans, W. H.; Parker, V. B.; Schumm, R. H.; Halow, I.; Bailey, S. M.; Churney, K. L.; Nuttall, R. L. *J. Phys. Chem. Ref. Data* **1982**, *11*, Supplementary 2. [h] See text. [i] Cox and Pilcher.[48]

formation of silaethylenes and the corresponding silicenium ions and listed in Table IV. The values of 27 and 11 kcal/mol for heats of formation of $H_2C{=}SiHCH_3$ and $H_2C{=}Si(CH_3)_2$, respectively, are estimated from heats of formation of methylene and silylenes in Table III by assuming a constant $D°(C{=}Si)$ of 119.4 kcal/mol for silaethylenes.[45] In addition, these values are 4 kcal/mol higher than Walsh's estimates[46] of 23 and 7 kcal/mol, respectively. These values lead to the proton affinities of 221 and 230 kcal/mol for $H_2C{=}SiHCH_3$ and $H_2C{=}Si(CH_3)_2$, respectively. The previous experimental values by Hehre and co-workers[25] are 204 ± 3 and 227 ± 3 kcal/mol, respectively. The experimental proton affinity[25b] for $H_2C{=}SiHCH_3$ may be in error, due to complications in identifying the onset of proton transfer, and detailed studies of deprotonation kinetics were unfortunately not reported. For the comparison of the proton affinities of silylenes and silaethylenes with their carbon analogues, the heats of formation and proton affinities for carbenes and ethylenes are included in Table III. Values of 85.8 and 76.6 kcal/mol for heats of formation of $CHCH_3$ and $C(CH_3)_2$, respectively, are evaluated from heats of formation of methylene and ethylenes in Table III by assuming a constant $D°(C{=}C)$ of 174.3 kcal/mol for ethylenes.[47] These values yield heats of formation of -2.7, -11.9, and -21.1 kcal/mol for $CH_3HC{=}CHCH_3$, $CH_3HC{=}C(CH_3)_2$, and $(CH_3)_2C{=}C(CH_3)_2$, respectively, using the above assumption, and are close to the accepted values[48] of -2.99, -10.12, and -16.42 kcal/mol, respectively. Uncertainties in the estimated heats of formation for $CHCH_3$ and $C(CH_3)_2$ may be as much as 2 kcal/mol. The calculated proton affinities for carbenes are 197.0, 235.9, and 250.3 kcal/mol for CH_2, $CHCH_3$, and $C(CH_3)_2$, respectively. Since these carbenes have triplet ground states,[49] the proton-transfer reactions of the singlet ground-state carbonium ions with bases to produce the triplet ground-state carbenes should be spin-forbidden and may not be observed. Instead, the spin-allowed proton-transfer reactions to yield the singlet excited-state carbenes would be observed and provide the singlet-triplet splittings of carbenes from the differences between the observed proton affinities of singlet carbenes and the estimated proton affinities of triplet carbenes. The calculated proton affinities of ethylenes from thermochemical data in Table III using eq 7 are 162.6, 178.6, and 194.5 kcal/mol for $H_2C{=}CH_2$, $H_2C{=}CH(CH_3)$, and $H_2C{=}C(CH_3)_2$, respectively. The values are ~40 kcal/mol lower than those of the corresponding silaethylenes.

Effects of Solvation and the Choice of Reference Base on the Relative Stabilities of Silicenium and Carbonium Ions. The hydride affinities for the silicenium ions are precisely determined from kinetics and equilibria of hydride-transfer reactions in the gas phase. It is experimentally confirmed that the silicenium ions are significantly more stable than the corresponding carbonium ions in the gas phase with hydride as a reference base. However, the relative stabilities between the silicenium and the carbonium ions are strongly dependent upon the reference bases. In addition to the hydride affinities of MR_3^+ (M = C or Si, R = H or CH_3), their gas-phase chloride and fluoride affinities are included in Table V with the calculated heat of solvation of MR_3^+ in CH_2Cl_2. For the comparison of the relative stabilities between the silicenium ions and their carbon analogues in the gas phase with those in solution, heats of solvation of the ions are estimated from the well-known Born[50] eq 8. This equation gives the electrical work

$$\Delta H_{sol}(M^+) = -\frac{1}{8\pi\epsilon_0}\frac{e^2}{r(M^+)}\left(1-\frac{1}{\epsilon_r}\right) \qquad (8)$$

involved in transferring an ion of radius r from a vacuum ($\epsilon_r = 1$) to the solvent, the latter being regarded as a continuous dielectric of relative permittivity ϵ_r ($\epsilon_r(CH_2Cl_2) = 9.08$).[51] Even

(45) $D°(C{=}Si) = \Delta H_f°_{298}(CH_2) + \Delta H_f°_{298}(SiH_2) - \Delta H_f°_{298}(H_2C{=}SiH_2)$.
(46) Walsh, R. *Acc. Chem. Res.* **1981**, *14*, 246.
(47) $D°(C{=}C) = 2\Delta H_f°_{298}(CH_2) - \Delta H_f°_{298}(H_2C{=}CH_2)$.
(48) Cox, J. D.; Pilcher, G. *Thermochemistry of Organic and Organometallic Compounds*; Academic Press: New York, 1970.
(49) Carter, E. A. Ph.D. Thesis, California Institute of Technology, Pasadena, CA, 1987.
(50) (a) Born, M. *Z. Phys.* **1920**, *21*, 45. (b) Bethell, D.; Gold, V. *Carbonium Ions, An Introduction*; Academic Press: London, 1967; Chapter 5. (c) For more elaborate studies, see: Cournoyer, M. E.; Jorgensen, W. L. *J. Am. Chem. Soc.* **1984**, *106*, 5104.
(51) Weast, R. C., Ed. *Handbook of Chemistry and Physics*, 63rd ed.; Chemical Rubber Co.: Cleveland, OH, 1982; p E-51.

Table V. Hydride, Chloride, Fluoride, and Hydroxide Affinities of MR_3^+ (M = C or Si, R = H or CH_3) and Their Heats of Solvation in CH_2Cl_2

molecule (M)	$D(M-H)$,[a] kcal/mol	$D(M^+-H^-)$,[b] kcal/mol	$D(M-Cl)$,[c] kcal/mol	$D(M^+-Cl^-)$,[b] kcal/mol	$D(M-F)$, kcal/mol	$D(M^+-F^-)$,[b] kcal/mol	$D(M-OH)$, kcal/mol	$D(M^+-OH^-)$,[b] kcal/mol	$r(M^+)$,[d] Å	$\Delta H_{sol}(M^+)$,[e] kcal/mol
CH_3	104.8	314.4	84.5	228.3	109.8[f]	258.3	92.1[g]	276.9	1.41	−104.8
SiH_3	91.5	261.4	110.6[h]	214.8	156.5[i]	265.4	127.9[j]	273.0	1.81	−81.6
$C(CH_3)_3$	96.5	233.6	84.8	156.1	110.6[k]	186.7	96.0[l]	208.3	2.41	−61.3
$Si(CH_3)_3$	90.3	220.5	112.9	177.3	156.5[m]	225.9	127.9[n]	233.5	2.75	−53.7

[a] From Table III and ref 16. [b] $D(M^+-X^-) = \Delta H_f°_{298}(M^+) + \Delta H_f°_{298}(X^-) - \Delta H_f°_{298}(MX)$. $\Delta H_f°_{298}(H^-) = 34.7$ kcal/mol, $\Delta H_f°_{298}(Cl^-) = -54.1$ kcal/mol, $\Delta H_f°_{298}(F^-) = -59.5$ kcal/mol, and $\Delta H_f°_{298}(OH^-) = -32.9$ kcal/mol. [c] From $\Delta H_f°_{298}(MCl)$ in Cox and Pilcher.[48] $\Delta H_f°_{298}(M)$ in Table III and ref 16, and $\Delta H_f°_{298}(Cl) = 29.1$ kcal/mol. [d] Calculated radii using the covalent radii for C (0.77 Å), Si (1.17 Å), and H (0.32 Å) from ref 36. [e] Calculated values using eq 8. [f] $\Delta H_f°_{298}(CH_3F) = -56 \pm 7$ kcal/mol from JANAF Table (1971). [g] $\Delta H_f°_{298}(CH_3OH) = -48.0$ kcal/mol and $\Delta H_f°_{298}(OH) = 9.3$ kcal/mol from JANAF Table (1982). [h] $\Delta H_f°_{298}(SiH_3Cl) = -33.9 \pm 2$ kcal/mol from JANAF Table (1982). [i] $\Delta H_f°_{298}(SiH_3F) = -90 \pm 5$ kcal/mol from JANAF Table (1978). [j] Assuming $D(SiH_3-OH) = D(Me_3Si-OH)$. [k] Assuming $D(i\text{-Pr}-F) = D(t\text{-Bu}-F)$. $\Delta H_f°_{298}(i\text{-PrF}) = -69.4 \pm 0.4$ kcal/mol from Cox and Pilcher.[48] [l] $\Delta H_f°_{298}(t\text{-BuOH}) = -74.7 \pm 0.2$ kcal/mol from Cox and Pilcher.[48] [m] Assuming $D(Me_3Si-F) = D(H_3Si-F)$. [n] $\Delta H_f°_{298}(Me_3SiOH) = -119.4 \pm 0.9$ kcal/mol from Cox and Pilcher.[48]

Table VI. Thermochemistry of Silane Thermal Decomposition

silanes	products	$\Delta H°$,[a] kcal/mol	log A[b]	E_a,[b] kcal/mol
SiH_4	$SiH_2 + H_2$	61	15.5[c]	59.6[c] (56.9)[d]
CH_3SiH_3	$H_2C{=}SiH_2 + H_2$	50		(96.3)[e]
	$SiH_2 + CH_4$	58	14.7[f]	66.7[f] (71.9)[e]
	$SiHCH_3 + H_2$	60	15.0[g]	63.2[g] (63.2)[e]
$(CH_3)_2SiH_2$	$H_2C{=}SiH_2 + CH_4$	48		
	$H_2C{=}SiHCH_3 + H_2$	50		
	$SiHCH_3 + CH_4$	58	14.8[h]	73.0[h]
	$Si(CH_3)_2 + H_2$	60	14.3[i]	68.0[i]
	$SiH_2 + C_2H_6$	72		
$(CH_3)_3SiH$	$H_2C{=}SiHCH_3 + CH_4$	48		
	$H_2C{=}Si(CH_3)_2 + H_2$	50		
	$Si(CH_3)_2 + CH_4$	58	(~14.8)[j]	(~80)[j]
	formation of CH_4		16.4[k]	76.5[k]
	formation of H_2		16.1[k]	80.3[k]
$(CH_3)_4Si$	$H_2C{=}Si(CH_3)_2 + CH_4$	48.5		
	$Si(CH_3)_2 + C_2H_6$	72		
	formation of CH_4		17.6[k]	84.8[k]

[a] The $\Delta H°$ values are esimated using heats of formation of silanes from Walsh,[46] silylenes and silaethylenes in Table III, and other thermochemical data from Cox and Pilcher.[48] [b] Experimental Arrhenius A factors and activation parameters; values in parenthesis are theor. results. [c] Newman et al.[56a] [d] Gordon et al.[56b] [e] Baldridge et al.[62] [f] Sawrey et al.[58a] [g] Neudorfl et al.[58b] [h] Rickborn et al.[59] [i] Neudorfl and Strausz.[57] [j] Estimated values, see text. [k] Baldwin et al.[60]

though this so-called "spherical ion in dielectric continuum" model is a crude approximation, it is useful in comparing the *relative* solvation effects between the silicenium ions and their carbon analogues. It is clear that the silicenium ions are less stable than the corresponding carbonium ions in the gas phase with F^- as a reference base. When Cl^- is used as a reference base in the gas phase, SiH_3^+ is more stable than CH_3^+ but $Si(CH_3)_3^+$ is less stable than $C(CH_3)_3^+$. Since the magnitude of heats of solvation is greater for the smaller ions, the nonspecific solvation effect favors the stabilization of the smaller carbonium ions than the corresponding silicenium ions. ***As a result, the silicenium ions are significantly less stable than the analogous carbonium ions in CH_2Cl_2 solution with both Cl^- and F^- as reference bases,[52] and the hydride affinity differences between the silicenium ions and the analogous carbonium ions are greatly attenuated in solution.[53]***

The OH^- affinity data are included in Table V for the comparison of the effects of OH^- as a reference base with those of hydride and halides. This may explain the failure to detect the $Si(CH_3)_3^+$ ion under conditions developed for the stabilization of the carbonium ions.[54] Also, the result suggests that the earlier observation of hydrogen–halogen exchange of optically active R_3Si^*H with trityl halides by Sommer and Bauman[55] may occur via transient formation of silicenium ions by the hydride transfer from R_3Si^*H to Ph_3C^+ and carbonium ions by the chloride transfer from Ph_3CCl to R_3Si^+, which results in the complete racemization of silicon chlorides in CH_2Cl_2 solution. Further investigation of the kinetics of hydrogen–halogen exchange reactions both in the gas phase and in solution may give some information pertinent to the silicenium ion question as viable reaction intermediates.

Acknowledgment. We acknowledge the support of the National Science Foundation (Grant No. CHE87-11567).

Appendix

Thermochemistry of Silane Thermal Decomposition. Thermal decomposition of silanes has been extensively studied to establish reliable thermochemistry of silicon containing compounds in the last two decades.[46,56-60] Recently, pyrolysis of silanes has been used to prepare thin silicon films for the fabrication of electric integrated circuits.[61] Understanding basic pyrolysis mechanisms, such as the lowest energy dissociation pathway and important reactive intermediates, under homogeneous or heterogeneous conditions is fundamental to developing mechanistic models for chemical vapor deposition film growth.[61] The newly derived heats of formation in Table III for some fundamental reactive intermediates, silylenes and silaethylenes,[24] can be used to evaluate reaction enthalpy changes for silane pyrolysis and may be helpful to elucidate pyrolysis mechanisms.

The $\Delta H°$ values for silane thermal decompositions involving silylenes or silaethylenes as products are listed in Table VI with previously reported Arrhenius parameters and available theoretical estimates for activation barriers.[56b,62] It is apparent in the pyrolysis of methylsilane[58] that three-center geminal elimination of molecular hydrogen forming methylsilylene is the lowest energy dissociation pathway. Although 1,2-elimination of hydrogen in the thermal decomposition of methylsilane is thermodynamically

(52) $D(R^+-X^-,s) = D(R^+-X^-) - \Delta H_{sol}(R^+) - \Delta H_{sol}(X^-) + \Delta H_{sol}(RX)$. $\delta(D) = D(R_3Si^+-X^-) - D(R_3C^+-X^-)$ and $\delta(D_s) = D(R_3Si^+-X^-,s) - D(R_3C^+-X^-,s)$. $\delta(D)$ and $\delta(D_s)$ are the X^- affinity differences between the silicenium and the carbonium ions in the gas phase and in solution, respectively. Assuming that $\Delta H_{sol}(R_3SiX) - \Delta H_{sol}(R_3CX)$ is considerably smaller than $\Delta H_{sol}(R_3Si^+) - \Delta H_{sol}(R_3C^+)$ leads to $\delta(D_s) = \delta(D) - (\Delta H_{sol}(R_3Si^+) - \Delta H_{sol}(R_3C^+))$. $\delta(D_s)$(R = H, X = H) = −29.8 kcal/mol, $\delta(D_s)$(R = CH_3, X = H) = −5.5 kcal/mol, $\delta(D_s)$(R = H, X = Cl) = 9.7 kcal/mol, $\delta(D_s)$(R = CH_3, X = Cl) = 28.8 kcal/mol, $\delta(D_s)$(R = H, X = F) = 30.3 kcal/mol, $\delta(D_s)$(R = CH_3, X = F) = 46.8 kcal/mol. $\delta(D_s)$(R = H, X = OH) = 19.3 kcal/mol, $\delta(D_s)$(R = CH_3, X = OH) = 32.8 kcal/mol. A positive value of $\delta(D_s)$ means that the silicenium ion is less stable than the corresponding carbonium ion in solution (CH_2Cl_2).

(53) $\delta(D)$(R = H, X = H) = −53.0 kcal/mol and $\delta(D_s)$(R = H, X = H) = −29.8 kcal/mol. $\delta(D)$(R = CH_3, X = H) = −13.1 kcal/mol and $\delta(D_s)$(R = CH_3, X = H) = −5.5 kcal/mol.

(54) Olah, G. A.; Mo, Y. K. *J. Am. Chem. Soc.* **1971**, *93*, 4942.
(55) Sommer, L. H.; Bauman, D. L. *J. Am. Chem. Soc.* **1969**, *91*, 7076.
(56) (a) Newman, C. G.; O'Neal, H. E.; Ring, M. A.; Leska, F.; Shipley, N. *Int. J. Chem. Kinet.* **1979**, *11*, 1167. (b) Gordon, M. S.; Gano, D. R.; Binkley, J. S.; Frisch, M. J. *J. Am. Chem. Soc.* **1986**, *108*, 2191, and earlier references therein.
(57) Neudorfl, P.; Strausz, O. P. *J. Phys. Chem.* **1978**, *82*, 241.
(58) (a) Sawrey, B. A.; O'Neal, H. E.; Ring, M. A.; Coffey, D., Jr. *Int. J. Chem. Kinet.* **1984**, *16*, 31. (b) Neudorfl, P.; Lown, E. M.; Safarik, I.; Jodhan, A.; Strausz, O. P. *J. Am. Chem. Soc.* **1987**, *109*, 5780, and earlier references therein.
(59) Rickborn, S. F.; Rogers, D. S.; Ring, M. A.; O'Neal, H. E. *J. Phys. Chem.* **1986**, *90*, 408, and earlier references therein.
(60) Baldwin, A. C.; Davidson, I. M. T.; Reed, M. D. *J. Chem. Soc., Faraday Trans. 1* **1978**, *74*, 2171, and earlier references therein.
(61) Jasinski, J. M.; Meyerson, B. S.; Scott, B. A. *Annu. Rev. Phys. Chem.* **1987**, *38*, 109.
(62) Baldridge, K. K.; Boatz, J. A.; Koseki, S.; Gordon, M. S. *Annu. Rev. Phys. Chem.* **1987**, *38*, 211.

the most favorable process, theoretical studies by Gordon and co-workers[62] suggest that the 1,2-elimination process has a higher activation barrier than a 1,1-elimination process. As a result, the direct formation of silaethylenes in the pyrolysis of silanes under homogeneous conditions is unlikely. The $\Delta H°$ values for 1,1-elimination of hydrogen in the pyrolysis of SiH_4,[56] CH_3SiH_3,[57,58] and $(CH_3)_2SiH_2$[57,59] are almost identical, but the E_a values tend to increase by ~4.2 kcal/mol per methyl group with increasing methyl substitution in place of hydrogen. The E_a values for 1,1-elimination of methane in the pyrolysis of CH_3SiH_3 and $(CH_3)_2SiH_2$ are slightly higher than those for 1,1-elimination of hydrogen and increase as a result of methyl substitution by ~6.7 kcal/mol per methyl group. This may indicate that methyl substitution at the silicon center in silylenes raises the activation energy for insertion into H–H or C–H bonds by ~4.2 or ~6.7 kcal/mol, respectively.[59] The pyrolysis mechanism of trimethylsilane[60] has not been well established because of the complexity of the mechanism and the lack of experimental data for most of its steps. It will be of particular interest to see if the pyrolysis of trimethylsilane involves a 1,1-elimination process to form $Si(CH_3)_2$. For this process, estimates of Arrhenius parameters are ~14.8 and ~80 kcal/mol for log A and E_a by analogy with pyrolysis reactions of CH_3SiH_3 and $(CH_3)_2SiH_2$. In the pyrolysis of tetramethylsilane, Davidson and co-workers[60] concluded that the formation of methane at high temperature (955–1055 K) relates to a nonchain mechanism rate-determined by the Si–C bond rupture process with E_a of 84.8 kcal/mol, while at low temperature (840–950 K), a short-chain sequence probably operates. This may indicate that the molecular process involving 1,2-elimination of methane or 1,1-elimination of ethane in the pyrolysis of tetramethylsilane requires a higher activation energy than the Si–C bond rupture process.

Chapter IV

Studies of the Gas-Phase Reactive Intermediate Formed by Heterogeneous Processes in Chlorosilane Chemical Vapor Deposition using Photoelectron Spectroscopy and Mass Spectrometry

Studies of the Gas-Phase Reactive Intermediate Formed by Heterogeneous Processes in Chlorosilane Chemical Vapor Deposition using Photoelectron Spectroscopy and Mass Spectrometry.

G. H. Kruppa, S. K. Shin, and J. L. Beauchamp*

Contribution No. 7843 from the Arthur Amos Noyes Laboratory of Chemical Physics
California Institute of Technology, Pasadena, California 91125

Abstract

Photoelectron spectroscopy and mass spectrometry have been employed to identify the gas-phase reactive intermediate in the chlorosilane (SiH_2Cl_2, $SiHCl_3$) CVD under the heterogeneous flash vacuum pyrolytic condition. Dichlorosilylene ($SiCl_2$) and hydrogen chloride (HCl) are the major gas phase products in the heterogeneous decomposition of SiH_2Cl_2 and $SiHCl_3$ on silicon surfaces above 600 °C and 800 °C, respectively. $SiCl_2$ and HCl desorb from the surface at these temperatures, and these species are likely to be important in the removal of excess chlorine and hydrogen from the growing polycrystalline thin silicon film. This result, combined with results of the detection of dichlorosilylene on the homogeneous IR multiphoton decomposition of dichlorosilane, indicates that monochlorosilylene (SiHCl) is not an abundant gas phase intermediate in both homogeneous and heterogeneous CVD systems using dichlorosilane as a source gas.

I. INTRODUCTION

The chlorosilanes, SiH_xCl_{4-x}, have commonly been used for the deposition of thin silicon films.[1] A wide variety of conditions have been employed for the chemical vapor deposition of silicon films, with pressures ranging from 0.1 torr (Low Pressure CVD, LPCVD) to 760 torr (Atomospheric Pressure CVD, APCVD), and surface temperatures ranging from 900-1100 °C. The importance of CVD to the electronics industry has led to a number of attempts to measure the concentrations and identities of the species present in CVD systems. The techniques employed to date include: thermodynamic equilibrium calculations,[2] gas chromatography,[3] mass spectrometry,[4] optical studies[5] and laser induced fluorescence[6]. The remainder of this paper will be confined to discussion of CVD systems using dichlorosilane and trichlorsilane as source gases. In spite of the extensive studies performed on chlorosilane CVD systems some controversy remains as to the identities and concentrations of the reactive intermediates present in these systems.

Sedgwick et al. used fluorescence scattering to profile the concentration of $SiCl_2$ in an APCVD reactor using $SiCl_4$ and SiH_2Cl_2 as input gases.[5a] $SiCl_2$ was found to be the major intermediate present, and the concentration profiles best fit a model where $SiCl_2$ is formed homogeneously in the gas phase above the hot susceptor. This result agrees with thermodynamic calculations which indicate that $SiCl_2$ is the dominant silicon containing species in the vapor phase under CVD conditions between 1000 and 1200 °C.[2] $SiCl_2$ has also been detected by mass spectrometric sampling of the hot gases in a reactor designed to simulate CVD conditions, with a variety of Si-Cl-H compounds and mixtures used as input gases.[4] However, in a more recent study, Ho and Breiland detected the laser-induced fluorescence spectrum of SiHCl in a CVD reactor under both APCVD and LPCVD conditions.[6] Ho and Breiland also asserted that the fluorescence observed by Sedgwick et al. was due to SiHCl and not $SiCl_2$. Finally, a recent study by Sausa and Ronn on the IR multiphoton dissociation of SiH_2Cl_2 showed that $SiCl_2$ and H_2 were the only

products observed in the homogeneous gas phase decomposition of dichlorosilane.[7] Further studies are clearly needed to determine the relative importance of intermediates such as $SiCl_2$ and SiHCl in CVD systems using the chlorosilanes as source gases.

In this report, results on the mechanism of the flash vacuum pyrolysis of dichlorosilane and trichlorosilane obtained using a combination of photoelectron spectroscopy (PES) and mass spectrometry are presented. The flash vacuum pyrolysis conditions employed in this study were 1-10 millitorr of the chlorosilane gas over a quartz pyrolyzer surface at 600-1100 °C (see experimental section for further details). While the conditions used in this study involve pressures considerably lower than typical CVD conditions,[1] the formation of a thin silicon film was observed on the pyrolyzer surface, showing that CVD does take place at these low pressures. In addition, under flash vacuum pyrolysis conditions thermal activation takes place primarily by contact with the hot pyrolyzer walls, so that processes observed in this study are the result of heterogeneous reactions. This is in contrast to many studies of CVD reactions where both heterogeneous and homogeneous reactions must be considered.[1] Hence, although the results in this study were not obtained under typical CVD conditions, they do have important implications for the mechanism of surface processes in CVD systems.

PES has previously been shown in our laboratory,[8] and by others,[9] to be a useful technique for studying reactive intermediates in gas-solid heterogeneous reactions. Bock et al. have previously measured the photoelectron spectrum of $SiCl_2$ produced by $SiCl_4$ thermal decomposition on solid silicon.[10] Unlike laser-induced fluorescence, where species of interest are selectively induced by a laser, PES detects all species present in a gas mixture simultaneously. Hence qualitative estimates of relative concentrations of the reactive intermediates and stable species in a gas mixture can be made, which is difficult to accomplish by laser induced fluorescence. Quantitative measurements of relative concentrations are hindered because

the relative photoionization cross sections of the species of interest must be known and often are unavailable. Mass spectrometric measurements on pyrolysis mixtures are often complicated by fragmentation of the ions formed by electron impact. The fragment ions produced often have the same masses as reactive intermediate species that are of interest. As will be shown in the results below, PES is a complimentary technique to mass spectrometry which allows the unambiguous detection of reactive intermediates and the determination of relative product concentrations in the heterogeneous decomposition of SiH_2Cl_2 and $SiHCl_3$ on a hot silicon surface.

II. EXPERIMENTAL SECTION

Figure 1a shows the photoelectron spectrometer used in these studies which has been specially modified to detect the reactive intermediate products of flash vacuum pyrolyses and has been described in detail previously.[11] Only details of the pyrolyzer will be discussed here, and a detail drawing of the pyrolzyer is shown in Figure 1b. The pyrolysis takes place within a quartz tube with an inner diameter of 3 mm. The pyrolyzer is heated by double stranded heating wire wound over a 2 cm length of the quartz tube, and temperatures up to 1100 °C may be obtained. The HeI photon beam intersects the sample about 0.5 cm downstream from the end of the pyrolysis region. Since the pyrolysis is done at low pressures (about 10^{-2} torr) the residence time in the pyrolyzer is kept to about 1 msec, and thermal activation results mainly from collisions with the walls. Because the distance from the end of the pyrolyzer to the detection region is short, all reactive intermediates that escape the surface should be detected.

As shown in Figure 1, a quadrupole mass spectrometer has recently been added to the apparatus used in these studies to help confirm the identification of reactive intermediates. The gases exiting the pyrolysis region traverse the scattering chamber (diameter = 1.7 cm, pressure about 10^{-3} torr) and exit the scattering chamber through a 4 mm aperture in the chamber directly opposite the pyrolysis tube. The ionizer region of the quadrupole mass spectrometer is 3 cm from the scattering

chamber exit and the pressure in this region is in the 10^{-6} torr range. Hence, while the gases exiting the pyrolyzer must traverse nearly 5 cm to the quadrupole ionizer, the pressures in this region are quite low, so recombination rates are slow, and reactive intermediates can easily be seen in the mass spectra.

The chlorosilane gases were obtained from Petrarch. HCl contamination due to reactions of the chlorosilanes with residual water and air in the sample handling system was a common problem. All samples were carefully put through several freeze-pump-thaw cycles to remove residual gases, and vacuum distillation at low temperatures was carried out to remove HCl when necessary. Room temperature spectra were recorded before and after all experiments to insure that the results obtained were not complicated by HCl contamination of the sample.

For temperature measurements a thermocouple was inserted between the heater coil and outside of the quartz tube. The temperature of the inner pyrolyzer surface was not measured directly, and the temperatures given in the spectra discussed below are probably somewhat higher than the true surface temperature. While the material used for the pyrolyzer tube was quartz, visual inspection of the pyrolysis region after operation at high temperature for one or more hours showed the deposition of a thin silicon film with 0.1 – 0.2 mm thickness. However, the surface has not been characterized in detail. The deposition of silicon films on SiO_2 surfaces by the chlorosilanes has previously been shown to occur.[12] Also, we obtained identical results in one experiment using a graphite tube. Hence both surfaces rapidly became coated with a silicon film similar to that observed under LPCVD conditions, and our results should have direct implications for surface processes that take place in CVD using the chlorosilanes as source gases.

III. RESULTS

Photoelectron spectroscopic and mass spectrometric results were not time dependent nor dependent on the use of a quartz or a graphite surface. The photoelectron spectra of the pyrolysis products of dichlorosilane at temperatures from room temperature to 780 °C are shown in Figure 2. The krypton present in all the spectra is used to calibrate the electron energy scale, and is admitted to the spectrometer at room temperature through an inlet system separate from the pyrolyzer. The first obvious change in the spectra with increasing temperature is the appearance of HCl peaks at 610 °C. At 780 °C a new peak appears at an ionization potential of 10.3 eV. Figure 3 shows a spectrum at 850 °C plotted with a spectrum of $SiCl_2$, obtained previously by Bock et al., produced by $SiCl_4$ thermal decomposition over solid silicon.[10] Comparison of the spectra, allowing for the presence of HCl, some undecomposed SiH_2Cl_2 and Kr in the spectra from this work, shows that the band with an IP of 10.3 eV is due to $SiCl_2$. No H_2 or SiHCl is observed in the photoelectron spectra at any temperature. The ionization potentials and photoelectron band shapes for the species that have been detected in previous CVD studies are given in Table 1. Also apparent in the spectrum at 850 °C is that the spectrometer resolution is degraded (the vibrational progression in the second HCl peak is no longer resolved). The degradation in spectrometer performance is due to $SiCl_2$ polymerizing on the electron energy analyzer surfaces, and photoelectron spectra could not be obtained above 850 °C.

Mass spectra could be obtained up to the maximum temperature of the pyrolyzer, 1100 °C. Mass spectra of the pyrolysis products of dichlorosilane at three different temperatures are shown in Figure 4. The electron impact source electron energy was reduced to 20 eV in all of the spectra presented in this paper, to reduce complications due to fragmentation. The room temperature mass spectra of SiH_2Cl_2 at 20 eV electron energy show the conspicuous peak of $SiHCl^+$ (Fig. 4a). This result indicates that $SiHCl^+$ is a stable molecular ion. Therefore, if SiHCl were

present as a parent neutral after the pyrolysis, then the prominent peak of $SiHCl^+$ at 20 eV electron energy would be expected. The results agree well with the photoelectron spectra, showing the appearance of HCl^+ at 600 °C. At 900 °C the parent dichlorosilane is completely decomposed, and only $SiCl_2^+$, HCl^+ and $SiCl^+$ (from loss of Cl from $SiCl_2^+$ after electron impact ionization) are observed in the mass spectrum. The peak at mass 64 which is about 5% of that at mass 63 is ascribed to $^{29}SiCl^+$ [the natural aboundances of silicon isotopes: ^{28}Si (92.2%), ^{29}Si (4.7%), and ^{30}Si (3.1%)]. The room temperature and high temperature mass spectra reported here also agree reasonably well with mass spectra reported previously for SiH_2Cl_2, $SiHCl_3$ and $SiCl_2$.[4] The small amount of Kr^+ present in the spectra was used to calibrate the mass scale. The water observed in the spectra is due to background water in the main vacuum chamber and not in the inlet system or sample. The sodium and potassium ions observed at the highest pyrolyzer temperature are due to thermal desorption of sodium and potassium from the sodium silicate ceramic cement used in construction of the pyrolyzer. Hence the combination of the mass spectra and photoelectron spectra shows unambiguously that the only products of the heterogeneous thermal decomposition of dichlorosilane are HCl and $SiCl_2$.

Trichlorosilane decomposed at higher temperatures than dichlorosilane, consistent with previous determinations that the activation energy for silicon deposition is higher for $SiHCl_3$ than for SiH_2Cl_2.[1] At temperatures above 900 °C emission of sodium and potassium from the pyrolyzer ceramic insulation made it impossible to obtain photoelectron spectra. Mass spectra could be obtained however, and these are shown in Figure 5. Comparison of these spectra with those for dichlorosilane shows the same general trend, disappearance of the parent molecule and appearance of HCl and $SiCl_2$ as the only pyrolysis products with increasing temperature.

IV. Discussion

The possible decomposition pathways for dichlorosilane along with the heat of reaction and estimated activation energy for each pathway are given in Table 2. $SiCl_2$ is the thermodynamically favored product by stepwise or one step molecular elimination decomposition of dichlorosilane. Sausa and Ronn observed $SiCl_2$ and H_2 as the only products of the homogeneous gas phase IR multiphoton dissociation of dichlorosilane,[7] which is not surprising since IR multiphoton dissociation is expected to yield the product resulting from the process with the lowest activation energy. This result is an interesting contrast to the results presented by Ho and Breiland and the results presented in this study, which clearly indicate that the mechanisms for heterogeneous and homogeneous decomposition of $SiCl_2$ are different. Ho and Breiland observed laser-induced fluorescence due to HSiCl and suggested that HSiCl is also formed by homogeneous decomposition above the hot silicon surface.[6] The results from this study show that in the heterogeneous decomposition of dichlorosilane $SiCl_2$ and HCl are the major pyrolysis products.

Given the results of Sausa and Ronn showing that $SiCl_2$ is the major silicon containing reactive intermediate in the homogeneous decomposition of dichlorosilane, and the results presented here which show that $SiCl_2$ is the major silicon containing intermediate formed in the heterogeneous decomposition, it is resonable to suggest that the observation of SiHCl by Ho and Breiland is due to the relative sensitivities of the detection methods, the different experimental conditions, and the activation energies for the decomposition pathways yielding the two intermediates. Although $SiCl_2$ is the thermodynamically favored product by 32.6 kcal/mol, the activation energy for the elimination of HCl from dichlorosilane yielding SiHCl is estimated from theoretical considerations to be only 13.0 kcal/mol higher than for the elimination of H_2.[13] At 1000 °C, a difference of 5 kcal/mol yields a ratio of reaction rates of 0.008. Hence small concentrations of SiHCl may be formed at high temperatures in a homogeneous system. The laser-induced fluorescence technique is capable of

detecting concentrations of species approximately 10^3 lower in concentration than the PES technique used in this study. Also, laser-induced fluorescence is a highly specific technique allowing the detection of one species at a time and Ho and Breiland were unable to comment on the relative concentration of SiHCl to $SiCl_2$, H_2 or HCl in their study. (SiHCl fluorescence was detected at wavelengths from 445-490 nm, while $SiCl_2$ fluorescence is observed between 310 nm and 350 nm[14]). As shown in Table 1, SiH_2 has an adiabatic ionization potential of 9.02 eV[15] and $SiCl_2$ has a vertical ionization potential of 10.35 eV.[10] The vertical ionization potentials of SiH_2, SiHCl, and $SiCl_2$ are estimated from the orbital energies of the highest occupied Si nonbonding orbitals at the Hartree-Fock level and are listed in Table 1. The theoretical ionization potentials of 9.19 and 10.29 eV for SiH_2 and $SiCl_2$ are in good agreement with an adiabatic IP of 9.02 eV for SiH_2 and a vertical IP of 10.35 eV for $SiCl_2$. The theoretical vertical IP of SiHCl is 9.54 eV, and if it were present in the experiments presented in this study at a concentration more than 5% of the $SiCl_2$ concentration, it would have been observed as another band at 9.54 eV in the photoelectron spectrum. Based on the studies discussed above, it appears that $SiCl_2$ is the major silicon containing reactive intermediate present in the gas phase in CVD systems using SiH_2Cl_2 as a source gas, formed in our experiments by heterogeneous decomposition of SiH_2Cl_2 over the decomposition film, while SiHCl is present as a minor species. Since identical results were obtained with quartz and graphite pyrolyzers and results were independent of time variation, we are confident that similar results would be obtained from silicon surfaces.

It is interesting to note from the mass spectra in Figures 4 and 5 that at temperatures where the precursor chlorosilane is completely decomposed, the relative concentrations of HCl and $SiCl_2$ are nearly the same for dichlorosilane and trichlorosilane. The ratio of $SiCl_2$/HCl is higher in the trichlorosilane case, presumably because there is more chlorine carried to the surface by this feed gas. This is in agreement with previous optical and mass spectrometric studies which

showed that the gas phase species present in CVD systems were independent of the chlorosilane source gas.[4,5] Gilbert and Ban,[4] using mass spectrometry, showed that the gas phase species found in CVD reactions were independent of the feed gas, and that their relative concentrations depended only on the temperature and Cl/H ratio of the feed gas. The IR multiphoton dissociation results of Sausa and Ronn showed that only H_2 and $SiCl_2$, and not HCl, are produced by the homogeneous gas phase decomposition of dichlorosilane.[7] The results in this study show that the HCl observed in previous studies of CVD systems using chlorosilanes as source gases is probably generated by heterogeneous surface decomposition of the chlorosilanes, followed by surface reactions.

V. Speculation Regarding Heterogeneous Decomposition Pathways of Chlorosilanes

The results presented in this study show that $SiCl_2$ and HCl are formed in the heterogeneous decomposition of SiH_2Cl_2 and $SiHCl_3$ on silicon surfaces deposited on both quartz and graphite above 600 °C and 800 °C respectively. $SiCl_2$ and HCl desorb from the surface at these temperatures, and these species are likely to be important in the removal of excess chlorine and hydrogen from the growing polycrystalline thin silicon film. Under heterogeneous conditions, where the dichlorosilane decomposes on the surface and not above it, species I and II in Scheme 1 would be likely to form by dissociative adsorption on the surface.

Scheme 1

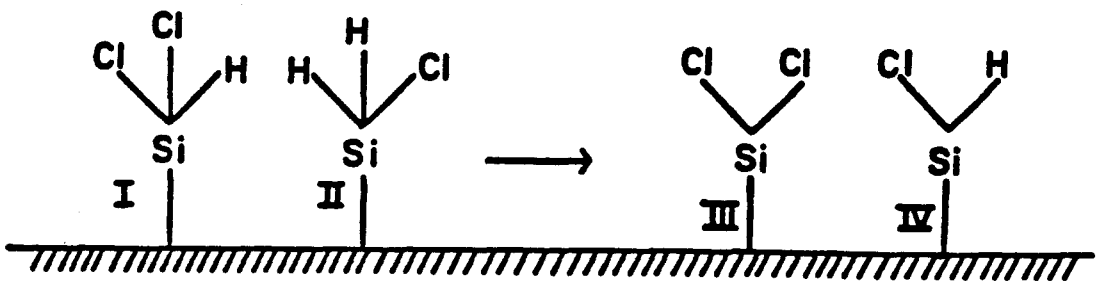

I and II can react further with the surface to form species such as III and IV. Because Si–Cl bonds are stronger than Si–H or Si–Si bonds (see Table 2 and the references to Table 2), and the Cl_2 bond is weak (58.0 kcal/mol[16]), a surface moiety such as III is most likely to desorb $SiCl_2$, rather than Cl_2. The results in this study indicate that species such as IV are most likely to lose HCl rather than SiHCl. In this case breaking the Si–Cl bond ($\sim$ 110 kcal/mol, see Table 1) is in large part compensated by the formation of the H–Cl bond (103 kcal/mol[16]). The results presented here, when combined with results on the homogeneous IR multiphoton decomposition of dichlorosilane, indicate that SiHCl is not an abundant intermediate in CVD systems using dichlorosilane as a source gas. A relative concentration of SiHCl to $SiCl_2$ of more than a few percent would have been observed by the PES technique used in this study. Further work is needed to quantify the relative concentrations of $SiCl_2$ and SiHCl in CVD systems.

Acknowledgment. We acknowledge the support of the National Science Foundation under Grant CHE87-11567.

References and Notes

(1) For recent reviews see: (a) Jasinski, J. M.; Meyerson, B. S.; Scott, B. A. *Ann. Rev. Phys. Chem.* **1987**, *38*, 109. (b) Bloem, J.; Giling, L. J. in *VLSI Electronics Microstructure Science*; Einspruch, N. G.; Huff, H. Ed.; Academic Press: Orlando; 1987, Vol. 12, p. 89.

(2) (a) Lever, R. F. *IBM J. Res. Dev.* **1964**, *8*, 460. (b) Hunt, L. P.; Sirtl, E. *J. Electrchem. Soc.* **1974**, *119*, 1741. (c) Sirtl, E.; Hunt, L. P.; Sawyer, D. H. *J. Electrochem. Soc.* **1974**, *121*, 919.

(3) (a) Duchemin, J. P.; Bonnet, M.; Beuchet, G. *J. Vac. Sci. Technol.* **1979**, *16*, 76. (b) Couchet, G.; Mellottee, H.; Delbourgo, R. *J. Electrochem. Soc.* **1978**, *113*, 487.

(4) (a) Ban, V. S.; Gilbert, S. L. *J. Cryst. Growth* **1975**, *31*, 284. (b) Ban, V. S.; Gilbert, S. L. *J. Electrochem. Soc.* **1975**, *122*, 1382.

(5) (a) Sedgwick, T. O.; Smith, J. E. *Thin Solid Films* **1977**, *40*, 1. (b) Nishizawa, J. E. *J. Cryst. Growth* **1982**, *56*, 273. and references therein.

(6) (a) Ho, P.; Breiland, W. G. *Appl. Phys. Lett.* **1983**, *43*, 125. (b) Breiland, W. G.; Ho, P.; Coltrin, M. E. *J. Appl. Phys.* **1986**, *60*, 1505.

(7) Sausa, R. C.; Ronn, A. M. *Chem. Phys.* **1985**, *96*, 183.

(8) Schultz, J. C.; Beauchamp, J. L. *J. Phys. Chem.* **1983**, *87*, 3587.

(9) Bock, H.; Solouki, B. *Angew. Chem. Int. Ed. Engl.* **1984**, *20*, 427.

(10) Bock, H.; Solouki, B.; Maier, G. *Angew. Chem. Int. Ed. Engl.* **1985**, *24*, 205.

(11) Houle, F. A.; Beauchamp, J. L. *J. Am. Chem. Soc.* **1978**, *100*, 3290.

(12) See the discussion in references 1 and 4 and also: Rosler, R. S. *Solid State Technol.* **1977**, *20*, 63.

(13) The recombination of radicals is generally assumed to occur without activation energy, so the reverse activation barriers for the stepwise decomposition processes should be near zero. Hence the activation energies for these processes

are equal to the reaction endothermicities. SiH_2 is known to insert into H_2 with an activation energy of less than 1 kcal/mol (Gordon, M. S.; Gano, D. R.; Stephen, B.; Frisch, M. J. *J. Am. Chem. Soc.* **1986**, *108*, 2191. ; Jasinski, J. M. *J. Phys. Chem.* **1986**, *90*, 555.), so by analogy the activation energy for the elimination of Cl_2 from dichlorosilane should approximately equal the endothermicity of the reaction. The order of reactivities for the insertion of SiXY into the Si–H bond is $SiH_2 > SiHCl \gg SiCl_2$ (Jenkins, R. L.; Vanderwielen, A.-J.; Ruis, S. P.; Gird, S. R.; Ring, M. A. *Inorg. Chem.* **1973**, *12*, 2968.). The activation energies for the elimination of HCl and H_2 from dichlorosilane were calculated assuming that the difference in reactivity in the reverse insertion reaction is caused by a difference in activation energy due to the difference in singlet-triplet splittings in the series SiH_2, SiHCl, $SiCl_2$. Calculations at the GVB-DCCI//MP2/6-31G** level show that the singlet-triplet splitting in $SiCl_2$ is 34.1 kcal/mol greater than SiH_2 and SiHCl has a singlet-triplet splitting 14.5 kcal/mol greater than SiH_2 (Shin, S. K.; Goddard, W. A. III; Beauchamp, J. L. results to be published). For SiHCl and $SiCl_2$ formation from dichlorosilane, the difference in singlet-triplet splitting between SiXY and SiH_2 was added to the reaction endothermicity to obtain the activation energy given in Table 1.

(14) Suzuki, M.; Washida, N.; Inoue, G. *Chem. Phys. Lett.* **1986**, *131*, 24. and references therein.

(15) Berkowitz, J.; Greene, J. P.; Cho, H.; Ruscic, B. *J. Chem. Phys.* **1987**, *86*, 1235.

(16) (a) Edwards, J. G.; Franklin, H. F.; Gilles, P. W. *J. Chem. Phys.* **1971**, *54*, 545. (b) Kant, A. *J. Chem. Phys.* **1968**, *49*, 5144.

Table 1. Photoelectron Spectrum Features for Species expected in CVD Systems.

Species	IP (eV)	IP_{SCF} (eV)[a]	Band Shape
SiH_2	9.02[b]	9.19[c]	No reference spectrum is available. But the IP is known from photoionization appearance potential measurements[d]
$SiCl_2$	10.35[e]	10.29[c]	Broad unstructured first band with several bands at higher IP. See Figure 3.
SiHCl		9.54[c]	No reference spectrum is available.
HCl[f,g]	12.75		Sharp doublet
	16.28		Sharp vibrational progression beginning at 16.25 eV.
H_2[f,g]	15.98		Sharp vibrational progression beginning at 15.45 eV.

[a] The theoretical ionization potentials are estimated from the orbital energies of the highest occupied Si nonbonding orbitals at the Hartree-Fock level with the MP2/6-31G** optimized geometries (reference 13). The following basis sets were used: Si($7s5p2d1f$), H($2s1p$), and Cl($4s3p1d$).

[b] An adiabatic IP.

[c] A vertical IP.

[d] Reference 15.

[e] Reference 10.

[f] Kimura, K.; Katsumata, S.; Achiba, Y.; Yamazaki, T.; Iwata, S. *Handbook of HeI Photoeletcrom Spectra of Fundamental Organic Molecules*; Halsted Press: New York; 1981.

[g] Turner, D. W.; Baker, C.; Baker, A. D.; Brundle, C. R. *Molecular Photoelectron Spectroscopy*; Wiley: New York; 1970.

Table 2. Heats of Reaction and Activation Energies for the Decomposition Pathways of Dichlorosilane.

Reactions			ΔH_{298} [a] (kcal/mol)	E_a [b] (kcal/mol)
Stepwise Processes				
SiH_2Cl_2	$\longrightarrow$	$SiH_2Cl + Cl$	111.3	$\sim$ 111.3
SiH_2Cl_2	$\longrightarrow$	$SiHCl_2 + H$	92.3	$\sim$ 92.3
$SiHCl_2$	$\longrightarrow$	$SiCl_2 + H$	48.8	$\sim$ 48.8
$SiHCl_2$	$\longrightarrow$	$SiHCl + Cl$	80.3	$\sim$ 80.3
Molecular Elimination				
SiH_2Cl_2	$\longrightarrow$	$SiH_2 + Cl_2$	143.5	$\sim$ 143.5
SiH_2Cl_2	$\longrightarrow$	$SiHCl + HCl$	69.5	$\sim$ 84.0
SiH_2Cl_2	$\longrightarrow$	$SiCl_2 + H_2$	36.9	$\sim$ 71.0

[a] Heats of reaction were calculated from heats of formation in: Ho, P.; Coltrin, M. E.; Binkley, J. S.; Melius, C. F. *J. Phys. Chem.* **1985**, *89*, 4647.

[b] Reference 13.

Figure Captions

Figure 1. Diagram of the instrument used in this work. (a) Cutaway view of the instrument showing the pyrolyzer, scattering chamber, electron energy analyzer, and quadrupole mass spectrometer. (b) Detail of the flash vacuum pyrolyzer.

Figure 2. Photoelectron spectra of SiH_2Cl_2 under flash vacuum pyrolysis conditions at three different temperatures. (a) Room temperature: This room temperature spectrum is in agreement with the published spectrum of SiH_2Cl_2 [Frost, D. C.; Herring, F. G.; Katrib, A.; McLean A. N.; Drake, J. E.; Westwood, N. P. C. *Can. J. Chem.* **1971**, *49*, 4033]. (b) 720 °C. (c) 780 °C.

Figure 3. Comparison of the photoelectron spectrum of $SiCl_2$, (a), obtained from the pyrolysis of $SiCl_4$ over solid Si (reference 10), with the photoelectron spectrum of SiH_2Cl_2 pyrolyzed at 850 °C (b). Kr and HCl are also present in the SiH_2Cl_2 pyrolysis products spectrum, but $SiCl_2$ is clearly a major component of the product mixture.

Figure 4. Mass spectra of the pyrolysis of SiH_2Cl_2 at three temperatures. (a) Room temperature. (b) 600 °C. (c) 900 °C.

Figure 5. Mass spectra of the pyrolysis of $SiHCl_3$ at three temperatures. (a) Room temperature. (b) 850 °C. (c) 1100 °C.

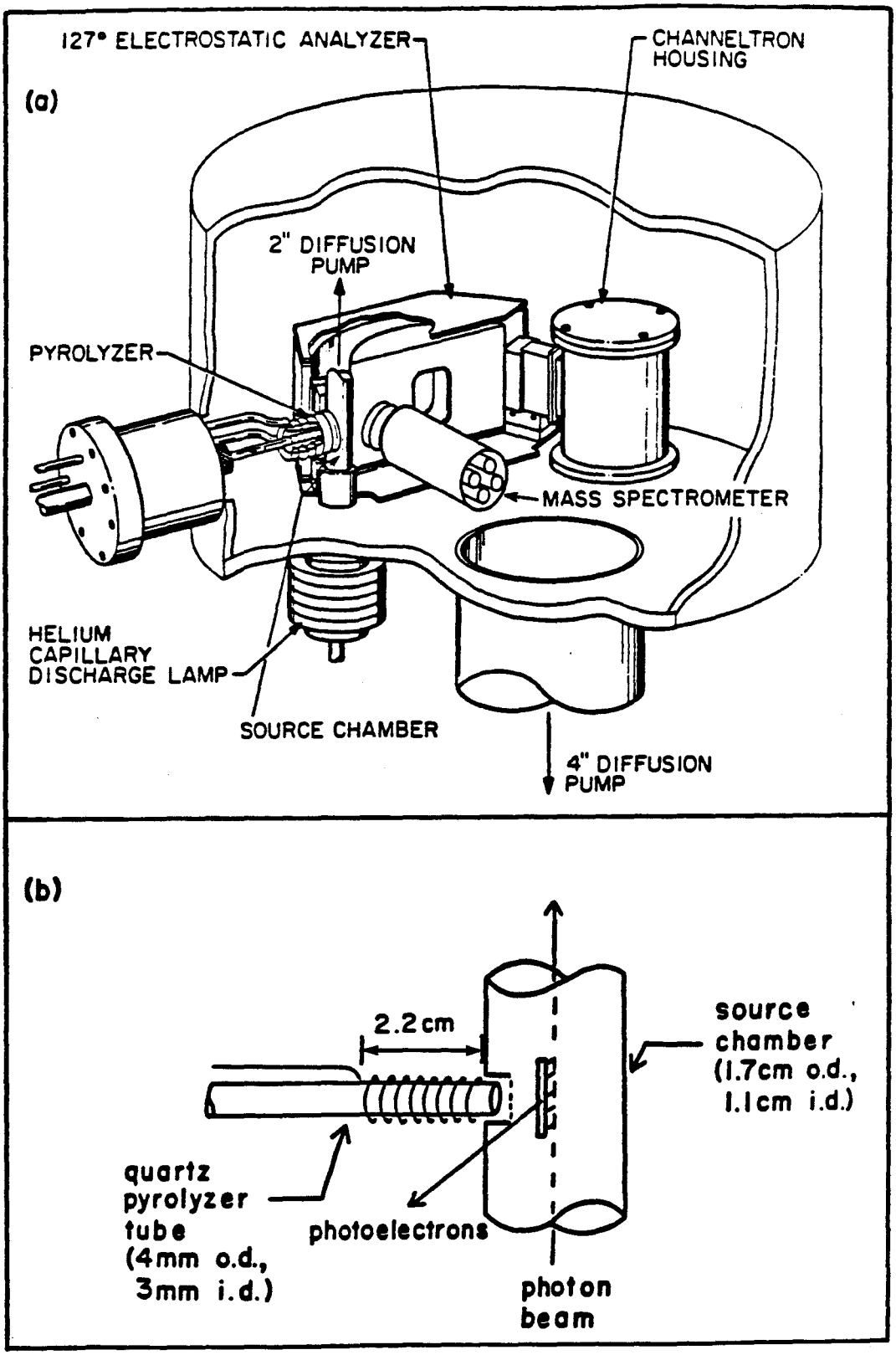
(a)
127° ELECTROSTATIC ANALYZER
CHANNELTRON HOUSING
2" DIFFUSION PUMP
PYROLYZER
MASS SPECTROMETER
HELIUM CAPILLARY DISCHARGE LAMP
SOURCE CHAMBER
4" DIFFUSION PUMP
(b)
2.2cm
source chamber (1.7cm o.d., 1.1cm i.d.)
quartz pyrolyzer tube (4mm o.d., 3mm i.d.)
photoelectrons
photon beam

Figure 1

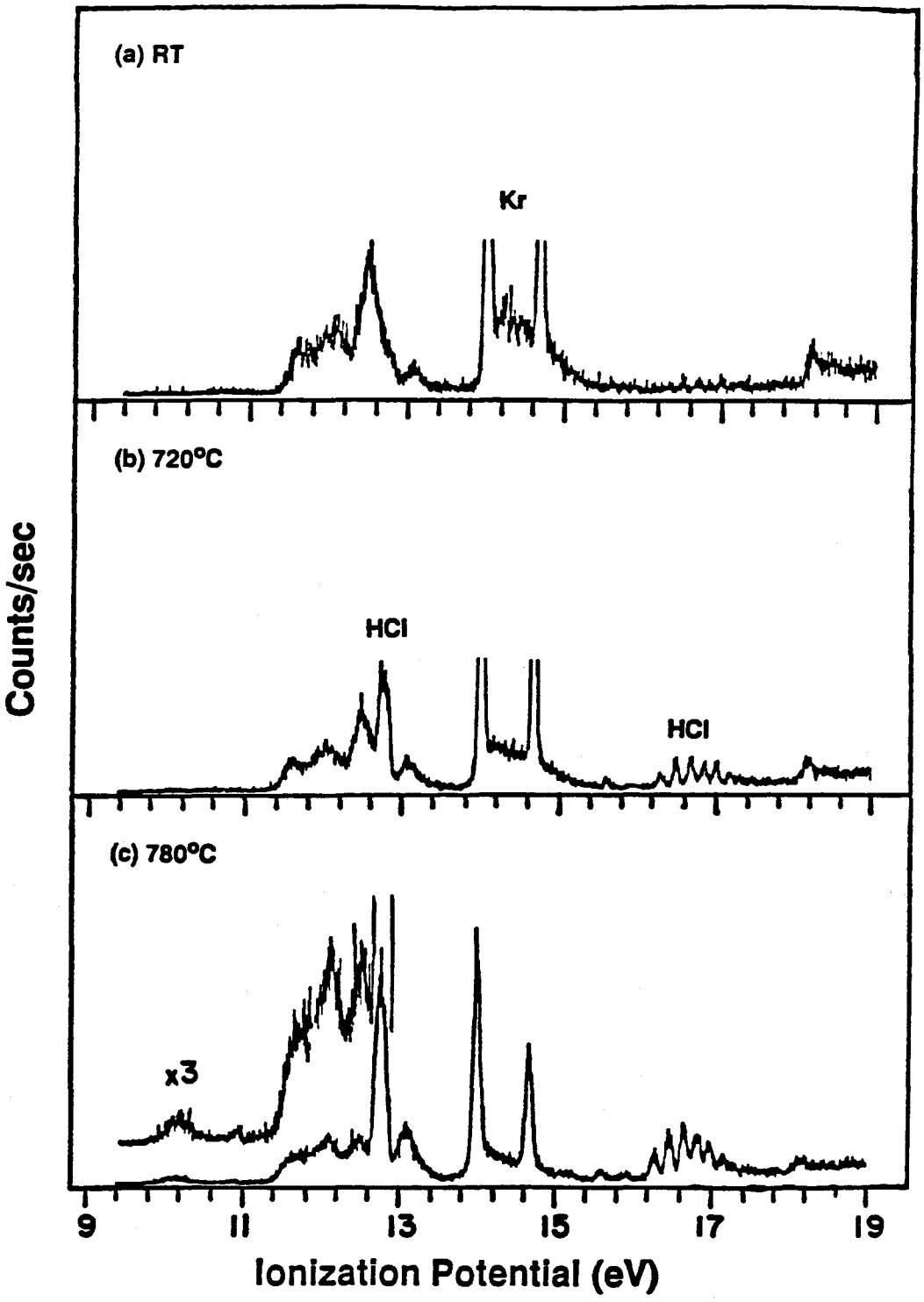
(a) RT
Kr
(b) 720°C
HCl
HCl
(c) 780°C
x3
Counts/sec
9
11
13
15
17
19
Ionization Potential (eV)

Figure 2

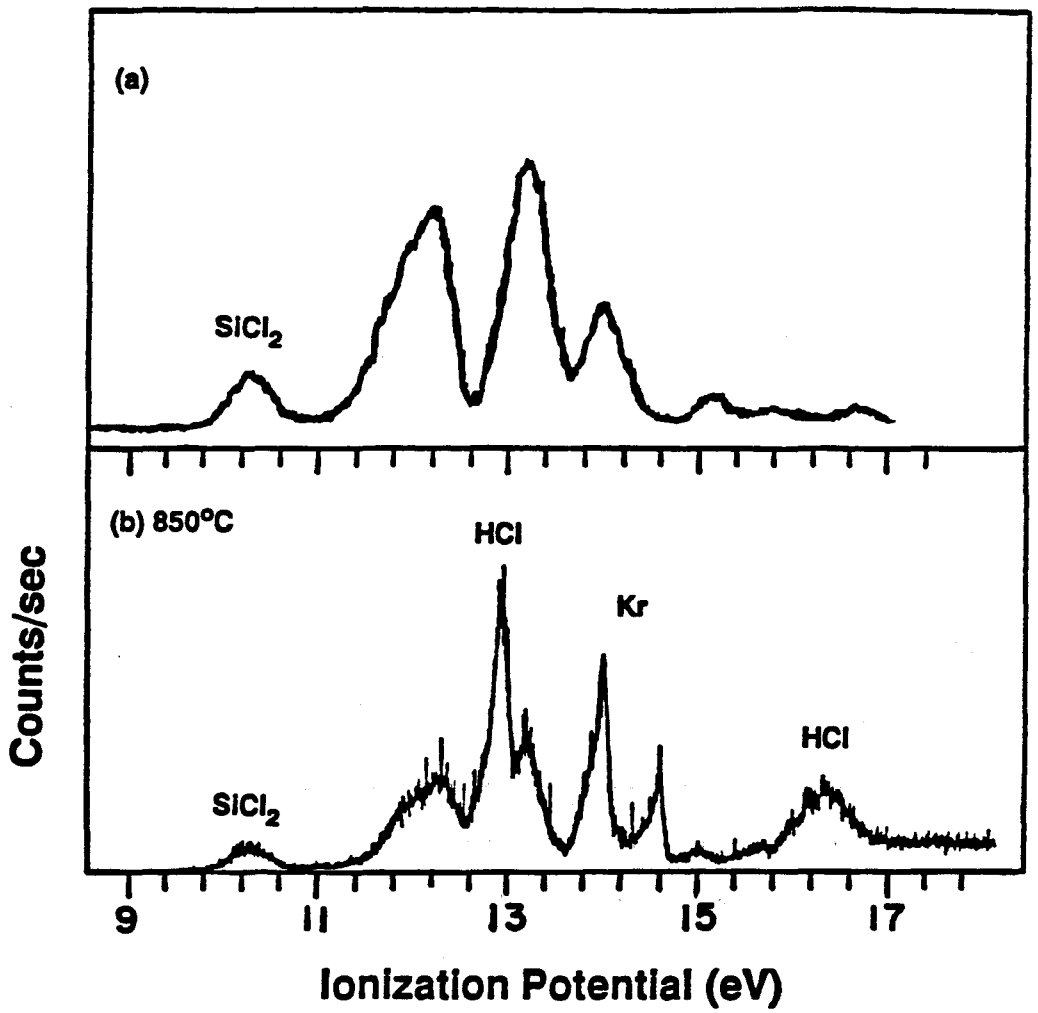
(a)
$SiCl_2$
(b) 850°C
HCl
Kr
HCl
$SiCl_2$
Counts/sec
9
11
13
15
17
Ionization Potential (eV)

Figure 3

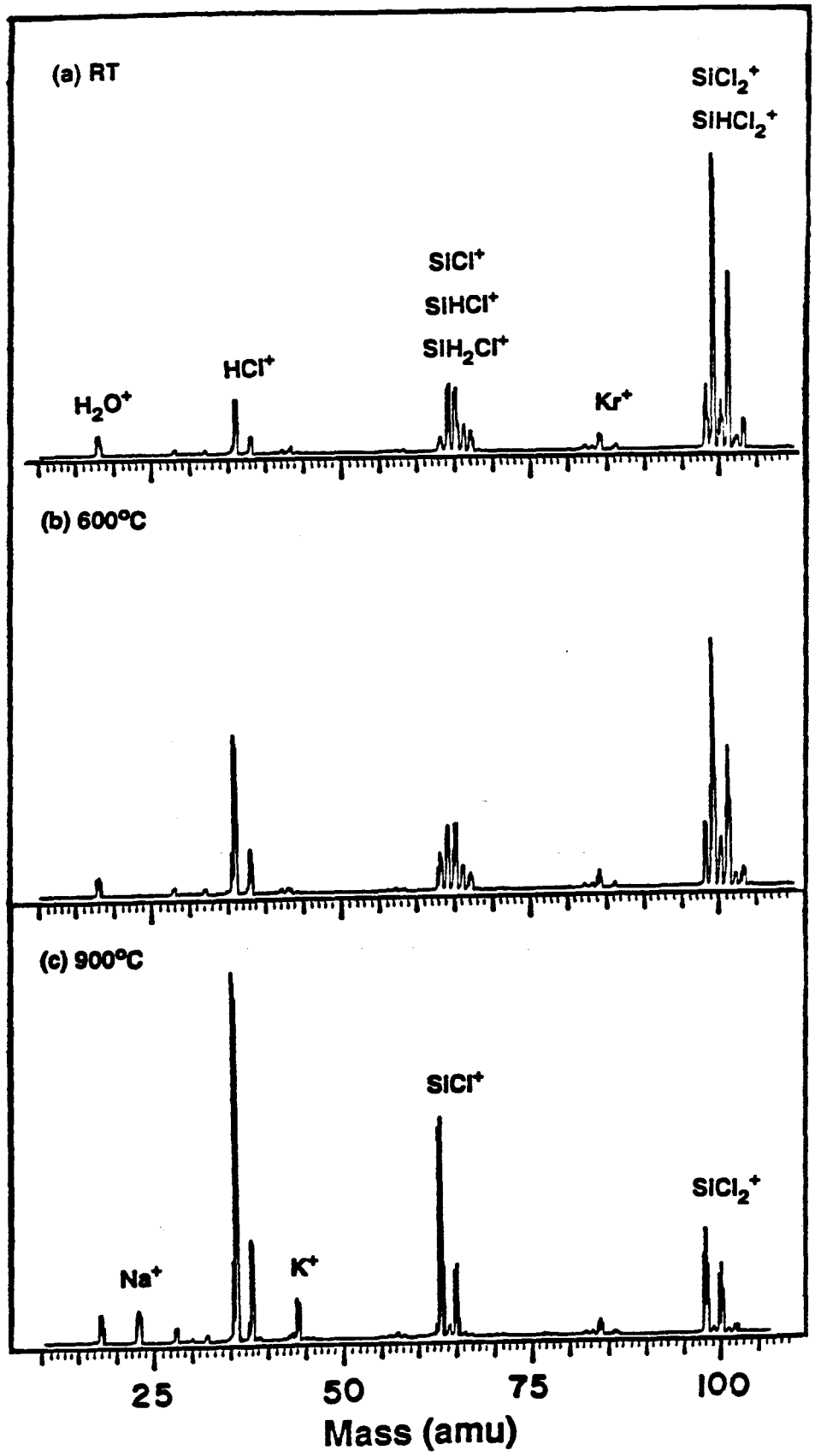
(a) RT
$SiCl_2^+$
$SiHCl_2^+$
$SiCl^+$
$SiHCl^+$
SiH_2Cl^+
HCl^+
H_2O^+
Kr^+
(b) 600°C
(c) 900°C
$SiCl^+$
$SiCl_2^+$
Na^+
K^+
25
50
75
100
Mass (amu)

Figure 4

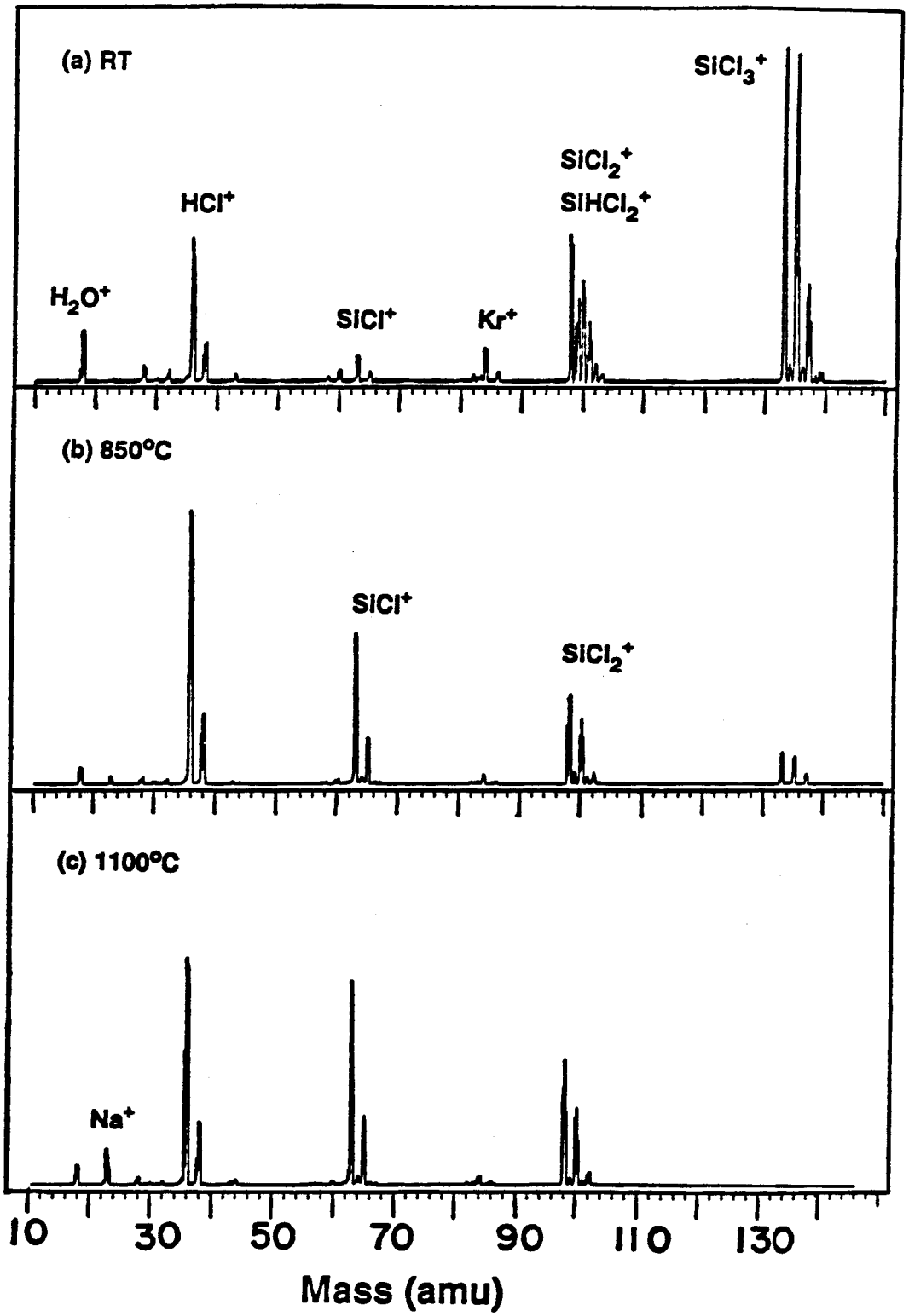
(a) RT
$SiCl_3^+$
$SiCl_2^+$
$SiHCl_2^+$
HCl^+
H_2O^+
$SiCl^+$
Kr^+
(b) 850°C
$SiCl^+$
$SiCl_2^+$
(c) 1100°C
Na^+
10
30
50
70
90
110
130
Mass (amu)

Figure 5

Chapter V

Singlet-Triplet Energy Gaps in Fluorine-Substituted Methylenes and Silylenes

Singlet-Triplet Energy Gaps in Fluorine-Substituted Methylenes and Silylenes

Seung Koo Shin, William A. Goddard III, and J. L. Beauchamp

Contribution No. 7894 from the Arthur Amos Noyes Laboratory of Chemical Physics, California Institute of Technology, Pasadena, California 91125

Abstract

We report singlet and triplet state splittings (ΔE_{ST}) for fluorine-substituted *methylenes* and *silylenes* using Dissociation-Consistent Configuration Interaction (DCCI) wavefunctions. These relatively simple CI calculations, starting with generalized valence bond wavefunctions, emphasize *correlation consistency* between the singlet and triplet states. Values of ΔE_{ST} for CH_2, CF_2, SiH_2, and SiF_2 are in excellent agreement with available experimental results [theory (T_e): −10.0, 57.1, 21.4, and 76.6 kcal/mol; experiment (T_e): −9.215, 56.7, 20.7, and 76.2 kcal/mol], and we expect the predictions for the other cases CHF(14.5) and SiHF(41.3) to be equally accurate. This result strongly suggests that the correct choice among the experimental values for ΔE_{ST} of CHF is 14.7 ± 0.2 kcal/mol.

I. INTRODUCTION

The structures, spectra, and reactivities of *methylenes* and *silylenes* have been of considerable experimental and theoretical interest.[1] The diverse chemical properties of *methylenes* and *silylenes* are strongly dependent upon the spin multiplicities of their low lying electronic states and the interstate energy gaps. The energetics of these low lying electronic states are prerequisite to understanding the chemistry of *methylenes* and *silylenes*. The parent molecules CH_2 and SiH_2 have been extensively studied, and their singlet-triplet energy gaps, ΔE_{ST}, have been determined to be -8.998 ± 0.014 and 21.0 ± 0.7 kcal/mol, respectively, from experiments[2,3] and corroborated by theoretical calculations[4] (a positive value indicates a singlet ground state). However, there are only a few experimental data for the singlet-triplet energy gaps of the fluorine-substituted *methylenes* and *silylenes*.[5-7] A value of 56.7 kcal/mol for $\Delta E_{ST}(CF_2)$ has been determined directly from observations of the $\tilde{a}\ ^3B_1 \rightarrow \tilde{X}\ ^1A_1$ phosphorescence transition of the triplet difluoromethylene produced in the reaction of oxygen atoms with tetrafluoroethylene in the gas phase.[5] A singlet-triplet splitting of 75.2 kcal/mol (or possibly 76.2 or 77.2) for SiF_2 has been assigned from the $\tilde{a}\ ^3B_1 \rightarrow \tilde{X}\ ^1A_1$ emission spectrum observed from a high frequency electrodeless discharge of flowing tetrafluorosilane.[6] The most recent photoelectron spectroscopic studies of the halocarbene anions yield bounds for ΔE_{ST} of the halocarbenes.[7] These studies suggest $\Delta E_{ST}(CHF)$ to be 14.7 ± 0.2, 11.4 ± 0.3, or 8.1 ± 0.4 kcal/mol (with 11.4 chosen as most likely) and a lower bound on $\Delta E_{ST}(CF_2)$ to be 50 ± 2 kcal/mol. No experimental observation exists for $\Delta E_{ST}(SiHF)$.

Previous theoretical values for ΔE_{ST} of the fluorine-substituted *methylenes* and *silylenes* are available at various calculational levels. Bauschlicher et al.[8] obtained ΔE_{ST} of 9.2 and 46.5 kcal/mol for CHF and CF_2, respectively, with relatively simple wavefunctions [Hartree-Fock (HF) for the triplet and GVB(1/2) for the singlet] using double-ζ plus polarization (DZP) basis sets. Dixon[9] also examined ΔE_{ST} of several fluorine-substituted carbenes at the same calculational level [with valence double-ζ

plus polarization (VDZP) basis sets] yielding 8.1 and 46.0 kcal/mol for CHF and CF_2, respectively. Colvin et al.[10] evaluated ΔE_{ST} of 37.7 and 73.5 kcal/mol for SiHF and SiF_2, respectively, using CI-SD (configuration interaction with all single and double excitations from HF) and the DZP basis. Krogh-Jespersen[11] also reported ΔE_{ST} of 73.8 kcal/mol for SiF_2 from CI-SD/6-31G* calculations. Luke et al.[12] calculated ΔE_{ST} of 12.7 and 37.7 kcal/mol for CHF and SiHF, respectively, at the MP4SDTQ (Møller-Plesset fourth-order perturbation theory) level using 6-31G* basis sets. Scuseria et al.[13] used CI-SD calculations with a triple-ζ basis augmented by two sets of polarization functions (TZ2P) to obtain 12.9 kcal/mol for ΔE_{ST}(CHF). From comparison of theoretical results outlined above with available experimental data, it is clear that all of the methods used above tend to underestimate ΔE_{ST} of singlet ground states of fluorine-substituted *methylenes* and *silylenes* due either to unbalanced levels of electron correlation for both singlet and triplet states or to basis set limitations. Recently, Carter and Goddard[14] proposed the correlation-consistent CI (CCCI) method for systematically obtaining excitation energies in substituted carbenes with the smallest CI wavefunctions. They reported values of 17.7 and 57.5 kcal/mol for ΔE_{ST} of CHF and CF_2, respectively.

Herein, we devise new level of CI that is correlation-consistent for both singlet and triplet states and balances their relative stabilities while retaining relative simplicity. Section II explains this dissociation-consistent configuration interaction (DCCI) method; Section III reports new results of ΔE_{ST} for CH_2, CHF, CF_2, SiH_2, SiHF, and SiF_2 obtained from the DCCI method. The convergence of the DCCI method with basis set in ΔE_{ST} of CH_2, SiH_2, and CHF is also included in Section III.

II. THEORETICAL METHODS

A. Basis sets

For the calculations of the singlet-triplet state splittings at various CI levels, we employed core double-ζ valence triple-ζ basis sets for carbon $(10s6p/5s3p)$[15,16] and

silicon $(11s7p/7s5p)$[17], augmented with two sets of d polarization functions centered at 0.62 for carbon and 0.42 for silicon with an internal ratio of 2.3 [ζ^d(C) = 0.940 and 0.409, ζ^d(Si) = 0.637 and 0.277]. In addition, one set of f functions was included, obtained by scaling the mean d exponents of 0.62 for carbon and 0.42 for silicon by 1.2 [ζ^f(C) = 0.893 and ζ^f(Si) = 0.605]. The s combination of d functions and p combination of f functions were excluded from all basis sets. Valence double-ζ basis sets[18] were used for hydrogen ($4s/2s$; scaled by 1.2 for hydrogen attached on carbon and unscaled for hydrogen attached on silicon) and fluorine ($9s5p/3s2p$), augmented with one set of p functions on hydrogen (ζ^p = 1.0 and 0.6 for hydrogen attached on carbon and silicon, respectively) and one set of d functions on fluorine (ζ^d = 0.9).

We also used the following basis sets for carbon, silicon, hydrogen, and fluorine to examine the convergence of ΔE_{ST} of CH_2, CHF, and SiH_2 with basis set:

C($3s2p1d$) and Si($4s3p1d$): Valence double-ζ basis sets were used for carbon $(9s5p/3s2p)$[18] and silicon $(11s7p/4s3p)$[19] augmented with one set of d functions on carbon (ζ^d = 0.62) and silicon (ζ^d = 0.42).

C($6s4p2d1f$): To the C($5s3p2d1f$) basis described above was added one set of diffuse s (ζ^s = 0.046) and p (ζ^p = 0.033) functions.

C($7s4p3d2f$): The Huzinaga ($11s7p$) basis[20] for carbon was contracted to ($6s3p$) triple-ζ for both core and valence, but diffuse s and p functions (ζ^s = 0.0388 and ζ^p = 0.0282) were added.[21] Three sets of carbon d polarization functions were added, centered at 0.620 with an internal ratio of 2.5 (leading to exponents ζ^d = 1.550, 0.620, and 0.248). Two sets of carbon f functions were included, centered at the previous f exponent of 0.893 with an internal ratio of 2.5 (ζ^f = 1.412 and 0.565).

H($3s2p$): The Huzinaga unscaled ($6s$) basis[16] was contracted to triple-ζ, with two sets of p functions centered at 1.0 with an internal ratio of 2.3 (ζ^p = 1.517 and 0.659).

H($3s2p1d$): To the H($3s2p$) basis was added one set of d functions ($\zeta^d = 1.0$).

F($5s3p2d1f$): The Dunning core double-ζ valence triple-ζ contractions[15] of the Huzinaga ($10s6p$) basis[16] were used with two sets of d functions centered at 0.90 with an internal ratio of 2.3 ($\zeta^d = 1.365$ and 0.593). In addition, one set of f functions was included, obtained by scaling the mean d-exponent of 0.90 by 1.2, yielding $\zeta^f = 1.296$.

B. Geometries

The geometries for *methylenes* in Table I were taken from the calculations of Harding and Goddard[22] (CH_2), Scuseria et al.[13] (CHF), and Bauschlicher et al.[8] (CF_2). The equlibrium geometries for the substituted *silylenes* were calculated at the MP2/6-31G** level using the Gaussian 86 program[23] and are listed in Table I with available experimental data.[24] For the singlet states of SiH_2 and SiF_2, the predicted bond angles are within 0.3° of the experimental values, while the Si−H and Si−F bond distances are longer than the experimental values by 0.008 and 0.026 Å, respectively.

C. DCCI Calculations

We have followed the philosophy of the CCCI methods previously described by Bair, Carter, and Goddard.[14,25] These approaches start with the generalized valence bond wavefunction (GVB), in which the carbene lone pair and the two bond pairs are correlated, followed by a small CI based on the GVB orbitals.[14] In order to calculate an accurate bond energy for a halogen-substituted double-bonded molecule, XYC = CZW, the DCCI prescription is to solve first for the GVB-PP (6/12) wavefunction in which the double bond and the four carbon-ligand bonds are correlated. In order to mimic the full GVB wavefunction in which various spin couplings (resonance structures) are included, we carry out a restricted CI (GVB-CI) in which all configurations having two electrons in each correlated pair are included. Since the orbitals of the double bond change dramatically as the bond is dissociated, we allow all quadruple excitations out of the double bond to obtain the wavefunction

RCI*SDTQ($\sigma\pi$). This allows (XYC) = (CZW) to dissociate smoothly to the wavefunction RCI*SD($\sigma\pi$) on each carbene fragment, leading to a consistent description for dissociation of the double bond. Carter and Goddard[14] showed that to obtain accurate ΔE_{ST} for halogen-substituted carbenes, the GVB-RCI must allow resonance structures in which the π-lone pair electrons in the CI can delocalize into the carbon π orbital. This leads to the RCI*[ΠCI + SDTQ($\sigma\pi$)] wavefunction for XYC = CZW, which dissociates to RCI*[ΠCI + SD($\sigma\pi$)] on each carbene product, designated as the CCCI by Carter and Goddard.[14] If calculated self-consistently, these wavefunctions would lead to accurate bond energies. However, since the orbitals are calculated at the GVB-PP level, we should also include all single excitations from the GVB-RCI wavefunction (S_{val}) to mimic the effects of full self-consistency. This leads to RCI*[ΠCI + S_{val} + SDTQ($\sigma\pi$)] for XYC = CZW. This choice of the wavefunction for CXY is so that as the double bond length in XYC = CXY is increased to R = ∞, it changes smoothly to the RCI*[ΠCI + S_{val} + SD($\sigma\pi$)] wavefunction for the carbenes. Thus we refer to this as DCCI. This DCCI wavefunction leads to a description of the carbenes that differs from the CCCI description only by inclusion of all single excitations from the GVB-RCI wavefunction (S_{val}). We find that this inclusion of S_{val} is important to properly balance the relative stabilities of the singlet and triplet states.

III. RESULTS

The values for ΔE_{ST} of CH_2, CHF, CF_2, SiH_2, SiHF, and SiF_2 using the DCCI method are shown in Table II with available experimental data and previous theoretical results. Table III summarizes the convergence of singlet-triplet state splittings of CH_2, CHF, and SiH_2 with basis set.

A. CH_2

The best estimate for the singlet-triplet splitting of CH_2 using the DCCI, is −9.99 kcal/mol, in reasonable agreement with experiment[2] (T_e = −9.215 kcal/mol). [DCCI consists of 11129/19758 spatial configurations/spin eigenfunctions for the

singlet state and 8120/23344 for the triplet state with 75 basis functions (nbfs) and C_s symmetry.] We believe that the remaining discrepancy of 0.7 kcal in ΔE_{ST} is mainly due to incompleteness of the basis set. Using 120 nbfs in C_{2v} symmetry with the CASSCF-SOCI involving over 700,000 configuration state functions, Bauschlicher *et al.*[4] obtain −9.24 kcal/mol, in essentially exact agreement with the experiment.

As indicated in Table III the values of ΔE_{ST} decrease smoothly as the basis is extended. For the HF wavefunction, the total change in ΔE_{ST} between the VDZ*p* basis (nbfs = 25) and the extended basis set (nbfs = 75) is 1.18 kcal/mol, while it is 3.52 kcal/mol for the GVB-RCI and 3.09 kcal/mol for the DCCI. For CASSCF-SOCI, the change in ΔE_{ST} is 2.73 kcal/mol between the C(4*s*2*p*1*d*)/H(2*s*1*p*) basis[26] (nbfs = 26) and the C(5*s*4*p*3*d*2*f*1*g*)/H(4*s*3*p*2*d*) basis[4] (nbfs = 120). This result indicates that the relatively simple DCCI have correlation consistency for both singlet and triplet states, correctly balance their relative stabilities, and are comparable to the big CASSCF-SOCI calculations.

B. CHF

Our best estimate for the singlet-triplet splitting of CHF using the DCCI with the extended basis set is 14.48 kcal/mol. Murray et al.[7] reported three possible triplet excitation energies of 14.7 ± 0.2, 11.4 ± 0.3, and 8.1 ± 0.4 kcal/mol from the photoelectron spectroscopic studies of CHF^- and suggested that 11.4 is the most likely (with 14.7 due to a hot band). The present calculational result strongly suggests that the actual singlet-triplet splitting of CHF is 14.7 ± 0.2 kcal/mol. [The DCCI with 87 nbfs consists of 15020/26972 spatial configurations/spin eigenfunctions for the singlet state and 10943/36787 for the triplet state.] The CI-SD calculations of CHF by Scuseria et al.[13] with the triple-ζ plus double polarization basis sets (67 nbfs) [involving 119604 and 73581 configurations for the singlet and triplet states] yielded ΔE_{ST} of 12.9 kcal/mol. Although possessing more configurations, CI-SD tend to underestimate the singlet state of CHF due to the higher electron

correlation error in the HF singlet state.

As indicated in Table III, the values of ΔE_{ST} vary smoothly as the basis is extended. For the uncorrelated HF wavefunction, the total change in ΔE_{ST} between the VDZp basis (nbfs = 35) and the extended basis set (nbfs = 87) is 0.20 kcal/mol, while it is 2.17 kcal/mol for the GVB-RCI and 2.09 kcal/mol for the DCCI. It is clear that the extension of the carbon basis is most important because the singlet-triplet splitting involves an electronic excitation between the nonbonding σ and π orbitals of the center carbon atom. The extension of hydrogen and/or fluorine basis exerts little influence on the singlet-triplet splitting of CHF.

C. CF_2

Using DCCI, the singlet-triplet splitting of CF_2 is 57.1 kcal/mol, in excellent agreement with the experimental result of 56.7 kcal/mol by Koda.[5]

D. SiH_2

The DCCI results in a singlet-triplet splitting for SiH_2 of 21.5 kcal/mol, in excellent agreement with the experiment[3] ($T_e = 20.7 \pm 0.7$ kcal/mol). [This DCCI wavefunction with 74 nbfs has 10148/17966 spatial configurations/spin eigenfunctions for singlet and 7373/21229 for triplet with C_s symmetry.] The DCCI result is comparable to the value of 20.38 kcal/mol obtained from the big CASSCF-SOCI+Q with 124 nbfs by Bauschlicher *et al.*[4] [The largest SOCI expansions involve over 700,000 configuration state functions in C_{2v} symmetry.]

As indicated in Table III, the values of ΔE_{ST} decrease smoothly as the basis is extended. For the uncorrelated HF wavefunction, the total change in ΔE_{ST} between the VDZp basis (nbfs = 29) and the extended basis set (nbfs = 74) is 0.33 kcal/mol, while it is 1.41 kcal/mol for the GVB-RCI and 2.72 kcal/mol for the DCCI. For CASSCF-SOCI+Q, the change in ΔE_{ST} is 2.87 kcal/mol between the Si($5s3p1d$)/H($2s1p$) basis[27] (nbfs = 36) and the Si($6s5p3d2f1g$)/H($4s3p2d$) basis[4] (nbfs = 124).

E. SiF_2

The singlet-triplet splitting of SiF_2 is 76.6 kcal/mol. [The DCCI involves 10685/19089 configurations/spin eigenfunctions for the singlet state and 7199/28879 for the triplet state with 74 nbfs and C_s symmetry.] The $\tilde{a}\ ^3B_1 \rightarrow \tilde{X}\ ^1A_1$ emission spectrum has been observed from a high frequency electrodeless discharge of flowing tetrafluorosilane.[6] The band origin at 26310 cm^{-1} with long vibrational progressions involving the bending frequency of $\omega'' = 343$ cm^{-1} has been assigned from a Deslandres Table without a Franck-Condon analysis. Since the observed transition involves a large change (18.2°) in the bond angle from the triplet to singlet states, the observed long vibrational progressions are reasonable. However, it is quite possible that weak features due to the band origin may be unobserved. Therefore, the correct band origin would be $26310 + 343n$ cm^{-1}, where $n = 0$, 1, or 2. Thus, in addition to the assigned value of $\Delta E_{ST} = 75.2$ kcal/mol, we must also consider 76.2 and 77.2 kcal/mol as possibilities. The present DCCI result suggests the actual singlet-triplet splitting of SiF_2 to be 76.2 kcal/mol. The previous CI-SD calculations on SiF_2 by Colvin et al.[10] with the double-ζ plus polarization basis sets (56 nbfs) involved more configurations (23009 and 14300 for the singlet and triplet states), but we conclude that CI-SD underestimates ΔE_{ST} by 2.7 kcal/mol.

F. SiHF

The DCCI predicts the singlet-triple splitting of SiHF to be 41.3 kcal/mol. [With 64 nbfs, this leads to 7739/13653 spatial configuration/spin eigenfunctions for the singlet state and 5297/19001 for the triplet state.] The previous CI-SD calculations on SiHF by Colvin et al.[10] with double-ζ plus polarization basis set (45 nbfs) [involving 13780 and 9156 for configurations for the singlet and triplet states] resulted in ΔE_{ST} of 37.7 kcal/mol. The MP4-SDTQ calculations using 6-31G* basis sets by Luke et al.[12] yielded ΔE_{ST} of 37.7 kcal/mol. We believe that these levels of theory underestimate the ΔE_{ST} of SiHF by 3 kcal/mol.

Comparing our calculations on CHF, CF_2, and SiF_2 with experiment [theory

(T_e): 14.5, 57.1, and 76.6 kcal/mol, experiment (T_e): 14.6, 56.7, and 76.2 kcal/mol], we estimate that the experimental value for SiHF is 41.3 ± 0.5 kcal/mol.

IV. DISCUSSION

The agreement between the relatively simple DCCI and the experiment is excellent where experimental ΔE_{ST}'s are available (CH_2, SiH_2, and CF_2). The DCCI result (14.5 kcal/mol) for the singlet-triplet splitting of CHF strongly suggests that the correct choice of experimental value is 14.7 ± 0.2 kcal/mol and suggests that the correct choice of experimental value for SiF_2 is 76.2 kcal/mol. We predict that ΔE_{ST} = 41.3 ± 0.5 kcal/mol for SiHF.

It is clear that fluorine substitution in place of hydrogen drastically stabilizes singlet state carbenes. Factors favoring singlet ground states by the fluorine substitution are (i) the donation of $p\pi$ lone pair electrons into an empty carbon or silicon $p\pi$ orbital of the singlet state and (ii) the increase of s-character in the nonbonding σ orbital due to the electron-withdrawing substitution.[14] The contribution of the $p\pi$ lone pair donation to the stabilization of the singlet state may be estimated from the difference between ΔE_{ST} at the RCI and that at the RCI*ΠCI shown in Table II (2.9 and 4.6 kcal/mol for CHF and CF_2; 0.4 and 0.7 kcal/mol for SiHF and SiF_2, respectively). The ΠCI contributions are greater for CHF and CF_2 than their silicon analogs because of the smaller C–F bond distance [r(C–F) ≅ 1.30 Å and r(Si–F) ≅ 1.62 Å; see Table I]. A quantitative indication of the s and p contributions may be evaluated by the Mulliken population analysis.[28] Table IV summarizes the total charges on each atom, the bond populations on the center atom, and the hybridizations in various orbitals of the center atom. The s character in the bonding orbitals varies slightly with fluorine substitution for single state carbenes (from 18.9% s in CH_2 to 17.6% s in CF_2 and from 18.2% s in SiH_2 to 21.8% s in SiF_2) but decreases significantly for triplet states (from 50.8% s in CH_2 to 45.0% s in CF_2 and from 51.4% s in SiH_2 to 42.6% s in SiF_2). For singlet state carbenes, the s contributions in the nonbonding σ orbitals increase slightly (~ 7%) from CH_2 to CF_2 or SiH_2 to

SiF_2. In contrast, fluorine substitution in triplet state carbenes greatly enhances s character in nonbonding σ orbitals (by $\sim$ 31%). This result indicates that the electron-withdrawing fluorine substitution induces an increase of s character in the nonbonding σ orbital of the center atom, stabilizing the σ orbital relative to the π orbital and disfavoring the triplet state due to the greater loss of $\sigma \rightarrow \pi$ excitation energy than the gain by the triplet exchange interaction.

The basis sets convergence tests of DCCI shows that basis extension of the center atom is most important. This is plausible since the process of interest involves electronic excitation between the nonbonding σ and π orbitals of the center atom. Thus, for CF_2, SiHF, and SiF_2, we employed the extended basis sets for carbon and silicon while utilizing the valence double-ζ plus polarization basis for hydrogen and fluorine. This choice of basis sets was large enough to yield accurate values of ΔE_{ST}. The very slow convergence in CH_2 compared with the rapid convergence in CHF and SiH_2 may be attributed to the electronegative charge population of the carbon in CH_2, as shown in Table IV. The electronegative carbon in CH_2 apparently requires more diffuse basis functions than the electropositive carbon and silicon in CHF and SiH_2.

V. CONCLUSIONS

Ab initio GVB-DCCI calculations have been carried out to estimate the singlet-triplet splittings for fluorine-substituted *methylenes* and *silylenes*. The relatively simple DCCI wavefunctions emphasizing correlation consistency in the double bond breaking process shows correlation consistency for both singlet and triplet states of carbene fragments. Hence, DCCI correctly balances relative stabilities of the singlet and triplet states of carbenes and leads to accurate singlet-triplet splittings. The convergence test of the DCCI method with basis sets reveals that the basis extension of the center atom is most important, allowing modest basis sets to be essentially complete for ΔE_{ST}. We find that a negatively-charged center atom requires more diffuse basis functions than the positively-charged center atom to obtain comparable

accuracy.

Acknowledgments.

We wish to acknowledge the support of the National Science Foundation under Grant Nos. CHE87-11567(J.L.B.) and CHE83-18041(W.A.G.).

References

(1) For reviews, see *Reactive Intermediates*, edited by R. A. Moss and M. Jones (Wiley, New York, 1985), Vol.3, and earlier references therein.

(2) P. Jensen and P. R. Bunker, J. Chem. Phys. **89**, 1327 (1988), and earlier references therein.

(3) J. Berkowitz, J. P. Greene, H. Cho, and B. Ruscic, J. Chem. Phys. **86**, 1235, (1987).

(4) C. W. Bauschlicher, Jr. and S. R. Langhoff, J. Chem. Phys. **87**, 387 (1987), and earlier references therein.

(5) (a) S. Koda, Chem. Phys. Lett. **55**, 353 (1978); (b) S. Koda, Chem Phys. **66**, 383 (1986).

(6) D. R. Rao, J. Mol. Spectry **34**, 284 (1970).

(7) K. K. Murray, D. G. Leopold, T. M. Miller, and W. C. Lineberger, J. Chem. Phys. **89**, 5442 (1988).

(8) C. W. Bauschlicher, Jr., H. F. Schaefer III, and P. S. Bagus, J. Am. Chem. Soc. **99**, 7106 (1977).

(9) D. Dixon, J. Phys. Chem. **90**, 54 (1986).

(10) M. E. Colvin, R. S. Grev, and H. F. Schaefer III, Chem. Phys. Lett. **99**, 399 (1983).

(11) K. Krogh-Jespersen, J. Am. Chem. Soc. **107**, 537 (1985).

(12) B. T. Luke, J. A. Pople, M.-B. Krogh-Jespersen, Y. Apeloig, M. Karni, J. Chandrasekhar, and P. v. R. Schleyer, J. Am. Chem. Soc. **102**, 7644 (1980).

(13) G. E. Scuseria, M. Durán, R. G. A. R. Maclagan, and H. F. Schaefer III, J. Am. Chem. Soc. **108**, 3248 (1986).

(14) E. A. Carter and W. A. Goddard III, J. Chem. Phys. **88**, 1752 (1988).

(15) T. H. Dunning, Jr., J. Chem. Phys. **55**, 716 (1970).

(16) S. Huzinaga, J. Chem. Phys. **42**, 1293 (1965).

(17) One set diffuse s ($\zeta^s = 0.03648$) and p ($\zeta^p = 0.02808$) were added to the Si($11s7p/6s4p$) basis (reference 18).

(18) T. H. Dunning, Jr. and P. J. Hay, in *Methods of Electronic Structure Theory*, edited by H. F. Schaefer III (Plenum Press, New York, 1977), Chap. 1.

(19) *Gaussian Basis Sets for Molecular Calculations*, edited by S. Huzinaga (Elsevier, Amsterdam, 1984).

(20) S. Huzinaga and Y. Sakai, J. Chem. Phys. **50**, 1371 (1969).

(21) E. A. Carter and W. A. Goddard III, J. Chem. Phys. **86**, 862 (1987).

(22) L. B. Harding and W. A. Goddard III, Chem. Phys. Lett. **55**, 217 (1978).

(23) M. J. Frisch, J. S. Binkley, H. B. Schlegel, K. Raghavachari, C. F. Melius, R. L. Martin, J. J. P. Stewart, F. W. Bobrowicz, C. M. Rohlfing, L. R. Kahn, D. J. Defrees, R. Seeger, R. A. Whiteside, D. J. Fox, E. M. Fleuder, and J. A. Pople, *Gaussian 86* (Carnegie-Mellon Quantum Chemistry Publishing Unit, Pittsburgh, 1984).

(24) M. D. Harmony, V. W. Laurie, R. L. Kuczkowski, R. H. Schwendeman, D. A. Ramsay, F. J. Lovas, W. J. Lafferty, and A. G. Maki, J. Phys. Chem. Ref. Data **8**, 619 (1979).

(25) (a) R. A. Bair, Ph. D. thesis, California Institute of Technology, 1981; (b) E. A. Carter and W. A. Goddard III, J. Am. Chem. Soc. **110**, 4077 (1988).

(26) C. W. Bauschlicher, Jr. and P. R. Taylor, J. Chem. Phys. **85**, 6510 (1986).

(27) C. W. Bauschlicher, Jr. and P. R. Taylor, J. Chem. Phys. **86**, 1420 (1987).

(28) Mulliken populations were obtained by summing over the electron populations of each carbon s, p, and d basis function within each natural orbital for each GVB pair. Although this analysis tends to be basis-dependent and at best provides a qualitative indication of charge transfer, relative trends and qualitative comparisons are expected to be reliable.

Table I. Geometries of fluorine-substituted methylenes and silylenes. [a]

molecule	state	r(C,Si–H) (Å)	r(C,Si–F) (Å)	Angle (degree)
CH_2 [b]	$^1A_1$	1.113		101.8
	$^3B_1$	1.084		133.2
CHF [c]	$^1A'$	1.104	1.294	103.3
	$^3A''$	1.073	1.304	121.1
CF_2 [d]	$^1A_1$		1.291	104.7
	$^3B_1$		1.303	118.2
SiH_2	$^1A_1$	1.508 (1.516[e])		92.4 (92.1[e])
	$^3B_1$	1.471		118.2
SiHF	$^1A'$	1.520	1.625	97.6
	$^3A''$	1.475	1.625	115.8
SiF_2	$^1A_1$		1.616 (1.590[e])	100.9 (100.8[e])
	$^3B_1$		1.617	115.8

[a] Calculational level/basis sets for geometry optimization of silylenes are MP2/6-31G** for the singlet state and UMP2/6-31G** for the triplet state.

[b] Reference 22.

[c] Reference 13.

[d] Reference 8.

[e] Experimental geometries are in parentheses. Reference 24.

Table II. Singlet-triplet splittings (ΔE_{ST}) for methylenes and silylenes.[a] The recommended theoretical values are DCCI. All quantities in units of kcal/mol.

Level	CH_2	CHF	CF_2	SiH_2	SiHF	SiF_2
HF	-24.9	-3.8	34.5	5.7	23.8	55.6
GVB(3/6)–PP	-6.9	13.1	49.8	21.4	39.3	69.5
RCI	-8.5	12.2	49.1	20.8	38.4	69.2
RCI*ΠCI	-8.5	15.1	53.7	20.8	38.8	69.9
RCI*[ΠCI + S_{val}]	-16.9	6.3	48.0	14.5	33.7	68.6
CCCI[b]	-5.1	19.9	60.3	26.7	45.6	78.1
DCCI[c,d]	-10.0	14.5	57.1	21.5	41.3	76.6
Experiment (T_e)[d]	-9.215	14.6[e]	56.7[f]	20.7[g]		76.2[h]
		11.3[e]		17.7[g]		75.2[h]
		8.0[e]				77.2[h]
Previous Theory (T_e)[d]	-9.1[i]	13.2[j]	46.5[k]	20.4[i]	37.7[l,m]	73.5[m]
		12.9[l]	46.0[n]			73.8[o]
		8.1[n]				

[a] The following basis sets were used: CH_2 (C(7*s*4*p*2*d*1*f*) / H(3*s*2*p*1*d*)); CHF (C(5*s*3*p*2*d*1*f*) / H(3*s*2*p*1*d*) / F(5*s*3*p*2*d*1*f*)); CF_2 (C(5*s*3*p*2*d*1*f*) / F(3*s*2*p*1*d*)); SiH_2 (Si(7*s*5*p*2*d*1*f*) / H(3*s*2*p*1*d*)); SiHF (Si(7*s*5*p*2*d*1*f*) / H(2*s*1*p*) / F(3*s*2*p*1*d*)); SiF_2 (Si(7*s*5*p*2*d*1*f*) / F(3*s*2*p*1*d*)).

[b] RCI*[ΠCI + SD($\sigma\pi$)].

[c] RCI*[ΠCI + S_{val} + SD($\sigma\pi$)].

[d] To estimate T_0 from T_e add 0.217 (CH_2), 0.3 (SiH_2), 0.1 (CHF and SiHF), and 0.0 kcal/mol (CF_2 and SiF_2).

[e] Reference 7.

[f] Reference 5.

[g] Reference 3.

[h] See text (ref. 6).

[i] CASSCF-SOCI+Q/Extended Basis (ref. 4).

[j] CI-SD+Davidson correction/TZ+2P (ref. 13).

[k] GVB(1/2) for $^1A_1$ and HF for $^3B_1$/DZP (ref. 8).

[l] MP4-SDTQ/6-31G* (ref. 12).
[m] CI-SD/DZP (ref. 10).
[n] GVB(1/2) for the singlet state and HF for the triplet state/DZP (ref. 9).
[o] CI-SD/6-31G* (ref. 11).

Table III. ΔE_{ST} (kcal/mol) of CH_2, CHF, and SiH_2 as a function of basis set.

Molecule	Basis set	HF	GVB-PP	GVB-RCI	CCCI[a]	DCCI[b]	Exp.
CH_2	C(3*s*2*p*1*d*)/H(2*s*1*p*)	-26.04	-9.01	-11.05	-8.87	-13.08	
	C(5*s*3*p*2*d*1*f*)/H(2*s*1*p*)	-25.43	-7.77	-9.39	-6.17	-10.91	
	C(5*s*3*p*2*d*1*f*)/H(3*s*2*p*1*d*)	-25.40	-7.73	-9.34	-6.02	-10.76	
	C(6*s*4*p*2*d*1*f*)/H(2*s*1*p*)	-25.32	-7.68	-9.29	-6.05	-10.79	
	C(7*s*4*p*3*d*2*f*)/H(3*s*2*p*)	-24.86	-6.93	-8.53	-5.05	-9.99	-9.215[c]
CHF	C(3*s*2*p*1*d*)/H(2*s*1*p*)/F(3*s*2*p*1*d*)	-4.01	12.10	10.99	17.76	12.39	
	C(5*s*3*p*2*d*1*f*)/H(2*s*1*p*)/F(3*s*2*p*1*d*)	-3.49	13.38	12.49	20.18	14.66	
	C(5*s*3*p*2*d*1*f*)/H(3*s*2*p*1*d*)/F(3*s*2*p*1*d*)	-3.55	13.31	12.43	20.16	14.60	
	C(5*s*3*p*2*d*1*f*)/H(3*s*2*p*1*d*)/F(5*s*3*p*2*d*1*f*)	-3.81	13.10	12.22	19.93	14.48	14.6[d]
SiH_2	Si(4*s*3*p*1*d*)/H(2*s*1*p*)	5.34	20.18	19.40	23.93	18.74	
	Si(7*s*5*p*2*d*1*f*)/H(2*s*1*p*)	5.74	21.49	20.86	26.67	21.44	
	Si(7*s*5*p*2*d*1*f*)/H(3*s*2*p*1*d*)	5.67	21.44	20.81	26.69	21.46	20.7[e]

[a] RCI*[ΠCI + SD($\sigma\pi$)].

[b] RCI*[ΠCI + S_{val} + SD($\sigma\pi$)].

[c] T_e (ref. 2).

[d] T_e (ref. 7).

[e] T_e (ref. 3).

Table IV. Total charges, bond populations, and carbon and silicon hybridization for CXY and SiXY.[a]

		Total Charges				Bond Population	Hybridization: Bonding Orbital			Hybridization: Nonbonding σ orbital		
Molecule	State	C,Si	H	F	Bond	on C and Si[b]	% s	% p	% d	% s	% p	% d
CH_2	$^1A_1$	6.21	0.89		C-H	1.06	18.9	79.0	1.9	61.8	37.9	0.2
CHF	$^1A'$	5.86	0.93	9.21	C-H	1.01	16.7	80.6	2.5	66.0	33.7	0.1
					C-F	0.52	17.1	76.5	4.8			
CF_2	$^1A_1$	5.60		9.20	C-F	0.53	17.6	75.6	5.4	68.8	30.7	0.3
SiH_2	$^1A_1$	13.63	1.18		Si-H	0.78	18.2	75.6	5.8	68.7	30.7	0.4
SiHF	$^1A'$	13.31	1.22	9.47	Si-H	0.73	19.7	72.2	7.5	71.9	27.0	0.1
					Si-F	0.34	20.3	60.1	15.4			
SiF_2	$^1A_1$	13.08		9.46	Si-F	0.34	21.8	57.0	16.7	76.3	22.4	1.4
CH_2	$^3B_1$	6.29	0.86		C-H	1.16	50.8	48.4	0.8	18.9	80.9	0.2
CHF	$^3A''$	5.89	0.87	9.25	C-H	1.18	59.8	39.3	1.0	34.0	65.0	0.9
					C-F	0.55	34.0	61.8	3.5			
CF_2	$^3B_1$	5.53		9.23	C-F	0.60	45.0	50.7	3.6	50.9	47.2	1.8
SiH_2	$^3B_1$	13.76	1.12		Si-H	0.91	51.4	45.2	3.4	36.1	62.1	1.9
SiHF	$^3A''$	13.42	1.12	9.47	Si-H	0.95	62.5	34.0	3.4	49.1	47.3	3.3
					Si-F	0.37	33.8	50.4	12.9			
SiF_2	$^3B_1$	13.12		9.44	Si-F	0.40	42.6	41.8	12.7	66.1	29.5	4.1

[a] Based on Mulliken populations with basis sets of C(5*s*3*p*2*d*1*f*), Si(7*s*5*p*2*d*1*f*), H(2*s*1*p*), and F(3*s*2*p*1*d*) (ref. 28).

[b] Perfect covalent bonding would lead to a carbon- or silicon-ligand bond population of 1.00.

Chapter VI

Singlet-Triplet Energy Gaps in Chlorine-Substituted Methylenes and Silylenes

Singlet-Triplet Energy Gaps in Chlorine-Substituted Methylenes and Silylenes

Seung Koo Shin, William A. Goddard III, and J. L. Beauchamp

Contribution No. 7953 from the Arthur Amos Noyes Laboratory of Chemical Physics, California Institute of Technology, Pasadena, California 91125

Abstract

The singlet-triplet splittings of chlorine-substituted methylenes and silylenes have been studied using the *ab initio* generalized valence bond (GVB) dissociation-consistent configuration interaction (DCCI) method. Extended basis sets for carbon and silicon combined with valence double-ζ plus polarization basis sets for hydrogen and chlorine were employed to obtain accurate values for the singlet-triplet splittings. All chlorine-substituted methylenes and silylenes have singlet ground states, with singlet-triplet splittings of 6.0, 20.5, 35.8, and 55.2 kcal/mol for CHCl, CCl_2, SiHCl, and $SiCl_2$, respectively. We expect these results to be within 1 kcal/mol of experiment. The DCCI result strongly suggests that the correct experimental singlet-triplet splitting of CHCl is 6.4 ± 0.7 kcal/mol. The sp^n hybridizations of nonbonding σ orbitals of carbon and silicon in substituted methylenes and silylenes correlate well with the singlet-triplet splittings and bond angle differences.

I. INTRODUCTION

Carbenes are highly reactive molecules containing a divalent carbon with an unshared pair of electrons.[1] There are two low-lying states, singlet and triplet, depending on whether the nonbonding electrons are σ^2 or $\sigma\pi$.

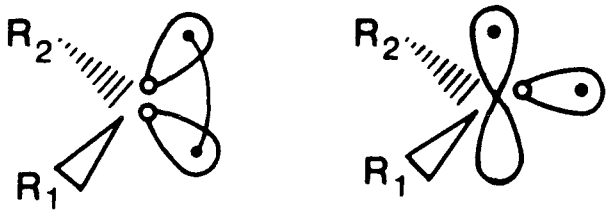

σ^2 $\sigma^1\pi^1$

Carbenes undergo characteristic chemical reactions such as insertion into a single bond, addition to a double bond, dimerization, and intramolecular rearrangement.[1] Their diverse chemical properties of carbenes are strongly dependent upon spin multiplicities. For example, Roth[2] has studied reactions of singlet and triplet methylenes with deuteriotrichloromethane using the chemically induced dynamic nuclear polarization (CIDNP) technique.

$$^1 : CH_2 + CDCl_3 \rightarrow [CH_2Cl\cdot \cdot CDCl_2] \rightarrow CH_2Cl - CDCl_2 \text{ (E)} \qquad (1)$$

$$^3 : CH_2 + CDCl_3 \rightarrow [CH_2D\cdot \cdot CCl_3] \rightarrow CH_2D - CCl_3 \text{ (A)} \qquad (2)$$

Singlet methylene generated from direct photolysis of diazirine abstracts chlorine atoms from $CDCl_3$ and yields an emission CIDNP signal of 1,1,2-trichloro-1-deuterioethane [Eq. (1)]. On the other hand, triplet methylene formed upon photosensitized decomposition of diazirine shows an absorption CIDNP signal of 1,1,1-trichloro-2-deuterioethane initiated by hydrogen abstraction [Eq. (2)]. Thus the chemical selectivities of carbenes depend upon whether the ground state of CXY is triplet or singlet, which in turn depends on which substituents X and Y are used.[3] In brief, the singlet state is stablized by electron-withdrawing substituents and substituents donating $p\pi$ lone pairs to the empty carbon $p\pi$ orbital. The triplet state

is favored by substitutents more electropositive than carbon and by sterically bulky substituents (which prefer large X-C-Y bond angles). The substituent effect to the carbenic selectivity in the addition of singlet carbenes to the double bond has been studied extensively.[1,4] Moss[4] has found that increasing $p\pi$–electron donation and increasing inductive electron withdrawal by X and Y both augment the selectivity of the singlet CXY in cyclopropanation reactions. Therefore, a knowledge of the ground spin state, the singlet-triplet splitting (ΔE_{ST}), and the effect of a particular substituent is of great importance in understanding the carbene chemistry. In recent years, the chemistry of silylenes (the silicon analogs of carbenes) has also become of great experimental interest. The chlorine-substituted silylenes, SiHCl and $SiCl_2$, have been detected during the chlorosilane chemical vapor deposition of thin silicon films and speculated as important gas phase intermediates.[5,6] However, the structures and energetics of SiHCl and $SiCl_2$ have not been well studied. In the present paper, we employed *ab initio* theoretical methods to study the singlet-triplet splittings of chlorine-substituted *methylenes* and *silylenes* and silylene structures.

The parent molecules, CH_2 and SiH_2, have been most extensively studied and their singlet-triplet energy gaps, ΔE_{ST}, (T_0) have been determined to be -8.998 ± 0.014 and 21.0 ± 0.7 kcal/mol, respectively, from experiments[7,8] and corroborated by theoretical calculations[9] (a positive value indicates a singlet ground state). However, there are only a few experimental data for the singlet-triplet energy gaps of the substituted *methylenes* and *silylenes*.[10–12] The recent photoelectron spectroscopic studies of the halocarbene anions yield bounds for ΔE_{ST} of the halocarbenes.[12] This study suggests ΔE_{ST}(CHCl) to be $(11.4 \pm 0.3) - n \cdot (2.5 \pm 0.2)$ kcal/mol, where $n = 0$, 1, 2, 3, or 4. No experimental observation exists for ΔE_{ST} of CCl_2, SiHCl, and $SiCl_2$.

Previous theoretical values for ΔE_{ST} of the chlorine-substituted *methylenes* and *silylenes* are available at various calculational levels. Scuseria et al.[13] used CI-SD calculations with a triple-ζ basis augmented by two sets of polarization functions (TZ2P) to obtain 5.4 kcal/mol for ΔE_{ST}(CHCl) after Davidson correction.

Bauschlicher et al.[14] obtained ΔE_{ST} of 1.6 and 13.5 kcal/mol for CHCl and CCl_2, respectively, at a relatively low level [Hartree-Fock (HF) for the triplet and generalized valence bond [GVB(1/2)] for the singlet] using double-ζ plus polarization on carbon (DZ*p*) basis sets. Nguyen et al.[15] estimated a vertical excitation energy of 21.9 kcal/mol from the singlet ground state of CCl_2 at the MP4SDQ (Møller-Plesset fourth-order perturbation theory) level using 6-31G** basis sets. Ha et al.[16] also utilized the UPM4SDQ method using 6-31G* basis sets to yield the vertical excitation energy of 54.9 kcal/mol for $SiCl_2$. Gosavi et al.[17] estimated ΔE_{ST} of 36.8 kcal/mol for $SiCl_2$ based on the restricted HF (RHF) calculations using 6-31G* basis sets. No *ab initio* calculational results for the singlet-triplet splitting of SiHCl have been reported. Carter and Goddard[3] designed the correlation-consistent CI (CCCI) method to obtain the singlet-triplet excitation energies in substituted carbenes. Their reported values of 9.3 and 25.9 kcal/mol for ΔE_{ST} of CHCl and CCl_2, respectively, are greater than other theoretical estimates by 4 kcal/mol.

Recently, we devised the *ab initio* GVB-DCCI method to have correlation consistency for both singlet and triplet states with their relative stabilities balanced.[18] The calculated singlet-triplet splittings for fluorine-substituted methylenes and silylenes using the DCCI method were in excellent agreement with available experimental results [theory (T_e): −10.0, 14.5, 57.1, 21.4, and 76.6 kcal/mol; experiment (T_e): -9.215, 14.6, 56.7, 20.7, and 76.2 kcal/mol for CH_2, CHF, CF_2, SiH_2, and SiF_2, respectively]. Herein we utilize this proven *ab initio* GVB-DCCI methodology to obtain accurate values for the singlet-triplet splittings of chlorine-substituted methylenes and silylenes. Furthermore, Mulliken populations[19] were analyzed to provide qualitative correlations between the sp^n hybridization of nonbonding σ orbitals of carbon and silicon in substituted methylenes and silylenes and the singlet-triplet splittings and bond angle differences.

II. RESULTS

The geometries for *methylenes* in Table I were taken from the calculations of

Scuseria et al.[13] (CHCl) and Bauschlicher et al.[14] (CCl_2). The equlibrium geometries for the substituted *silylenes* were calculated at the MP2/6-31G** level using the Gaussian 86 program[20] and are listed in Table I with available experimental data.[21,22] The values for ΔE_{ST} of CHCl, CCl_2, SiHCl, and $SiCl_2$ using the DCCI method are shown in Table II with available experimental data and other previous theoretical results. Table III summarizes total charges on each atom, bond populations, and *spd* hybridizations in bonding orbitals and nonbonding σ orbitals of carbon and silicon.

A. CHCl

The best estimate for the singlet-triplet splitting of CHCl using the DCCI method is 6.0 kcal/mol. [The DCCI with 96 basis functions (nbfs) consists of 17216/31005 spatial configurations/spin eigenfunctions for the singlet state and 12344/41231 for the triplet state.] The CI-SD calculations by Scuseria et al.[13] yielded ΔE_{ST} of 3.7 kcal/mol. [With the triple-ζ plus double polarization basis sets (67 nbfs), this involves 74546 and 48368 configurations for the singlet and triplet states of CHCl.] Despite the large number of configurations, the CI-SD method tends to underestimate ΔE_{ST} of carbons due to the larger electron correlation error for single-states. Indeed, the singlet-triplet splittings of CHCl increases to 5.4 kcal/mol after Davidson corrections. Murray et al.[12] reported triplet excitation energies of $(11.4 \pm 0.3) - n\cdot(2.5 \pm 0.2)$ kcal/mol from the photoelectron spectroscopy studies of $CHCl^-$. The present calculational result strongly suggests that the actual singlet-triplet splitting of CHCl is 6.4 ± 0.7 kcal/mol.

Our previous studies suggest that errors in the ΔE_{ST} from DCCI calculations are mainly due to limitations in basis sets. We have previously shown that the electronegative carbon atom in CH_2 requires more diffuse functions to balance the relative stabilities between the singlet and triplet states accurately.[18] An extension of CH_2 basis sets from C($5s3p2d1f$)/H($2s1p$) to C($7s4p3d2f$)/H($3s2p$) resulted in greater stabilization of the singlet state by 0.9 kcal/mol. Simi-

larly, the extension of CHCl basis sets from C($5s3p2d1f$)/H($2s1p$)/Cl($4s3p1d$) to C($7s4p3d2f$)/H($3s2p$)/Cl($6s4p2d$) increases ΔE_{ST} by 0.9 kcal/mol. Since the carbon atoms in CHCl have negative charge populations, as shown in Table III (total charges of 6.09 and 6.12 for carbon atoms in $^1A'$ and $^3A''$ CHCl, respectively), the basis limitation error of 0.8 kcal/mol estimated from the error in CH_2 (T_e(DCCI) = -9.99 kcal/mol and T_e(EXP) = -9.215 kcal/mol) suggests a singlet-triplet splitting of 6.8 kcal/mol for CHCl, in good agreement with our selected experimental value of 6.4 ± 0.7 kcal/mol.

The GVB one-electron orbitals are shown in Figs. 1 and 2 for the ground ($^1A'$) and excited ($^3A''$) states of CHCl, respectively. All valence orbitals for each state show a visible difference in the sp hybridization and charge transfer. The greater contribution of the $p\pi$ lone pair donation of chlorine into the carbon $p\pi$ orbital in the singlet CHCl is apparent from comparison of the chlorine $p\pi$ orbital in $^1A'$ CHCl (Fig. 1d) with that in $^3A''$ CHCl (Fig. 2d). Analyses of Mulliken populations for both $^1A'$ and $^3A''$ states in Table III quantify the hybridization and charge transfer in the CHCl bonds. $^1A'$ CHCl has more p character in the C–H and C–Cl bonds (C–H:79.2% p and C–Cl:76.1% p) and less p character in the nonbonding σ orbital (34.6% p), while $^3A''$ CHCl has less p character in the C–H and C–Cl bonds (C–H:44.6% p and C–Cl:51.0% p) and more p character in the nonbonding σ orbital (70.8% p).

B. CCl_2

The singlet-triplet splitting of CCl_2 using the DCCI method is 20.5 kcal/mol. The DCCI with 74 nbfs consists of 9308/16576 spatial configurations/spin eigenfunctions for the singlet state and 6296/25590 for the triplet state.

The $^1A_1$ ground state has 19.6% s/77.4% p character in the C–Cl bonds and 69.5 % s/30.3% p in the carbon nonbonding σ orbital. The $^3B_1$ excited state has 52.0% s/46.6% p character in the C–Cl bonds and 37.6% s/61.6% p in the carbon nonbonding σ orbital.

C. SiHCl

The predicted bond angle for singlet SiHCl differs by 7.6° from the experimental bond angle determined by Herzberg and Verma! [21] The Si−Cl bond distance for singlet SiHCl is longer than the experimental value by 0.014 Å; however, the predicted Si–H bond distance of 1.509 Å is significantly shorter than the experimental value of 1.561 Å. These discrepancies in θ(Si-H-Cl) and r(Si–H) are several times larger than expected from comparisons with other systems, and we suggest that these discrepancies may be due to analyzing the rovibrational spectra of this asymmetric top molecule SiHCl using a symmetric top approximation and assuming zero inertia defect.

The DCCI predicts the singlet-triplet splitting of SiHCl to be 35.8 kcal/mol. [With 68 nbfs, there are 7739/13653 spatial configurations/spin eigenfunctions for the singlet state and 5297/19001 for the triplet state.]

The GVB one-electron orbitals are shown in Figs. 3 and 4 for the ground (^{1}A′) and excited (^{3}A″) states of SiHCl, respectively. Comparison with the bond pairs of CHCl in Figs. 1 and 2 shows that the Si–Cl bonds are more ionic than the C–Cl bonds, as expected from the electronegativity. Also, the $p\pi$ lone pair donation of chlorine into the silicon $p\pi$ orbital in SiHCl is visibly smaller than that in CHCl. The hybridizations of the Si–H and Si–Cl bonds show the trend of more silicon p character for the singlet than for the triplet (Si–H:73.6% p and Si–Cl:62.3% p for ^{1}A′ vs. Si–H:38.5% p and Si–Cl:44.8% p for ^{3}A″). The nonbonding σ orbital at silicon has concurrently less p character for the singlet (27.7% p) than for the triplet (51.2% p).

D. $SiCl_2$

The predicted bond angle for singlet $SiCl_2$ is within 0.2° of an experimental value by Suzuki *et al.*[22] The Si−Cl bond distance in singlet state $SiCl_2$ is longer than the experimental value by 0.007 Å.

The DCCI singlet-triplet splitting of $SiCl_2$ is 55.2 kal/mol. [With 82 nbfs,

there are 10685/19089 configurations/spin eigenfunctions for the singlet state and 7199/28879 for the triplet state.]

The hybridizations of the Si–Cl bond follow the general trend of more silicon p character for the singlet than for the triplet (61.1% p for $^1A_1$ and 39.6% p for $^3B_1$). The nonbonding σ orbital at silicon has concomitantly less p character for the singlet (23.3% p) than for the triplet (37.2% p).

III. DISCUSSION

The DCCI results (calculated 6.0 kcal/mol; estimated 6.8 for complete basis) for the singlet-triplet splitting of CHCl suggests that the correct experimental value is 6.4 ± 0.7 kcal/mol. The predicted values for ΔE_{ST} of CCl_2, SiHCl, and $SiCl_2$ are 20.5, 35.8, and 55.2 kcal/mol, respectively, and expected to be equally accurate (about 1 kcal/mol low due to the basis set limitations). The stabilization of the singlet state by the chlorine substitution in place of hydrogen results from (i) the increase of s character in the nonbonding σ orbital of the center atom due to the electron-withdrawing substituent and (ii) the concomitant increase of the electron density in the empty $p\pi$ orbital of the center atom due to the back donation of $p\pi$ lone pair of chlorine as shown in Scheme I.

Scheme I

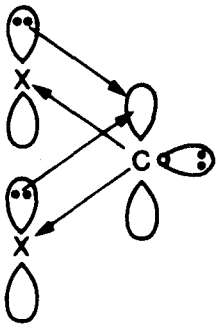

The greater increase of s character in the nonbonding σ orbital of the triplet state carbene leads to the stabilization of the σ orbital relative to the $p\pi$ orbital, disfavoring the triplet state due to the greater loss of $\sigma \rightarrow \pi$ excitation energy than

the gain by the triplet state exchange interaction. The contribution of the $p\pi$ lone pair donation to the stabilization of the singlet state (estimated from the difference between ΔE_{ST} at the RCI and that at the RCI*ΠCI) is 2.6 and 5.5 kcal/mol for CHCl and CCl_2, respectively, and 0.2 kcal/mol for SiHCl and $SiCl_2$. The $p\pi$ lone pair donation enhances the singlet stabilization of CHCl and CCl_2 more than their corresponding silicon analogues because of the shorter bond distance for methylenes.

Bauschlicher et al.[14] have previously utilized Mulliken gross populations of the carbon atom for singlet and triplet states to correlate with the qualitative trends of the singlet-triplet splittings of carbenes. Also, Harrison et al.[23] have suggested that the electronegativity of the substituents is an important factor in determining the multiplicities of the ground state. Herein we employ Mulliken populations of bonding orbitals to provide the more quantitative correlations between the singlet-triplet splittings and the sp^n hybridizations in nonbonding σ orbitals for both states. Since the singlet-triplet splitting involves an electronic excitation between the nonbonding σ and π orbitals, its dependence on the halogen substitution can be understood in terms of the very different sp^n hybridization in the nonbonding σ orbital for the singlet [n(S)] and triplet [n(T)] states, where n is the ratio of p character to s character. Table IV summarizes the sp^n hybridization of nonbonding σ orbitals in methylenes and silylenes with bond angles and the calculated singlet-triplet splittings. Previous data[18] for CXY and SiXY (where X, Y = H, F) were included in Table IV. The ratio n(T) for the triplet state decreases more effectively than n(S) for the singlet state with the more electronegative halogen substitution. Figure 5 shows the visible decrease of p character in nonbonding σ orbitals of the triplet state methylenes due to the halogen substitutions. The dependence of the bond angle on the sp^n hybridization is peculiar. As the ratio n increases, the triplet state bond angle θ(T) decreases as expected from the decrease of s character in the sp^n hybridizations of bond orbitals, while the singlet state bond angle θ(S) increases. This increase of the singlet state bond angle θ(S) with halogen substitution may be attributed (a) to the size of halogen substituent and (b) to $p\pi$ lone pair dona-

tion of halogen into the empty $p\pi$ orbital of the center atom (developing a partial double bond). We take the ratio of n(S) to n(T) as a measure of the relative sp^n hybridization changes in nonbonding σ orbitals due to the halogen substitutions for the singlet and triplet states.

$$R = \frac{n(\mathrm{S})}{n(\mathrm{T})} = \frac{\text{singlet } p \text{ character}/s \text{ character}}{\text{triplet } p \text{ character}/s \text{ character}} \tag{3}$$

The singlet-triplet splittings correlate linearly with R, as shown in Fig. 6, whereas the bond angle differences are inversely related, as shown in Fig. 7. A deviation for CCl_2 may be ascribed to the greater size of chlorine atom. This bulky chlorine substituent in CCl_2 leads to a large Cl–C–Cl bond angle of 109.4° for the singlet state, which results in small values of n(S) and R.

IV. SUMMARY

Ab initio GVB-DCCI calculations have been carried out to estimate the singlet-triplet splittings for chlorine-substituted *methylenes* and *silylenes*. The DCCI result suggests that the experimental singlet-triplet splitting of CHCl is 6.4 ± 0.7 kcal/mol (singlet ground state). The equilibrium geometry for the singlet SiHCl optimized at the MP2/6-31G* level differs significantly from the experimental geometry. We recommend reanalyses of rovibrational data for an asymmetric top molecule SiHCl. Mulliken population analyses provide the quantitative correlation between the singlet-triplet splittings and the sp^n hybridizations in nonbonding σ orbitals of methylenes and silylenes. The more electronegative substituent induces increase of s character in the nonbonding σ orbital for the triplet state as compared to the singlet state. The relative ratio of sp^n hybridizations of the singlet state to the triplet state correlates linearly with the singlet-triplet splittings and inversely with the bond angle differences.

V. CALCULATIONAL DETAILS

A. Basis sets

For calculations of singlet-triplet state splittings at various CI levels and for Mulliken population analyses, we employed core double-ζ valence triple-ζ basis sets for carbon $(10s6p/5s3p)$[24,25] and silicon $(11s7p/7s5p)$[26], augmented with two sets of d polarization functions centered at 0.62 for carbon and 0.42 for silicon with an internal ratio of 2.3 [ζ^d(C) = 0.940 and 0.409, ζ^d(Si) = 0.637 and 0.277]. In addition, one set of f functions was included, obtained by scaling the mean d exponents of 0.62 for carbon and 0.42 for silicon by 1.2 [ζ^f(C) = 0.893 and ζ^f(Si) = 0.605]. The s combination of d functions and p combination of f functions were excluded from all basis sets. Valence double-ζ basis sets[27] were used for hydrogen $(4s/2s$; scaled by 1.2 for hydrogen attached on carbon and unscaled for hydrogen attached on silicon) and chlorine $(11s8p/4s3p)$,[28] augmented with one set of p functions on hydrogen (ζ^p = 1.0 and 0.6 for hydrogen attached on carbon and silicon, respectively) and one set of d functions on chlorine (ζ^d = 0.6). We also extended basis sets for carbon, hydrogen, and chlorine to examine the convergence of ΔE_{ST} of CHCl:

C$(7s4p3d2f)$: The Huzinaga $(11s7p)$ basis[29] for carbon was contracted to $(6s3p)$ triple-ζ for both core and valence, but diffuse s and p functions (ζ^s = 0.0388 and ζ^p = 0.0282) were added.[30] Three sets of carbon d polarization functions were added, centered at 0.620 with an internal ratio of 2.5 (leading to exponents ζ^d = 1.550, 0.620, and 0.248). Two sets of carbon f functions were included, centered at the previous f exponent of 0.893 with an internal ratio of 2.5 (ζ^f = 1.412 and 0.565).

H$(3s2p)$: The Huzinaga scaled $(6s)$ basis[25] was contracted to triple-ζ, with two sets of p functions centered at 1.0 with an internal ratio of 2.3 (ζ^p = 1.517 and 0.659).

Cl$(6s4p2d)$: The double-ζ basis[27] $(11s7p/6s4p)$ were used with two sets of d functions centered at 0.60 with an internal ratio of 2.3 (ζ^d = 0.91 and 0.40).

B. Geometries

The geometries for *methylenes* were taken from HF/GVB(1/2) geometry optimizations for the $^1A'/^3A''$ states of CHCl using TZ2P basis sets by Scuseria et al.[13] and the HF/GVB(1/2) calculations for $^1A_1/^3B_1$ states of CCl_2 using DZ*p* basis sets by Bauschlicher *et al.*[14] The equlibrium geometries for the singlet/triplet states of SiHCl and $SiCl_2$ were optimized at the MP2/UMP2 level with 6-31G** basis sets using the Gaussian 86 program.[20]

C. DCCI Calculations

The GVB-DCCI approach starts with a GVB wavefunction in which the carbene lone pair and the two bond pairs are correlated, followed by a small CI based on the GVB orbitals.[3,18] In order to calculate an accurate bond energy for a halogen-substituted double-bonded molecule, XYC = CZW, the DCCI prescription is to solve first for the GVB-PP (6/12) wavefunction in which the double bond and the four carbon-ligand bonds are correlated. Then, to relax the perfect spin-pairing restriction imposed on the GVB-PP wavefunction, we allow a full CI restricted so that each correlated pair has two electrons (GVB-RCI). Then all quadruple excitations are allowed out of the double bond, leading to the RCI*SDTQ($\sigma\pi$) wavefunction. This wavefunction dissociates smoothly to the RCI*SD($\sigma\pi$) wavefunction on each carbene fragment, leading to a consistent description for dissociation of the double bond. For the halogen-substituted systems, Carter and Goddard[3] showed that to obtain accurate ΔE_{ST} for carbenes one must include the π-lone pair orbitals in the RCI. Hence, we would consider the RCI*[ΠCI + SDTQ($\sigma\pi$)] wavefunction for XYC = CZW, which dissociates to RCI*[ΠCI + SD($\sigma\pi$)] on each carbene product. This was designated CCCI by Carter and Goddard.[3] If calculated self-consistently, these wavefunctions would lead to accurate bond energies. However, since the orbitals are calculated at the GVB-PP level, we also include all single excitations from the GVB-RCI wavefunction (S_{val}), leading to RCI*[ΠCI + S_{val} + SDTQ($\sigma\pi$)] for XYC = CZW and RCI*[ΠCI + S_{val} + SD($\sigma\pi$)] for the carbenes. This choice of the

wavefunction for CXY insures that the double bond in XYC=CXY is calculated at the same level as the bond length is increased to R = ∞. Hence, we refer to this as *dissociation-consistent* CI. The DCCI (RCI*[ΠCI + S_{val} + SD($\sigma\pi$)]) extends the previous CCCI (RCI*[ΠCI + SD($\sigma\pi$)]), with inclusion of all single excitations from the GVB-RCI wavefunction (S_{val}). We find that inclusion of S_{val} is important to balance the relative stabilities of the singlet and triplet states.[18]

Acknowledgments

We wish to acknowledge the support of the National Science Foundation under Grant Nos. CHE87-11567 (J.L.B.) and CHE83-18041 (W.A.G.).

References

(1) (a) Kirmse, W. *Carbene Chemistry*, Academic Press: New York, 1971; (b) *Carbenes*, Moss, R. A.; Jones, M. Ed.; Wiely: New York, 1975; Vol. 2; (c) *Reactive Intermediates*, Moss, R. A.; Jones, M. Ed.; Wiely: New York, 1978; Vol. 1, 1981; Vol. 2; 1985, Vol. 3; (d) Davidson, E. R. In *Diradicals*, Borden, W. T. Ed.; Wiley: New York, 1982; (e) Wentrup, C. *Reactive Molecules*, Wiley: New York 1984.

(2) Roth, H. D. *Acc. Chem. Res.* **1977**, *10*, 85.

(3) Carter, E. A.; Goddard, W. A. III *J. Chem. Phys.* **1988**, *88*, 1752.

(4) Moss, R. A. *Acc. Chem. Res.* **1980**, *13*, 58.

(5) (a) Jasinski, J. M.; Meyerson, B. S.; Scott, B. S. *Ann. Rev. Phys. Chem.* **1987**, *38*, 109; (b) Breiland, W. G.; Ho, P.; Coltrin, M. E. *J. Appl. Phys.* **1986**, *60*, 1505.

(6) Kruppa, G. H.; Shin, S. K.; Beauchamp, J. L. *J. Phys. Chem.* submitted for publication.

(7) Jensen, P.; Bunker, P. R. *J. Chem. Phys.* **1988**, *89*, 1327 and earlier references therein.

(8) Berkowitz, J.; Greene, J. P.; Cho, H.; Ruscic, B. *J. Chem. Phys.* **1987**, *86*, 1235.

(9) (a) Shavitt, I. *Tetrahedron*, **1985**, *41*, 1531; (b) Goddard, W. A. III *Science*, **1985**, *227*, 917; (c) Schaefer, H. F. III *Science*, **1986**, *231*, 1100; (d) Bauschlicher, C. W. Jr.; Langhoff, S. R. *J. Chem. Phys.* **1987**, *87*, 387 and earlier references therein.

(10) (a) Koda, S. *Chem. Phys. Lett.* **1978**, *55*, 353; (b) Koda, S. *Chem Phys.* **1986**, *66*, 383.

(11) Rao, D. R. *J. Mol. Spectry* **1970**, *34*, 284.

(12) Murray, K. K.; Leopold, D. G.; Miller, T. M.; Lineberger, W. C. *J. Chem.*

Phys. **1988**, *89*, 5442.

(13) Scuseria, G. E.; Durán, M.; Maclagan, R. G. A. R.; Schaefer, H. F. III *J. Am. Chem. Soc.* **1986**, *108*, 3248.

(14) Bauschlicher, C. W. Jr.; Schaefer, H. F. III; Bagus, P. S. *J. Am. Chem. Soc.* **1977**, *99*, 7106.

(15) Nguyen, M. T.; Kerins, M. C.; Hegarty, A. F.; Fitzpatrick, N. J. *Chem. Phys. Lett.* **1985**, *117*, 295.

(16) Ha, T.-K.; Nguyen, M. T.; Kerins, M. C.; Fitzpatrick, N. J. *Chem. Phys.* **1986**, *103*, 243.

(17) Gosavi, R. K.; Strausz, O. P. *Chem. Phys. Lett.* **1986**, *123*, 65.

(18) Shin, S. K.; Goddard, W. A. III; Beauchamp, J. L. *J. Chem. Phys.* submitted for publication.

(19) Mulliken populations were obtained by summing over the electron populations of each *s*, *p*, and *d* basis function on carbon and silicon within each natural orbital for each GVB pair. Although this analysis tends to be basis dependent, relative trends and comparisons are expected to be reliable.

(20) Frisch, M. J.; Binkley, J. S.; Schlegel, H. B.; Raghavachari, K.; Melius, C. F.; Martin, R. L.; Stewart, J. J. P.; Bobrowicz, F. W.; Rohlfing, C. M.; Kahn, L. R.; Defrees, D. J.; Seeger, R.; Whiteside, R. A.; Fox, D. J.; Fleuder, E. M.; Pople, J. A. *Gaussian 86*; Carnegie-Mellon Quantum Chemistry Publishing Unit: Pittsburgh, 1984.

(21) Herzberg, G.; Verma, R. D. *Can. J. Phys.* **1964**, *42*, 395.

(22) Suzuki, M.; Washida, N.; Inoue, G. *Chem. Phys. Lett.* **1986**, *131*, 24.

(23) Harrison, J. F.; Liedtke, R. C.; Liebman, J. F. *J. Am. Chem. Soc.* **1979**, *101*, 7162.

(24) Dunning, T. H. Jr. *J. Chem. Phys.* **1970**, *55*, 716.

(25) Huzinaga, S. *J. Chem. Phys.* **1965**, *42*, 1293.

(26) One set diffuse $s(\zeta^s = 0.03648)$ and $p(\zeta^p = 0.02808)$ were added to the Si($11s7p/6s4p$) basis (refernce 27).

(27) Dunning, T. H. Jr.; Hay, P. J. In *Methods of Electronic Structure Theory*, Schaefer, H. F. III Ed.; Plenum Press: New York, 1977; Chap. 1.

(28) *Gaussian Basis Sets for Molecular Calculations*, Huzinaga, S. Ed.; Elsevier: Amsterdam, 1984.

(29) S. Huzinaga and Y. Sakai, J. Chem. Phys. **50**, 1371 (1969).

(30) E. A. Carter and W. A. Goddard III, J. Chem. Phys. **86**, 862 (1987).

Table I. Geometries of chlorine substituted methylenes and silylenes.[a]

Molecule	State	r(C,Si–H) (Å)	r(C,Si–Cl) (Å)	Angle (degree)
CHCl [c]	$^1A'$	1.092	1.725	102.1
	$^3A''$	1.070	1.699	124.4
CCl_2 [d]	$^1A_1$		1.756	109.4
	$^3B_1$		1.730	125.5
SiHCl	$^1A'$	1.509 (1.561[b])	2.078 (2.064[b])	95.2 (102.8[b])
	$^3A''$	1.473	2.054	115.9
$SiCl_2$	$^1A_1$		2.073 (2.066[c])	101.7 (101.5[c])
	$^3B_1$		2.049	118.2

[a] Calculational level/basis sets for geometry optimization of silylenes are MP2/6-31G** for the singlet state and UMP2/6-31G** for the triplet state and experimental geometries are in parentheses.

[b] Reference 21.

[c] Reference 22.

Table II. Singlet-triplet splittings (ΔE_{ST}) for methylenes and silylenes.[a] The recommended theoretical values are DCCI. All quantities in units of kcal/mol.

Level	CHCl	CCl_2	SiHCl	$SiCl_2$
HF	-11.9	-0.3	19.1	36.7
GVB(3/6)–PP	4.6	16.2	34.1	50.2
RCI	3.5	15.3	33.3	49.9
RCI*ΠCI	6.1	20.8	33.5	50.1
RCI*[ΠCI + S_{val}]	-2.8	12.0	28.3	47.3
CCCI[b]	10.3	24.8	40.1	57.5
Estimated Limit	(6.8)	(20.5)	(35.8)	(55.2)
DCCI[c]	6.0	20.5	35.8	55.2
Experiment (T_0)	6.4[d]			
	8.9[d]			
	11.4[d]			
Previous Theory (T_e)				
HF, GVB				36.8[g]
CI-SD, MP4	5.4[e]	21.9[f]		54.9[f]

[a] The following basis sets were used: C(7*s*4*p*2*d*1*f*), Si(7*s*5*p*2*d*1*f*), H(2*s*1*p*), and Cl(4*s*3*p*1*d*).
[b] RCI*[ΠCI + SD($\sigma\pi$)].
[c] RCI*[ΠCI + S_{val} + SD($\sigma\pi$)].
[d] CI-SD + Davidson correction/TZ+2P (ref. 13).
[e] Vertical excitation energy at the MP4SDQ/6-31G** level using $^1A_1$ geometry (ref. 15).
[f] Vertical excitation energy at the UMP4SDQ/6-31G* level using $1A_1$ geometry (ref. 16).
[g] RHF/6-31G* (ref. 17).

Table III. Total charges, bond populations, and carbon and silicon hybridization for CXY and SiXY.[a]

		Total Charges				Bond Population	Hybridization					
							Bonding Orbital			Nonbonding σ orbital		
Molecule	State	C,Si	H	Cl	Bond	on C and Si[b]	% s	% p	% d	% s	% p	% d
CHCl	$^1A'$	6.09	0.88	17.03	C-H	1.07	18.8	79.2	1.9	65.3	34.6	0.1
					C-Cl	0.73	20.6	76.1	2.7			
CCl_2	$^1A_1$	6.00		17.00	C-Cl	0.76	19.6	77.4	2.7	69.5	30.3	0.1
SiHCl	$^1A'$	13.51	1.18	17.31	Si-H	0.78	19.3	73.6	6.7	71.5	27.7	0.6
					Si-Cl	0.39	27.6	62.3	9.0			
$SiCl_2$	$^1A_1$	13.43		17.24	Si-Cl	0.41	28.5	61.1	9.4	74.1	23.3	2.4
CHCl	$^3A''$	6.12	0.84	17.04	C-H	1.18	54.7	44.6	0.8	28.8	70.8	0.5
					C-Cl	0.84	47.3	51.0	1.5			
CCl_2	$^3B_1$	5.98		17.01	C-Cl	0.89	52.0	46.6	1.4	37.6	61.6	0.9
SiHCl	$^3A''$	13.64	1.10	17.26	Si-H	0.95	58.2	38.5	3.4	46.0	51.2	2.7
					Si-Cl	0.49	48.6	44.8	6.2			
$SiCl_2$	$^3B_1$	13.53		17.24	Si-Cl	0.52	54.0	39.6	6.0	59.0	37.2	3.6

[a] Based on Mulliken populations with basis sets of C(5s3p2d1f), Si(7s5p2d1f), H(2s1p), and Cl(4s3p1d) (ref. 19).

[b] Perfect covalent bonding would lead to a carbon- or silicon-ligand bond population of 1.00.

Table IV. Summary of sp^n Hybridizations[a] of Nonbonding σ Orbitals in Methylenes and Silylenes, Bond Angles (in degree), and Singlet-Triplet Splittings (in kcal/mol) at the DCCI Level.[b]

	Singlet		Triplet				
Molecule	n(S)	θ(S)	n(T)	θ(T)	R^c	$\Delta\theta^d$	ΔE_{ST}
CH_2	0.61	101.8	4.28	133.2	0.14	31.4	−10.0
CHCl	0.53	102.1	2.46	124.4	0.22	22.3	5.1
CHF	0.51	103.3	1.91	121.1	0.27	17.8	14.5
CCl_2	0.44	109.4	1.64	125.5	0.27	16.1	20.5
CF_2	0.45	104.7	0.93	118.2	0.48	13.5	57.1
SiH_2	0.45	92.4	1.72	118.2	0.26	25.8	21.5
SiHCl	0.39	95.2	1.11	115.9	0.35	20.7	35.8
SiHF	0.38	97.6	0.96	115.8	0.40	18.2	41.3
$SiCl_2$	0.31	101.7	0.63	118.2	0.49	16.6	55.2
SiF_2	0.29	100.9	0.45	115.8	0.64	14.9	76.6

[a] n = % p character/% s character.

[b] Data for CXY and SiXY (X,Y = H, F) are taken from Shin et al. (ref. 18).

[c] $R = n(\mathrm{S})/n(\mathrm{T})$.

[d] $\Delta\theta = \theta(\mathrm{T}) - \theta(\mathrm{S})$.

Figure Captions

Figure 1. The GVB(3/6)-PP one-electron orbitals for $^1A'$ CHCl: (a) the C–H bond pair, (b) the C–Cl pair, (c) the C nonbonding σ natural orbital (nearly doubly-occupied), and (d) the Cl $p\pi$ orbital. Contours reflect regions of constant amplitude ranging from -1.0 to 1.0 a.u., with increments of 0.04 a.u.

Figure 2. The GVB(2/4)-PP one-electron orbitals for $^3A''$ CHCl: (a) the C–H bond pair, (b) the C–Cl pair; (c) the C nonbonding σ orbital (singly-occupied), and (d) the Cl $p\pi$ orbital.

Figure 3. The GVB(3/6)-PP one-electron orbitals for $^1A'$ SiHCl: (a) the Si–H bond pair, (b) the Si–Cl pair, (c) the Si nonbonding σ natural orbital (nearly doubly-occupied), and (d) the Cl $p\pi$ orbital.

Figure 4. The GVB(2/4)-PP one-electron orbitals for $^3A''$ SiHCl: (a) the Si–H bond pair, (b) the Si–Cl pair, (c) the Si nonbonding σ orbital (singly-occupied), and (d) the Cl $p\pi$ orbital.

Figure 5. Evolution of the carbon nonbonding σ orbitals (singly-occupied) of the triplet methylenes with the halogen substitution.

Figure 6. The singlet-triplet splittings of methylenes and silylenes as a function of the relative ratio $[n(\mathrm{S})/n(\mathrm{T})]$ of sp^n hybridization of nonbonding σ orbitals.

Figure 7. The singlet-triplet bond angle differences of methylenes and silylenes as a function of the relative ratio $[n(\mathrm{S})/n(\mathrm{T})]$ of sp^n hybridization of nonbonding σ orbitals.

CHCl ($^1A'$)

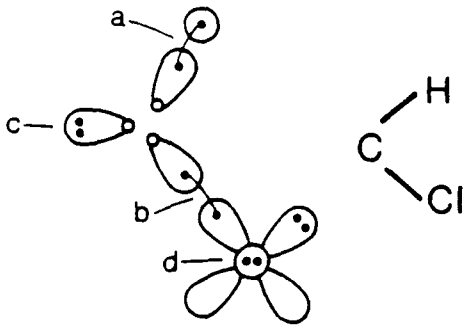

a) C – H BOND PAIR

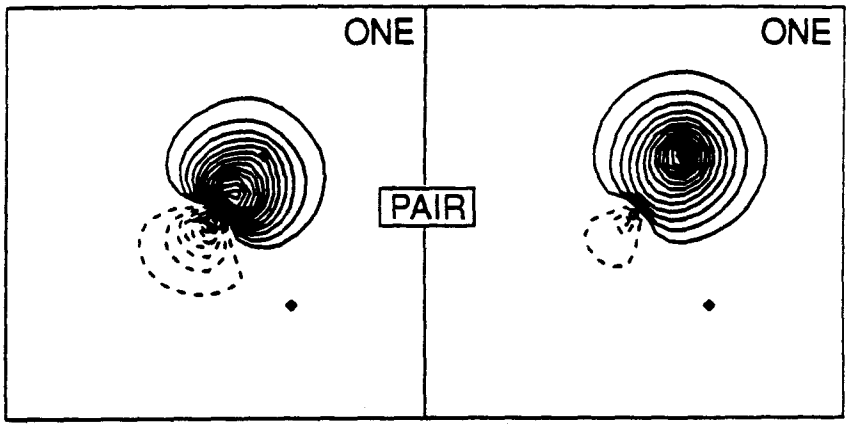

b) C – Cl BOND PAIR

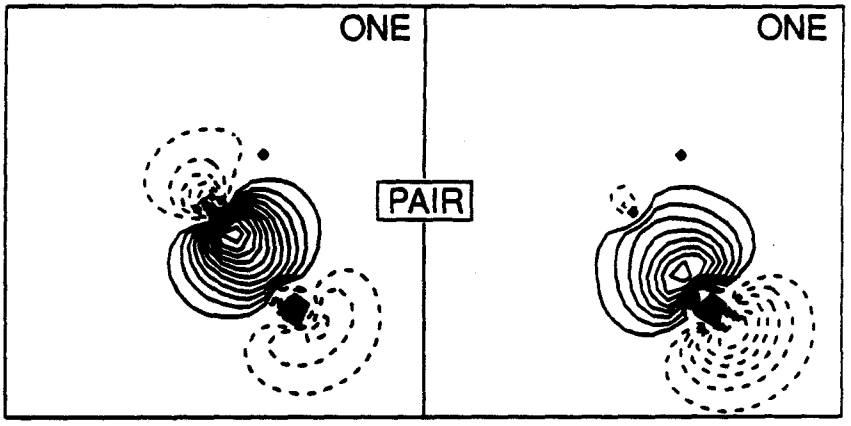

c) C σ ORBITAL

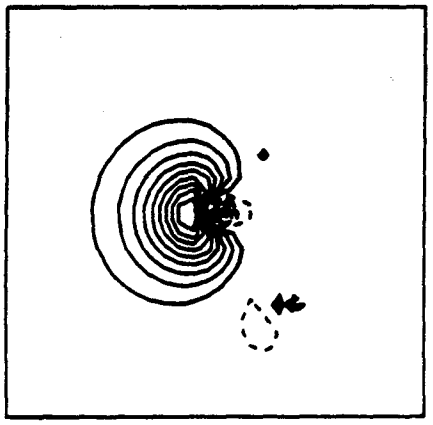

d) Cl p_π ORBITAL

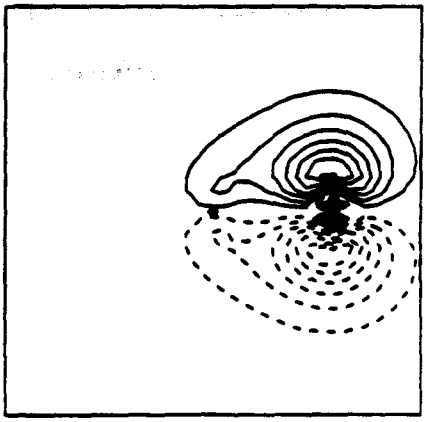

Figure 1

CHCl ($^3A''$)

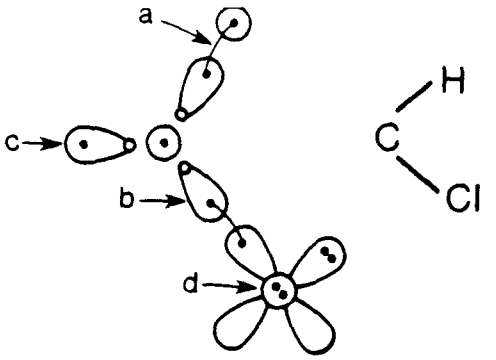

a) C – H BOND PAIR

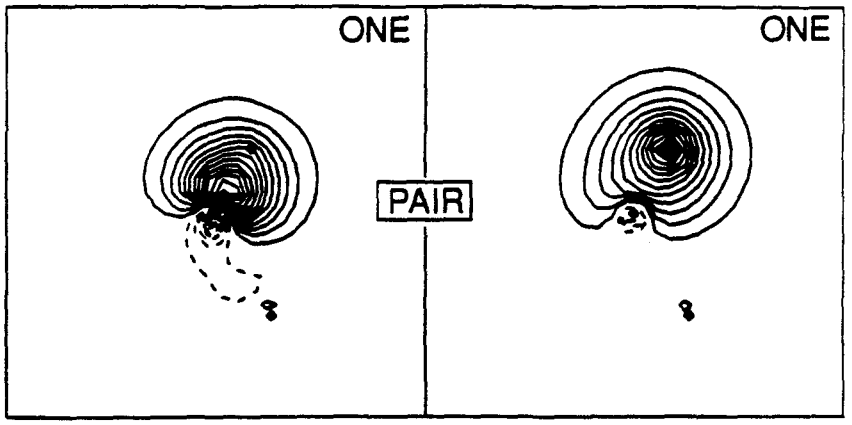

b) C – Cl BOND PAIR

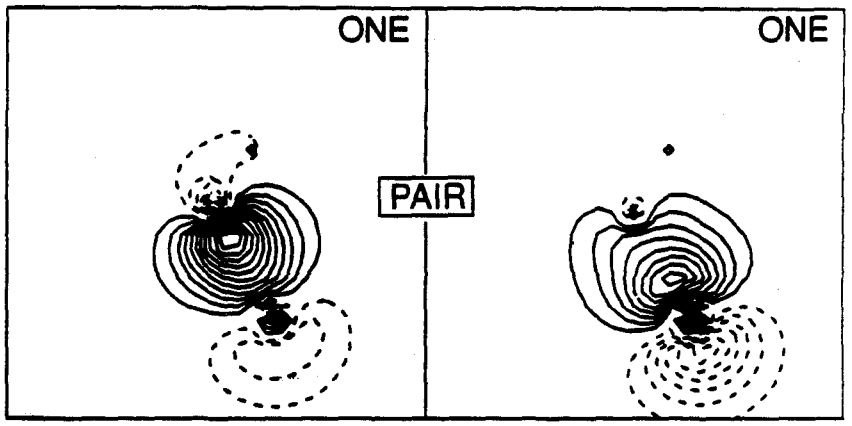

c) C σ ORBITAL

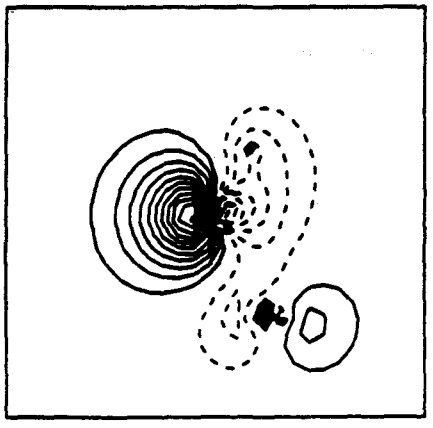

d) Cl p_π ORBITAL

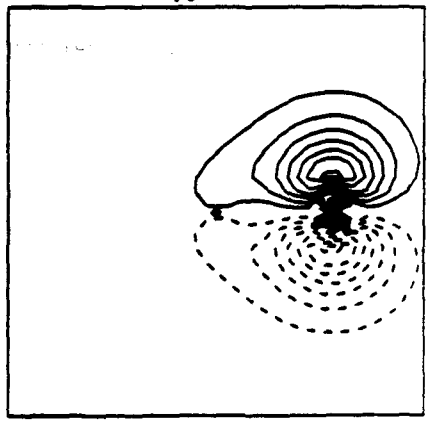

Figure 2

SiHCl ($^1A'$)

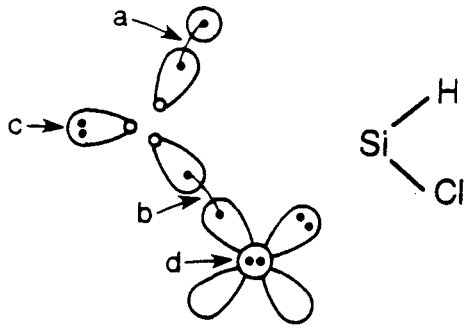

a) Si– H BOND PAIR

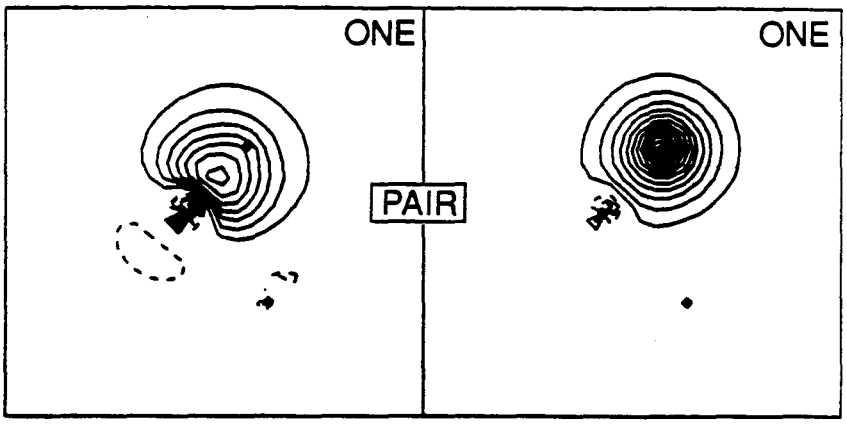

b) Si– Cl BOND PAIR

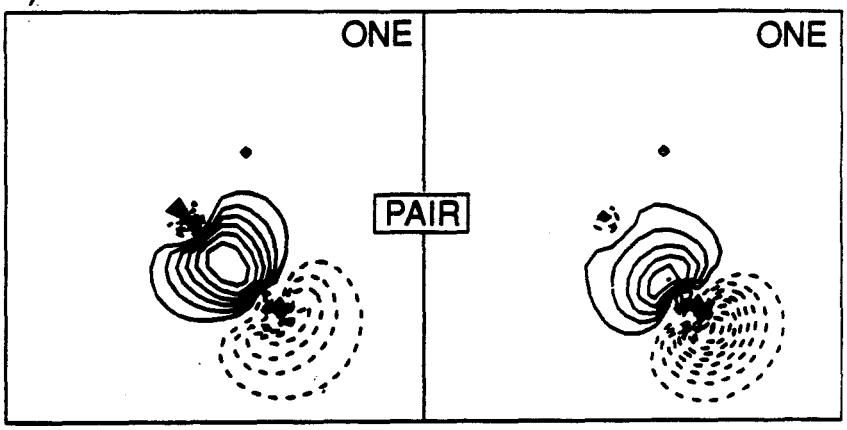

c) Si σ ORBITAL

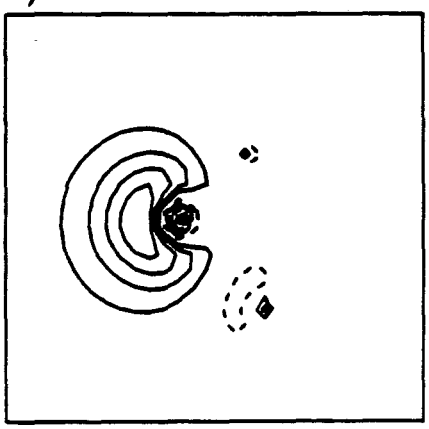

d) Cl p_π ORBITAL

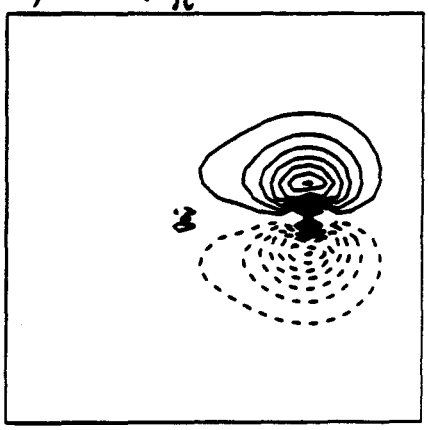

Figure 3

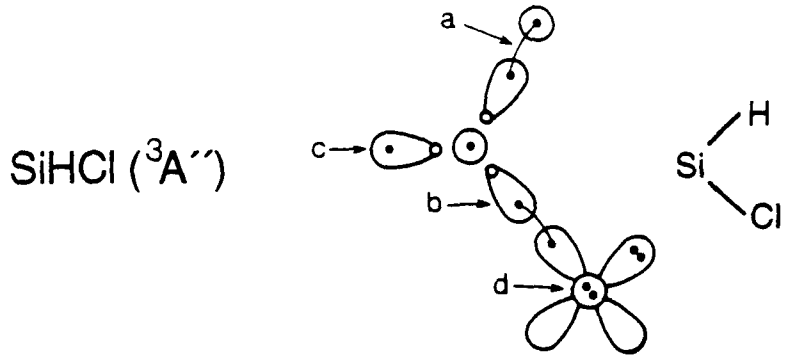
SiHCl ($^3A''$)
a
b
c
d
H
Si
Cl

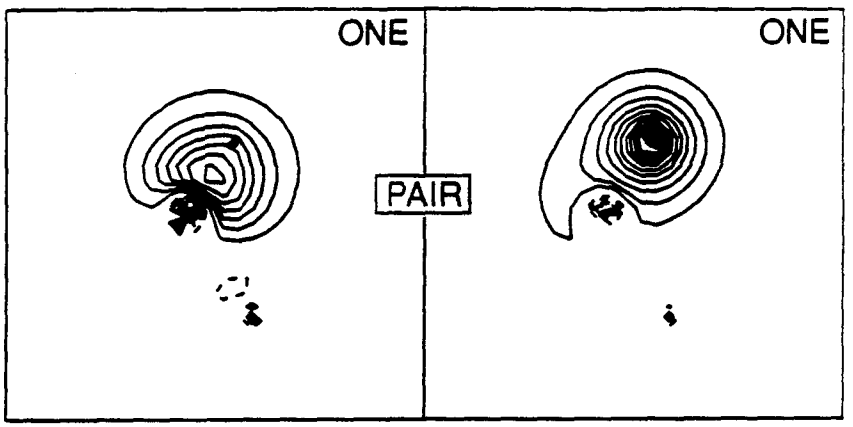
a) Si– H BOND PAIR
ONE
ONE
PAIR

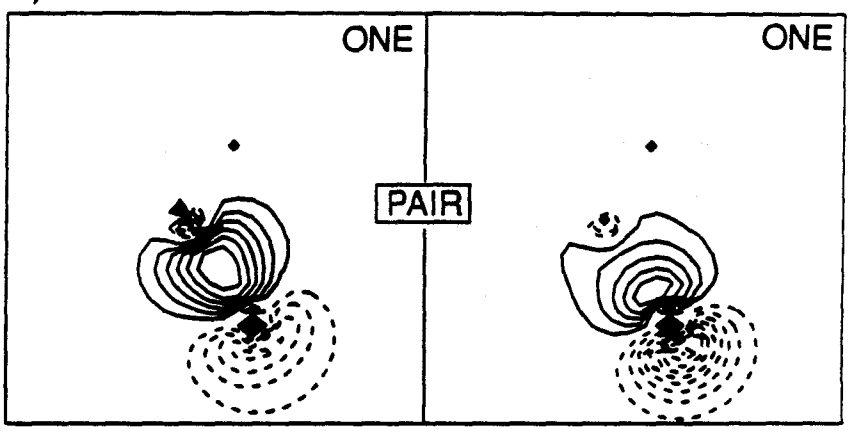
b) Si– Cl BOND PAIR
ONE
ONE
PAIR

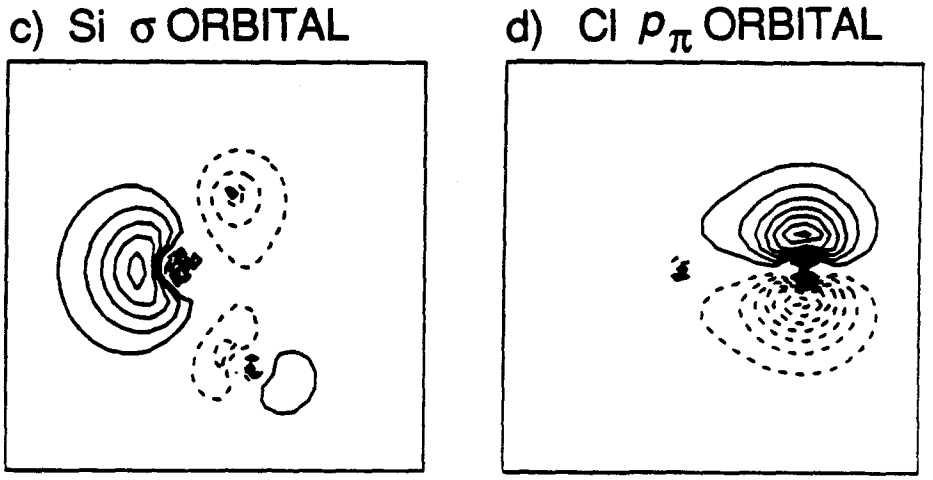
c) Si σ ORBITAL
d) Cl p_π ORBITAL

Figure 4

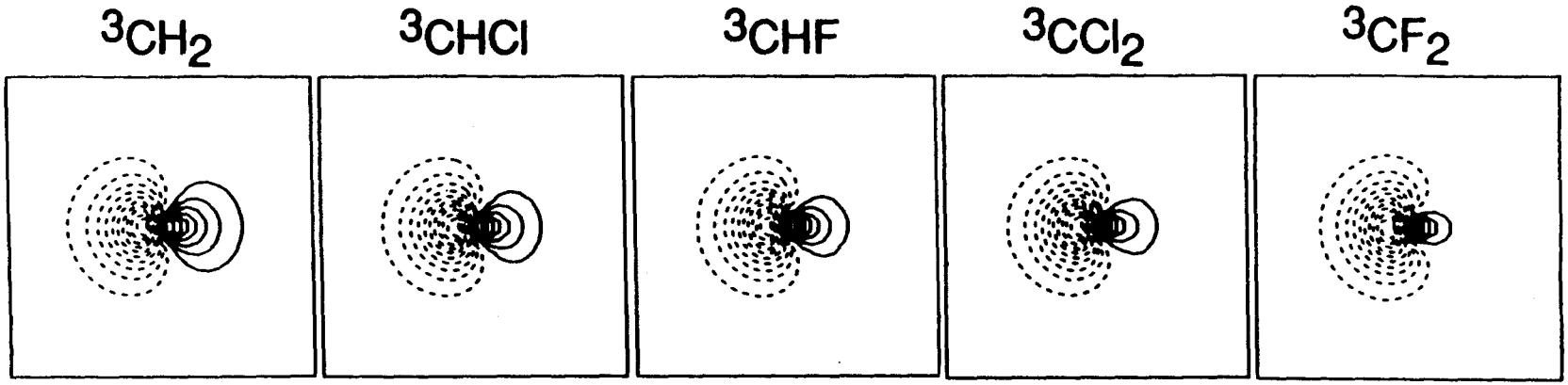

Figure 5

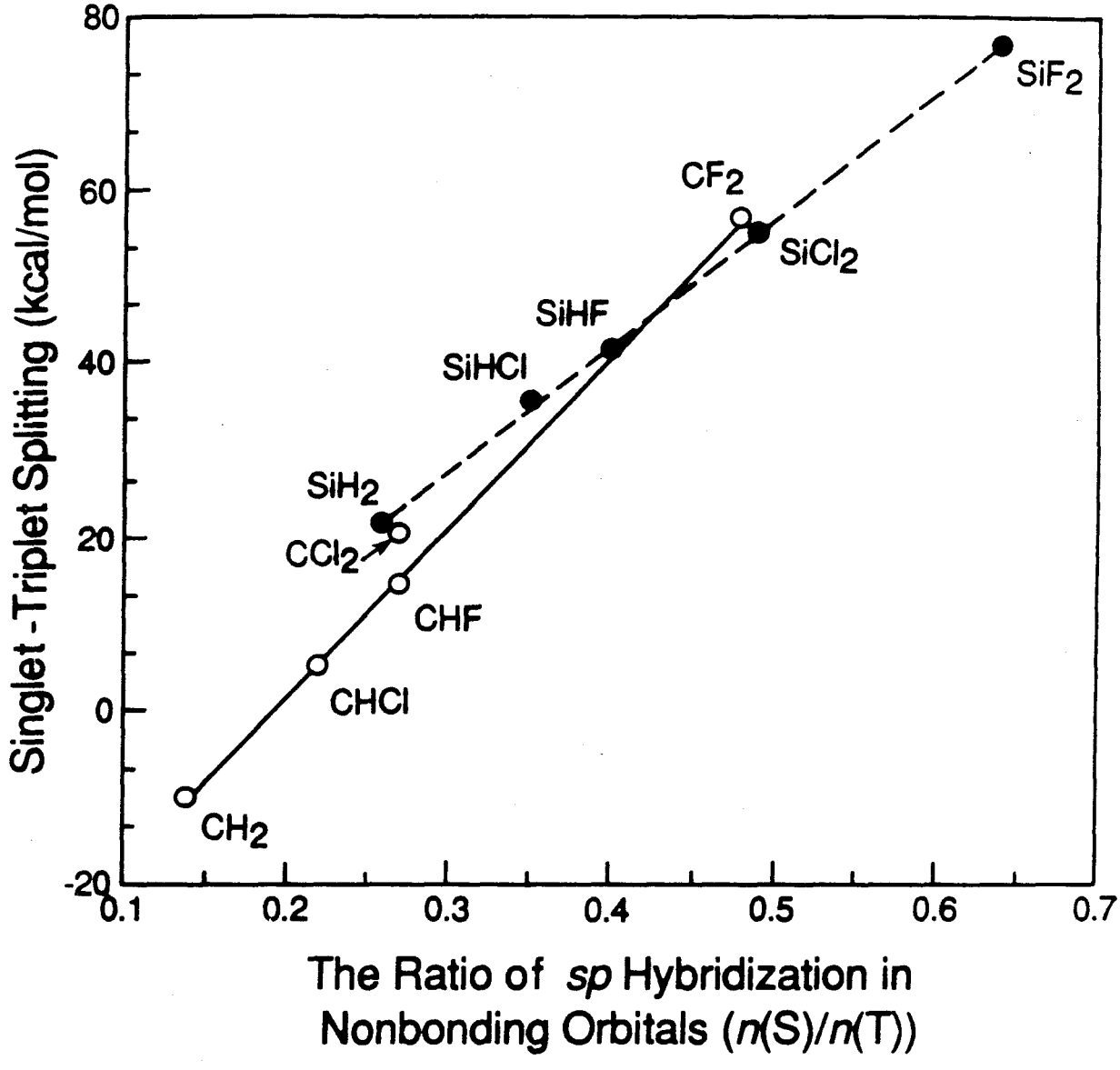
80
60
40
20
0
-20
0.1
0.2
0.3
0.4
0.5
0.6
0.7
Singlet - Triplet Splitting (kcal/mol)
The Ratio of sp Hybridization in Nonbonding Orbitals (n(S)/n(T))
SiF2
CF2
SiCl2
SiHF
SiHCl
SiH2
CCl2
CHF
CHCl
CH2

Figure 6

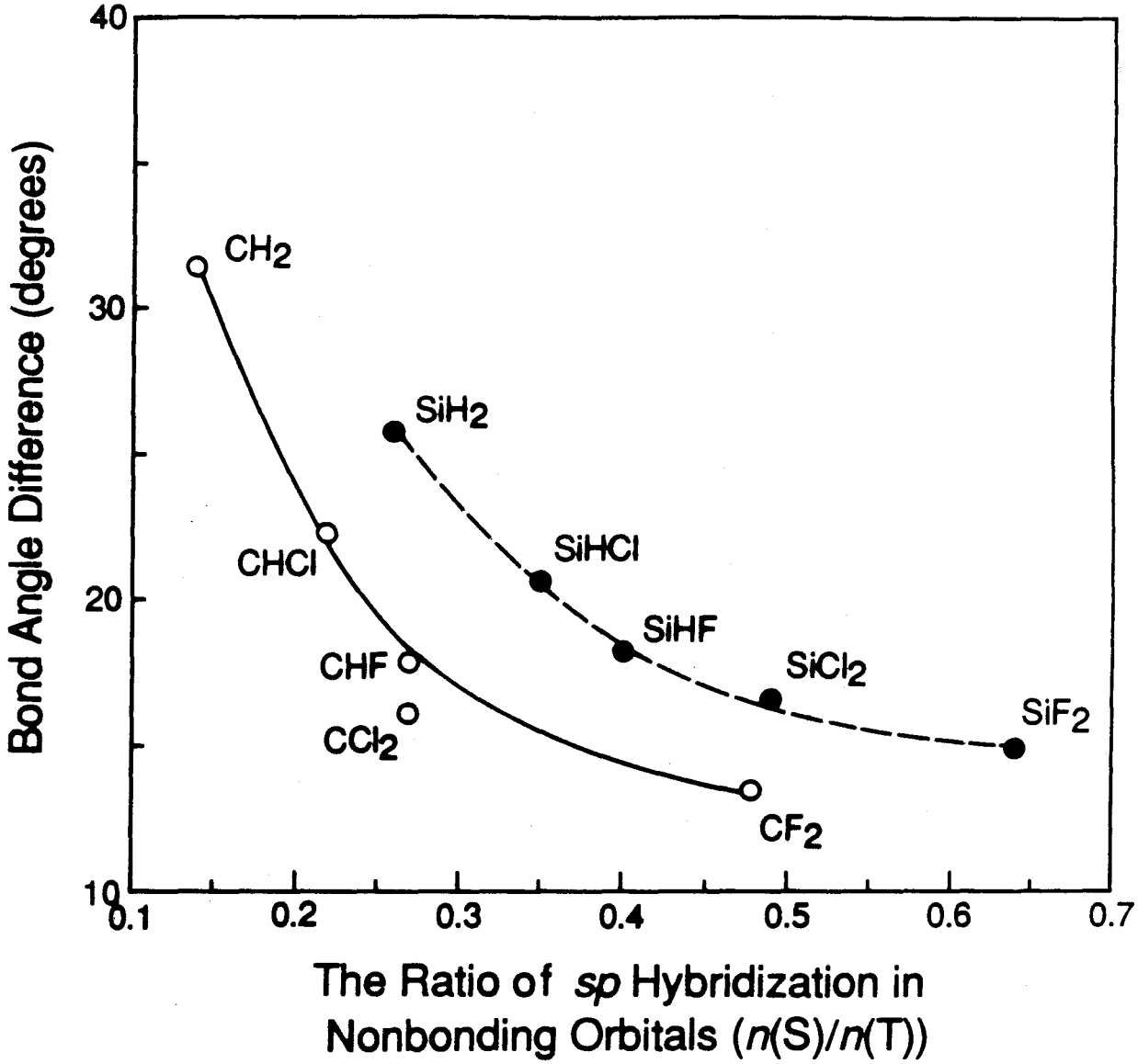
40
30
20
10
0.1
0.2
0.3
0.4
0.5
0.6
0.7
Bond Angle Difference (degrees)
The Ratio of sp Hybridization in Nonbonding Orbitals (n(S)/n(T))
CH2
SiH2
CHCl
SiHCl
SiHF
CHF
SiCl2
SiF2
CCl2
CF2

Figure 7

Chapter VII

Identification of $Mn(CO)_nCF_3^-$ (n=4,5) Structural Isomers by IR Multi-Photon Dissociation, Collision-Induced Dissociation, and Reactivities of Ligand Displacement Reactions

Identification of $Mn(CO)_nCF_3^-$ (n=4,5) Structural Isomers by IR Multi-Photon Dissociation, Collision-Induced Dissociation, and Reactivities of Ligand Displacement Reactions:

Seung Koo Shin, and J. L. Beauchamp*

Contribution No. 7951 from the Arthur Amos Noyes Laboratory of Chemical Physics

California Institute of Technology, Pasadena, California 91125

Abstract

The trifluoromethyl-migration reaction involving decarbonylation from the trifluoroacetylmanganese tetracarbonyl anion to the trifluoromethylmanganese tetracarbonyl anion is studied in the gas phase using Fourier transform ion cyclotron resonance spectroscopy. The dissociative electron attachment of trifluoroacetylmanganese pentacarbonyl produces $Mn(CO)_5CF_3^-$ and $Mn(CO)_4CF_3^-$ ions. $Mn(CO)_5CF_3^-$ slowly decomposes to yield $Mn(CO)_4CF_3^-$ with loss of CO. In order to identify the structures of these two ions, we have employed infrared multiphoton dissociation in conjuction with collision-induced dissociation and kinetics of ligand displacement reactions. $Mn(CO)_4CF_3^-$ ion derived from the dissociative electron attachment of a different precursor, trifluoromethylmanganese pentacarbonyl, is also used to confirm the identity of the trifluoromethyl-migration product ion. $Mn(CO)_5CF_3^-$ ion generated from trifluoroacetylmanganese pentacarbonyl does not undergo infrared multiphoton dissociation in the CO_2 wavelength range, which indicates the trifluoroacetyl structure $CF_3COMn(CO)_4^-$. $Mn(CO)_4CF_3^-$ ions derived from the two different precursors show identical infrared multiphoton dissociation spectral features within experimental errors. Two absorption maxima at 1052 and 945 cm^{-1} are assigned as a symmetric C–F stretch of A_1-type symmetry and a degenerate C–F stretch of E-type symmetry, respectively. Collision-induced dissociation of $Mn(CO)_4CF_3^-$ yields indistinguishable fragment mass spectra from the

two different precursors. Identical rate constants within experimental error are measured for $Mn(CO)_4CF_3^-$ from the two precursors in ligand displacement reactions with NO to yield $Mn(CO)_3(NO)CF_3^-$ with loss of CO. Displacement of CO by ^{13}CO or PF_3 is not observed for either ion. These results support identical structures for $Mn(CO)_4CF_3^-$ from the two different precursors, with the CF_3 ligand directly bonded to manganese, $CF_3Mn(CO)_4^-$. It is postulated that this ion from trifluoromethylmanganese pentacarbonyl is produced directly by electron attachment accompanied by loss of one equatorial CO. With trifluoroacetylmanganese pentacarbonyl, electron attachment leads to loss of an equatorial CO followed by the migration of CF_3 from the acetyl carbon to the vacant equatorial site on the manganese center with loss of another CO in the equatorial position to the CF_3 ligand. The CF_3 group is an ideal infrared chromophore to investigate the infrared photochemistry of organometallic complexes, $L_nM–CF_3$, structures, and reaction mechanisms of their coordinatively unsaturated intermediates containing metal bonded CF_3 groups.

I. Introduction

Organometallic migration reactions have been studied extensively in recent years.[1] Many kinetic and stereochemical studies of alkyl to acyl migratory-insertion reactions have been reported. The generally accepted two-step mechanism for migratory-insertion which is presented in equation 1 invokes a coordinatively unsaturated acyl intermediate.

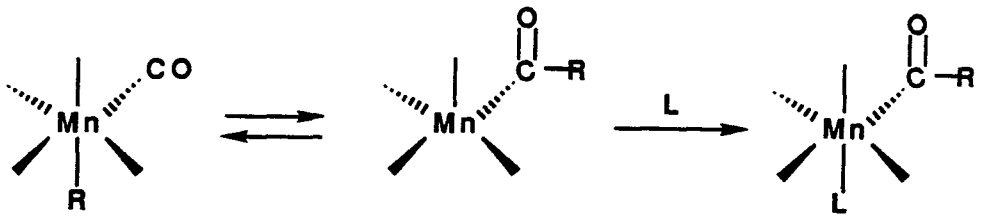

(1)

In the first step there is an equilibrium between the coordinatively saturated alkyl complex and the coordinatively unsaturated acyl complex. The second step involves the addition of the external ligand affording the product, a saturated acyl complex. Most of the cases have been studied under conditions whereby the equilibrium lies far to the right.

Considerable attention has been directed to determine whether these reactions proceed by CO insertion or alkyl-migration,[2] but information on the reverse alkyl-migration step from the acyl intermediate to the alkyl complex has been rarely studied.[2] The direct kinetic studies of the reverse methyl-migration step have been reported by Kubota et al..[3] They prepared five-coordinated phenylacetyliridium complexes (I) from the oxidative additions of phenylacetyl chlorides to *trans*-chlorobis(triphenylphosphine)dinitrogeniridium. These five-coordinated iridium complexes rearrange in solution to six-coordinated benzyl(carbonyl) complexes (II). They found that electron-withdrawing groups retard this alkyl migration.

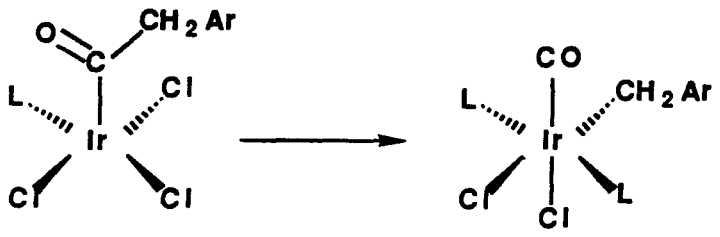

(I) (II)

Recently, Casey et al.[4] have studied reductive elimination of acetophenone from $N(CH_3)_4^+[cis\text{-}Mn(CO)_4(COCH_3)(COC_6H_5)]^-$ (III) to measure relative migratory aptitudes between methyl and benzyl in the conversion of acyl-metal to alkyl-metal complexes. Their results were interpreted in terms of a mechanism involving loss of CO from III and formation of a five-coordinated intermediate $Mn(CO)_3(COCH_3)(COC_6H_5)^-$ (IV), which is in rapid equilibrium with a benzoyl-methyl intermediate $Mn(CO)_4(CH_3)(COC_6H_5)^-$ due to the facile methyl migration. Conversion of IV to the acetylphenyl intermediate $Mn(CO)_4(COCH_3)(C_6H_5)^-$ is followed by reductive elimination to give acetophenone and $Mn(CO)_4^-$. The formation of a coordinatively unsaturated $Mn(CO)_4^-$ intermediate was trapped by forming the complex $Mn(CO)_4(P(C_6H_5)_3)^-$ with triphenylphosphine.

To provide a fundamental undertanding of these complex organometallic reaction mechanisms, it is prerequisite to devise methods to isolate the coordinatively unsaturated intermediates, identify the structures, and examine the reaction kinetics in the absence of solvent effects. However, there has been no report of kinetic studies of methyl-migration reactions in the gas phase. In the present paper we employ Fourier transform ion cyclotron resonance spectroscopy to isolate the coordinatively unsaturated intermediates and examine structures, reactivities, and spectroscopic properties of the isolated intermediates for one such reaction.

Dissociative electron attachment[5] of trifluoroacetylmanganese pentacarbonyl, $CF_3COMn(CO)_5$, generates $Mn(CO)_5CF_3^-$ and $Mn(CO)_4CF_3^-$ ions. The former ion is considered to be a 17 e^- trifluoroacetylmanganese tetracarbonyl anion (V), $CF_3COMn(CO)_4^-$, because the other possiblity of a 19 e^- trifluoromethylmanganese pentacarbonyl anion, $CF_3Mn(CO)_5^-$, is most unlikely. However, $Mn(CO)_4CF_3^-$ affords the possibility of being either trifluoroacetyl (VI) or trifluoromethyl (VII) manganese ions of the same mass-to-charge ratio. $Mn(CO)_5CF_3^-$ slowly decomposes to yield $Mn(CO)_4CF_3^-$ with loss of CO, leaving the chance of observing the trifluoromethyl migratory decarbonylation reaction, if $Mn(CO)_5CF_3^-$ and $Mn(CO)_4CF_3^-$

ions are trifluoroacetyl (V) and trifluoromethyl (VII) manganese tetracarbonyl anions, respectively.

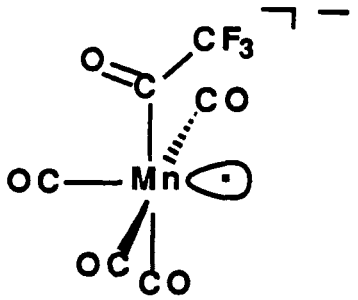

(V)

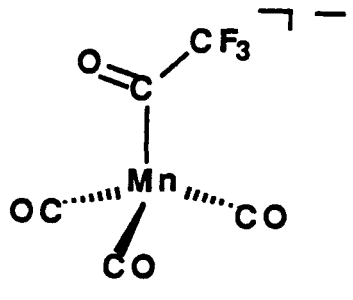

(VI)

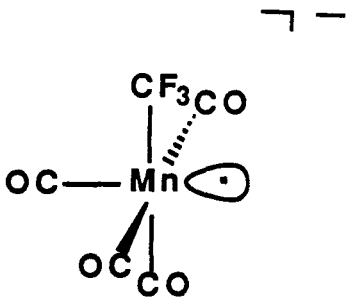

(VII)

Since trifluoromethylmanganese pantacarbonyl, $CF_3Mn(CO)_5$, also produces $Mn(CO)_4CF_3^-$ by dissociative electron attachment, results from $Mn(CO)_4CF_3^-$ ions derived from the two different precursors, $CF_3COMn(CO)_5$ and $CF_3Mn(CO)_5$, can be directly compared. $Mn(CO)_4CF_3^-$ ion obtained from the $CF_3Mn(CO)_5$ precursor is considered to be trifluoromethyl tetracarbonyl anion, $CF_3Mn(CO)_4^-$ (VII), because the migration of CF_3 from CF_3–$Mn(CO)_4^-$ to the carbonyl carbon yielding CF_3CO–$Mn(CO)_3^-$ is estimated to be endothermic by 33 kcal/mol.[6]

The structural differentiation between iosomeric ions with the same mass-to-charge ratio has been explored using several mass spectrometric techniques. These approaches, which are successful with certain classes of ions, include collision-induced dissociation (CID)[7], specific reactivity in bimolecular processes[8], and photodissociation[9].

The most widely used technique is high energy collision-induced dissociation of a mass-selcted ion, which often yield a characteristic fragmentation pattern distinguishing isomeric structures. For example, Peake et al.[10] have probed the structures of $FeC_nH_{2n}^+$ species formed by reaction of $Fe(CO)^+$ with olefins ($n = 2 - 14$) and

cycloalkanes ($n = 3-6$) using high energy collision-induced dissociation of the iron-olefin complex in a tandem mass spectrometer (MS/MS). Freiser and co-workers[11] have utilized collision-induced dissociation techniques to distinguish isomeric structures, generate unprecedented ions, and deduce reaction mechanisms and thermochemistry.

The second method utilizes distinguishable reactivities of isomeric ions in low energy bimolecular ion-molecule collisions. Small hydrocarbon ions have been investigated with this method.[8] For instance, Halle et al.[12] have distinguished a bisethylene complex, $Ni(C_2H_4)_2^+$, formed by dehydrogenation of *n*-butane with Ni^+, from a metallacycle complex, $NiC_4H_8^+$, yielded from decarbonylation of cyclopentanone with Ni^+, by different reaction products of reactive collisions of isomeric complexes with HCN. Jacobson and Freiser[13] have probed the structures of $Rh(C_7H_6)^+$ isomers obtained from reaction of Rh^+ with toluene using H/D exchange reactions with D_2.

Isomeric ions may be differentiated if they have different photodissociation spectra or if their photoproducts differ. Energies required for cleavage of typical bonds necessitate visible or ultraviolet radiation for single-photon events. Such photodissociation resulting from VIS and UV irradiation have been quite useful for structure elucidation of gaseous ions.[9] Recent experiments employing infrared multiphoton dissociation (IRMPD) processes[14] have also demonstrated the possibility of isomeric differentiation based on the observed IRMPD spectra.[9b] For example, $C_3F_6^+$ molecular ions formed from either perfluoropropylene or perfluorocyclopropane, affording the possibility of observing cyclic or acyclic ions of the same mass-to-charge ratio, have identical photodissociation spectra upon gated cw CO_2 laser irradiation.[15] Wright and Beauchamp[16] have successfully differentiated between benzyl and cycloheptatrienyl anions generated from different precursors using their distinguishable infrared multiphoton electron attachment spectra. Recently, Baykut et al.[17] have observed different infrared multiphoton dissociation products from $C_4H_9O_2^+$ ions arising from different precursors. Hanratty et al.[18]

have probed the potential energy surfaces for reactions of cobalt ions with C_5H_{10} isomers. Infrared multiphoton dissociation of Co(1-pentene)$^+$ and Co(2-pentene)$^+$ adducts yields distinguishable photoproducts, $Co(C_3H_6)^+$ with loss of ethylene and $Co(C_4H_6)^+$ with loss of methane, respectively, in processes which can be interpreted as resulting from the facile insertion of the metal ion into an allylic carbon-carbon bond.

In the present paper we employ infrared multiphoton dissociation, combined with collision-induced dissociation and ligand displacement reactions in the trapping ion cyclotron resonance cell[19] to distinguish the structures and reactivities of $Mn(CO)_nCF_3^-$ $(n = 4, 5)$ ions.

Experimental Section

Experimental techniques associated with ICR spectroscopy,[8a-c] and in particular Fourier transform ion cyclotron resonance spectroscopy,[20] have been previously described in detail. Experiments were performed using an Ion Spec FT–ICR data system in conjunction with a 1-in. cubic trapping cell[19] built by Bio-Med Tech[21] situated between the poles of a Varian 15-in. electromagnet maintained at 2 Tesla.

All experiments were carried out in the range of 10^{-7}–10^{-5} Torr, corresponding to neutral particle densities of 3.5×10^9 to 3.5×10^{11} molecule cm^{-3}. Pressures were measured with a Schulz-Phelps ion gauge[22] calibrated against an MKS Baratron (Model 390 HA-0001) capacitance manometer. The principal errors in the rate constants (estimated to be $\pm 20\%$) arise from uncertainties in pressure measurements.[23] Sample mixtures were prepared directly in the instrument using three sample inlets and the Schulz-Phelps gauge.

Where available, chemicals were obtained commercially in high purity and used as supplied except for multiple freeze-pump-thaw cycles to remove noncondensable gases. Manganese compounds were synthesized with the assitance of J. W. Park of Professor R. H. Grubbs' group at Caltech. Trifluoroacethylmanganese pen-

tacarbonyl, $CF_3COMn(CO)_5$, was prepared by treatment of $NaMn(CO)_5$ with trifluoroacetic anhydride. Trifluoromethylmamganese pentacarbonyl, $CF_3Mn(CO)_5$, was obtained by heating $CF_3COMn(CO)_5$ at 110 °C.[24] Melting points were measured using a Thomas-Hoover melting apparatus ($CF_3COMn(CO)_5$: 55 – 56 °C; $CF_3Mn(CO)_5$: 82 – 83 °C). Fluorine-19 nuclear magnetic resonance (84.57 MHz) spectra were obtained on a Jeol FX-90 spectrometer. $CF_3COMn(CO)_5$ and $CF_3Mn(CO)_5$ in benzene-d_6 show sharp singlets at 81.2 and 28.3 ppm downfield from C_6F_6, respectively.

ICR modifications for infrared photochemistry are described elsewhere.[25] The unfocused infrared beam from a grating tuned Apollo 550A CW CO_2 laser enters the vacuum system through an antireflection coated NaCl window (25.4 mm diameter × 3.5 mm thick) supplied by Oriel, Inc. and passes a 92% transmittance mesh to allow irradiation of trapped ions. The transmitter plate reflects the beam for a second pass through the ion-trapping region and out of the apparatus. Assuming that the plate reflects 100% of the incident laser beam and taking into account the 92% mesh transmittance, the beam power inside the cell is 1.84 times the power of the beam entering the vacuum system. Beam shape is monitored with an Optical Engineering Model 22A thermal imaging plate. Infrared wavelengths are measured with an Optical Engineering Model 16A spectrum analyzer. Bandwidths are estimated to be 100 MHz. Beam power is measured with a Scientech, Inc. Model 36-0001 surface absorbing disc calorimeter. Power fluctuations are typically ±5% during an experiment. The CO_2 laser beam is triggered by the control pulse from the computer. Laser beam duration is typically 20 msec with laser intensity of about 8 W cm^{-2} inside the cell. Although laser intensity in the cell can be varied because of the Gaussian beam profile, irradiation of trapped ions is uniform as indicated by the fact that small translations of the laser beam do not alter photoproduct distributions.

Gas-phase infrared absorption spectra of manganese compounds were recorded with the assistance of J. E. Hanson of Professor P. B. Dervan's group at Caltech

using a Mattson Instruments, Inc. Sirius 100 FT-IR spectrometer having a Hg-Cd-Te detector cooled by liquid N_2. A 10-cm path length cell equipped with NaCl windows were used.

The negative ions were generated by dissociative electron attachment with 2 eV electrons. Since both anions and electrons are trapped in the cell during the negative-ion mode experiment, electrons are ejected from the cell shortly after the electron beam pulse by applying an oscillating electric field (about 5 V_{pp} amplitude and 6.72 MHz frequency at -1 V trapping voltage) across the trapping plates. Ions formed by dissociative electron attachment are stored in the trapping ICR cell and mass-selected by a series of ion ejection pulses. Translational excitation of the reactant ion was minimized by using the lowest possble rf fields. The infrared multiphoton dissociation spectra of mass-selected ions are obtained with a constant power (8 W cm^{-2}) and 20 msec duration laser beam at all lines in the 925–1085 cm^{-1} wavelength range. In the ligand displacement reactions of $CF_3Mn(CO)_4^-$ ions with ^{13}CO, PF_3, and NO, the temporal variations of reactant and product ion abundances starting from $CF_3Mn(CO)_4^-$ were recorded and used to calculate rate constants. The temperature in the ICR cell is assumed to be 298 °K.

Results and Discussion

Infrared Spectra of $CF_3COMn(CO)_5$ and $CF_3Mn(CO)_5$. Figure 1 shows gas-phase infrared absorption spectra of trifluoroacetylmanganese pentacarbonyl (top) and trifluoromethylmanganese pentacarbonyl (bottom). Spectrometer resolution is 0.5 cm^{-1}. The same samples are used for the rest of the experiments described below. Note the absence of cross contamination of the two samples.

Vibrational frequencies for $CF_3COMn(CO)_5$ are assigned from the comparison with reported results for CF_3COCl[26], $CF_3Mn(CO)_5$[27], and $C_2F_5COMn(CO)_5$[28] and are listed in Table I. There are four infrared absorption bands for the CF_3 group in $CF_3COMn(CO)_5$. The peak at 1254 cm^{-1} is assigned as a symmetric C–F stretch and peaks at 1191 and 1141 cm^{-1} are assigned as a in-plane C–F stretch and a out-of-plane C–F stretch, respectively.[29] The small peak at 719 cm^{-1} is due to a F–CF_2 deformation. No vibrational bands fall within the CO_2 laser wavelength range (925–1085 cm^{-1}).

Infrared absorption bands of trifluoromethylmanganese pentacarbonyl have been assigned previously in the literature[27] and summarized in Table I. The strong peak at 1063 cm^{-1} has been identified as a C–F stretch of A_1-type symmetry and the peak at 1043 cm^{-1} as a degenerate C–F stretch of E-type symmetry.[27a] Since the trifluoromethyl ligand exhibits strong absorption bands within CO_2 laser wavelength range, it is an ideal probe ligand to study the infrared multiphoton dissociation processes of organometallic compounds.

The CO stretching vibrations for $CF_3COMn(CO)_5$ are symmetric stretching of equatorial CO at 2134 cm^{-1} (A_1-type symmetry), degenerate stretching of equatorial CO at 2050 cm^{-1} (E-type symmetry), symmetric stretching of axial CO at 2028 cm^{-1} (A_1-type symmetry), and an acetyl CO stretch at 1673 cm^{-1}. $CF_3Mn(CO)_5$ shows symmetric and degenerate stretchings of equatorial CO at 2142 (A_1) and 2055 (E) cm^{-1}, respectively, which are slightly greater than those for $CF_3COMn(CO)_5$ by 8 and 5 cm^{-1}, respectively. This result indicates that the CF_3 ligand is the

poorer σ donor than the CF_3CO ligand, leading to less electron density on manganese available to the π back donation to the equatorial CO.[30,31] The symmetric stretching vibration for the axial CO in $CF_3Mn(CO)_5$ peaks at 2026 cm^{-1} which is 2 cm^{-1} smaller than axial CO stretch in $CF_3COMn(CO)_5$. It has been previously suggested that the force constants of all carbonyl groups in $LMn(CO)_5$ complexes will change by the same amount owing to the change in inductive effect in going from one ligand to another; while the differences in π bonding between two ligands will affect the *trans* force constant twice as much as the *cis*.[31] This means that the CF_3CO ligand considerably increases an axial CO stretching frequency due to its greater π-acceptor ability than the CF_3 ligand. However, it is evident that both CF_3 and CF_3CO ligands are weaker π-acceptors than CO,[31] because stretching vibrations for axial carbonyls *trans* to these ligands are much weaker than those for equatorial carbonyls *trans* to the carbonyls. This result also implies that the $Mn-(CO)_{ax}$ bond is significantly stronger than the $Mn-(CO)_{eq}$ bond. Bond energies of of $D[(CO)_5Mn-CF_3]$ = 48.9 kcal/mol and $D[(CO)_5Mn-COCF_3]$ = 42.9 kcal/mol have been reported previously.[6] The CF_3 ligand forms a stronger bond than the CF_3CO ligand because the σ orbital of trifluoromethyl has considerably more carbon 2*s* character than that of trifluoroacetyl resulting in a significant bond shortening in $Mn-CF_3$ bond.[32]

Reactions of $Mn(CO)_nCF_3^-$ Ions. Dissociative electron attachment of $CF_3COMn(CO)_5$ produces $Mn(CO)_nCF_3^-$ ($n = 2-5$) and $Mn(CO)_5^-$ fragment ions as shown in Figure 2a and that of $CF_3Mn(CO)_5$ yields $Mn(CO)_nCF_3^-$ ($n = 2-4$) ions as shown in Figure 2b. $Mn(CO)_5CF_3^-$ and $Mn(CO)_5^-$ ions are the chracteristics of the $CF_3COMn(CO)_5$ precursor. $Mn(CO)_5CF_3^-$ ion derived from the $CF_3COMn(CO)_5$ precursor slowly decomposes by thermal collisions with parent molecule to yield $Mn(CO)_4CF_3^-$ with loss of CO with a rate constant of 2.5×10^{-11} cm^3 $molecule^{-1}$ sec^{-1} as shown in Figure 3. The most abundant ions, $Mn(CO)_4CF_3^-$, formed from the two precursors are very stable and unreactive with

their neutral precursors. $Mn(CO)_3CF_3^-$ ion generated from the two precursors also slowly decomposes to yield $Mn(CO)_2CF_3^-$ with loss of CO with a rate constant of 4.4×10^{-11} cm^3 molecule^{-1} sec^{-1}. The 18 e$^-$ $Mn(CO)_5^-$, which is a distinguishing trait of $CF_3COMn(CO)_5$, does not react with the neutral presursor. $Mn(CO)_2CF_3^-$ ions are unreactive with their netrual partners.

Infrared Multiphoton Dissociation Spectra of $Mn(CO)_4CF_3^-$ Ions. $Mn(CO)_4CF_3^-$ ions formed by dissociative electron attachment of two different precursors, trifluoroacetyl- or trifluoromethylmanganese pentacarbonyl, affords the possibility of observing trifluoroacetyl or trifluoromethyl manganese ions of the same mass-to-charge ratio (VI and VII, respectively).

Figure 4a presents a spectrum of the isolated $CF_3Mn(CO)_4^-$ ion generated from $CF_3COMn(CO)_5$ just after a series of ejection pulses. Figure 4b shows the appearance spectrum of the photodissociation fragments of $Mn(CO)_4CF_3^-$ at 944 cm^{-1} with the 20 msec duration of 8 W cm^{-2} laser beam. $Mn(CO)_4CF_3^-$ loses CO to yield $Mn(CO)_3CF_3^-$ which undergoes infrared multiphoton dissociation to form $Mn(CO)_2CF_3^-$. The photodissociation spectrum of $Mn(CO)_4CF_3^-$ is obtained by taking the ratio of photofragment intensities ($Mn(CO)_3CF_3^-$ + $Mn(CO)_2CF_3^-$) to the total ion intensity ($Mn(CO)_4CF_3^-$ + $Mn(CO)_3CF_3^-$ + $Mn(CO)_2CF_3^-$) as a function of laser wavelength.

Figure 5 shows the infrared absorption spectrum of the CF_3 group in $CF_3Mn(CO)_5$ over the CO_2 laser wavelength range (top), the infrared multiphoton dissociation spectra of $Mn(CO)_4CF_3^-$ derived from $CF_3COMn(CO)_5$ (middle), and $Mn(CO)_4CF_3^-$ obtained from $CF_3Mn(CO)_5$ (bottom). The infrared photodissociation spectrum of $Mn(CO)_4CF_3^-$ derived from $CF_3COMn(CO)_5$ (Figure 5, middle) shows broad bands at two maxima at 1052 and 945 cm^{-1} which, within experimental errors, coincides exactly with spectral features in the photodissociation spectrum of the same mass ion generated from $CF_3Mn(CO)_5$. Further investigation of the trifluoroacetyl-containing anion is described below.

Figure 6 shows the photoproduct appearance spectra of $Mn(CO)_3CF_3^-$ from the infrared multiphoton dissociation of $Mn(CO)_4CF_3^-$. Two spectra from different presursors, $CF_3COMn(CO)_5$ (top) and $CF_3Mn(CO)_5$ (bottom), match well with each other. The further photodissociation of $Mn(CO)_3CF_3^-$ ions during laser irradiation resulted in $Mn(CO)_2CF_3^-$ with loss of CO. The photoproduct spectra of $Mn(CO)_2CF_3^-$ ions in Figure 7 shows similar appearance bands as $Mn(CO)_3CF_3^-$ ions. This indicates that $Mn(CO)_3CF_3^-$ has infrared absorption bands which strongly overlap those of the $Mn(CO)_4CF_3^-$ ion.

Collision-Induced Dissociation Spectra of $Mn(CO)_4CF_3^-$ Ions. Figure 8 shows the collision-induced dissociation spectra of $Mn(CO)_4CF_3^-$ ions from $CF_3COMn(CO)_5$ (top) and $CF_3Mn(CO)_5$ (bottom) precursors. If the $Mn(CO)_4CF_3^-$ ion derived from $CF_3COMn(CO)_5$ contains the trifluoroacetyl group, then the $Mn(CO)_3^-$ ion would be present in the collision-induced dissociation spectrum by loss of CF_3CO. Collisions of $Mn(CO)_4CF_3^-$ ions from two different precursors with Ar or Kr buffer gas induce identical dissociation patterns without any indication of $Mn(CO)_3^-$ fragment ions expected from the $CF_3COMn(CO)_3^-$ ion if present. The translational energy imparted to an ion is estimated to be about 84 eV (corresponding to center of mass collision energies of 12 and 22 eV, respectively, for Ar and Kr). $MnCF_3^-$ is the most intense fragment ion observed after the collision-induced dissociation. The intensity of the $Mn(CO)_3CF_3^-$ ion is very weak compared with the infrared multiphoton dissociation process, which manifests that the collision-induced dissociation is a higher energy activation process than the infrared multiphoton dissociation which proceeds selectively by the pathway with the lowest activation energy.[18,33]

Ligand Displacement Reactivities of $Mn(CO)_4CF_3^-$ Ions. We have examined ligand displacement reactions of $Mn(CO)_4CF_3^-$ ions from the two precursors with the strong π-acids[34], ^{13}CO, PF_3, and NO. If $Mn(CO)_4CF_3^-$ generated from $CF_3COMn(CO)_5$ is $CF_3COMn(CO)_3^-$, the reactivity of ligand displacement of this

15 e^- anion with the strong π-acids would be quite different from that of the 17 e^- $CF_3Mn(CO)_4^-$ ion.

The thermoneutral ligand displacement reaction of $Mn(CO)_4CF_3^-$ ions with ^{13}CO does not occur. No ligand displacement is observed in the reaction of $Mn(CO)_4CF_3^-$ ions with the more strong π-acceptor PF_3.[34] Coderman and Beauchamp[35] have observed the ligand displacement reaction of the 17 e^- η^5-$CpCo(CO)^-$ (cyclopentadienylcobalt carbonyl) ion with PF_3 to yield the 17 e^- η^5-$CpCoPF_3^-$ ion with loss of CO, presumably via the ring slippage forming the 15 e^- η^3-$CpCo(CO)^-$ intermediate. In light of these results, it is reasonable to suggest that $Mn(CO)_4CF_3^-$ is the 17 e^- complex and does not undergo the CF_3 migration forming the 15 e^- $CF_3COMn(CO)_3^-$ intermediate during the thermal bimolecular encounter.

However, nitric oxide, NO, which can be considered as either 1 e^- or 3 e^- donor, reacts with $Mn(CO)_4CF_3^-$ ions to yield a nitrosyl-containing complex $Mn(CO)_3(NO)CF_3^-$ with loss of one CO (Eq. 2).

$$Mn(CO)_4CF_3^- + NO \longrightarrow Mn(CO)_3(NO)CF_3^- + CO \qquad (2)$$

$Mn(CO)_4CF_3^-$ ion derived from the $CF_3COMn(CO)_5$ precursor undergoes reaction 2 as shown in Figure 9a with a rate constant of $3.7\pm0.7\times10^{-12}$ cm^3 $molecule^{-1}$ sec^{-1}, which is in good agreement with the observed rate constant of $4.2 \pm 0.8 \times 10^{-12}$ cm^3 $molecule^{-1}$ sec^{-1} for the ligand displacement reaction of $Mn(CO)_4CF_3^-$ ion obtained from the $CF_3Mn(CO)_5$ precursor with NO as shown in Figure 9b. If this slow rate is due to a barrier, assuming the typical ion-molecule collision frequency of 1.0×10^{-9} cm^3 $molecule^{-1}$ sec^{-1} leads to an estimated activation energy of 2 kcal/mol.

In light of the similar infrared multiphoton dissociation spectra, the indistinguishable collision-induced dissociation patterns, and the identical rate constant within experimental errors for the ligand displacement reaction with NO, *it is quite reasonable to conclude that* $Mn(CO)_4CF_3^-$ *ions generated from the dis-*

sociative electron attachment of two different precursors, $CF_3COMn(CO)_5$ *and* $CF_3Mn(CO)_5$, *are the same 17* e^- *species having the trifluoromethyl group directly bonded to the manganese, which is a trifluoromethylmanganese tetracarbonyl ion* (VII), $CF_3Mn(CO)_4^-$.

Infrared Multiphoton Dissociation of $CF_3COMn(CO)_4^-$ and the Migratory Decarbonylation Reaction. $Mn(CO)_5CF_3^-$ and its decomposition product $Mn(CO)_4CF_3^-$, which are trapped in the ICR cell after 1 sec delay from the initial isolation of $Mn(CO)_5CF_3^-$, are irradiated with 8 W cm^{-2} CO_2 laser beam for 10 msec. Figure 10 shows the mass spectra before (top) and after (bottom) the CO_2 laser irradiation at 944 cm^{-1}. The absolute intensity of $Mn(CO)_5CF_3^-$ remains constant, while $Mn(CO)_4CF_3^-$ dissociates first to $Mn(CO)_3CF_3^-$ and subsequently yield $Mn(CO)_2CF_3^-$. $Mn(CO)_5CF_3^-$ does not undergo the infrared multiphoton dissociation in the 925–1085 cm^{-1} wavelength range. Since the CF_3CO group bonded to manganese has no infrared absorption bands in the CO_2 laser wavelength range and the decomposition product $Mn(CO)_4CF_3^-$ is proven as $CF_3Mn(CO)_4^-$, $Mn(CO)_5CF_3^-$ ion generated from $CF_3COMn(CO)_5$ is clearly a trifluoroacetylmanganese tetracarbonyl anion, $CF_3COMn(CO)_4^-$. This assignment rules out the possibility of $CF_3COMn(CO)_3^-$ having the very similar infrared absorption bands as $CF_3Mn(CO)_4^-$ and substantiates the previous structural indentification of $CF_3Mn(CO)_4^-$.

Since the decomposition of $CF_3COMn(CO)_4^-$ yields $CF_3Mn(CO)_4^-$ with loss of CO, it is necessary to involve the migration of the CF_3 group from the acetyl carbon to the manganese during the dissociation process. This implies that $CF_3COMn(CO)_4^-$ has a vacant site for the CF_3 migration. The structures of the d^7 complexes, $CF_3COMn(CO)_4^-$ and $CF_3Mn(CO)_4^-$, are presumed to be a square-based pyramidal with CF_3CO and CF_3 in the basal plane, respectively, from comparisons with results for other d^6 and d^7 five-coordinated manganese complexes. An infrared spectroscopic study of the five-coordinated d^6 complex, $CH_3COMn(CO)_4$,

in methane matrix at 12 K indicates the square-based pyramidal strcture with a η^1-acetyl bonding.[36] Spectroscopic studies of the d^7 complex, $Mn(CO)_5$, generated in $Cr(CO)_6$ crystals or in low-temperature solid matrices, support a square pyramidal structure with C_4v point group.[37] Extended Hückel calculations by Elian and Hoffmann[38] also suggest the square pyramidal structure for the five-coordinated d^7 complex carrying its odd electron in a relatively high-lying, directional orbital of A_1 symmetry. Low-lying occupied d orbitals for the d^7 square-pyramidal $LMn(CO)_4^-$ ($L = CF_3CO, CF_3$) are shown in scheme I.

Scheme I

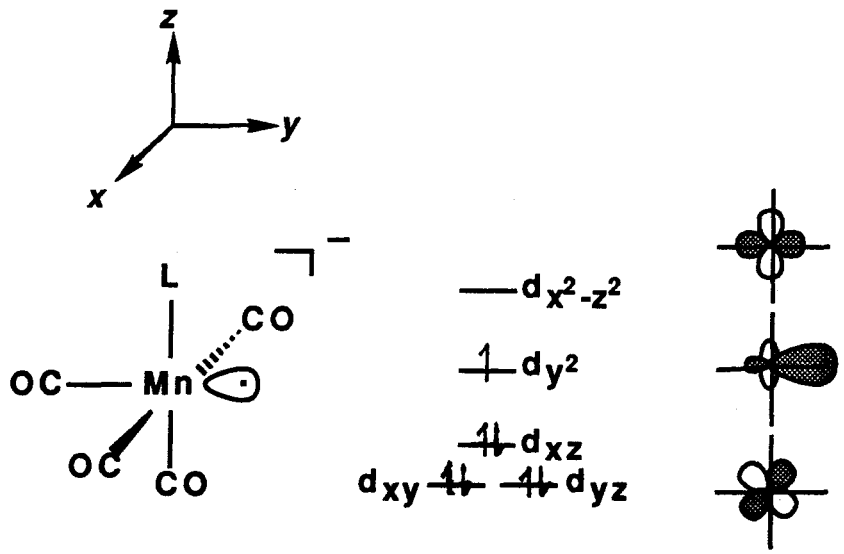

The present experimental result combined with the presumed square-pyramidal structures for ions of interest elucidates the stepwise dissociative electron attachment process in the generation of $CF_3Mn(CO)_4^-$ from the $CF_3COMn(CO)_5$ precursor as shown in scheme II. Since the Mn–$(CO)_{eq}$ bond is weaker than the Mn–$(CO)_{ax}$ and the decomposition of $CF_3COMn(CO)_4^-$ ion necessitates the migration of the CF_3 group to an empty apical site, the generation of $CF_3Mn(CO)_4^-$ from the $CF_3COMn(CO)_5$ precursor involves an electron attachment with loss of an equato-

rial CO forming $CF_3COMn(CO)_4^-$ (V) followed by the migration of the CF_3 group from the acetyl carbon to the apical position with loss of the second carbonyl *cis* to CF_3.

Scheme II

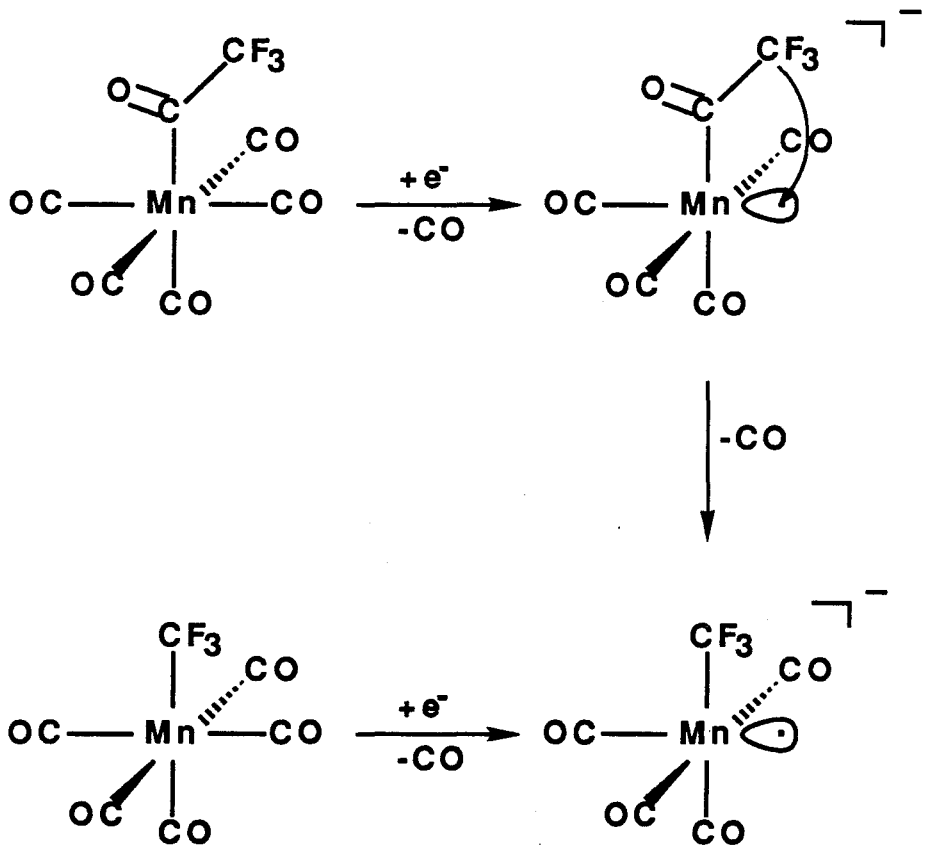

It will be of particular experimental interest to see whether this CF_3 migratory decarbonylation occurs via a stepwise or concerted mechanism. The acetyl oxygen-18 labelled $CF_3C^{18}OMn(CO)_5$ precursor would produce $CF_3C^{18}OMn(CO)_4^-$ by dissociative electron attachment and its subsequent decomposition would yield the unlabelled $CF_3Mn(CO)_4^-$ by the concerted loss of acetyl $C^{18}O$ or both the oxygen-18 labelled and unlabelled products by the stepwise loss of CO.

The production of $CF_3Mn(CO)_4^-$ from the $CF_3Mn(CO)_5$ precursor is presumably via the electron attachment with loss of an equatorial CO, because the π back bonding with an axial CO is significantly stronger than that with an equatorial

CO ($\nu_s(CO_{ax})$ = 2026 cm^{-1} and $\nu_s(CO_{eq})$ = 2142 cm^{-1}) and the difference in $CF_3Mn(CO)_5$ is even greater than that in $CF_3COMn(CO)_5$ ($\Delta\nu_s(CO_{ax})$ = 116 cm^{-1} and $\Delta\nu_s(CO_{eq})$ = 106 cm^{-1}). This likely results in a square pyramidal structure (VII) for $CF_3Mn(CO)_4^-$.

The enthalpy change for migratory decarbonylation reaction 3 is estimated to be 2.7 ± 1.7 kcal/mol from the gas phase heats of formation of $CF_3COMn(CO)_5$, $CF_3Mn(CO)_5$, and CO.[39]

$$CF_3COMn(CO)_5 \rightleftharpoons CF_3COMn(CO)_4 + CO \longrightarrow CF_3Mn(CO)_5 + CO \quad (3)$$

Since reaction 3 involves a rate-determining decarbonylation step followed by the methyl migration, an activation energy as high as the Mn–CO bond dissociation energy would be required. Providing that $D[CF_3COMn(CO)_4–CO]$ is equal to $D[Mn_2(CO)_9–CO]$ = 36 ± 2 kcal/mol[40] leads to an activation barrier estimate of 36 kcal/mol for reaction 3. If the slow migratory decarbonylation rate of reaction 4 is due to a barrier, assuming the typical ion-molecule collision frequency of 1.0×10^{-9} cm^3 $molecule^{-1}$ sec^{-1} yields the activation barrier estimate of 2 kcal/mol which is significantly smaller than that of reaction 3.

$$CF_3COMn(CO)_4^- \longrightarrow CF_3Mn(CO)_4^- + CO \quad (4)$$

Scheme III illustrates a potential energy surface difference between reaction 3 and 4. Electron affinities of 2.35 eV for five-coordinated complexes, $CF_3COMn(CO)_4$ and $CF_3Mn(CO)_4$, are assumed to be equal to that of $Mn(CO)_5$, which is estimated from the gas phase acidity of 318 ± 3 kcal/mol for $HMn(CO)_5$[41] combined with $D[(CO)_5Mn–H]$ = 59 kcal/mol[42] and IP(H) = 13.598 eV. The small activation barrier for reaction 4 indicates that the CF_3 migration occurs prior to the decarbonylation which requires a high activation barrier. However, it is yet to be explored whether the decarbonylation undergoes a stepwise mechanism involving a transient 19 e^- intermediate or a concerted mechanism involving exclusive loss of acetyl carbonyl.

Scheme III

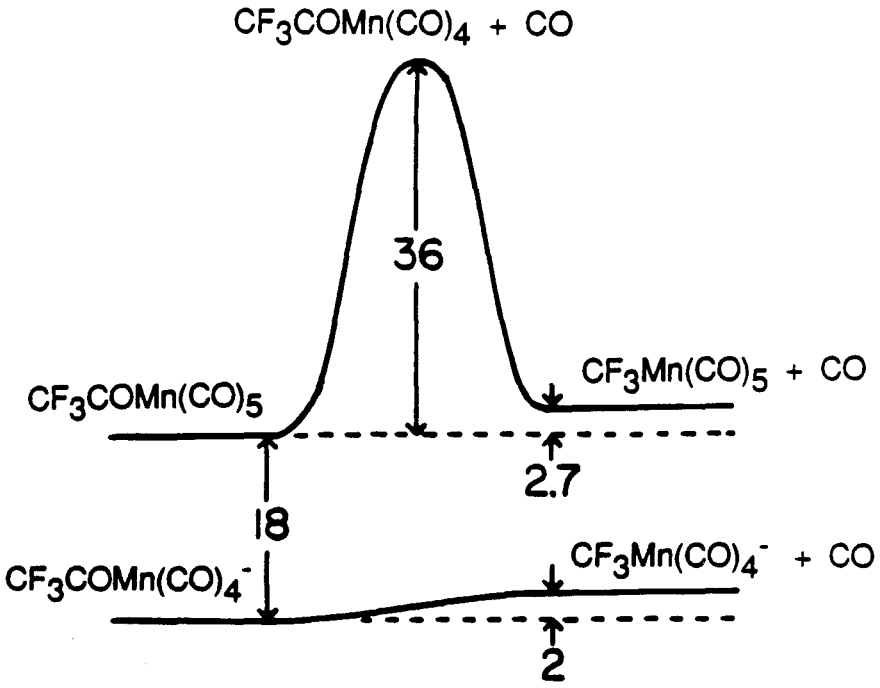

The overall decompostion reaction 4 is probably endothermic by 2 kcal/mol. However, the free energy change for the migratory decarbonylation reaction is expected to be quite negative due to loss of free CO. Since the translational and rotational contribution to the entropy of CO is about 47.4 cal mol^{-1} K^{-1},[43] the overall entropy change for the process is probably not less than this CO entropy increase. The estimated free energy change for reaction 4 at 298 K° is about −12 kcal/mol.

For the comparison with other decarbonylation reactions 5, Table II summarizes heats of reaction and free energy changes obtained from the gas phase heats of formation and the entropy increase of CO released from reaction.

$$RCOMn(CO)_5 \longrightarrow RMn(CO)_5 + CO \qquad (5)$$

$D[R(CO)_4Mn\text{–}CO]$ of 36 ± 2 kcal/mol is assumed to be equal to $D[Mn_2(CO)_9\text{–}CO]$. The gas phase free energy for the decarbonylation reaction 5 changes in order R = CH_3 (−6.1 kcal/mol) > R = C_6H_5 (−9.1 kcal/mol) > R = CF_3 (−11.4 kcal/mol).

The reverse order for the carbonylation reaction is expected. In pratice, the carbonylation of $CH_3Mn(CO)_5$ is readily accomplished; in contrast, $CF_3Mn(CO)_5$ resists direct carbonylation, even under high pressures of CO, and the decarbonylation of $CF_3COMn(CO)_5$ is the preferred route to $CF_3Mn(CO)_5$.[44] The reverse order of the carbonylation reactions is in agreement with Casey's observation that the $L_nMn-COCH_3$ intermediate is in rapid equlibrium with the $L_n(CO)Mn-CH_3$ intermediate, the methyl-benzoyl bond formation ($CH_3-COC_6H_5$) is a kinetically preferred process, and the acetyl-phenyl bond formation ($CH_3CO-C_6H_5$) is a thermodynamically favored process.[4,45]

Vibrational Frequency Assignments. The assignments of the observed C–F stretching frequencies in the infrared multiphoton dissociation spectra of $Mn(CO)_4CF_3$ are made by comparison with results for other CF_3X molecules[27,28] summarized in Table III. It has been noticed previously that the nondegenerate C–F stretching mode is higher in frequency than the degenerate C–F stretching mode, where the CF_3 group is attached to a carbon atom in a molecule of C_{3v} symmetry.[27] This holds for molecules of D_{3d} symmetry (e.g. CF_3CF_3 and $CF_3C{\equiv}CCF_3$) if the mean of the two nondegenerate stretching vibrations (A_{1g} and A_{1u}) is compared with the mean of the two degenerate vibrations (E_g and E_u). If the CF_3 group is attached to a hydrogen or halogen atom, the degenerate stretch is the higher. Cotton and Wing[28] have also concluded that the nondegenerate C–F stretching frequency in $CF_3Mn(CO)_5$ is higher than the degenerate C–F stretching mode. Assuming the higher frequency for the nondegenerate C–F stretching mode leads to the assignments of 1052 cm^{-1} as a symmetric C–F stretch of A_1-type symmetry and 945 cm^{-1} as a degenerate C–F stretch of E-type symmetry. It is quite surprising to observe that the symmetric C–F stretching mode has changed very little in frequency from 1063 cm^{-1} for $CF_3Mn(CO)_5$ to 1052 cm^{-1} for $CF_3Mn(CO)_4^-$, whereas the frequency of the degenerate C–F stretching mode of E-type symmetry has decreased from 1043 cm^{-1} for $CF_3Mn(CO)_5$ to 945 cm^{-1} for $CF_3Mn(CO)_4^-$.

Ligand Displacement Reaction Mechanism. The square-based pyramidal $CF_3Mn(CO)_4^-$ ion reacts with NO to produce $CF_3Mn(CO)_3(NO)^-$ with loss of CO. The proposed association mechanism for the ligand displacement reaction is shown in scheme IV.

Scheme IV

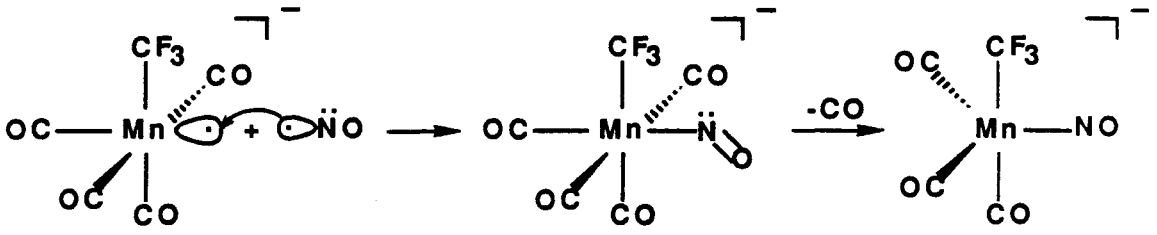

It is suggested that the reaction of NO with the 17 e^- $CF_3Mn(CO)_4^-$ ion (VII) involves an approach of NO to a singly occupied orbital on the apical site to form an 18 e^- intermediate (VIII) having a bent Mn–NO bond (1 electron donor) followed by loss of equatorial carbonyl *trans* to NO, with charge transfer from nitrogen to metal forming a linear Mn–N–O bond (3 electron donor). It has been previously shown that several metal nitrosyl carbonyl compounds (e.g. $V(CO)_5(NO)$, $Mn(CO)_4(NO)$, and $Co(CO)_3(NO)$) undergo ligand displacement reactions via an associative (SN_2) pathway involving a bent metal nitrosyl intermediate.[46] Lionel *et al.*[47] have observed the electron paramagnetic resonance spectrum of $Mn(CO)_4(NO)^-$ doped in $Cr(CO)_6$ single crystals suggesting that the Mn–N–O moiety is bent. These observations support the proposed associative mechanism for the ligand displacement

reaction. The resulting ion is formally an 18 e^- complex and presumed to have a trigonal bipyramidal structure with a linear Mn–NO in equatorial position. Frenz et al.[48] have determined the crystal structure of $Mn(CO)_4(NO)$, revealing that the nitrosyl group is in an equatorial position in the trigonal-bipyramidal structure and the Mn–CO and Mn–NO bonds are linear. $Mn(CO)_5^-$ also has a trigonal bipyramidal structure in the solid state.[49]

Conclusion

The CF_3 migratory decarbonylation reaction of $CF_3COMn(CO)_4^-$ yielding $CF_3Mn(CO)_4^-$ with loss of CO is observed in the gas phase. Infrared photochemistry, structures, and reactivities of the two ions are examined using Fourier transform ion cyclotron resonance spectroscopy. $CF_3Mn(CO)_4^-$ ions generated from two different precursors, trifluoroacetylmanganese pentacarbonyl and trifluoromethylmanganese pentacarbonyl, show identical features in IRMPD spectra, CID spectra, and ligand displacement reactivities. The observed IR frequencies for the CF_3 group of $CF_3Mn(CO)_4^-$ in the infrared multiphoton dissociation spectrum are assigned from comparisons with the assignments of other CF_3X molecules. The higher frequency at 1052 cm^{-1} is due to a symmetric C–F stretch of A_1-type symmetry and the lower frequency at 945 cm^{-1} is ascribed to a degenerate C–F stretch of E-type symmetry. In going from the 18 e^- complex $CF_3Mn(CO)_5$ to the 17 e^- ion $CF_3Mn(CO)_4^-$, the nondegenerate symmetric C–F stretching frequency changes very little, while the degenerate C–F stretching frequency decreases about 100 cm^{-1}. $CF_3COMn(CO)_4^-$ ion derived from $CF_3COMn(CO)_5$ does not undergo the infrared multiphoton dissociation. Electron attachment to $CF_3Mn(CO)_5$ is accompanied by loss of equatorial CO generating $CF_3Mn(CO)_4^-$ and that of $CF_3COMn(CO)_5$ involves the removal of equatorial CO producing $CF_3COMn(CO)_4^-$ followed by the CF_3 migration from the acetyl carbon to the manganese and loss of another CO yielding $CF_3Mn(CO)_4^-$. $CF_3Mn(CO)_4^-$ under-

goes a ligand displacement reaction with NO via an associative pathway involving an 18 e^- intermediate $CF_3Mn(CO)_4(NO)^-$ having a bent nitrosyl group (1 e^- donor) and yielding an 18 e^- product $CF_3Mn(CO)_3(NO)^-$ having a linear Mn–NO bond in equatorial position.

The CF_3 group bonded to metal is an ideal infrared chromophore to investigate the infrared photochemistry of organometallic complexes, which yields information related to the structure and reaction mechanisms of coordinatively unsaturated intermediates. It will be of further experimental and theoretical interest to see how the C–F stretching frequencies vary with the number and variety of ligand substituents in complexes containing metal bonded CF_3 groups.

Acknowledgement. We acknowledge the support of the National Science Foundation (Grant No. CHE87-11567) and the Petroleum Research Fund administered by the American Chemical Society.

References

(1) (a) Collman, J. P.; Hegedus, L. S. *Principles and Applications of Organotransition Metal Chemistry*; University Science Books: Mill Valley; 1980, Chapter 5. (b) Collman, J. P.; Hegedus, L. S.; Norton, J. R.; Finke, R. G. *Principles and Applications of Organotransition Metal Chemistry*; University Science Books: Mill Valley; 1987, Chapter 6.

(2) Basolo, F.; Pearson, R. G. *Mechanisms of Inorganic Reactions*; 2nd Ed; Wiley: New York; 1967, pp 578-609.

(3) Kubota, M; Blake, D. M.; Smith, S. A. *Inorg. Chem.* **1971**, *10*, 1430.

(4) Casey, C. P.; Scheck, D. M. *J. Am. Chem. Soc.* **1980**, *102*, 2728.

(5) (a) Foster, M. S.; Beauchamp, J. L. *Chem. Phys. Lett.* **1975**, *31*, 1975. (b) Woodin, R. L.; Foster, M. S.; Beauchamp, J. L. *J. Chem. Phys.* **1980**, *72*, 4223. (c) Squires, R. R. *Chem. Rev.* **1987**, *87*, 623.

(6) Estimated from $D[(CO)_5Mn-COCF_3]$ = 42.9 kcal/mol, $D[(CO)_5Mn-CF_3]$ = 48.9 kcal/mol, $D[Mn_2(CO)_9-CO]$ = 36 kcal/mol, and $D(CF_3-CO)$ = 9 kcal/mol; see reference 1b, p 240 and 368.

(7) (a) *Collision Spectroscopy*; Cooks, R. G. Ed; Plenum: New York, 1978. (b) Cody, R. B.; Freiser, B. S. *Int. J. Mass Spectrom. Ion Phys.* **1982**, *41*, 199. (c) Cody, R. B.; Burnier, R. C.; Freiser, B. S. *Anal. Chem.* **1982**, *54*, 96. (d) Cody, R. B.; Burnier, R. C.; Cassady, C. J.; Freiser, B. S. *Anal. Chem.* **1982**, *54*, 2225.

(8) (a) Baldeschwieler, J. D. *Science* **1968**, *159*, 263. (b) Beauchamp, J. L. *Ann. Rev. Phys. Chem.* **1971**, *22*, 527. (c) Lehman, T. A.; Bursey, M. M. *Ion Cyclotron Resonance Spectrometry*; Wiley: New York, 1976. (d) Gross, M. L.; Russell, D. H.; Aerni, R. J.; Bronczyk, S. A. *J. Am. Chem. Soc.* **1977**, *99*, 3603. (e) Ausloos, P. J. *J. Am. Chem. Soc.* **1981**, *103*, 3931. (f) Jackson, J. A. A.; Lias, S. C.; Ausloos, P. J. *J. Am. Chem. Soc.* **1977**, *99*, 7515. (g) Eyler, J. R.; Campana, J. E. *Int. J. Mass Spectrom. Ion Phys.* **1983/1984**,

55, 171. (h) Fetterolf, D. D.; Yost, R. A.; Eyler, J. R. *Org. Mass Spectrom.* **1984**, *19*, 104.

(9) (a) Dunbar, R. C. In *Gas Phase Ion Chemistry*; Bowers, M. T. Ed.; Academic Press: New York, 1979; vol. 2, pp. 181; 1984, vol.3, pp. 130. (b) Thorne, L. R.; Beauchamp, J. L. In *Gas Phase Ion Chemistry*; Bowers, M. T. Ed.; Academic Press: New York, 1984; vols. 3, pp. 42. (c) Harris, F. M.; Beynon, J. H. In *Gas Phase Ion Chemistry*; Bowers, M. T. Ed.; Academic Press: New York, 1984; vols. 3, pp. 100. (d) *Molecular Ions: Spectroscopy, Structure, and Chemistry* Miller, T. A.; Bondybey, V. E. Ed; North-Holland Publishing: Amsterdam; 1983, 231. (e) *Molecular Photodissociation Dynamics* Ashfold, M. N. R.; Baggott, J. E. Ed; The Royal Society of Chemistry: London; 1987.

(10) Peake, D. A.; Gross, M. L.; Ridge, D. P. *J. Am. Chem. Soc.* **1984**, *106*, 4307.

(11) (a) Freiser, B. S. *Talanta* **1985**, *32*, 697. (b) Jacobson, D. B.; Freiser, B. S. *J. Am. Chem. Soc.* **1983**, *105*, 736. (c) Jacobson, D. B.; Freiser, B. S. *J. Am. Chem. Soc.* **1983**, *105*, 7484.

(12) Halle, L. F.; Houriet, R.; Kappes, M. M.; Staley, R. H.; Beauchamp, J. L. *J. Am. Chem. Soc.* **1982**, *104*, 6293.

(13) Jacobson, D. B.; Freiser, B. S. *J. Am. Chem. Soc.* **1984**, *106*, 1159.

(14) (a) Lupo, D. W.; Quack, M. *Chem. Rev.* **1987**, *87*, 181 and earlier references therein. (b) Bomse, D. S.; Berman, D. W.; Beauchamp, J. L. *J. Am. Chem. Soc.* **1978**, *100*, 3248. (c) Cassassa, M. P.; Bomse, D. S.; Beauchamp, J. L.; Janda, K. C. *J. Chem. Phys.* **1980**, *72*, 6805.

(15) (a) Bomse, D. S.; Berman, D. W.; Beauchamp, J. L. *J. Am. Chem. Soc.* **1981**, *103*, 3967. (b) Woodin, R. L.; Bomse, D. S.; Beauchamp, J. L. *Chem. Phys. Lett.* **1979**, *63*, 630.

(16) Wright, C. A.; Beauchamp, J. L. *J. Am. Chem. Soc.* **1981**, *103*, 6499. (b) Wright, C. A.; Beauchamp, J. L. *Chem. Phys.* **1989** in press.

(17) Baykut, G.; Watson, C. H.; Weller, R. R.; Eyler, J. R. *J. Am. Chem. Soc.*

1985, *107*, 8036.

(18) Hanratty, M. A.; Paulsen, C. M.; Beauchamp, J. L. *J. Am. Chem. Soc.* **1985**, *107*, 5074.

(19) Comisarow, M. B. *Int. J. Mass. Spectrom. Ion Phys.* **1981**, *37*, 251.

(20) Marshall, A. G. *Acc. Chem. Res.* **1985**, *18*, 316 and references therein.

(21) Bio-Med Tech, 2001 E. Galbreth, Pasadena, CA 91104.

(22) Schulz, G. J.; Phelps, A. V. *Rev. Sci. Instrum.* **1957**, *28*, 1051.

(23) Blint, R. J.; McMahon, T. B.; Beauchamp, J. L. *J. Am. Chem. Soc.* **1974**, *96*, 1269.

(24) (a) McClellan, W. R. *J. Am. Chem. Soc.* **1961**, *83*, 1598. (b) Coffield, T. H. Kozikowski, J.; Closson, R. D. *Abstr. 5th Intern. Conf. Coordination Chem. London*; The Chemical Society Special Publication 13: London, 1959; p. 126. (c) King, R. B. *Organometallic Synthesis*; Academic Press: New York, 1965; vol. 1, p. 145.

(25) Bomse, D. S.; Woodin, R. L.; Beauchamp, J. L. *J. Am. Chem. Soc.* **1979**, *101*, 5503.

(26) Berney, C. V. *Spectrochimica Acta* **1964**, *20*, 1437.

(27) (a) Cotton, F. A.; Wing, R. M. *J. Organometal. Chem.* **1967**, *9*, 511. (b) Cotton, F. A.; Musco, A.; Yagupsky, G. *Inorg. Chem.* **1967**, *6*, 1357.

(28) Pitcher, E.; Stone, F. G. *Spectrochimica Acta* **1962**, *18*, 585.

(29) Ogilvie, J. F. *J. C. S. Chem. Commun.* **1970**, 323.

(30) Avanzino, S. C.; Bakke, A. A.; Chen, H.-W.; Donahue, C. J.; Jolly, W. L.; Lee, T. H.; Ricco, A. J. *Inorg. Chem.* **1980**, *19*, 1931.

(31) Graham, A. G. *Inorg. Chem.* **1968**, *7*, 315.

(32) Hall, M. B.; Fenske, R. F. *Inorg. Chem.* **1972**, *11*, 768.

(33) Watson, C. H.; Baykut, G.; Battiste, M. A.; Eyler, J. R. *Anal. Chim. Acta.* **1985**, *178*, 125.

(34) (a) Cotton, F. A.; Wilkinson, G. *Advanced Inorganic Chemistry*; Wiley: New York; 1980, 4th ed. (b) Avanzino, S. C.; Chen, H.-W.; Donahue, C. J.; Jolly,

W. L. *Inorg. Chem.* **1980**, *19*, 2201.

(35) Coderman, R. R.; Beauchamp, J. L. *Inorg. Chem.* **1977**, *16*, 3135.

(36) Hitam, R. B.; Narayanaswamy, R.; Rest, A. J. *J. Chem. Soc. Dalton Trans.* **1983**, 615.

(37) (a) Hughey, J. L.; Anderson, C. P.; Meyer, T. J. *J. Organomet. Chem.* **1977**, *125*, C49. (b) Waltz, W. L.; Hackelberg, O.; Dorfman, L. M.; Wojcicki, A. *J. Am. Chem. Soc.* **1978**, *100*, 7259. (c) Church, S. P.; Poliakoff, M.; Timney, J. A.; Turner, J. J. *J. Am. Chem. Soc.* **1981**, *103*, 7515. (d) Symons, M. C. R.; Sweany, R. L. *Organometallics* **1982**, *1*, 834. (e) Fairhurst, S. A.; Morton, J. R.; Perutz, R. N.; Preston, K. F. *Organometallics* **1984**, *3*, 1389. (f) Howard, J. A.; Morton, J. R.; Preston, K. F. *Chem. Phys. Lett.* **1981**, *83*, 226. (g) Lionel, T.; Morton, J. R.; Preston, K. F. *Chem. Phys. Lett.* **1981**, *81*, 17.

(38) Elian, M.; Hoffmann, R. *Inorg. Chem.* **1975**, *14*, 1058.

(39) Connor, J. A.; Zafarani-Moattar, M. T.; Bickerton, J.; El Saied, N. I.; Suradi, S.; Carson, R.; Al Takhin, G.; Skinner, H. A. *Organometallics* **1982**, *1*, 1166.

(40) See reference 1b, pp 240.

(41) Stevens, A. E. Ph. D. Thesis, California Insitute of Technology, Pasadena, 1981.

(42) Heats of formation of -177 ± 2 kcal/mol for $HMn(CO)_5$ and -379 ± 1 kcal/mol for $Mn_2(CO)_{10}$ (reference 39), combined with $D[(CO)_5Mn\text{–}Mn(CO)_5] = 38 \pm 5$ kcal/mol and ΔH°_{f298} (H) = 52.1 kcal/mol, lead to $D[(CO)_5Mn\text{–}H] = 59 \pm 6$ kcal/mol. The value for D(Mn–Mn) is taken from recent photoacoustic calorimetry studies (Goodman, J. L.; Peters, K. S.; Vaida, V. *Organometallics* **1986**, *6*, 815), which is in agreement with a value of 41 ± 9 kcal/mol obtained from ion cyclotron resonance and photoelectron studies (Simões, J. A. M.; Schultz, J. C.; Beauchamp, J. L. *Organometallics* **1985**, *4*, 1238).

(43) Calculated from formulae in *JANAF Thermochemical Tables*; 2nd Ed; Stull. D. R.; Prophet, H. Ed.; NBS: Washington, D. C.; 1971.

(44) (a) Calderazzo, F.; Cotton, F. A. *Abstr. 8th Intern. Conf. Coordination Chem. Stockholm and Uppsala*; The Chemical Society Special Publication: London, 1962; p. 296. (b) Bamford, C. H.; Mullik, S. U. *J. C. S. Faraday I* **1977**, *74*, 1648. (c) Saddei, D.; Freund, H.-J.; Hohlneicher, G. *J. Organometal. Chem.* **1980**, *186*, 63.

(45) Casey, C. P.; Scheck, D. M. *J. Am. Chem. Soc.* **1980**, *102*, 2723.

(46) Basolo, F. *Inorg. Chim. Acta* jacsform 1985 100 33

(47) Lionel, T.; Morton, J. R.; Preston, K. F. *J. Phys. Chem.* **1982**, *86*, 367.

(48) Frenz, B. A.; Enemark, J. H.; Ibers, J. A. *Inorg. Chem.* **1969**, *8*, 1288.

(49) Frenz, B. A.; Ibers, J. A. *Inorg. Chem.* **1972**, *11*, 1109.

Table I. Infrared frequency assigments for $CF_3COMn(CO)_5$ and $CF_3Mn(CO)_5$.

$CF_3COMn(CO)_5$ [a]		$CF_3Mn(CO)_5$ [b]	
ν (cm^{-1})	assignment	ν (cm^{-1})	assignment
2134	sym. str. of $(CO)_{eq}$	2142	sym. str. of $(CO)_{eq}$ (A_1)
2050	degen. str. of $(CO)_{eq}$	2055	degen. str. of $(CO)_{eq}$ (E)
2028	str. of $(CO)_{ax}$	2026	str. of $(CO)_{ax}$ (A_1)
1673	str. of acetyl CO		
1254	sym. str. of CF_3	1063	sym. str. of CF_3 (A_1)
1191	F–CF_2 in plane str.	1043	degen. str. of CF_3 (E)
1141	F–CF_2 out of plane str.		
865	C–C str.		
719	F–CF_2 deform.		
650	Mn–CO wagging	650	Mn–CO wagging

[a] References 28 and 29.

[b] Reference 27.

Table II. The enthalpy changes[a] and free energies[b] for the migratory decarbonylation reactions in the gas phase.

Reactions	ΔH_{298} (kcal/mol)	ΔG_{298} (kcal/mol)
$CH_3COMn(CO)_5 \longrightarrow CH_3Mn(CO)_5 + CO$	8.0 ± 2.6	-6.1
$C_6H_5COMn(CO)_5 \longrightarrow C_6H_5Mn(CO)_5 + CO$	5.6 ± 2.1	-9.1
$CF_3COMn(CO)_5 \longrightarrow CF_3Mn(CO)_5 + CO$	2.7 ± 1.7	-11.4
$RCOMn(CO)_5 \longrightarrow RCOMn(CO)_4 + CO$	36 ± 2 [c]	22

[a] From heats of formation of $RCOMn(CO)_5$, $RMn(CO)_5$, and CO (reference 39).

[b] $\Delta G = \Delta H - T\Delta S$; ΔS is assumed to be equal to the translational and rotational contribution to the entropy of free CO (47.4 cal mol^{-1} K^{-1}).

[c] $D[RCOMn(CO)_4\text{–}CO]$ is assumed to be equal to $D[Mn_2(CO)_9\text{–}CO]$ (reference 1b, p. 240).

Table III. The C–F stretching frequencies of CF_3X molecules.[a]

molecule	$\nu_s(a_1)$ (cm^{-1})	$\nu_s(e \text{ or } f)$ (cm^{-1})
CF_3	1084	1250
CF_3H	1137	1157
CF_3D	1111	1210
CF_3I	1076	1183
CF_3Br	1087	1206
CF_3Cl	1102	1210
CF_3F	904	1265
CF_3CH_3	1278	1230
CF_3CCl_3	1255	1227
CF_3CF_3	1417, 1117	1250, 1250.5
	(1267) [b]	(1250) [b]
$CF_3C{\equiv}CCF_3$	1245, 1294	1181, 1198
	(1270) [b]	(1190) [b]
$CF_3C{\equiv}CH$	1254	1182
$CF_3C{\equiv}N$	1226	1212
$CF_3Mn(CO)_5$ [c]	1063	1043
$CF_3Mn(CO)_4^-$ [d]	1052	945

[a] From reference 26.

[b] Mean value

[c] Reference 27 and this work.

[d] This work.

Figure Captions

Figure 1. Gas-phase infrared absorption spectra of trifluoroacetylmanganese pentacarbonyl (top) and trifluoromethylmanganese pentacarbonyl (bottom). See Table 1 for the frequency assignment.

Figure 2. Anion mass spectra of trifluoroacetylmanganese pentacarbonyl (top) and trifluoromethylmanganese pentacarbonyl (bottom) with 2-eV electron energy at 4×10^{-7} torr.

Figure 3. Temporal variation of $Mn(CO)_5CF_3^-$, generated from dissociative electron attachment of trifluoroacetylmanganese pentacarbonyl, and its decomposition product $Mn(CO)_4CF_3^-$ at 6.3×10^{-7} torr.

Figure 4. (a) Mass spectrum of $Mn(CO)_4CF_3^-$ derived from $CF_3COMn(CO)_5$ shortly after a series of ion ejection pulses. (b) Photodissociation mass spectrum of $Mn(CO)_4CF_3^-$ at 944 cm^{-1} with 8 W cm^{-2} laser beam and 20 msec duration. The parent neutral pressure is 2.5×10^{-6} torr.

Figure 5. The infrared absorption spectra of the CF_3 group in trifluoromethylmanganese pentacarbonyl (top) and photodissociation spectra of $Mn(CO)_4CF_3^-$ ions over the CO_2 laser spectral range from the two different precursors, trifluoroacetylmanganese pentacarbonyl (middle) and trifluoromethylmanganese pentacarbonyl (bottom). parent neutral pressures are 2.5×10^{-6} torr. Data points are the ratio (in percentage) of the intensity of $Mn(CO)_4CF_3^-$ to the total ion intensity $[Mn(CO)_4CF_3^- + Mn(CO)_3CF_3^- + Mn(CO)_2CF_3^-]$ as a function of wavelength. The mass-selected ion of interest is irradiated for 20 msec at 8 W cm^{-2}.

Figure 6. Photoappearance spectra of $Mn(CO)_3CF_3^-$ ions over the CO_2 laser spectral range from the two different precursors, trifluoroacetylmanganese pentacarbonyl (top) and trifluoromethylmanganese pentacarbonyl (bottom). Data points are the

ratio (in percentage) of the intensity of $Mn(CO)_3CF_3^-$ to the total ion intensity $[(Mn(CO)_4CF_3^- + Mn(CO)_3CF_3^- + Mn(CO)_2CF_3^-]$ as a function of wavelength.

Figure 7. Photoappearance spectra of $Mn(CO)_2CF_3^-$ ions over the CO_2 laser spectral range from the two different precursors, trifluoroacetylmanganese pentacarbonyl (top) and trifluoromethylmanganese pentacarbonyl (bottom). Data points are the ratio (in percentage) of the intensity of $Mn(CO)_2CF_3^-$ to the total ion intensity $[Mn(CO)_4CF_3^- + Mn(CO)_3CF_3^- + Mn(CO)_2CF_3^-]$ as a function of wavelength.

Figure 8. The collision induced dissociation spectra of $Mn(CO)_4CF_3^-$ ions from the two different precursors, trifluoroacetylmanganese pentacarbonyl (top) and trifluoromethylmanganese pentacarbonyl (bottom) with Ar buffer gas; P(the parent neutral) $= 4 \times 10^{-7}$ torr, $P(Ar) = 4 \times 10^{-6}$ torr, and E_{CM} (collision) = 12-eV.

Figure 9. Temporal variation of $Mn(CO)_4CF_3^-$ ions, generated from the two different precursors, trifluoroacetylmanganese pentacarbonyl (top) and trifluoromethylmanganese pentacarbonyl (middle), and $Mn(CO)_3(NO)CF_3^-$ in the ligand displacement reaction; top: $P[CF_3COMn(CO)_5] = 4.1 \times 10^{-7}$ torr and $P(NO) = 6.7 \times 10^{-6}$ torr; bottom: $P[CF_3Mn(CO)_5] = 4 \times 10^{-7}$ torr and $P(NO) = 6 \times 10^{-6}$ torr.

Figure 10. (a) Mass spectrum of $Mn(CO)_5CF_3^-$ derived from $CF_3COMn(CO)_5$ and its decomposition product $Mn(CO)_4CF_3^-$ after 1 sec delay from the initial isolation of $Mn(CO)_5CF_3^-$. (b) Photodissociation mass spectrum of $Mn(CO)_5CF_3^-$ and $Mn(CO)_4CF_3^-$ at 944 cm^{-1} with 8 W cm^{-2} laser beam and 10 msec duration. The parent neutral pressure is 5×10^{-7} torr.

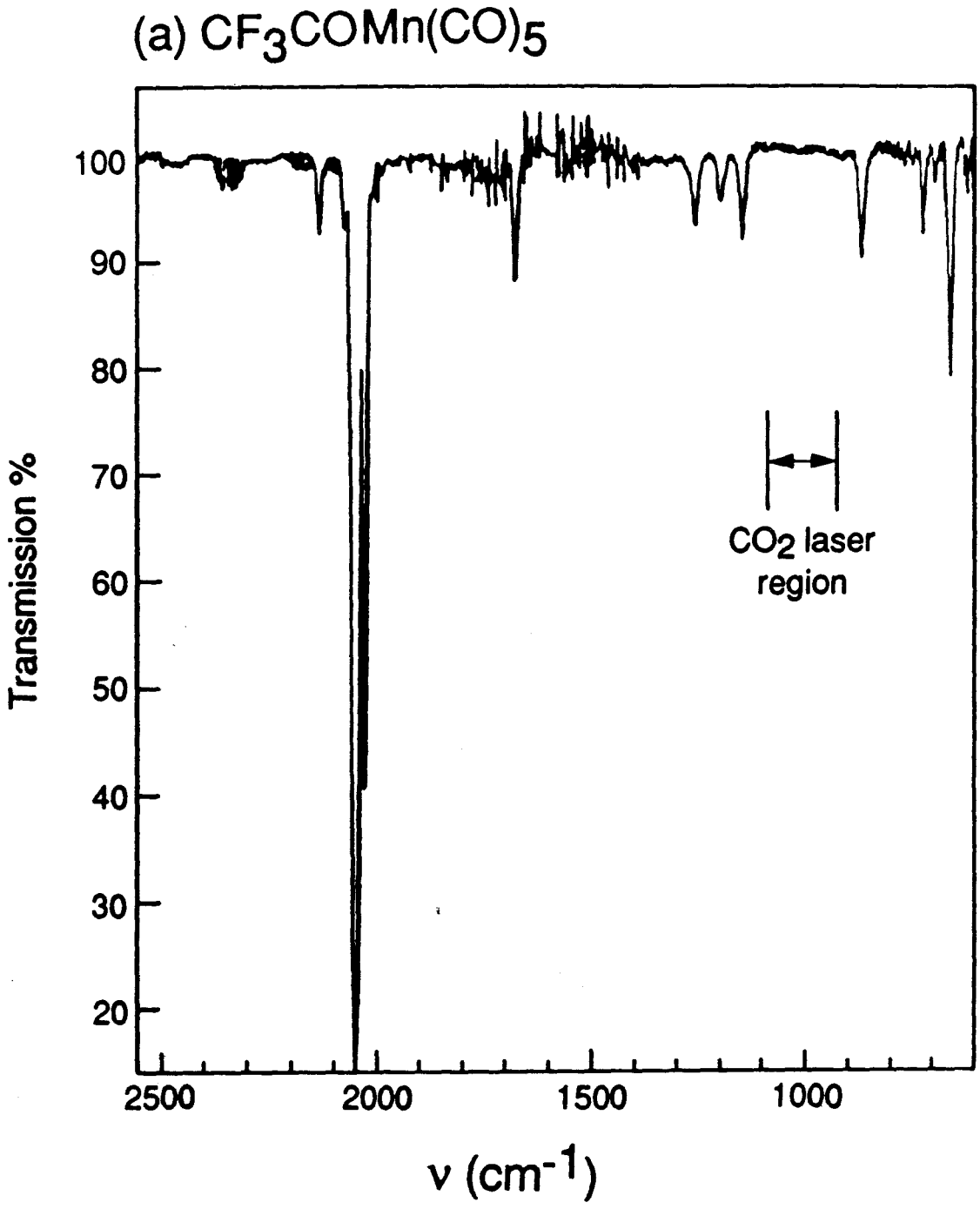
(a) $CF_3COMn(CO)_5$
Transmission %
100
90
80
70
60
50
40
30
20
2500
2000
1500
1000
ν (cm^{-1})
CO_2 laser region

Figure 1.

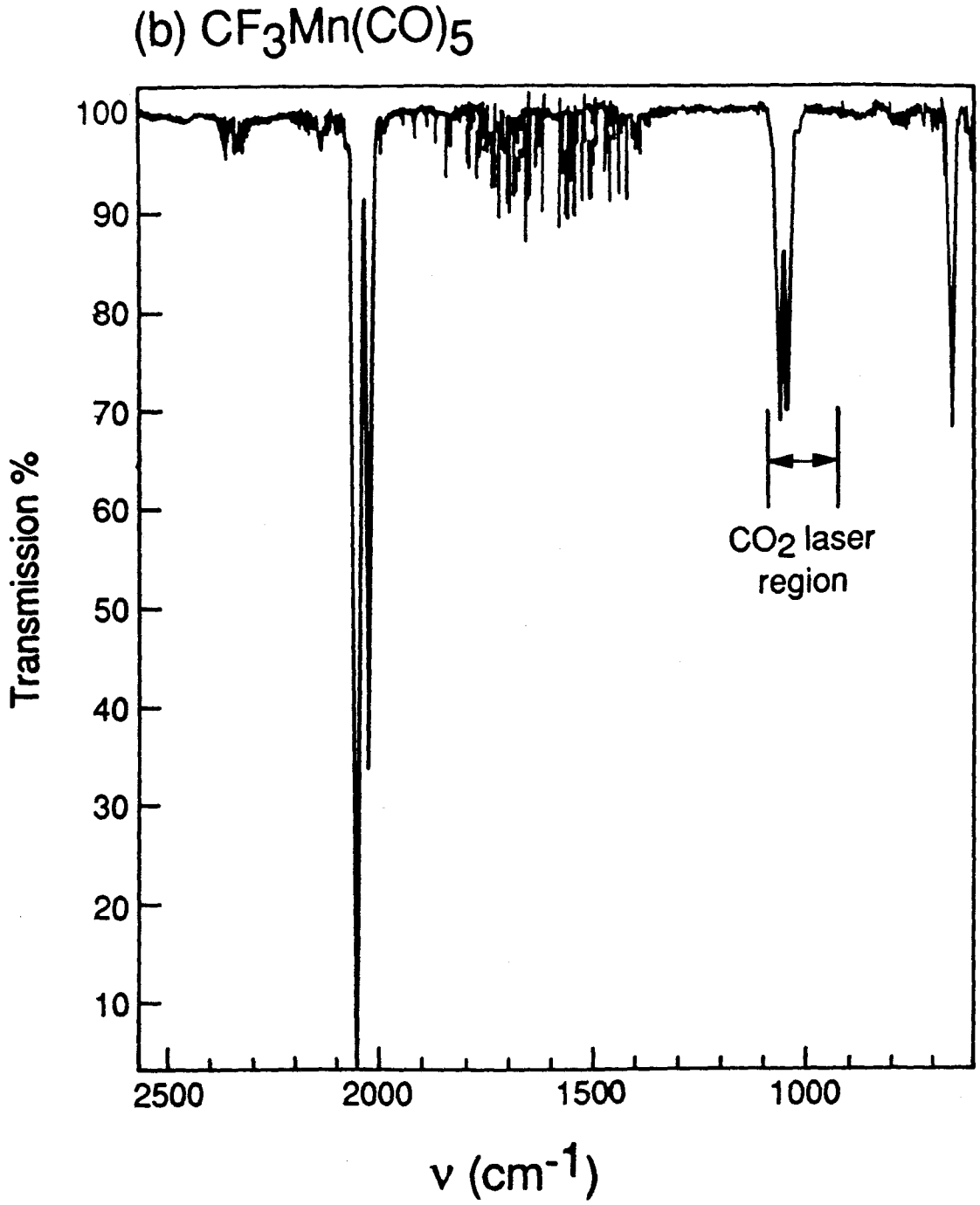
(b) $CF_3Mn(CO)_5$
Transmission %
100
90
80
70
60
50
40
30
20
10
2500
2000
1500
1000
ν (cm^{-1})
CO_2 laser region

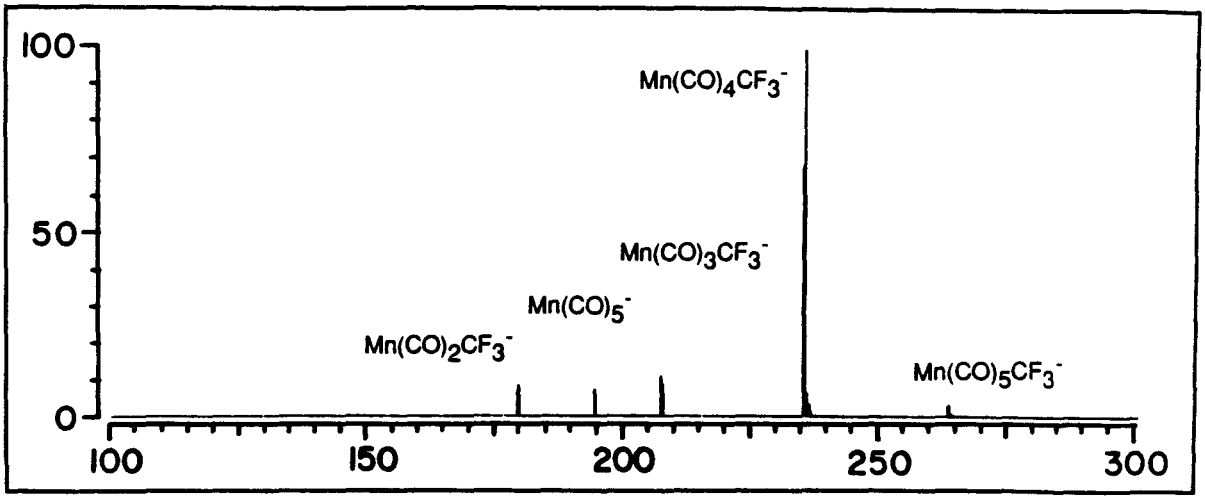
100
50
0
100
150
200
250
300
$Mn(CO)_4CF_3^-$
$Mn(CO)_3CF_3^-$
$Mn(CO)_5^-$
$Mn(CO)_2CF_3^-$
$Mn(CO)_5CF_3^-$

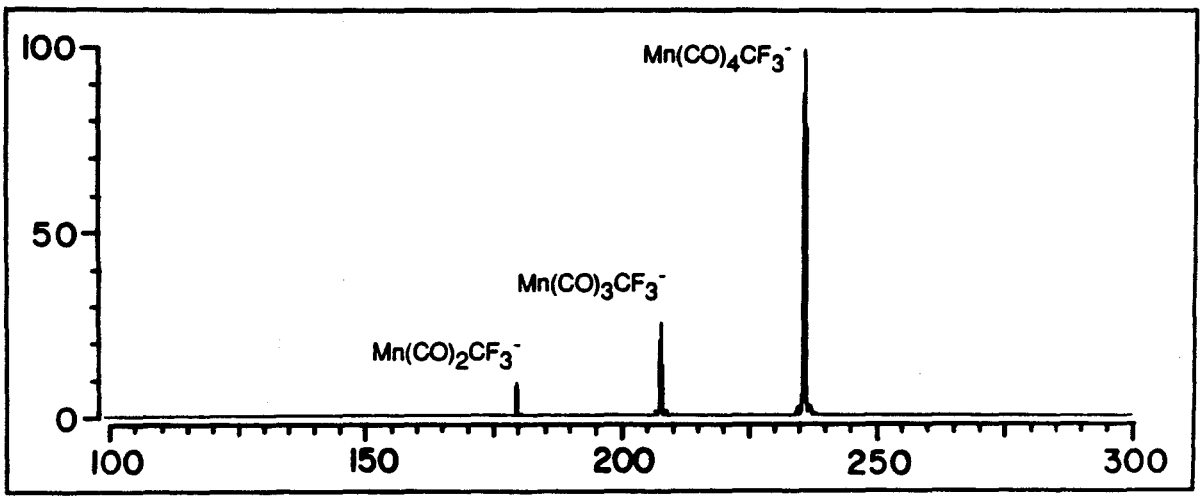
100
50
0
100
150
200
250
300
$Mn(CO)_4CF_3^-$
$Mn(CO)_3CF_3^-$
$Mn(CO)_2CF_3^-$

Figure 2

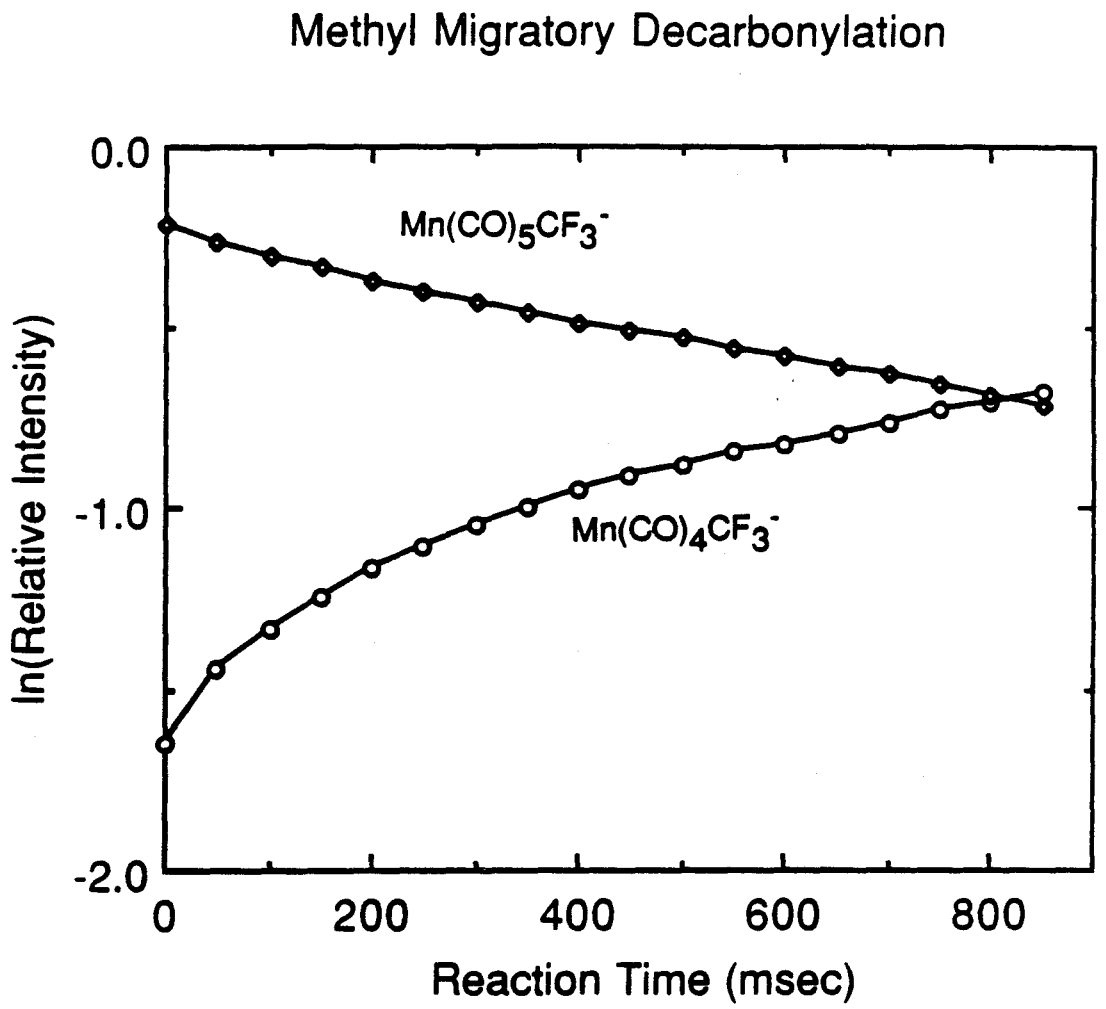
Methyl Migratory Decarbonylation
0.0
-1.0
-2.0
ln(Relative Intensity)
Mn(CO)5CF3-
Mn(CO)4CF3-
0
200
400
600
800
Reaction Time (msec)

Figure 3

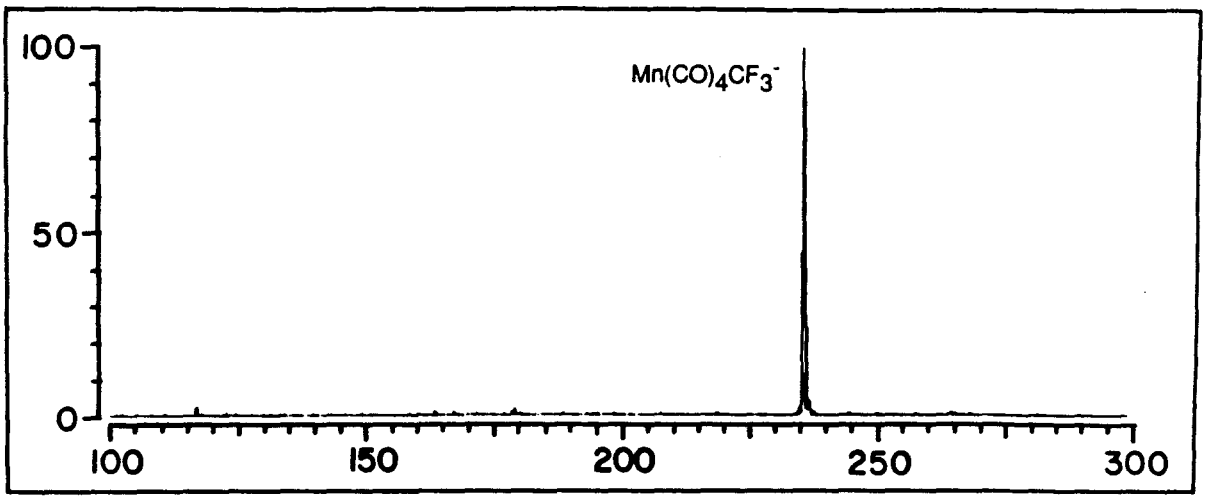
100
50
0
100
150
200
250
300
$Mn(CO)_4CF_3^-$

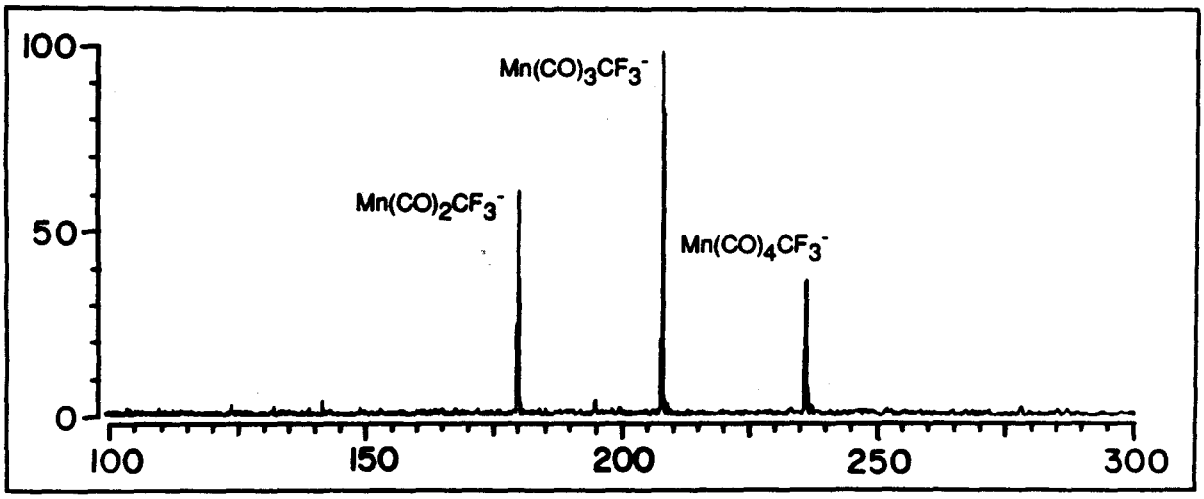
100
50
0
100
150
200
250
300
$Mn(CO)_3CF_3^-$
$Mn(CO)_2CF_3^-$
$Mn(CO)_4CF_3^-$

Figure 4

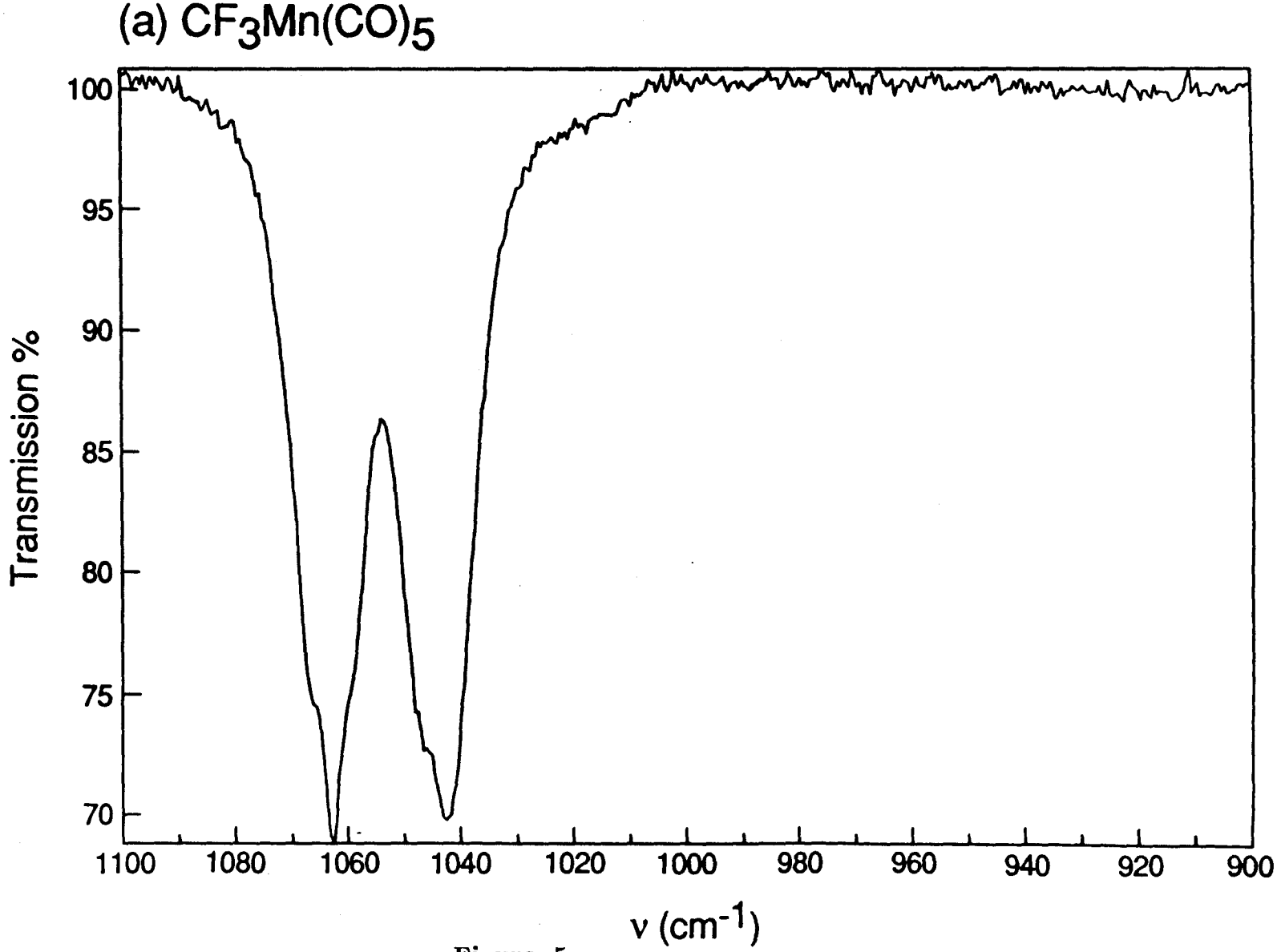
(a) $CF_3Mn(CO)_5$
Transmission %
100
95
90
85
80
75
70
1100
1080
1060
1040
1020
1000
980
960
940
920
900
ν (cm^{-1})

Figure 5

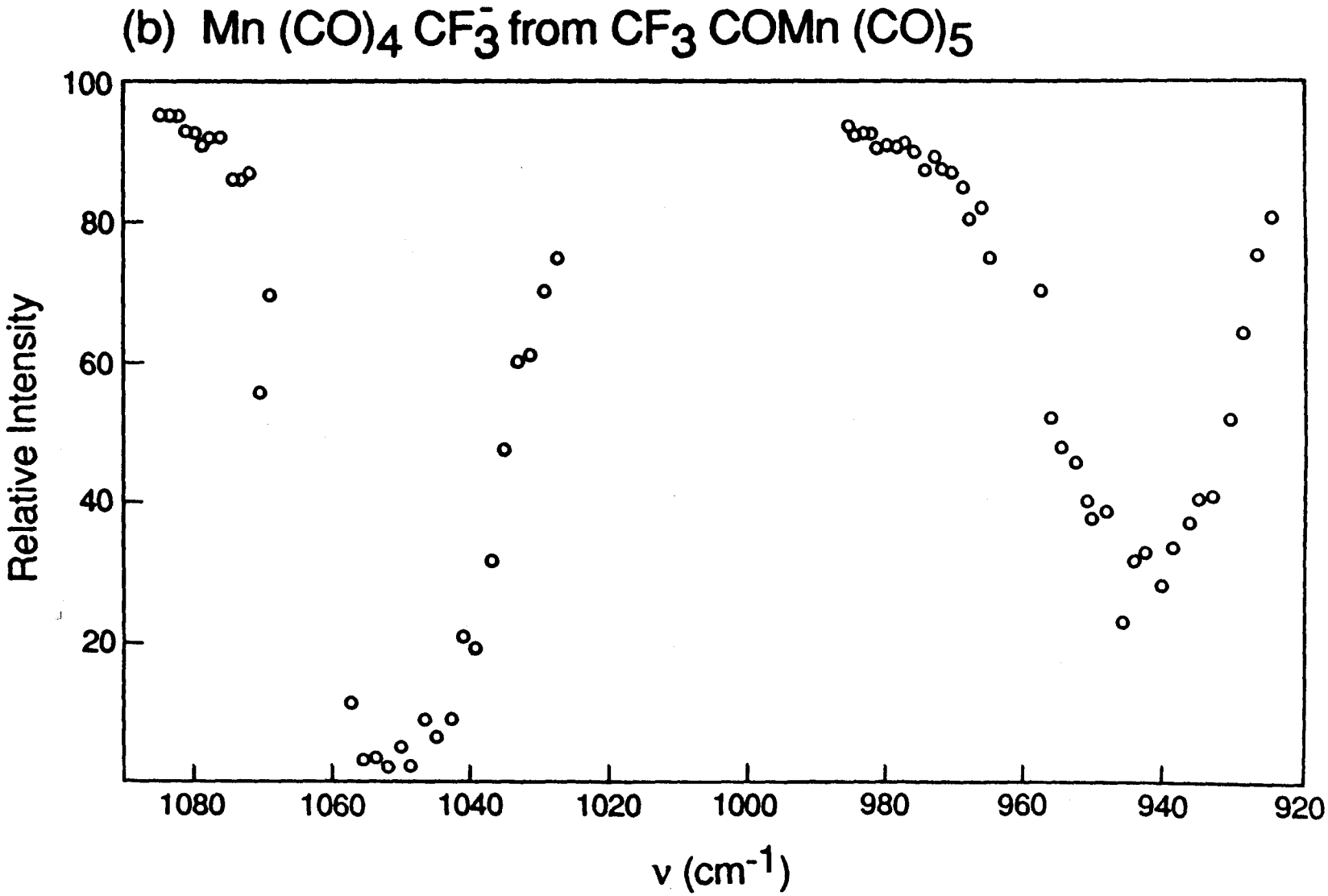
(b) Mn (CO)4 CF3- from CF3 COMn (CO)5
Relative Intensity
100
80
60
40
20
1080
1060
1040
1020
1000
980
960
940
920
ν (cm-1)

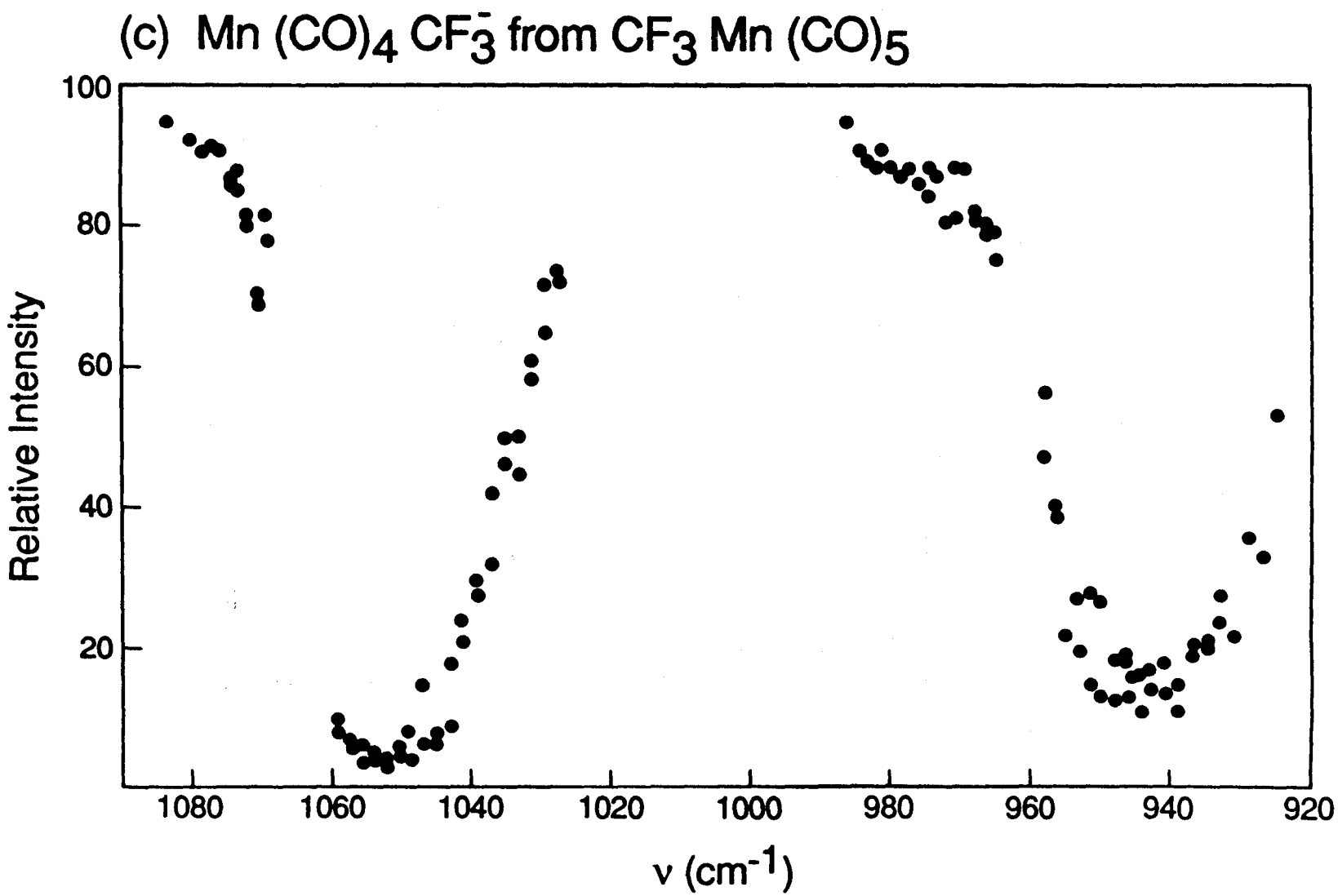
(c) Mn (CO)4 CF3 from CF3 Mn (CO)5
Relative Intensity
100
80
60
40
20
1080
1060
1040
1020
1000
980
960
940
920
ν (cm-1)

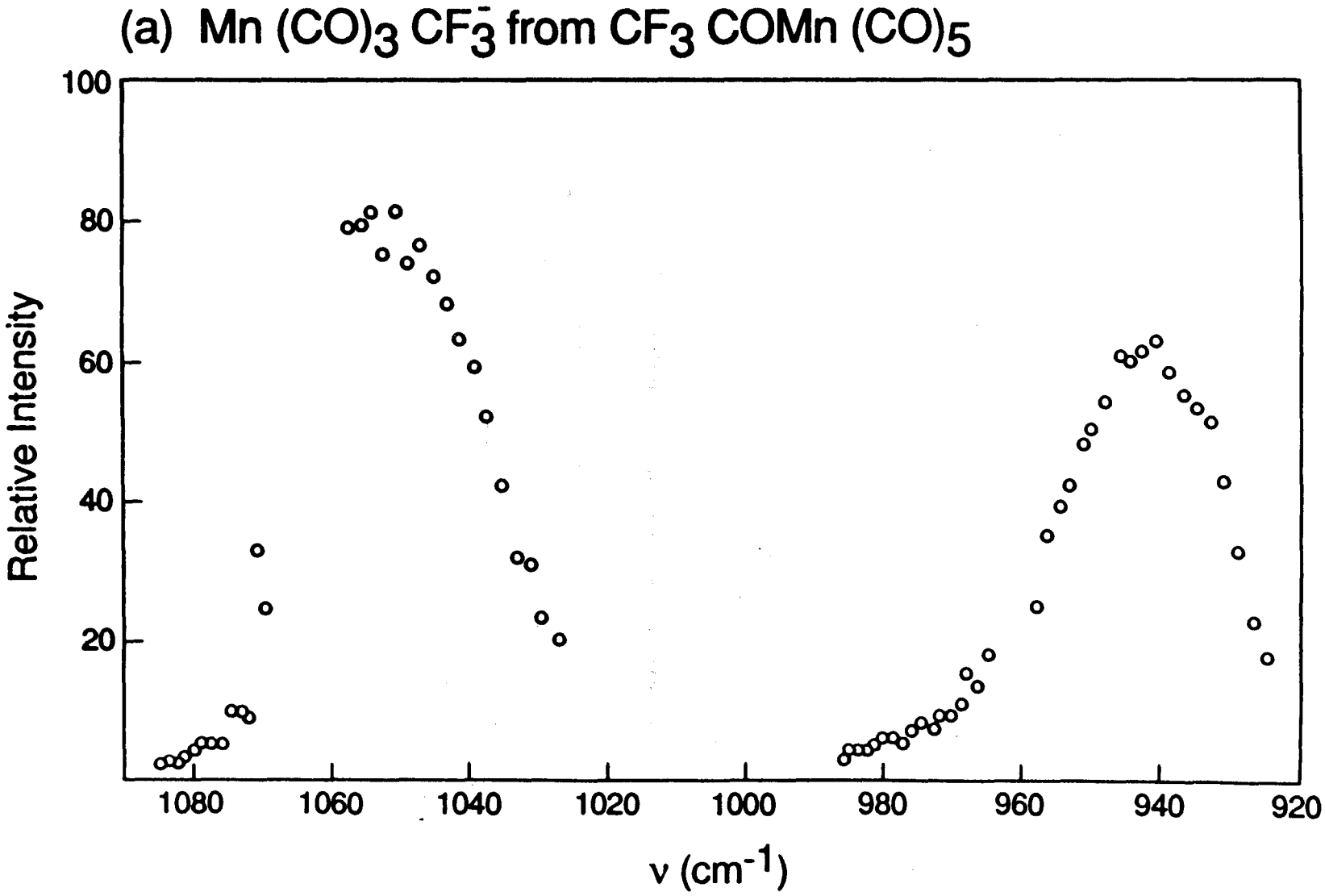
(a) Mn (CO)3 CF3 from CF3 COMn (CO)5
Relative Intensity
100
80
60
40
20
1080
1060
1040
1020
1000
980
960
940
920
ν (cm-1)

Figure 6

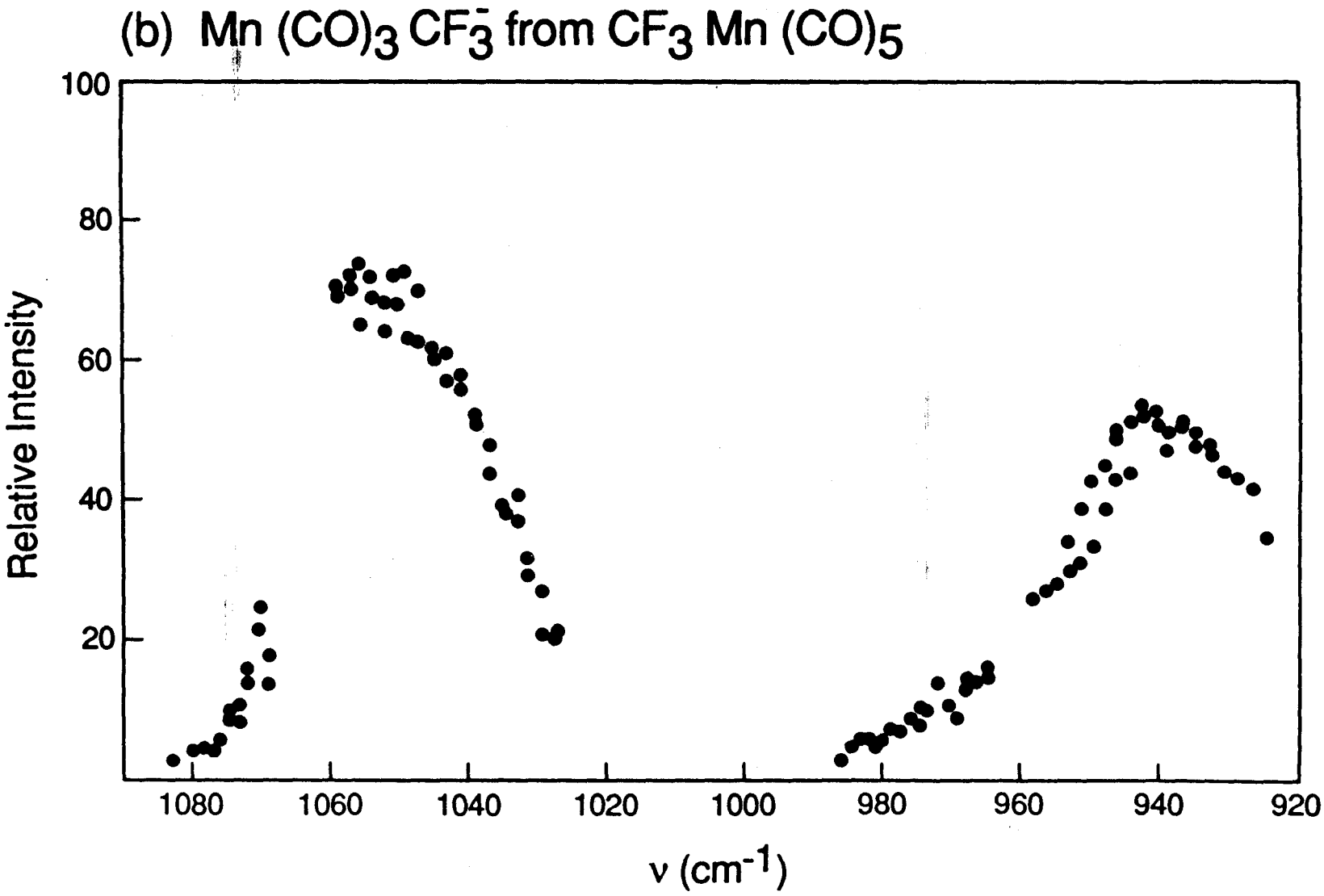
(b) Mn (CO)3 CF3 from CF3 Mn (CO)5
Relative Intensity
100
80
60
40
20
1080
1060
1040
1020
1000
980
960
940
920
ν (cm-1)

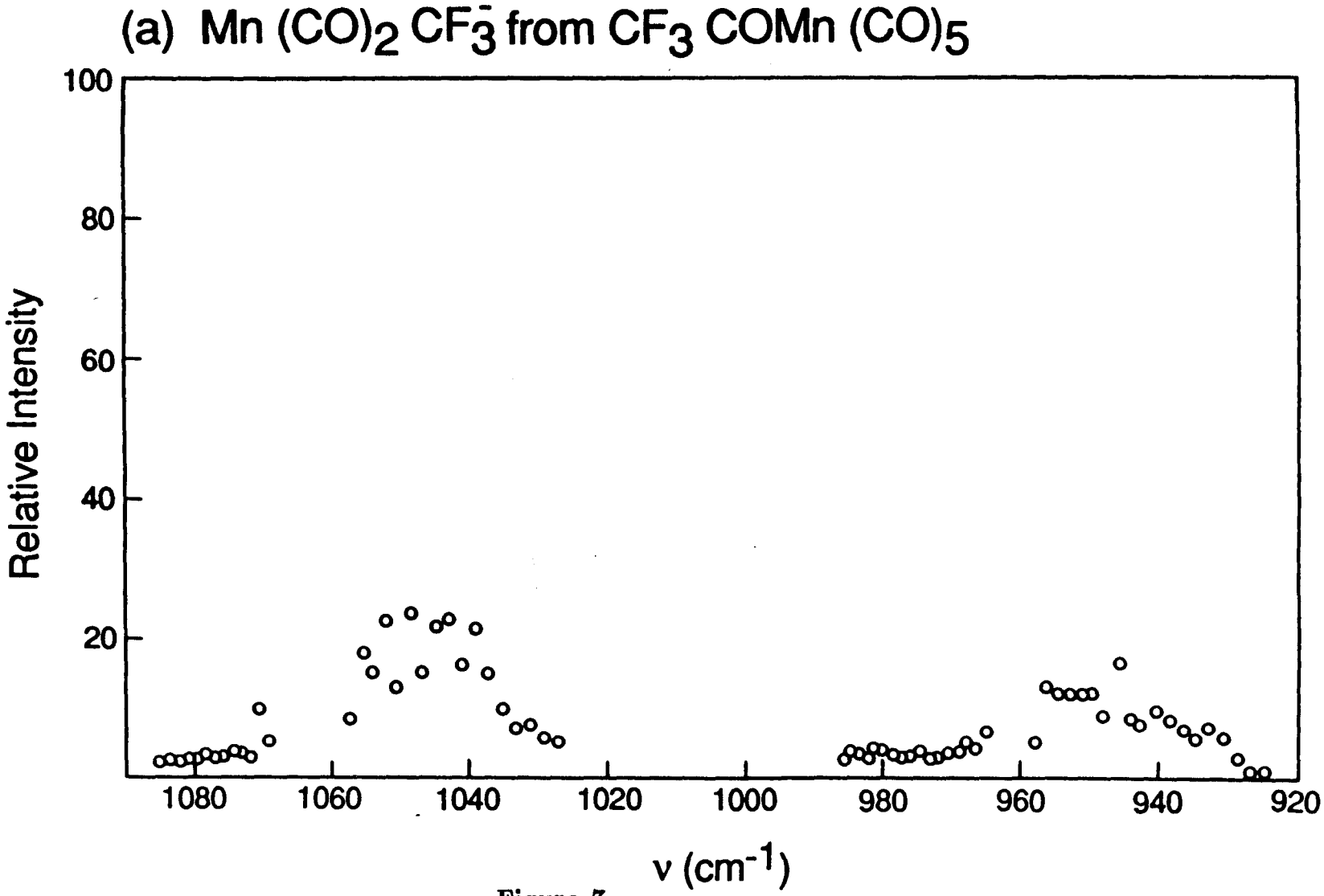
(a) Mn (CO)2 CF3 from CF3 COMn (CO)5
Relative Intensity
100
80
60
40
20
1080
1060
1040
1020
1000
980
960
940
920
ν (cm-1)

Figure 7

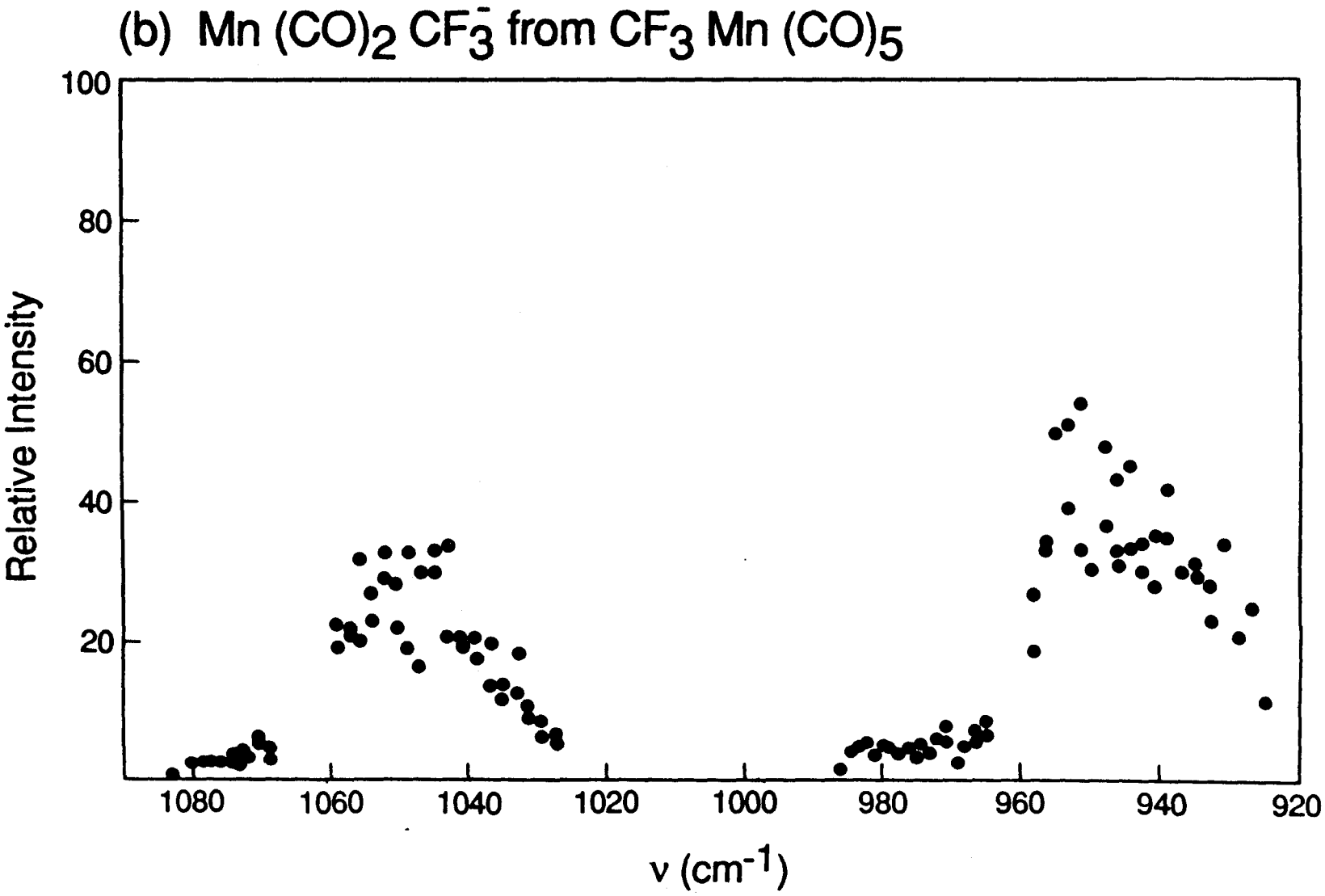
(b) Mn (CO)2 CF3 from CF3 Mn (CO)5
Relative Intensity
100
80
60
40
20
1080
1060
1040
1020
1000
980
960
940
920
ν (cm-1)

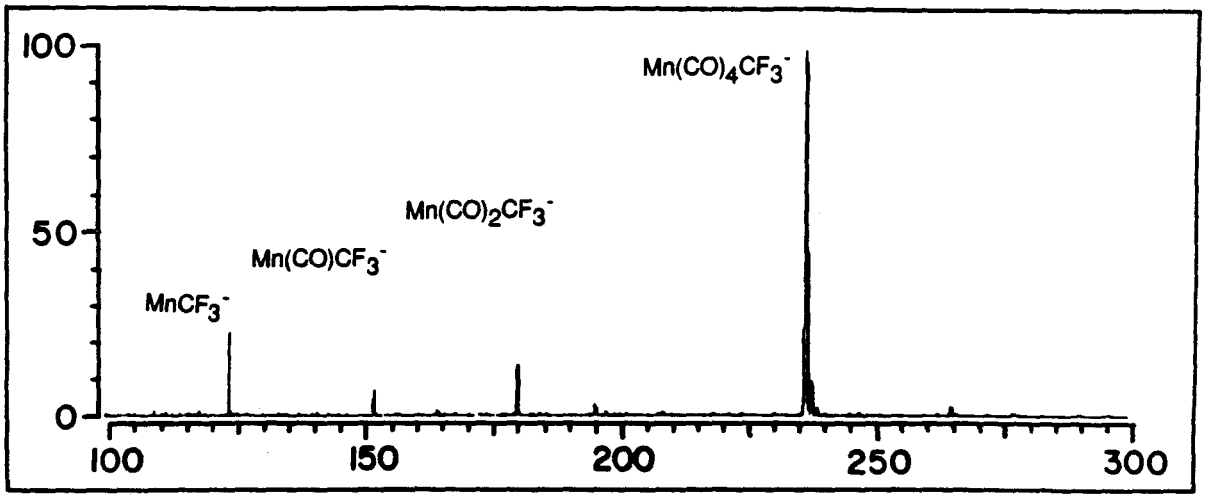
100
50
0
100
150
200
250
300
$Mn(CO)_4CF_3^-$
$Mn(CO)_2CF_3^-$
$Mn(CO)CF_3^-$
$MnCF_3^-$

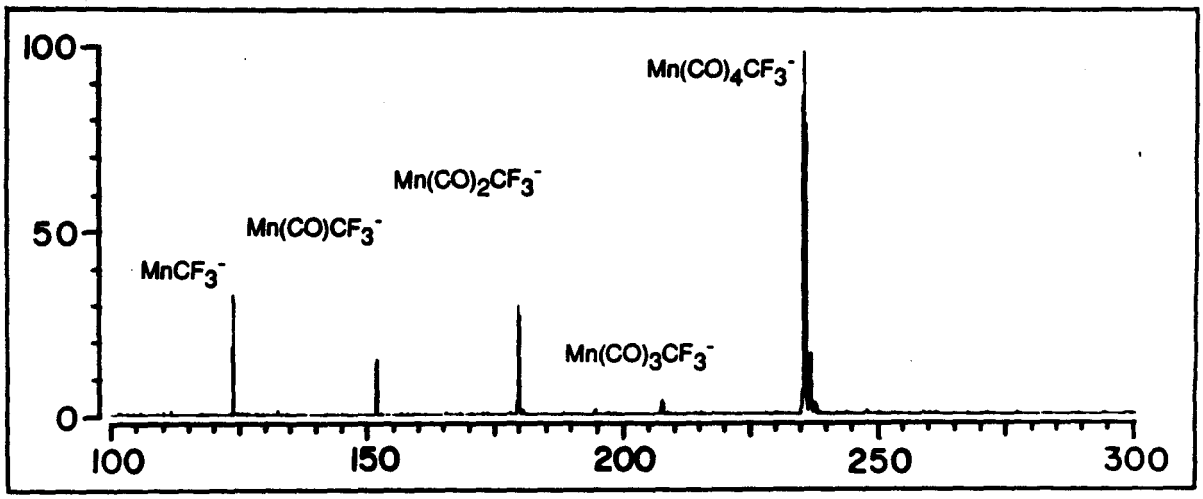
100
50
0
100
150
200
250
300
$Mn(CO)_4CF_3^-$
$Mn(CO)_2CF_3^-$
$Mn(CO)CF_3^-$
$MnCF_3^-$
$Mn(CO)_3CF_3^-$

Figure 8

Trifluoroacetylmanganese pentacarbonyl

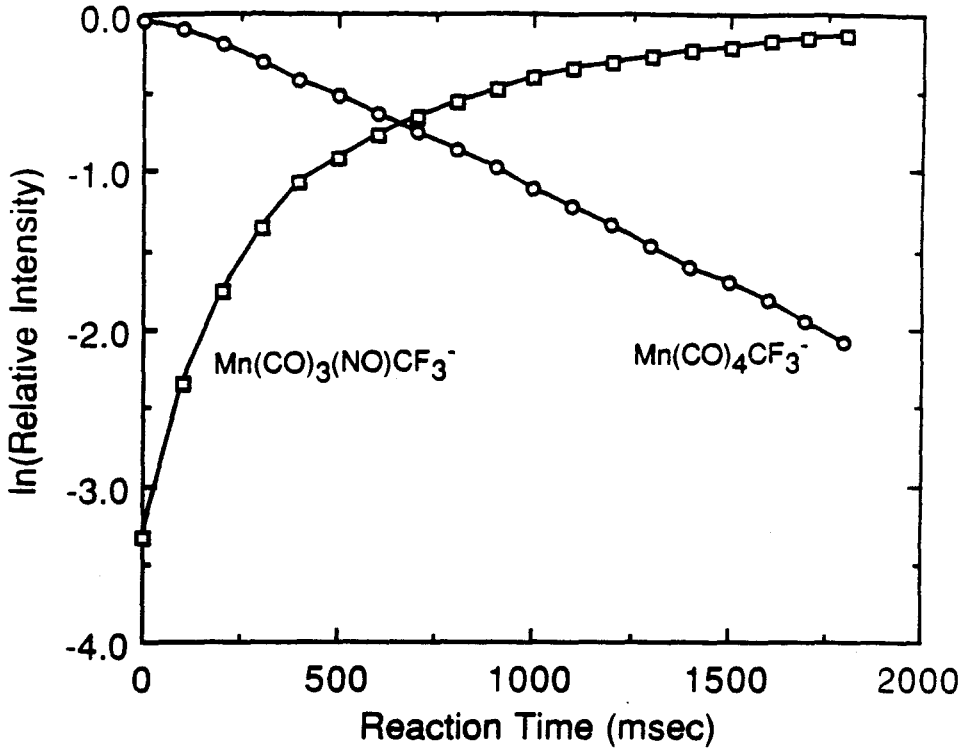

Trifluoromethylmanganese pentacarbonyl

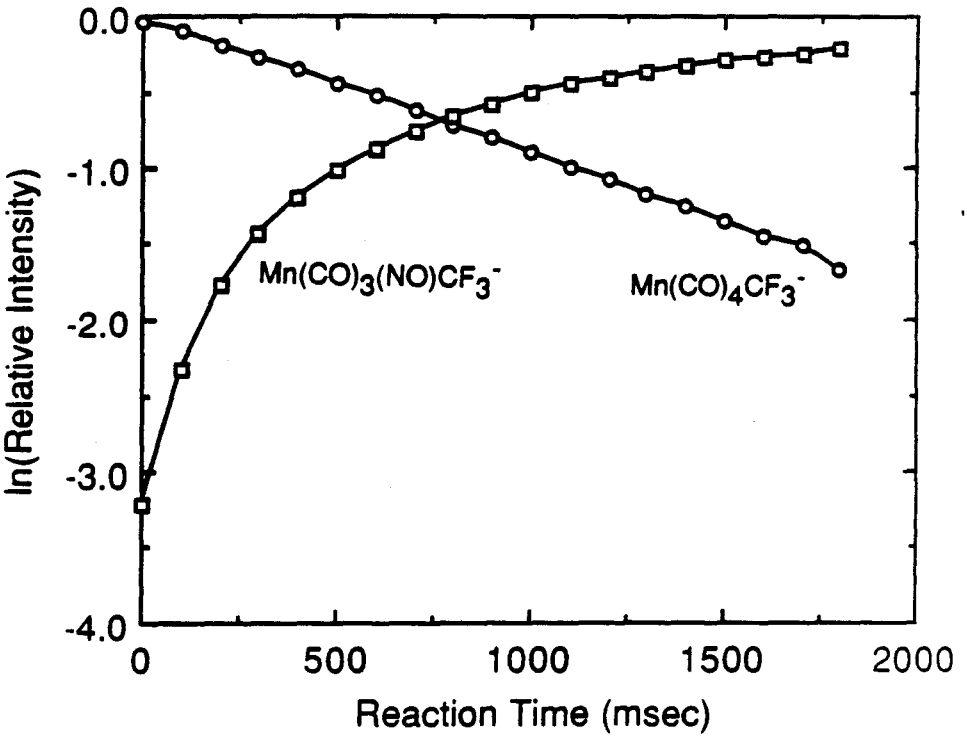

Figure 9

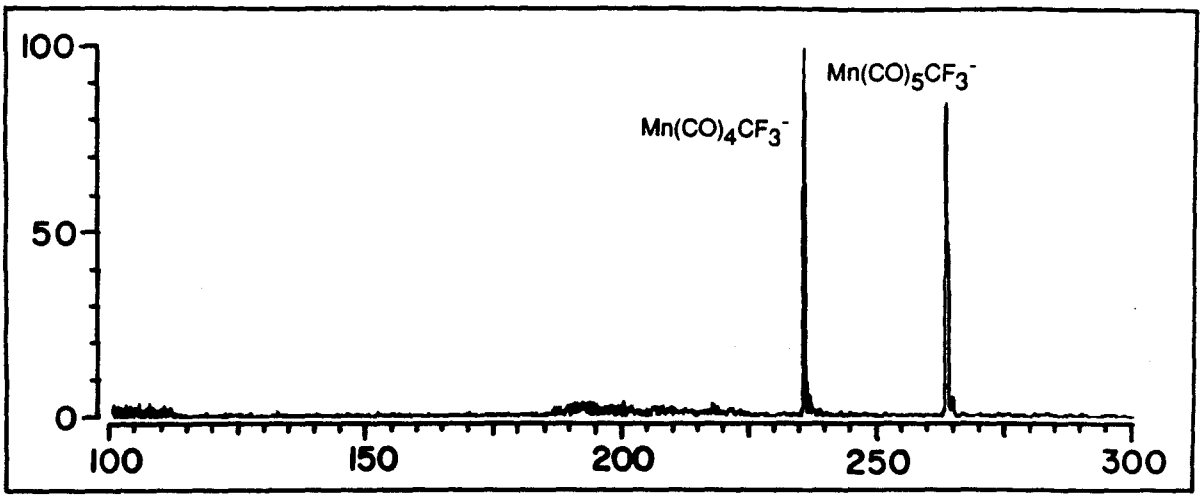
100
50
0
100
150
200
250
300
$Mn(CO)_4CF_3^-$
$Mn(CO)_5CF_3^-$

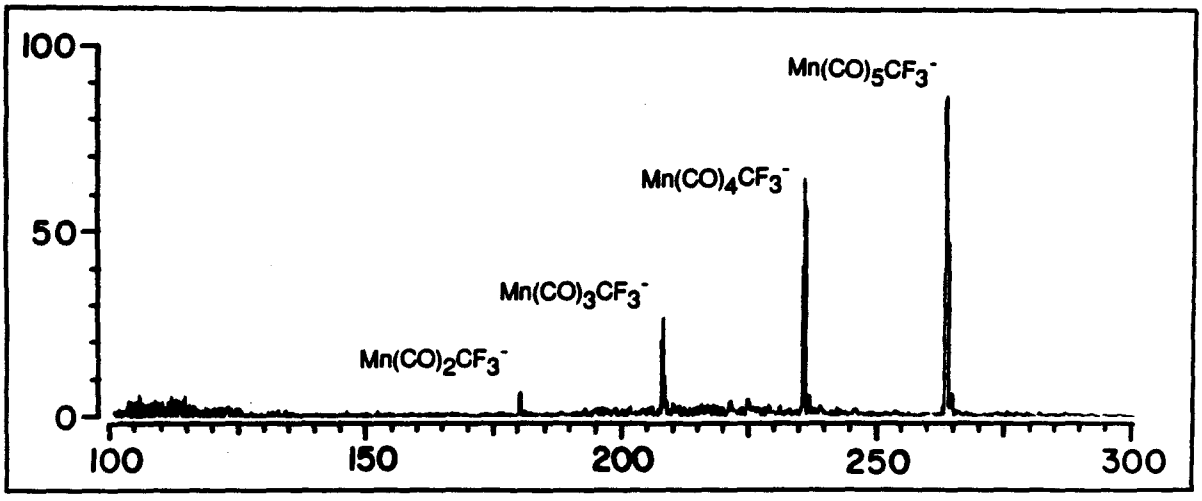
100
50
0
100
150
200
250
300
$Mn(CO)_2CF_3^-$
$Mn(CO)_3CF_3^-$
$Mn(CO)_4CF_3^-$
$Mn(CO)_5CF_3^-$

Figure 10

Chapter VIII

Infrared Multiphoton Dissociation Spectrum of $CF_3Mn(CO)_3(NO)^-$

Infrared Multiphoton Dissociation Spectrum of $CF_3Mn(CO)_3(NO)^-$

Seung Koo Shin, and J. L. Beauchamp*

Contribution No. 7952 from the Arthur Amos Noyes Laboratory of Chemical Physics

California Institute of Technology, Pasadena, California 91125

Abstract

An infrared multiphoton dissociation spectrum of $CF_3Mn(CO)_3(NO)^-$ has been obtained using Fourier transform ion cyclotron resonance spectroscopy combined with a line-tunable CW CO_2 laser in the 925–1085 cm^{-1} wavelength range. The trifluoromethyl group in the anion shows two absorption maxima at 1045 and 980 cm^{-1}. The peak at 1045 is assigned as a C–F stretch of A_1-type symmetry and the peak at 980 cm^{-1} is ascribed to a C–F stretch of E-type symmetry. It is quite interesting to observe that the symmetric C–F stretching mode changes little in frequency from 1063 cm^{-1} for $CF_3Mn(CO)_5$ to 1046 cm^{-1} for $CF_3Mn(CO)_3(NO)^-$, while the C–F stretching frequency of E-type symmetry decreases from 1043 cm^{-1} for the 18 e^- neural precursor to 980 cm^{-1} for the 18 e^- anion. Comparison with the infrared multiphoton dissociation spectrum of $CF_3Mn(CO)_4^-$ ion reveals that the degenerate C–F stretch of E-type symmetry increases from 945 cm^{-1} for the 17 e^- $CF_3Mn(CO)_4^-$ to 980 cm^{-1} for the 18 e^- $CF_3Mn(CO)_3(NO)^-$, whereas the symmetric C–F stretching bands overlap with each other quite well within experimental uncertainties. Variations of the electron density and hybridization in the σ donor orbital of the CF_3 ligand due to the different *d* orbital splittings of the complexes may be responsible for the distinctive C–F stretching frequencies observed in $CF_3Mn(CO)_5$ (18 e^-), $CF_3Mn(CO)_4^-$ (17 e^-), and $CF_3Mn(CO)_3(NO)^-$ (18 e^-).

Spectroscopy of molecular ions has been of great experimental interest in recent years.[1] Various techniques have been employed to obtain information about the structures, vibrational and electronic spectra, and photodissociation dynamics of molecular ions.[2] Recent developments in high-resolution infrared spectroscopy made it possible to study the individual vibration-rotation levels of relatively simple ions such as HD^+, HeH^+, CH^+, and H_3^+. However, there have been only a few experimental observation of infrared spectra of organometallic ions in the gas phase.

We have recently explored the technique of multiphoton dissociation[3] using a low power CO_2 laser to obtain infrared spectrum of the C–F stretching mode of the CF_3 ligand in organometallic anions.[4] The infrared multiphoton dissociation spectrum of $CF_3Mn(CO)_4^-$ ion exhibits two infrared absorption maxima at 1052 and 945 cm^{-1}. The peaks at 1052 and 945 cm^{-1} were assigned as a C–F stretch of A_1-type symmetry and that of E-type symmetry, respectively, from comparisons with results for CF_3X molecules. In going from a 18 e^- neutral precursor $CF_3Mn(CO)_5$ to a 17 e^- ion $CF_3Mn(CO)_4^-$, the nondegenerate C–F stretching mode changes little in frequency (from 1063 to 1052 cm^{-1}, while the degenerate C–F stretch of E-type symmetry decreases about 100 cm^{-1} (from 1043 to 945 cm^{-1}).

It has been previously observed that the negative charge reduces the C–O stretching force constant and NO substitution in place of an equatorial CO increases an axial C–O stretching force constant in trigonal bipyramidal $LM(CO)_4$ complexes.[5] This relationship is in accord with the observed decrease of the C–F stretching frequency in going from $CF_3Mn(CO)_5$ to the $CF_3Mn(CO)_4^-$ ion.[4] In light of this emperical observation, NO substitution in place of an equatorial CO is expected to enhance the C–F stretching frequencies in $CF_3Mn(CO)_3(NO)^-$ compared with those in $CF_3Mn(CO)_4^-$.

In the present paper, we have investigated the infrared multiphoton dissociation of the 18 e^- ion $CF_3Mn(CO)_3(NO)^-$ to see how each C–F stretching mode varies with NO substitution.

Experimental techniques associated with Fourier transform ion cyclotron res-

onance spectroscopy[6] and its modification for infrared photochemistry have been previously described in detail.[4,7] Briefly, the anion of interest is formed by the ligand displacement reaction of $CF_3Mn(CO)_4^-$ ion generated from the dissociative electron attachment[8] of $CF_3Mn(CO)_5$ with nitric oxide as shown in reactions 1 and 2.

$$CF_3Mn(CO)_5 + e^- \longrightarrow CF_3Mn(CO)_4^- + CO \quad (1)$$

$$CF_3Mn(CO)_4^- + NO \longrightarrow CF_3Mn(CO)_3(NO)^- + CO \quad (2)$$

All ions except $CF_3Mn(CO)_3(NO)^-$ were removed from a trapping ICR cell[9] using a series of ion ejectron pulses after 1 second delay from an initial isolation of $CF_3Mn(CO)_4^-$ ion in 10:1 mixtures of trifluoromethylmanganese pentacarbonyl and nitric oxide with a total pressure of 1.0×10^{-5} Torr. The $CF_3Mn(CO)_3(NO)^-$ ion is unreactive with $CF_3Mn(CO)_5$ and NO. The isolated ion of interest is irradiated with the unfocused output of a line-tunable CW CO_2 laser (Appolo Lasers Model 550A). The infrared spectrum of the $CF_3Mn(CO)_3(NO)^-$ ion is obtained by monitoring the extent of photodissociation as function of laser wavelength at a fixed intensity (8 W cm^{-2}) and irradiation period (20 msec). Irradiation of $CF_3Mn(CO)_3(NO)^-$ results in loss of CO yielding $CF_3Mn(CO)_2(NO)^-$ (reaction 3). The photodissociation of $CF_3Mn(CO)_2(NO)^-$ with loss of CO followed by the NO substitution reaction results in the formation of the $CF_3Mn(NO)_2^-$ ion (reaction 4).

$$CF_3Mn(CO)_3(NO)^- + h\nu \longrightarrow CF_3Mn(CO)_2(NO)^- + CO \quad (3)$$

$$CF_3Mn(CO)_2(NO)^- + NO + h\nu \longrightarrow CF_3Mn(NO)_2^- + 2CO \quad (4)$$

The infrared absorption spectrum of the neutral precursor, $CF_3Mn(CO)_5$, is shown in Figure 1a. The infrared multiphoton dissociation spectrum of $CF_3Mn(CO)_4^-$ and $CF_3Mn(CO)_3(NO)^-$ are presented in Figure 1b and 1c, respectively, for the comparison. The peaks at 1046 and 980 cm^{-1} are assigned as a C–F stretch of A_1-type symmetry and that of E-type symmetry, respectively, from comparisons with results for $CF_3Mn(CO)_4^-$.

Comparison of the infrared spectrum of $CF_3Mn(CO)_5$ (Figure 1a) with infrared multiphoton dissociation spectra of $CF_3Mn(CO)_4^-$ (Figure 1b) and $CF_4Mn(CO)_3(NO)^-$ (Figure 1c) leads to the interesting observation that the C–F stretching frequencies of the anionic species have decreased from those of the neutral molecule, the nondegenerate C–F stretching mode has changed very little in frequency, whereas the degenerate C–F stretching frequency has varied effectively with changes in total charge of the molecule and ligand substituents. The decrease of the C–F stretching frequency for the anionic species may be due to an increase of the electron density in the carbon σ-donor orbital of the CF_3 group in the anionic species.

In order to illustrate the hybridization changes at carbon in the C–F bond orbitals and σ-donor orbital due to the negative charge, the GVB[10] one electron C–F bond orbitals and carbon nonbonding σ orbitals are presented in Figure 2 for the CF_3 radical and CF_3^- ion. Analyses of Mulliken populations[11] for both radical and anion quantify the hybridization and charge transfer in the C–F bonds and carbon nonbonding σ orbital [charge population: C (5.27) and F (9.24) for the radical; C (5.96) and F (9.35) for the ion]. The CF_3^- ion has visibly more *p*-character at the C–F bond carbon than the radical (36 % *s* and 64 % *p* for the radical; 100 % p for the ion). This increase of carbon *p*-character in the C–F bond orbitals of the CF_3^- ion would increase the C–F bond distance and decrease the C–F stretch force constant.

Moreover, since a contraction of one C–F bond would increase the carbon *s*-character of the contracting bond and induce a concurrent increase of the carbon *p*-character of the other two C–F bonds, it would tend to be more easily accompanied by an extension than the contraction of the other two bonds resulting in E-type vibration.[12] Therefore, one would expect that changes of hybridization during vibration could be more effective for the degenerate E-type vibration than the symmetric vibration. This qualitative explanation is in agreement with the observation that the anionic species have the lower C–F stretching frequencies than the

neutral and the E-type stretch is less stiff than the A_1-type vibration. Previous observation of changes in the C–F stretching frequencies from the CF_3 radical[13] (C_{3v}: $\nu_s(A_1) = 1084\ cm^{-1}$ and $\nu_s(E) = 1252\ cm^{-1}$) to the CF_3^+ ion[13] (D_{3h}: $\nu_s(A') = 1125\ cm^{-1}$ and $\nu_s(E') = 1667\ cm^{-1}$) shows that the positive ion has the higher C–F stretching frequencies than the radical and the E-type stretch increases about 410 cm^{-1}, while the A_1-type stretch mode varies as little as about 40 cm^{-1}. This result also supports the proposed explanation.

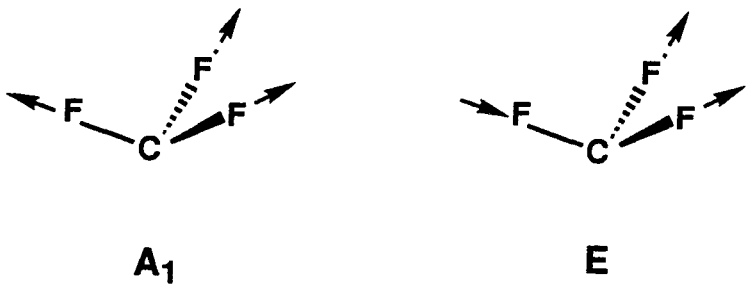

A_1 E

The observed increase of the degenerate C–F stretching frequency of E-type symmetry for $CF_3Mn(CO)_3(NO)^-$ compared with that of $CF_3Mn(CO)_4^-$ may afford the possibility of differentiating their structures.

The structure of the d^7 complex $CF_3Mn(CO)_4^-$ is presumed to be a square-based pyramidal with CF_3 in the basal plane, from comparisons with results for other five-coordinate d^6 and d^7 complexes. An infrared spectroscopic study of the five-coordinate d^6 complex, $CH_3COMn(CO)_4$, in methane matrix at 12 K° indicates the square-based pyramidal structure with a η^1-acetyl bonding.[14] Spectroscopic studies of the five-coordinate d^7 complex, $Mn(CO)_5$, generated in $Cr(CO)_6$ crystals or in low-temperature solid matrices, support a square pyramidal structure with C_{4v} point group.[15] Extended Hückel calculations by Elian and Hoffman[16] also suggested the square pyramidal structure for the five-coordinate d^7 complex carrying its odd electron in a relatively high-lying directional orbital occupying an empty apical site. The d orbital splitting schemes for $CF_3Mn(CO)_4^-$ are shown in scheme I with those for $CF_3Mn(CO)_5$, $CF_3Mn(CO)_3(NO)^-$, and $CF_3Mn(CO)_4^{2-}$.

d Orbital Splitting Scheme

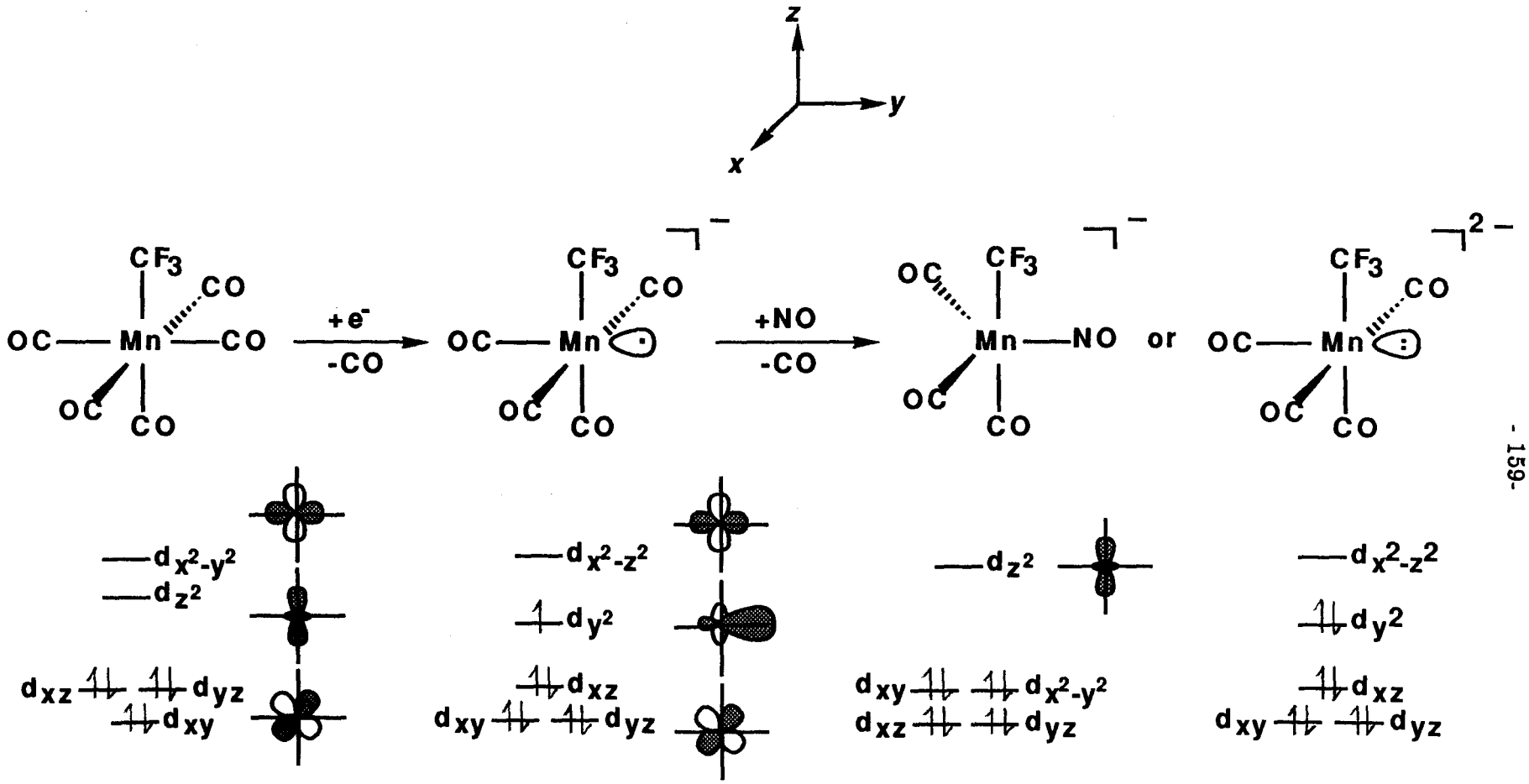

In going from the octahedral d^6 complex $CF_3Mn(CO)_5$ to the square pyramidal d^7 complex $CF_3Mn(CO)_4^-$, the number of electrons occupying the nonbonding directional orbital (d_{y^2}) increases and the C–F stretching frequencies decrease. Assuming that the $CF_3Mn(CO)_3(NO)^-$ ion has a square-based pyramidal structure would lead to the similar d orbital splittings as $CF_3Mn(CO)_4^-$ bearing its nonbonding lone pair electrons in a directional d_{y^2} orbital occupying an empty apical site. If the NO substituted ion is analogous to the square pyramidal $CF_3Mn(CO)_4^{2-}$,[17] one would expect that the C–F stretching frequencies of $CF_3Mn(CO)_4^{2-}$ would decrease due to its doubly occupied d_{y^2} orbital. However, this expectation, which resulted from viewing $CF_3Mn(CO)_3(NO)^-$ as a square pyramidal $CF_3Mn(CO)_4^{2-}$, is inconsistent with the observed increase of the degenerate C–F stretching frequency. Therefore, it is quite reasonable to suggest that the structure of $CF_3Mn(CO)_3(NO)^-$ is different from a square pyramidal.

The structure of the d^8 complex $CF_3Mn(CO)_3(NO)^-$ is considered to be a trigonal bipyramidal with a linear Mn–NO in the equatorial position from comparison with the structures of the five-coordinate d^8 complexes $Mn(CO)_4(NO)$ and $Mn(CO)_5^-$. Frenz et al.[17] have determined the crystal structure of $Mn(CO)_4(NO)$ revealing that the nitrosyl group is in equatorial position in the trigonal bipyramidal structure and the Mn–CO and Mn–NO bonds are linear. $Mn(CO)_5^-$ is also a trigonal bipyramidal in the solid state.[18]

The trigonal bipyramidal d^8 complex $CF_3Mn(CO)_3(NO)^-$ has an unoccupied d_{z^2} orbital which can easily accomodate the electron density on the σ-donor orbital of the CF_3 ligand. This delocalization of the σ-donor electrons of the CF_3 ligand to the d_{z^2} orbital would reduce the charge population on carbon and lead to concurrent decrease of carbon p character in the C–F bond orbitals resulting in the increase of the C–F stretching force constant. Since the degenerate C–F stretch of E-type symmetry changes more effectively with changes of hybridization as noted earlier, the E-type C–F stretching frequency is expected to increase more readily

than the A_1-type vibration. The observed increase of the E-type C–F stretching frequency in $CF_3Mn(CO)_3(NO)^-$ is in agreement with the expectation from the trigonal bipyramidal structure.

This result strongly suggests that NO substitution in place of CO induces structural change from the square pyramidal for $CF_3Mn(CO)_4^-$ to the trigonal bipyramidal for $CF_3Mn(CO)_3(NO)^-$.

In conclusion, infrared photochemistry of organometallic intermediates containing the CF_3 group directly bonded to metal is explored using Fourier transform ion cyclotron resonance spectroscopy. The C–F stretching frequency shift, which is sensitive to the net charge of the complex and ligand substituents, is used to differentiate the structures of intermediates. It will be of further experimental and theoretical interest to see how each C–F stretch mode varies with ligand substituents and the coordination number.

Acknowledgement. We acknowledge the support of the National Science Foundation (Grant No. CHE87-11567) and the Petroleum Research Fund administered by the American Chemical Society.

References

(1) (a) In *Gas Phase Ion Chemistry*; Bowers, M. T. Ed.; Academic Press: New York, 1984, vol.3. (b) *Molecular Ions: Spectroscopy, Structure, and Chemistry* Miller, T. A.; Bondybey, V. E. Ed; North-Holland Publishing: Amsterdam; 1983, 231.

(2) *Molecular Photodissociation Dynamics* Ashfold, M. N. R.; Baggott, J. E. Ed; The Royal Society of Chemistry: London; 1987.

(3) (a) Thorne, L. R.; Beauchamp, J. L. In *Gas Phase Ion Chemistry*; Bowers, M. T. Ed.; Academic Press: New York, 1984; vols. 3, pp. 42. and earlier references therein (b) Hanratty, M. A.; Paulsen, C. M.; Beauchamp, J. L. *J. Am. Chem. Soc.* **1985**, *107*, 5074. (c) Lupo, D. W.; Quack, M. *Chem. Rev.* **1987**, *87*, 181 and earlier references therein. (d) Schulz, P. A.; Sudbo, A. S.; Krajnovich, D. J.; Kwok, H. S.; Shen, Y. R.; Lee, Y. T. *Annu. Rev. Phys. Chem.* **1979**, *30*, 379.

(4) Shin, S. K.; Beauchamp, J. L. *J. Am. Chem. Soc.* to be submitted.

(5) Timney, J. A. *Inorg. Chem.* **1979**, *18*, 2502.

(6) (a) Baldeschwieler, J. D. *Science* **1968**, *159*, 263. (b) Beauchamp, J. L. *Ann. Rev. Phys. Chem.* **1971**, *22*, 527. (c) Lehman, T. A.; Bursey, M. M. *Ion Cyclotron Resonance Spectrometry*; Wiley: New York, 1976. (d) Marshall, A. G. *Acc. Chem. Res.* **1985**, *18*, 316 and references therein.

(8) (a) Foster, M. S.; Beauchamp, J. L. *Chem. Phys. Lett.* **1975**, *31*, 1975. (b) Woodin, R. L.; Foster, M. S.; Beauchamp, J. L. *J. Chem. Phys.* **1980**, *72*, 4223. (c) Squires, R. R. *Chem. Rev.* **1987**, *87*, 623.

(9) Comisarow, M. B. *Int. J. Mass. Spectrom. Ion Phys.* **1981**, *37*, 251.

(10) The generalized valence bond (GVB) method describes each valence bond with two natural orbitals: Bobrowicz, F. W.; Goddard, W. A. III, In *Methods of Electronic Structure Theory*; Schaefer, H. F. Ed.; Plenum Press: New York; 1977, Chapter 4. The geometry of r(C–F) = 1.332 Å and ∠(F-C-F) = 109°

from experimental values for CHF_3 is used for the GVB calculation (Ghosh, S. N.; Trambarulo, R.; Gordy, W. *J. Chem. Phys.* **1952**, *20*, 605.).

(11) Mulliken populations were obtained by summing over the electron populations of each *s*, *p*, and *d* basis function on carbon within each natural orbital for each GVB pair. Although this analysis tends to be basis dependent, relative trends and comparisons are expected to be reliable. Valence double-ζ plus polarization basis sets for carbon and fluorine are used: Dunning, T. H. Jr.; Hay, P. J. In *Methods of Electronic Structure Theory*; Schaefer, H. F. Ed.; Plenum Press: New York; 1977, Chapter 1.

(12) Wilson, E. B. Jr.; Decius, J. C.; Cross, P. C. *Molecular Vibrations*; Dover: New York; 1955, pp 180-181.

(13) Prochaska, F. T.; Andrews, L. *J. Am. Chem. Soc.* **1978**, *100*, 2102.

(14) Hitam, R. B.; Narayanaswamy, R.; Rest, A. J. *J. Chem. Soc. Dalton Trans.* **1983**, 615.

(15) (a) Hughey, J. L.; Anderson, C. P.; Meyer, T. J. *J. Organomet. Chem.* **1977**, *125*, C49. (b) Waltz, W. L.; Hackelberg, O.; Dorfman, L. M.; Wojcicki, A. *J. Am. Chem. Soc.* **1978**, *100*, 7259. (c) Church, S. P.; Poliakoff, M.; Timney, J. A.; Turner, J. J. *J. Am. Chem. Soc.* **1981**, *103*, 7515. (d) Symons, M. C. R.; Sweany, R. L. *Organometallics* **1982**, *1*, 834. (e) Fairhurst, S. A.; Morton, J. R.; Perutz, R. N.; Preston, K. F. *Organometallics* **1984**, *3*, 1389. (f) Howard, J. A.; Morton, J. R.; Preston, K. F. *Chem. Phys. Lett.* **1981**, *83*, 226. (g) Lionel, T.; Morton, J. R.; Preston, K. F. *Chem. Phys. Lett.* **1981**, *81*, 17.

(16) Elian, M.; Hoffmann, R. *Inorg. Chem.* **1975**, *14*, 1058.

(17) Frenz, B. A.; Enemark, J. H.; Ibers, J. A. *Inorg. Chem.* **1969**, *8*, 1288.

(18) Frenz, B. A.; Ibers, J. A. *Inorg. Chem.* **1972**, *11*, 1109.

Figure Captions

Figure 1. The infrared absorption spectra of the CF_3 group in trifluoromethylmanganese pentacarbonyl (top) and photodissociation spectra of $CF_3Mn(CO)_4^-$ (middle) and $CF_3Mn(CO)_3(NO)^-$ over the CO_2 laser spectral range. Data points for photodissociation spectra of $CF_3Mn(CO)_3(NO)^-$ are the ratio (in percentage) of the intensity of $CF_3Mn(CO)_3(NO)^-$ to the total ion intensity [$CF_3Mn(CO)_3(NO)^-$ + $CF_3Mn(CO)_2(NO)^-$ + $CF_3Mn(NO)_2^-$] as a function of wavelength. The mass-selected ion of interest is irradiated for 20 msec at 8 W cm^{-2}.

Figure 2. The GVB(3/6)-PP one electron orbitals for the CF_3 radical and the CF_3^- ion: (a) the C–F bond pair for the radical; (b) the nonbonding σ orbital (singly occupied) for the radical; (a) the C–F bond pair for the ion; (d) the nonbonding σ natural orbital (doubly occupied) for the ion.

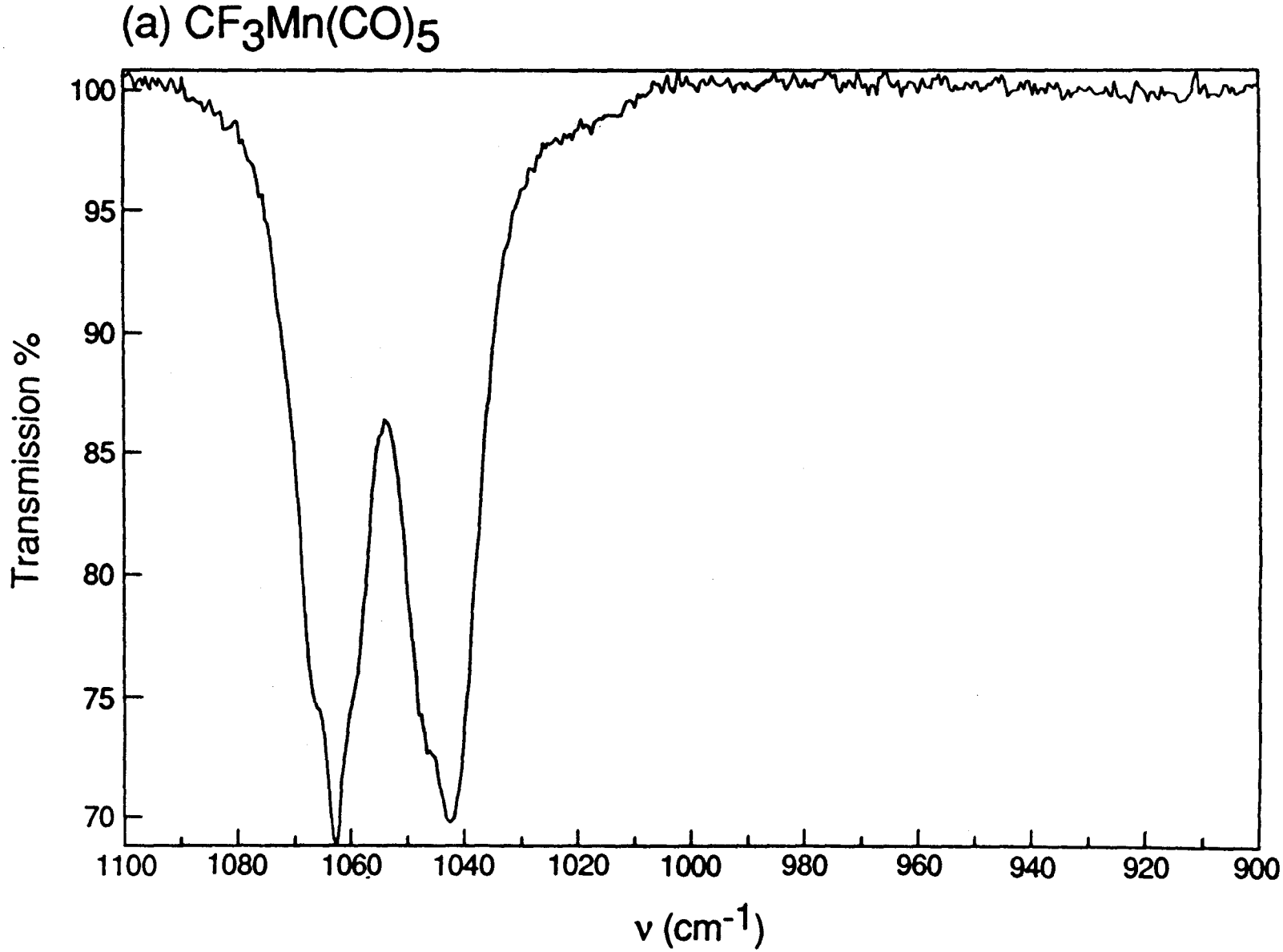
(a) $CF_3Mn(CO)_5$
Transmission %
100
95
90
85
80
75
70
1100
1080
1060
1040
1020
1000
980
960
940
920
900
ν (cm^{-1})

Figure 1

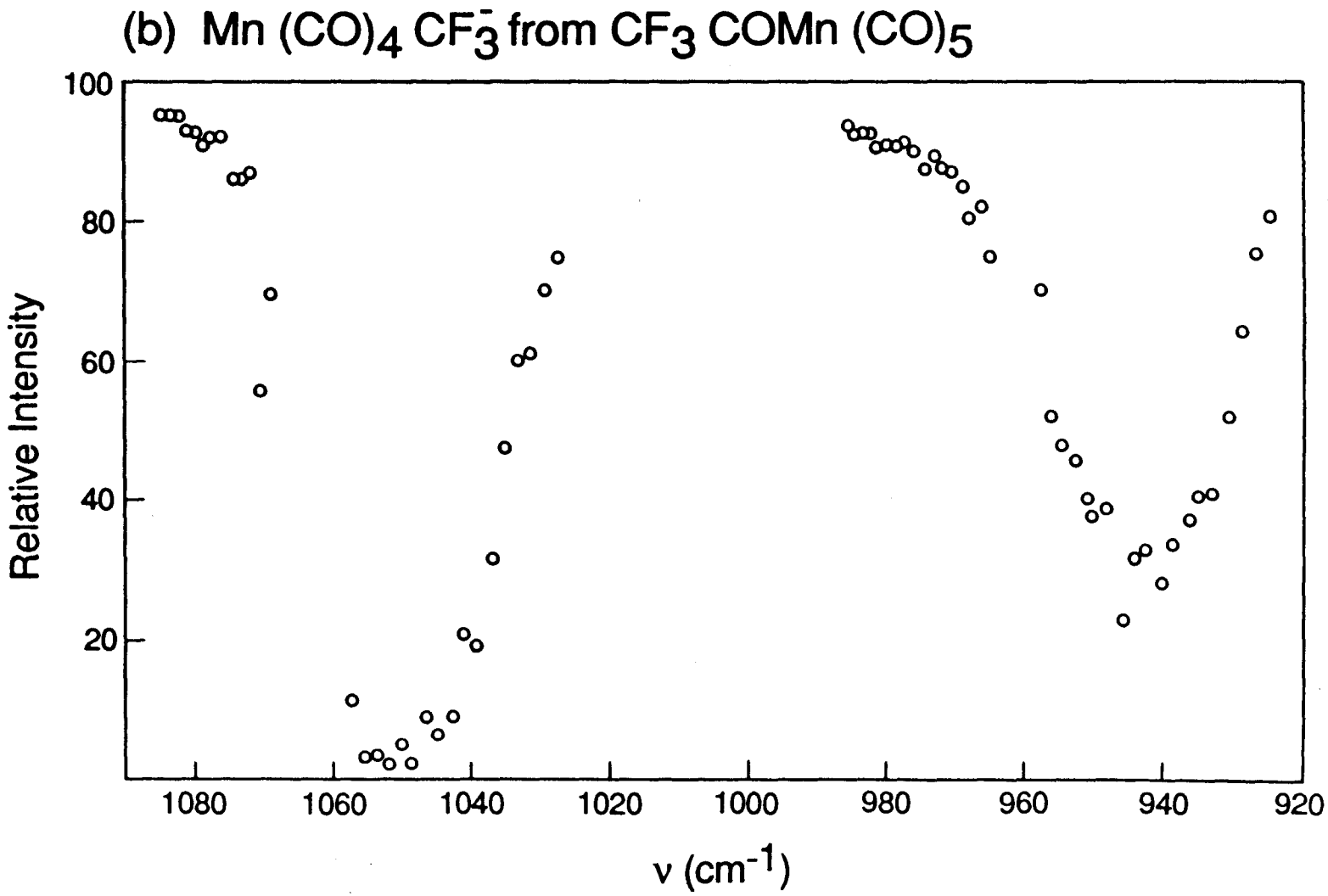
(b) Mn (CO)4 CF3 from CF3 COMn (CO)5
Relative Intensity
100
80
60
40
20
1080
1060
1040
1020
1000
980
960
940
920
ν (cm-1)

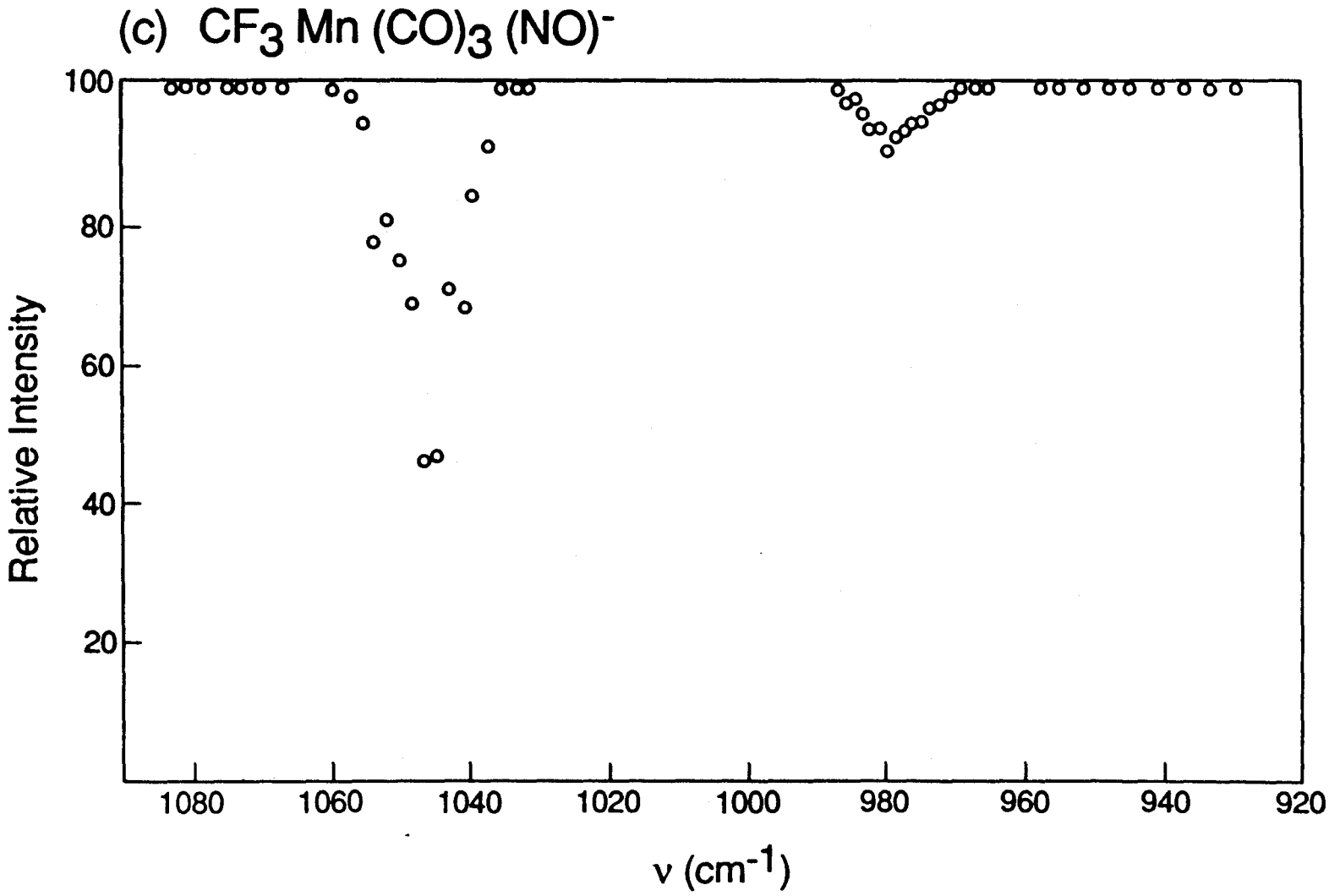
(c) $CF_3 Mn (CO)_3 (NO)^-$
Relative Intensity
100
80
60
40
20
1080
1060
1040
1020
1000
980
960
940
920
ν (cm^{-1})

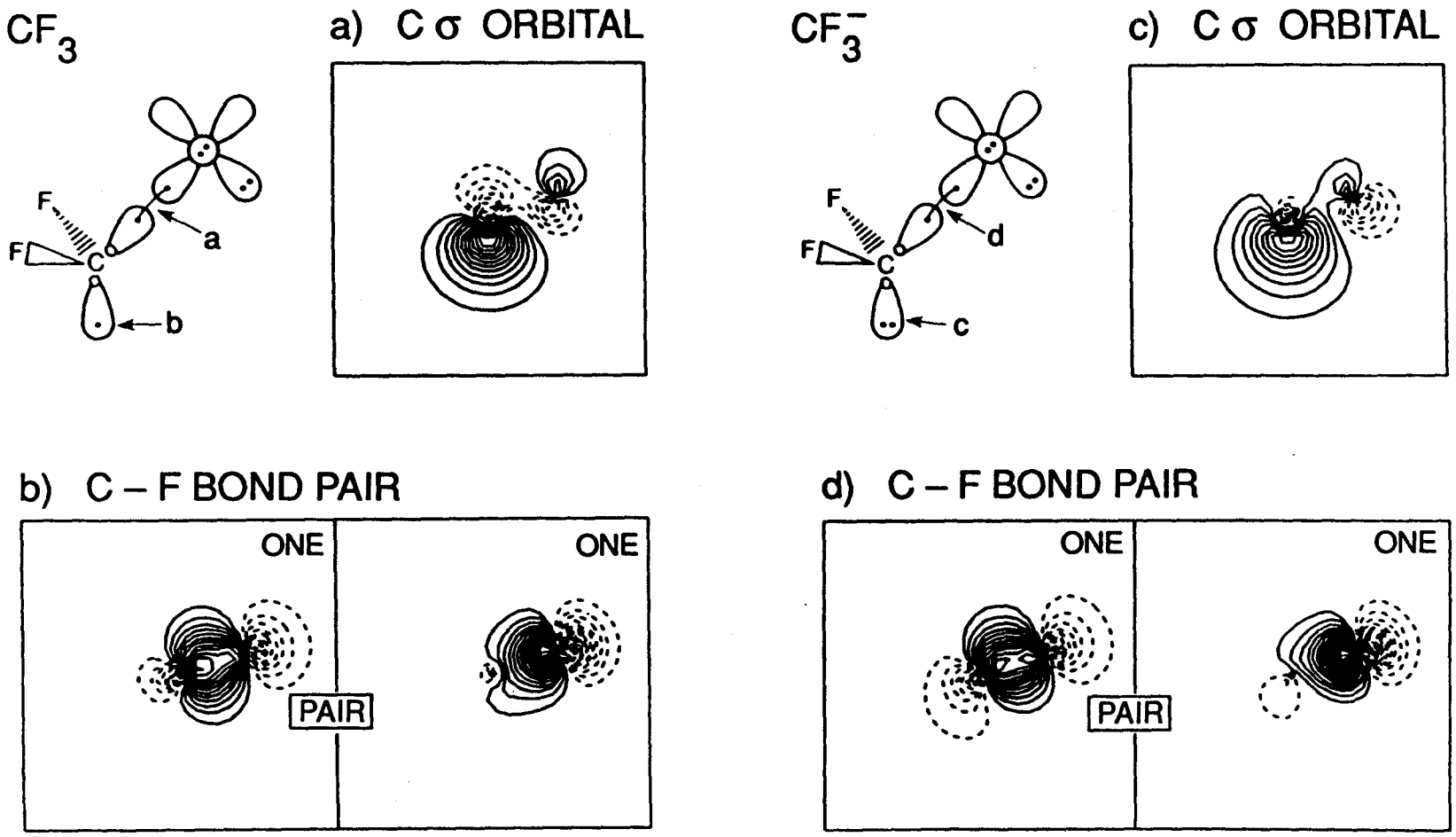
CF3
a) C σ ORBITAL
F
F
C
a
b
CF3−
c) C σ ORBITAL
F
F
C
d
c
b) C – F BOND PAIR
ONE
ONE
PAIR
d) C – F BOND PAIR
ONE
ONE
PAIR

Figure 2

Appendix I

Reactions of Transition Metal Ions with Methyl Silanes in the Gas Phase: The Formation and Characteristics of Strong Transition Metal-Silylene Bonds

Reprinted from the Journal of the American Chemical Society, 1986, *108*, 5668.

Reactions of Transition-Metal Ions with Methylsilanes in the Gas Phase. The Formation and Characteristics of Strong Transition Metal–Silylene Bonds

Heon Kang,[1] Denley B. Jacobson,[2a] Seung Koo Shin,[2a] J. L. Beauchamp,*[2a] and M. T. Bowers[2b]

Contribution No. 7322 from the Arthur Amos Noyes Laboratory of Chemical Physics, California Institute of Technology, Pasadena, California 91125, and Department of Chemistry, University of California, Santa Barbara, California 93106. *Received March 12, 1986*

Abstract: Reactions of transition-metal ions (Ti^+, V^+, Cr^+, Fe^+, Co^+, and Ni^+) with organosilanes are investigated in the gas phase with an ion beam apparatus. Co^+ and Ni^+ react with silane to yield metal silylenes as exothermic products. Collision-induced dissociation studies of the product $CoSiH_2^+$ and nascent $CoSiH_4^+$ adducts provide additional information concerning the product structure and reaction mechanisms. Reactions with methylsilanes lead to formation of metal silylenes as major reaction channels, along with several other processes including hydride abstraction, dehydrogenation, and methane loss. Reactions with hexamethyldisilane are also investigated, with major products indicating Si–Si bond cleavage. An examination of the reaction enthalpies for the observed metal silylene products provides estimates for metal ion–silylene bond energies, which include $D°(M^+ - SiH_2) = 67 \pm 6$ kcal mol^{-1} (M = Co, Ni). Correlation between the metal ion–silylene bond energies and the electronic structure of the metal ions supports a bonding scheme in which silylene donates its nonbonding lone pair electrons to an empty 4s orbital of the metal center. For Co^+ and Ni^+, back-donation of paired 3d electrons from the metal into the empty 3p orbital on silicon is suggested to account for the stronger bond deduced for these metals.

Studies of molecular transformations involving the reactions of silicon compounds at transition-metal centers are numerous. Hydrosilation, for example, which results in the addition of Si–H bonds to unsaturated hydrocarbons, is catalyzed by transition-metal complexes.[3-5] However, catalytic hydrosilations are often very complex, and their mechanisms are not well understood. Oxidative addition of a Si–H bond to the metal center is presumed to be an obligatory step in the hydrosilation process, and direct evidence for this reaction is provided by several spectroscopic studies at low temperatures.[6,7] Nevertheless, relatively little is known about the nature, strengths, and specific reactions leading to the formation and rupture of single and multiple bonds between transition metals and silicon.

Recent studies of the reactions of transition-metal ions with small organic molecules in the gas phase have been very successful

* To whom correspondence should be addressed.

(1) Present address: Department of Chemistry, University of Houston, 4800 Calhoun Road, Houston, Texas 77004.
(2) (a) California Institute of Technology. (b) University of California, Santa Barbara.
(3) Khan, M. M. T.; Martell, A. E. *Homogeneous Catalysis by Metal Complexes*; Academic: New York, 1974; Vol. 2, p 66.
(4) Collman, J. P.; Hegedus, L. S., *Principles and Applications of Organotransition Metal Chemistry*; University Science Books: New York, 1980; p 384.
(5) Noll, W. *Chemistry and Technology of Silicons*; Academic: New York, 1986.
(6) Fernandez, M.-J.; Bailey, P. M.; Bentz, P. O.; Ricci, J. S., Koetzle, T. F.; Maitlis, P. M. *J. Am. Chem. Soc.* **1984**, *106*, 5458.
(7) Fernandez, M.-J.; Maitlis, P. M. *Organometallics* **1983**, *2*, 164.

0002-7863/86/1508-5668$01.50/0

Table I. Lower Electronic States of Transition-Metal Ions and Their Relative Populations

metal ion	state[a]	config	energy,[b] eV	filament temp, K	population, %
Ti^+	X^4F	$3d^24s$	0.00	2290	62
	^4F	$3d^3$	0.11		36
	^2F	$3d^24s$	0.56		2
	^2D	$3d^24s$	1.05		<1
V^+	X^5D	$3d^4$	0.00	2290	81
	^5F	$3d^34s$	0.34		19
	^3F	$3d^34s$	1.08		<1
Cr^+	X^6S	$3d^5$	0.00	2000	100
	^6D	$3d^44s$	1.52		<1
Fe^+	X^6D	$3d^64s$	0.00	2560	74
	^4F	$3d^7$	0.25		25
	^4D	$3d^64s$	0.98		1
	^4P	$3d^7$	1.64		<1
Co^+	X^3F	$3d^8$	0.00	2560	78
	^5F	$3d^74s$	0.43		22
	^3F	$3d^74s$	1.21		<1
Ni^+	X^2D	$3d^9$	0.00	2490	98
	^4F	$3d^84s$	1.09		2
	^2F	$3d^84s$	1.68		<1

[a] Data from ref 22. [b] State energies cited are averaged over J states.

in providing valuable information concerning the reaction mechanisms[8-13] and thermochemistry of organometallic fragments in the absence of complicating solution phenomena.[14-18] In the present work, we have examined reactions of several first-row transition-metal ions with a series of methylsilanes in the gas phase. A surprising observation, with no precedent in condensed phase chemistry, is prevalent formation of transition-metal silylenes as major products. The silicon center in organosilanes completely dominates the observed reactions, which are very different from the reactions of transition-metal ions with alkanes in the gas phase.[9,10,16] These differences can be attributed to the special stability of metal silylenes. Correlation of metal–silicon bond energies with the electronic structures of the metal ions provides interesting insights into the nature of transition metal–silylene bonds.

Experimental Section

The ion-beam apparatus used for these investigations is described in detail elsewhere.[19] Briefly, transition-metal ions, Ti^+, V^+, Cr^+, Fe^+, Co^+, and Ni^+, are generated from organic compounds, $TiCl_4$, $VOCl_3$, $Cr(CO)_6$, $FeCl_3$(anhydrous), $CoCl_2$(anhydrous), and $NiCl_2$(anhydrous), respectively, by surface ionization. Ions are extracted from the source, mass and energy selected, and allowed to interact with the target gas in a collision chamber. Product ions scattered in the forward direction are focused into a quadrupole mass filter and detected with a channeltron electron multiplier operated in a pulse counting mode. Ion signal intensities are corrected for the mass discrimination of the quadrupole mass filter. The surface ionization source minimizes the production of excited state metal ions which can often react differently from ground state species.[17,20,21] The relative populations of the electronic states[22] of metal ions are estimated by assuming a Boltzmann distribution at the source temperature employed 2000–2600 K (Table I). CH_3SiH_3, CH_3SiD_3, and $(CH_3)_2SiD_2$ were prepared by reducing CH_3SiCl_3 and $(CH_3)_2SiCl_2$ with $LiAlH_4$ and $LiAlD_4$.[23] The other silicon compounds were obtained commercially and used without further purification. One sample of CH_3SiD_3 was kindly provided by Professor F. S. Rowland (U. C. Irvine).

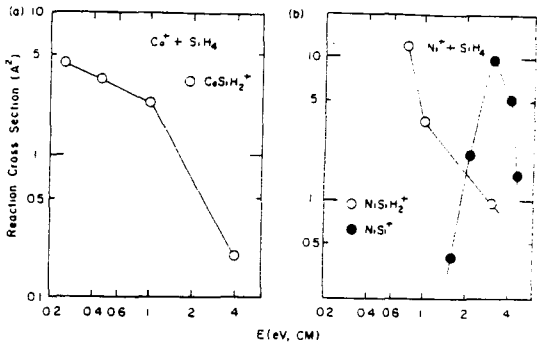

Figure 1. Variation in experimental cross section with center of mass kinetic energy for (a) the reaction of Co^+ with silane and (b) the reaction of Ni^+ with silane.

Collision-induced dissociation (CID) studies[24-26] were performed on nascent $CoSiH_4^+$ adducts as well as $CoSiH_2^+$ to probe their structures and fragmentation processes. These studies were performed with a reverse geometry double focusing mass spectrometer (VG Instruments ZAB-2F).[24] Cobalt ions were formed from 150 eV electron impact on $Co(CO)_3NO$. Metal–silane adducts were formed in a high-pressure source operated typically at $<3 \times 10^{-3}$ Torr of total pressure. Under these conditions metal–silane clusters were formed and extracted from the source before undergoing subsequent collisions. The source was operated under nearly field-free conditions to avoid imparting translational energy to the reactant species. Ions exited the source, were accelerated to 8 kV, and were mass selected. Products resulting from collision-induced dissociation of mass selected ions in the second field-free region between the magnet and electric sectors were detected by scanning the energy of the electric sector. CID experiments used He as the target admitted into the collision cell situated at the focal point between the magnetic and electric sectors until 50% attenuation of the main beam intensity was observed.

It is important to point out that neutral products are not detected in these experiments. However, except where noted below, the identity of these products can usually be inferred without ambiguity. In addition, these experiments provide no direct structural information about the ionic products. The CID studies in addition to thermochemical arguments can often distinguish possibilities for isomeric structures.

Results and Discussion

In the present study, the transition-metal ions, Ti^+, V^+, Cr^+, Fe^+, Co^+, and Ni^+, are reacted with silane, the methylsilanes, and hexamethyldisilane in the gas phase. Reactions observed in these systems are considered in the following section, along with plausible mechanisms. In general, Ni^+ and Co^+ are observed to be most reactive toward organosilanes, followed by Ti^+, V^+, and Fe^+. The specific reactions of Ti^+ and V^+ distinguish these ions from the late transition metals. Cr^+ is unreactive with organosilanes, as is the case with hydrocarbons.[27] This is followed by an examination of reaction thermochemistry in which several transition metal–silylene bond energies are bracketed. Finally, these bond energies are related to the electronic structures of the metal ions

(8) Hanratty, M. A.; Beauchamp, J. L.; Illies, A. J.; Bower, M. T. *J. Am. Chem. Soc.*, in press.
(9) (a) Halle, L. F.; Armentrout, P. B.; Beauchamp, J. L. *Organometallics* **1982**, *1*, 963. (b) Houriet, R.; Halle, L. F.; Beauchamp, J. L. *Organometallics* **1983**, *2*, 1818.
(10) Byrd, G. D.; Burnier, R. O.; Freiser, B. S. *J. Am. Chem. Soc.* **1982**, *104*, 3565.
(11) Jacobson, D. B.; Freiser, B. S. *J. Am. Chem. Soc.* **1985**, *107*, 4373 and references therein.
(12) Larsen, B. S.; Ridge, D. F. *J. Am. Chem. Soc.* **1984**, *106*, 1912.
(13) Walba, D. M.; Depuy, C. H.; Grabowski, J. J.; Bierbaum, V. M. *Organometallics* **1984**, *3*, 498.
(14) Aristov, N.; Armentrout, P. B. *J. am. Chem. Soc.* **1984**, *106*, 4065.
(15) Sallans, L.; Lane, K. R.; Squires, R. R.; Freiser, B. S. *J. Am. Chem. Soc.* **1984**, *106*, 4065.
(16) Armentrout, P. B.; Beachamp, J. L. *J. Am. Chem. Soc.* **1981**, *103*, 784.
(17) Mandich, M. L.; Halle, L. F.; Beauchamp, J. L. *J. Am. Chem. Soc.* **1984**, *106*, 4403.
(18) Hanratty, M. A.; Beauchamp, J. L.; Illies, A. J.; Bowers, M. T. *J. am. Chem. Soc.* **1985**, *107*, 1788.
(19) Armentrout, P. B.; Beauchamp, J. L. *J. Chem. Phys.* **1981**, *74*, 2819.
(20) Halle, L. F.; Armentrout, P. B.; Beauchamp, J. L. *J. Am. Chem. Soc.* **1981**, *103*, 962.
(21) Aristov, N.; Armentrout, P. B., to be published.
(22) Moore, C. E. *Atomic Energy Levels*; National Bureau of Standards: Washington, D.C., 1949.
(23) Gaspar, P. P.; Levy, C. A.; Adair, G. M., *Inorg. Chem.* **1970**, *9*, 1272.
(24) For a description of the experimental instrumentation and methodology, see: (a) Illies, A. J.; Bowers, M. T. *Chem. Phys.* **1982**, *65*, 281. (b) Illies, A. J.; Jarold, M. F.; Bass, L. M.; Bowers, M. T. *J. Am. Chem. Soc.* **1983**, *105*, 5775.
(25) For details of the kinetic energy release calculations, see: Jarold, M. F.; Illies, A. J.; Kirchner, N. J.; Wagner-Redeker, W.; Bowers, M. T.; Mandich, M. L.; Beauchamp, J. L. *J. Phys. Chem.* **1983**, *87*, 2213.
(26) For a general discussion of collision-induced dissociation, see: Cooks, R. G. *Collision Spectroscopy*; Plenum: New York, 1978.
(27) Beauchamp, J. L., unpublished results.

Table II. Low Energy Product Distributions for Reactions of Transition-Metal Ions with Silicon Compounds[a]

metal ion	Neutral Reactant					
	SiH_4	SiH_3Me	SiH_2Me_2	$SiHMe_3$	$SiMe_4$	Si_2Me_6
Ni^+	[17][b] H_2 (100)[c]	[34] H_2 (100)	[126] H_2 (95) CH_4 (5)	[120] H_2 (9) CH_4 (30) NiH (61)	[110] NiMe (100)	[370] $SiHMe_3$ (66) $SiMe_4$ (34)
Co^+	[3.7] H_2 (100)	[117] H_2 (100)	[64] H_2 (95) CH_4 (5)	[190] H_2 (12) CH_4 (33) CoH (55)	[47] CoMe (100)	[300] $SiHMe_3$ or CoMe (97) $SiMe_4$ (3)
Fe^+	n.r.	n.r.	[43] H_2 (100)	[23] H_2 (40) CH_4 (60)	n.r.	[180] $SiHMe_3$ (15) $SiMe_4$ (85)
Cr^+	n.r.	n.r.	n.r.	n.r.	n.r.	n.r.
V^+	n.r.	[1.9] H_2 (100)	[17] H_2 (45) CH_4 (55)	[7.6] H_2 (100)	[2.7] H_2 (10) CH_4 (90)	[280] H_2 (23) $2H_2$ (8) CH_4 (10) CH_4, H_2 (20) SiC_2H_8 (10) SiC_3H_{10} (29)
Ti^+	[0.8] H_2 (100)	[57] H_2 (94) CH_4 (6)	[95] H_2 (58) CH_4 (42)	[133] H_2 (95) CH_4 (5)	[44] H_2 (66) CH_4 (34)	[310] H_2 (18) $2H_2$ (5) CH_4 (17) CH_4, H_2 (31) SiC_2H_8 (11) SiC_3H_{10} (18)

[a] Only the neutral products are listed. No reaction indicated by n.r. The product distribution was measured at 0.5 eV center of mass kinetic energy. [b] Approximate total cross section, Å^2. Estimated uncertainty ±50% due to discrimination in measuring reactant and product ion intensities. [c] % of total reaction.

to deduce a favorable bonding scheme for transition-metal silylenes.

Silane. The products observed in the exothermic reactions with organosilanes are shown in Table II. Both Co^+ and Ni^+ dehydrogenate silane at low energies (reaction 1). Experimental reaction cross sections for these products are characteristic of exothermic processes, decreasing with increasing kinetic energy as shown in Figure 1. V^+, Cr^+, and Fe^+ are all unreactive with

$$M^+ + SiH_4 \rightarrow MSiH_2^+ + H_2 \ (M = Ni, Co) \qquad (1)$$

silane. Ti^+ undergoes an exothermic reaction with silane (eq 1). The maximum experimental cross section at low energy is very small ($\sigma < 0.8$ Å^2) in this instance.

Collision-induced dissociation (CID) of $CoSiH_2^+$, formed in reaction 1, yields reactions 2–4. The small amount of $CoSiH^+$ and $CoSi^+$, processes 2 and 3, suggests that the structure of

$$[CoSiH_2^+]^* \xrightarrow{3.5\%} CoSiH^+ + H \qquad (2)$$
$$\xrightarrow{14.5\%} CoSi^+ + H_2 \qquad (3)$$
$$\xrightarrow{82.0\%} Co^+ + SiH_2 \qquad (4)$$

$CoSiH_2^+$ can be formulated as a cobalt–silylene complex, **1**. If the $CoSiH_2^+$ structure were better described by either **2** and **3**, then processes 2 and 3 would be expected to dominate. CID of

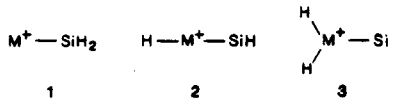

1 **2** **3**

the nascent $CoSiH_4^+$ cluster yields processes 5–10. Processes

$$[CoSiH_4^+]^* \xrightarrow{0.8\%} CoSiH_3^+ + H \qquad (5)$$
$$\xrightarrow{10.9\%} CoSiH_2^+ + H_2 \qquad (6)$$
$$\xrightarrow{19.0\%} CoSiH^+ + H_2 + H \qquad (7)$$
$$\xrightarrow{24.1\%} CoSi^+ + 2H_2 \qquad (8)$$
$$\xrightarrow{3.5\%} CoH^+ + SiH_3 \qquad (9)$$
$$\xrightarrow{41.7\%} Co^+ + SiH_4 \qquad (10)$$

Scheme I

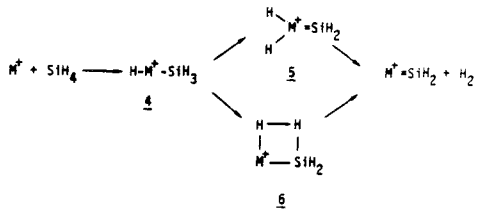

4 **5** **6**

5 and 9 may indicate competitive dissociations from intermediate **4**, which may be formed by insertion of Co^+ into a Si–H bond.

$$H—M^+—SiH_3$$
4

$CoSiH_3^+$, formed by process 5, probably dissociates further into $CoSiH^+$ and H_2 as indicated in process 7, and hence the yield of $CoSiH_3^+$ may actually be much higher. This suggests $D°$ (Co^+ – SiH_3) ~ $D°$ (Co^+ – H) = 52 kcal mol^{-1}.[9] With this bond energy, insertion of Co^+ into the silane Si–H bond is energetically favorable.

A mechanism for the dehydrogenation of silane is proposed in Scheme I and involves the insertion of a metal ion into the Si–H bond to form **4** as an initial step. This is then followed by an α-hydrogen transfer forming **5** which can eliminate H_2 to yield $M—SiH_2^+$ (M = Co, Ni).[28] Alternatively, dehydrogenation may proceed through the four-centered intermediate **6** in Scheme I. Such four-centered intermediates have been proposed in theoretical studies of the H/D exchange reaction of Cl_2MH (M = Sc, Ti, Ti^+) with D_2 with generalized valence bond methods.[29] In ad-

(28) We use $M{=}SiH_2^+$ in representing metal silylenes to be consistent with the valence of the silicon atom. However, this should not be interpreted as two σ-bonds between the metal and silicon, because, as discussed in the text, the metal–silylene bond is considered as σ-donation of a nonbonding lone-pair orbital of silylene to a metal and in some cases additional π-back-donation from metal to silicon.

Table III. Thermochemical Data Used in the Text

	kcal mol^{-1}	ref		kcal mol^{-1}	ref
$D(H_3Si-H)$	90.3	*a*	$\Delta H_f(SiH_4)$	8.2	*a*
$D(H_3Si-Me)$	88	*a*	$\Delta H_f(SiH_3Me)$	−7	*a*
$D(Me_3Si-SiMe_3)$	80.5	*a*	$\Delta H_f(SiH_2Me_2)$	−23	*a*
$\Delta H_f(CH_4)$	−17.9	*b*	$\Delta H_f(SiHMe_3)$	−39	*a*
$\Delta H_f(C_2H_6)$	−20.2	*b*			
$\Delta H_f(C_2H_4)$	12.5	*b*	$\Delta H_f(SiMe_4)$	−55.4	*a*
$\Delta H_f(CH_2)$	93.7	*e*	$\Delta H_f(SiMe_6)$	−87	*b*
			$\Delta H_f(SiH_2)$	69	*a*
			$\Delta H_f(SiHMe)$	53	*c*
			$\Delta H_f(SiMe_2)$	37	*c*
			$\Delta H_f(CH_2{=}SiMe_2)$	7	*a*
			$\Delta H_f(CH_2{=}SiH_2)$	39	*a*
			$\Delta H_f(SiH_3^+)$	234.1	*d*

[a] Reference 31. [b] Pedley, J. B.; Rylance, J. *Sussex-N.P.L. Computer Analyzed Thermochemical Data: Organic and Organometallic Compounds*; University of Sussex: Sussex, 1977. [c] Estimated from the values of ref 31. [d] Reference 41. [e] Rosenstock, H. M.; Draxl, K.; Steiner, B. W.; Herron, J. T. *J. Phys. Chem., Ref. Data. Suppl.* **1977**, *6*.

dition, Watson[30] has recently observed an interesting methane exchange reaction which may proceed through a four-centered transition state.

The metal ions which dehydrogenate silane do not undergo a similar reaction with methane. The reaction enthalpy[31] for process 11 forming silylene from silane is only 61 kcal mol^{-1} (Table III). This can be compared with carbene formation from methane, reaction 12, which requires 112 kcal mol^{-1}, rendering 1,1-dehydrogenation a very demanding process in the corresponding reactions of metal ions with methane.[32] Theory and experiment[33-35] suggest that the reverse of reaction 11 has a very low activation energy (<2 kcal mol^{-1}).

$$SiH_4 \rightarrow SiH_2(^1A_1) + H_2 \quad (11)$$

$$CH_4 \rightarrow CH_2(^3B_1) + H_2 \quad (12)$$

The variation of product abundances as a function of kinetic energy for reactions of Co^+ and Ni^+ with silane is shown in Figure 1. For the cobalt system only a decrease in the $Co{=}SiH_2^+$ product is observed with increasing energy, and no other products are detected ($\sigma < 0.3$ Å^2). For the nickel system, however, $NiSi^+$ is observed at higher energy as an endothermic product. This result suggests that dehydrogenation of $Ni{=}SiH_2^+$ is more facile than that of $Co{=}SiH_2^+$.

Methyl-Substituted Silanes. Ni^+, Co^+, and V^+ undergo exothermic reactions with CH_3SiH_3 to yield $M(SiCH_4)^+$ and H_2 (reaction 13). An examination of these reactions with CH_3SiD_3

$$M^+ + CH_3SiH_3 \rightarrow MSiCH_4^+ + H_2 \ (M = Ni, Co, V) \quad (13)$$

$$M^+ + CH_3SiD_3 \rightarrow MSiDCH_3^+ + D_2 \ (M = Co, V) \quad (14)$$

results in D_2 loss for Co^+ and V^+, indicating exclusively a 1,1-dehydrogenation process (reaction 14).[36] The observed 1,1-dehydrogenation process suggests that the product is a metal silylene ($M{=}SiDCH_3^+$). Formation of the other isomers such as a metal-silaethylene complex $[M(SiH_2{=}CH_2)^+]$ and metal-silylmethylene $[M{=}CH(SiH_3)^+]$ would be expected to yield HD and H_2 losses, respectively.[37] Ti^+ reacts with methylsilane to yield both H_2 and CH_4 losses (reactions 15 and 16). In the same reaction with CH_3SiD_3, D_2, and CH_3D losses are observed. This

$$Ti^+ + CH_3SiH_3 \xrightarrow{94\%} TiSiCH_4^+ + H_2 \quad (15)$$
$$\xrightarrow{6\%} TiSiH_2^+ + CH_4 \quad (16)$$

is again consistent with the formulation of product structures as metal silylenes, $Ti{=}SiDCH_3^+$ and $Ti{=}SiD_2^+$. Fe^+ and Cr^+ do not undergo exothermic reactions with methylsilane.

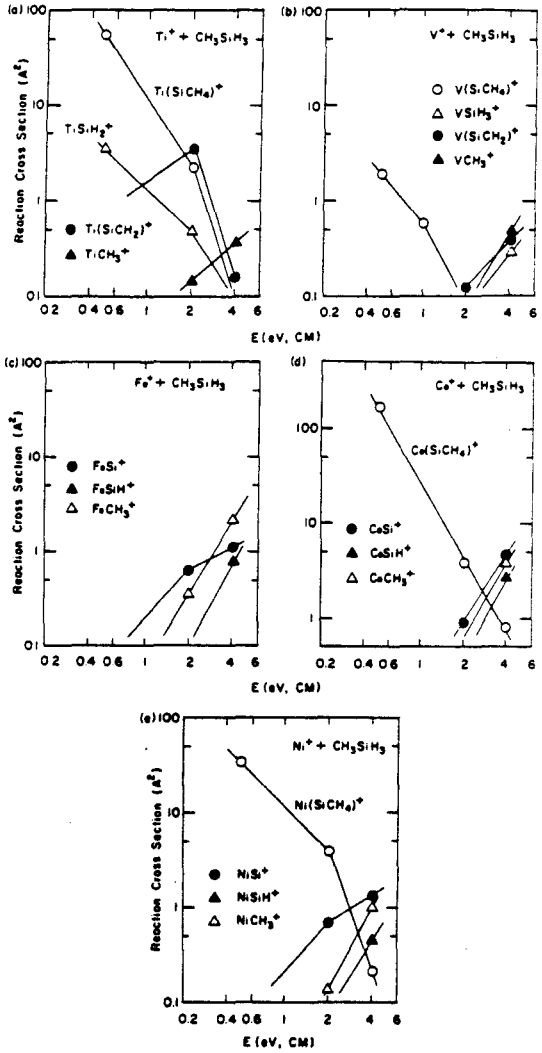

Figure 2. Variation in experimental cross section with center of mass kinetic energy for the reactions of (a) Ti^+ with methylsilane, (b) V^+ with methylsilane, (c) Fe^+ with methylsilane, (d) Co^+ with methylsilane, and (e) Ni^+ with methylsilane. Lines drawn through single data points are extrapolated to smaller experimentally determined cross sections.

(29) Steigerwald, M. L.; Goddard, W. A., III *J. Am. Chem. Soc.* **1984**, *106*, 308.
(30) Watson, P. L. *J. Am. Chem. Soc.* **1983**, *105*, 6491.
(31) Walsh, R. *Acc. Chem. Res.* **1981**, *14*, 246. We have recently determined a new value for $\Delta H_f(SiH_2)$ of 69 ± 3 kcal mol^{-1} by studying the deprotonation of SiH_3^+ with a series of *n*-donor bases (Shin, S. K.; Beauchamp, J. L. *J. Phys. Chem.* **1986**, *90*, 1507). This is in good agreement with recent ab initio calculations [Ho, P.; coltrin, M. E.; Binkley, J. S.; Melius, C. F. *J. Phys. Chem.* **1985**, *89*, 4647] which give a value of 68.1 kcal mol^{-1}. Several of Walsh's recommended heats of formation accordingly require revision.
(32) The 1,1-dehydrogenation process is not observed in the gas-phase reactions of the first-row transition-metal ions with methane or with larger hydrocarbons.
(33) (a) Blomberg, M. R. A.; Brandemark, U.; Siegbahn, P. E. M. *J. Am. Chem. Soc.* **1983**, *105*, 5557. (b) Blomberg, M. R. A.; Siegbahn, P. E. M.; Bauschlicher, C. W. *J. Chem. Phys.* **1984**, *81*, 1373.
(34) Sax, A.; Olbrich, G. *J. Am. Chem. Soc.* **1985**, *107*, 4868.
(35) (a) Viswanathan, R.; Thompson, D. L.; Raff, L. M. *J. Chem. Phys.* **1984**, *80*, 4230–4240. (b) Jasinski, J. M. *J. Phys. Chem.* **1986**, *90*, 555–557. (c) Gordon, M. S.; Gano, D. R.; Binkley, J. S.; Frisch, M. J. *J. Am. Chem. Soc.* **1986**, *108*, 2191–2199.
(36) Ni^+ was not included in this study because of the limited amount of CH_3SiD_3 available for the experiment.
(37) The energy difference between methylsilylene and silaethylene is controversial. The data in Table III suggest that the latter is more stable by ~14 kcal mol^{-1}. Theoretical results are not generally in accord with this result; however, see, for example: Schaefer, H. F. *Acc. Chem. Res* **1982**, *15*, 283.

Scheme II

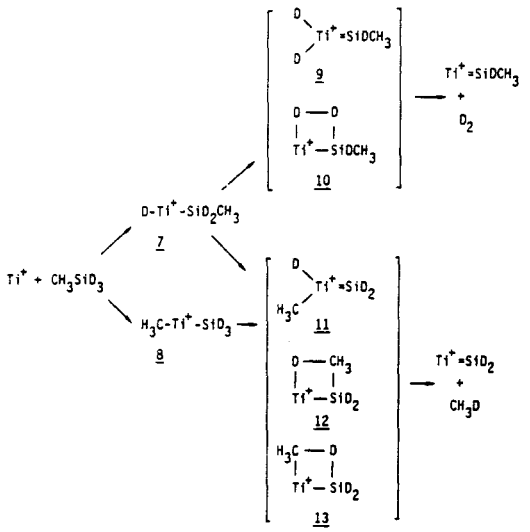

The observed processes can be rationalized by the mechanisms proposed in Scheme II with the reactions of Ti^+ as an example. Ti^+ may first insert into a Si–D bond of CH_3SiD_3 to form an intermediate **7**. Then, D_2 loss can result from either α-D transfer to the metal center (**9**) or, alternatively, the dissociation of a four-centered intermediate (**10**). **7** may either undergo α-methyl transfer (**11**) or form a four-centered intermediate **12** to eliminate CH_3D. Initial insertion of Ti^+ into a Si–Me bond can also be postulated, with loss of CH_3D occurring via intermediate **11** or **13**.

Products observed at different collision energies in the reactions with methylsilane are shown in Figure 2. Most of the metal ions except Cr^+ react with methylsilane at high energies to yield minor products of endothermic reactions. Although Fe^+ does not yield products involving exothermic reactions with methylsilane, several products are observed at high energies, including $FeSi^+$, $FeSiH^+$, and $FeCH_3^+$. Similar products are observed for Co^+ and Ni^+ at high energies, including MSi^+, $MSiH^+$, and MCH_3^+ (M = Co, Ni), illustrating very similar reactivities between Fe, Co, and Ni. On the other hand, Ti^+ and V^+ yield quite different high-energy products from those of the late transition metals. The double dehydrogenation product $M(SiCH_2)^+$ is unique for M = Ti and V. Metal silicides (MSi^+) are not produced from these metals. A common high-energy product for all of these metals is MCH_3^+ (M = Ti, V, Fe, Co, and Ni), which might be expected to be formed by the dissociation of a Si–C bond insertion intermediate (**8** in Scheme II) via an endothermic bond cleavage at high energies. Considering that $MSiH_3^+$ is not produced except for V, this could imply $D°(M^+–CH_3) > D°(M^+–SiH_3)$. Alternatively, this observation could also imply that the bond cleavage product $M^+–SiH_3$ further dissociates to yield other products, as indicated by the formation of MSi^+ and $MSiH^+$ (M = Fe, Co, and Ni) at high energies. The reaction of V^+ yields comparable amounts of VCH_3^+ and $VSiH_3^+$. Assuming that the structure is $V^+–SiH_3$, $D°(V^+–SiH_3) \sim D°(V^+–CH_3) = 49$ kcal mol^{-1} is implied.[21]

It is interesting to compare the reactions of methylsilane and those of ethane. Reaction of Ti^+ with methylsilane, for example, yields $Ti{=}SiH_2^+$ and $Ti{=}SiHCH_3^+$, the metal silylenes. On the other hand, reaction of Ti^+ with ethane yields the metal–ethylene complex $Ti(CH_2{=}CH_2)^+$, and the corresponding metal–carbene species $Ti{=}CHCH_3^+$ is not produced.[10] This is confirmed by the reaction of Ti^+ with CH_3CD_3, which eliminates predominately HD in a 1,2-dehydrogenation process.[38] It has been suggested that $M{=}CHCH_3^+$ (M = Fe, Co) species readily rearrange to the corresponding $M(ethene)^+$ isomer.[39]

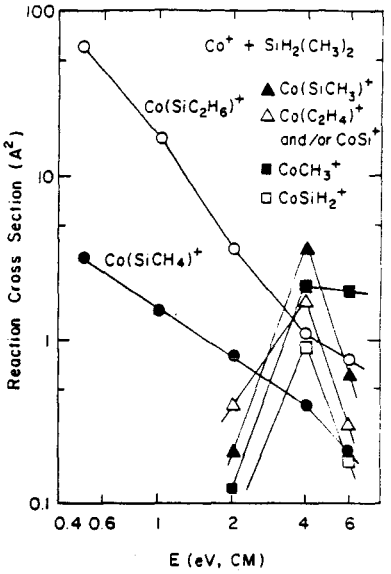

Figure 3. Variation in experimental cross section with center of mass kinetic energy for the reaction of Co^+ with dimethylsilane.

Reactions of Ti^+, V^+, Co^+, and Ni^+ with dimethylsilane yield H_2 and CH_4 loss as exothermic products. Reaction of Fe^+ exhibits H_2 loss as the only product channel. Both exothermic and endothermic products formed in the reaction of Co^+ with dimethylsilane are shown as an example in Figure 3. The exothermic products include $Co(SiC_2H_6)^+$ and $Co(SiCH_4)^+$ (reactions 17 and 18). These products can be rationalized by a mechansim

$$Co^+ + SiH_2(CH_3)_2 \xrightarrow{95\%} Co(SiC_2H_6)^+ + H_2 \quad (17)$$
$$\xrightarrow{5\%} Co(SiCH_4)^+ + CH_4 \quad (18)$$

analogous to Scheme II, which involves an initial insertion of Co^+ into a Si–H or Si–C bond followed by an α-Me or α-H transfer. Assuming similar pathways for the reactions with methylsilane and dimethylsilane, the products $M(SiC_2H_6)^+$ and $M(SiCH_4)^+$ observed for Ti, V, Fe, Co, and Ni are assumed to be metal silylenes. This was confirmed in the reaction of Co^+ with $(CH_3)_2SiD_2$, where the major product involved loss of D_2 (>85%) rather than HD or H_2. High-energy products in the reaction of Co^+ with dimethylsilane include $Co(SiCH_3)^+$, $CoCH_3^+$, $Co(C_2H_4)^+$ and/or $CoSi^+$, and $CoSiH_2^+$. Formation of $CoCH_3^+$ may result from direct bond cleavage of a Si–C insertion intermediate analogous to **8** in Scheme II. Formation of the other product may involve further molecular rearrangements in the high-energy intermediates.

Trimethylsilane shows somewhat different reactivity than mono- and dimethylsilanes. Reaction of Co^+ with trimethylsilane, reactions 19–21, leads to formation of $Si(CH_3)_3^+$ as the major product channel, along with methane loss and dehydrogenation.

$$Co^+ + SiH(CH_3)_3 \xrightarrow{58\%} CoH + Si(CH_3)_3^+ \quad (19)$$
$$\xrightarrow{33\%} Co(SiC_2H_8)^+ + CH_4 \quad (20)$$
$$\xrightarrow{12\%} Co(SiC_3H_8)^+ + H_2 \quad (21)$$

These three product channels dominate the reaction, and only small amounts of $Co(SiCH_4)^+$ and $Co(SiH_2)^+$ are formed at high energies (Figure 4). The product $Si(CH_3)_3^+$ results from hydride abstraction by Co^+ to generate CoH as a neutral product (reaction 19). The hydride abstraction reaction is observed only for Co^+ and Ni^+, indicating $D°(M^+–H^-) > D°(SiMe_3^+–H^-)$ for these metals. This observation is consistent with the fact that heterolytic

(38) Tolbert, M. A. Ph.D. Thesis, California Institute of Technology, 1986.

(39) Jacobson, D. B.; Freiser, B. S. *J. Am. Chem. Soc.*, in press

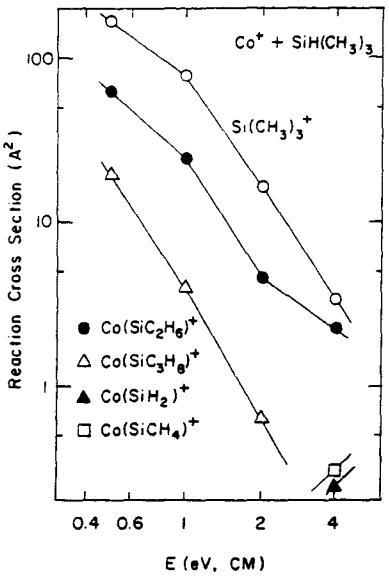

Figure 4. Variation in experimental cross section with center of mass kinetic energy for the reaction of Co^+ with trimethylsilane.

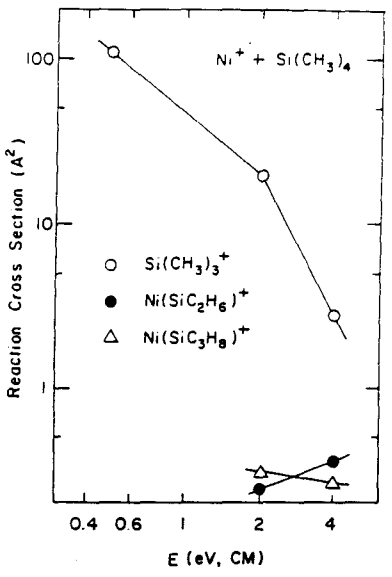

Figure 5. Variation in experimental cross section as a function of center of mass kinetic energy for the reaction of Ni^+ with tetramethylsilane.

Table IV. Heterolytic M^+–H^- Bond Dissociation Energies[a]

	Sc	Ti	V	Cr	Mn	Fe	Co	Ni
$D°(M^+ - H^-)$, kcal mol^{-1}	163	178	178	179	196	194	206 >218[b]	214 >218[b]

[a] Reference 40. [b] This study.

M^+–H^- bond dissociation energy is higher for Ni and Co than for the other first-row transition metals[40] (Table IV). The Me_3Si^+–H^- heterolytic bond dissociation energy of 218 kcal mol^{-1} is calculated with use of eq 22, with $AP(SiMe_3^+) = 10.20 \pm 0.03$ eV obtained from photoionization mass spectrometry measurements.[41] This value suggests somewhat higher values for the heterolytic bond dissociation energies for nickel and cobalt hydride than the values summarized in Table IV.

$$D°(Me_3Si^+–H^-) = AP(SiMe_3^+) - EA(H) \qquad (22)$$

Reaction 21, in which H_2 is eliminated, yields the ion product $Co(SiC_3H_8)^+$. The dehydrogenation process is observed to be the major channel in the reaction of Ti^+ and V^+. The structures of the ionic products $M(SiC_3H_8)^+$ (M = Ti, V, Fe, Co, and Ni) are not known. A metal–dimethylsilaethylene complex [$M(H_2C{=}SiMe_2)^+$] may be thermodynamically feasible. Since formation of dimethylsilaethylene from trimethylsilane (reaction 23) requires 46 kcal mol^{-1} (Table III), the exothermic formation of $M(H_2C{=}SiMe_2)^+$ would require a binding energy between the metal

$$SiHMe_3 \rightarrow H_2C{=}SiMe_2 + H_2 \qquad (23)$$

ion and dimethylsilaethylene greater than this value. The binding energy of Co^+ and the corresponding alkene, 2-methylpropene, is estimated to be ~50 kcal mol^{-1}.[8] For comparison, reactions with 2-methylpropane exhibit H_2 loss as a major process for all of these metals.[9,10,16] Isotope labeling has been used to confirm a 1,2-dehydrogenation of 2-methylpropane in several instances.[9b]

Reactions of Ni^+ and Co^+ with tetramethylsilane yield $SiMe_3^+$ as the only exothermic product. Cross-section data for the Ni system are shown in Figure 5. This product represents formal methyl anion abstraction from tetramethylsilane by Co^+ or Ni^+. As discussed in the case of trimethylsilane, a lower limit for

Table V. Reaction Enthalpies for the Formation of Silylenes from Several Silicon Compounds (kcal mol^{-1})[a]

silicon compd	eliminated fragment			
	H_2	CH_4	C_2H_6	$Si(CH_3)_4$
SiH_4	61			
CH_3SiH_3	60	58		
$SiH_2(CH_3)_2$	60	58	72	
$SiH(CH_3)_3$		58	72	
$Si(CH_3)_4$			72	
$Si_2(CH_3)_6$				69

[a] Reference 31.

M^+–Me^- heterolytic bond dissociation energy can be estimated as $D°(M^+–Me^-) > D°(Me^-–SiMe_3^+) = 229$ kcal mol^{-1} (M = Co, Ni).[42] Using this value, homolytic bond dissociation energies $D°(Ni–CH_3) > 55$ kcal mol^{-1} and $D°(Co–CH_3) > 50$ kcal mol^{-1} are derived.[43] Both Ti^+ and V^+ react with tetramethylsilane to cause loss of H_2 and CH_4. Although Fe^+ undergoes a facile reaction with 2,2-dimethylpropane to lose methane, no exothermic reaction is observed with tetramethylsilane.

Hexamethyldisilane. The reactions with hexamethyldisilane (Me_3Si–$SiMe_3$) exhibit very large experimental cross sections for product formation, which indicates that these reactions are extremely facile. Fe^+, Co^+, and Ni^+ yield products of exothermic reactions which include $M(SiC_3H_8)^+$ and $M(SiC_2H_6)^+$ (M = Fe, Co, and Ni). Figure 6 presents cross-section data for the reaction of Ni^+ with hexamethyldisilane as an example of these late transition-metal systems. The observed products in these systems indicate that cleavage of the weak Si–Si bond (80.5 kcal mol^{-1})[31] completely dominates the reaction pathways. The reactions of Ti^+ and V^+, on the other hand, are distinguished from those of Fe^+, Co^+, and Ni^+, yielding a variety of products including dehydrogenation, methane loss, as well as Si–Si bond cleavage products.

Bond Energies. As is amply illustrated by the above results, metal silylenes are often observed as a major product in the

(40) Martinho Simoes, J. A.; Beauchamp, J. L. *Chem. Rev.*, to be published. See also: Sallans, L.; Lane, K. R.; Squires, R. R.; Freiser, B. S. *J. Am. Chem. Soc.* **1985**, *107*, 4379.

(41) Cordermann, R. R. Ph.D. Thesis, California Institute of Technology, 1977.

(42) Calculated with $D(Me_3Si^+–Me^-) = AP(SiMe_3^+) - EA(Me)$, where the appearance potential of $SiMe_3^+$ from tetramethylsilane, $AP(SiMe_3^+)$, is 10.03 ± 0.04 eV from the following: Murphy, M. K.; Beauchamp, J. L. *J. Am. Chem. Soc.* **1977**, *99*, 2085. $EA(CH_3) = 0.08$ eV from the following: Ellison, G. B.; Engelking, P. C.; Lineberger, W. C. *J. Am. Chem. Soc.* **1978**, *100*, 2556.

(43) Calculated with $D°(M–Me) = D°(M^+–Me^-) + EA(Me) - IP(M)$.

Table VI. Transition Metal Ion–Silylene Bond Energies

metal ion	ground state electronic config (term)	bond energies, kcal mol^{-1}		
		$M^+ - SiH_2$	$M^+ - SiHCH_3$	$M^+ - Si(CH_3)_2$
Ni^+	$d^9(^2D)$	$67 \pm 6^{a,b}$	$>60^d$	$>69^e$
Co^+	$d^8(^3F)$	$67 \pm 6^{a,b}$	$>60^d$	$>69^e$
Fe^+	$s^1d^6(^6D)$	$<72^b$		$>69^e$
V^+	$d^4(^5D)$		$>60^d$	$>60^f$
Ti^+	$s^1d^2(^4F)$	$>58^c$	$>60^d$	$>60^f$

$^a M^+ + SiH_4 \rightarrow MSiH_2^+ + H_2$, $\Delta H < 0$. $^b M^+ + SiH_2Me_2 \rightarrow MSiH_2^+ + C_2H_6$, $\Delta H > 0$. $^c M^+ + SiH_3Me \rightarrow MSiH_2^+ + CH_4$, $\Delta H < 0$. $^d M^+ + SiH_3Me \rightarrow MSiHMe^+ + H_2$, $\Delta H < 0$. $^e M^+ + Si_2Me_6 \rightarrow MSiMe_2^+ + SiMe_4$, $\Delta H < 0$. $^f M^+ + SiH_2Me_2 \rightarrow MSiMe_2^+ + H_2$, $\Delta H < 0$.

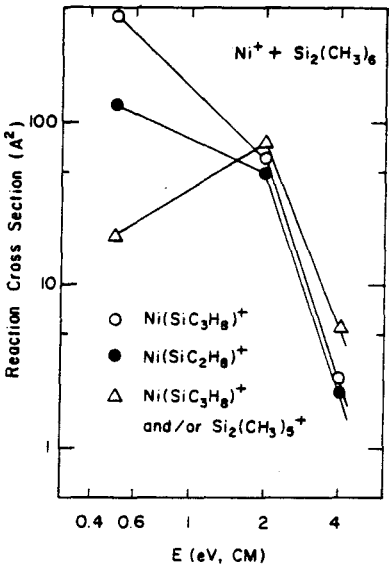

Figure 6. Variation in experimental cross section as a function of center of mass kinetic energy for the reactions of Ni^+ with hexamethyldisilane.

reactions of atomic metal ions with methylsilanes. By examining the reaction thermochemistry of the observed processes, limits on the dissociation energies of metal–silylene bonds can be obtained. For example, the reactions of Co^+ and Ni^+ with silane yield $M{=}SiH_2^+$ as an exothermic product reaction (reaction 1 and Figure 1). This provides a lower limit for the M^+–SiH_2 bond energy (M = Co, Ni) of 61 kcal mol^{-1} (Table VI). Similarly, a lower limit for the M^+–$SiHCH_3$ bond dissociation energy can be obtained from the exothermic formation of this species in the reactions with methyl silane (reaction 13). In several reactions with the methylsilanes and hexamethyldisilane, $M(SiC_2H_6)^+$ is produced as an exothermic product. On the condition that the structure is a metal silylene $M{=}Si(CH_3)_2^+$, this provides a lower limit for the metal–silylene bond energy (Table VI). Interestingly, the reactions with dimethylsilane yield $M{=}SiH_2^+$ as a *high energy product* for Fe^+, Co^+, and Ni^+. Cross sections for the formation of these products exhibit the typical behavior of an endothermic reaction, which is shown in Figure 4 for $Co{=}SiH_2^+$. Provided that no substantial energy barrier is present which might inhibit the formation of $M{=}SiH_2^+$ at low energy, the endothermicity of $M{=}SiH_2^+$ formation provides an upper limit of 72 kcal mol^{-1} for the M^+–SiH_2 bond energy (M = Fe, Co, and Ni). The bond dissociation energies estimated in this fashion are summarized in Table VI along with the reactions used to infer the various limits. Reaction enthalpies used in this determination may require additional attention. One of the important quantities in deriving these reaction enthalpies is the controversial heat of formation of SiH_2, for which several values have been previously reported, including 58[31] and 81 kcal mol^{-1}.[44] Considering the probable experimental uncertainties in these measurements, we have chosen to use the value determined recently in our laboratory,[31] $\Delta H_f°(SiH_2) = 69$ kcal mol^{-1}.

The Nature of the Transition Metal–Silylene Bond. The present study shows two distinct features of transition-metal silylenes. First, the transition-metal silylenes are fairly stable, which often renders metal silylenes as major products in the reactions of transition-metal ions with the silanes. The stability of metal silylenes may be illustrated further by the enthalpy change of reaction 24, for which $\Delta H° = 46 \pm 10$ kcal mol^{-1}.[45] Second,

$$NiSiH_2^+ + CH_2{=}CH_2 \rightarrow NiCH_2^+ + CH_2{=}SiH_2 \quad (24)$$

the metal–silylene bond is stronger for Ni^+ and Co^+ than the other transition-metal ions studied, as illustrated by the exothermic formation of $M{=}SiH_2^+$ (M = Ni and Co) from silane. These observations provide a basis to describe the bonding between transition-metal ions and silylene as follows.

Silylene has a singlet ground state ($^1A_1$) and a low-lying triplet excited state ($^3B_1$) at ~20 kcal mol^{-1}.[46] The ground-state silylene is expected to form a donor–acceptor type σ-bond to the metal ion by donating its nonbonding lone-pair electrons to the metal center. Hence, metal ions with an empty 4s orbital (ground state derived from a $3d^n$ valence electronic configuration) can make a strong metal–silylene bond by accepting the lone-pair electrons from silylene. Observation of the strong bond for $Ni^+(3d^9)$ and $Co^+(3d^8)$ supports this conjecture. In addition to accepting lone-pair electrons from silylene, both Ni^+ and Co^+ can also back-donate electrons from their paired $3d_\pi$ orbital to the empty $3p_\pi$ orbital of silicon, enhancing the transition metal–silylene bond strength.[47]

One way to test the validity of the bonding analysis for transition-metal silylenes described above is to apply this scheme to the other metal ions. Fe^+ and Ti^+ have $4s^13d^n$ valence electronic configurations, and we expect that their metal–silylene bond strength is weakened due to the half-filled 4s orbital. This argument is supported by the absence of $FeSiH_2^+$ as well as a very small amount of $TiSiH_2^+$ formation from the exothermic reactions of Ti^+ with silane. Although the ground state of V^+ is derived from a $3d^4$ electronic configuration with an empty 4s orbital, V^+ is unreactive toward silane. Comparing V^+ with Ni^+ and Co^+, V^+ has only singly occupied 3d orbitals. Hence, the amount of back-donation in the metal–silylene bond may be reduced for V^+ compared with Ni^+ or Co^+. Cr^+ has a stable $3d^5$ valence electronic configuration and may not initiate reaction toward silane or methyl-substituted silanes by the insertion into a Si–H or Si–Me bond. We have previously found that the Cr^+ is unreactive toward alkanes for the same reason.[27]

Conclusion

The present results are the first experimental observation and bond energy determination of transition-metal silylenes. The metal silylenes are the major products from the reactions of transition-metal ions with the silanes, providing a contrast to the formation of metal–alkene complexes from the reactions of transi-

(44) Saalfeld, F. E.; McDowell, M. V. *Inorg. Chem.* **1967**, *6*, 96.

(45) $D°(Ni^+–CH_2) = 86 \pm 6$ kcal mol^{-1} from ref 9a.

(46) Meadows, J. H.; Schaefer, H. F., III *J. Am. Chem. Soc.* **1976**, *98*, 3998. Calvin, M. E.; Grev, R. S.; Schaefer, H. F., III; Bicerano, J. *Chem. Phys. Lett.* **1983**, *99*, 399.

(47) Nakatsuji, H.; Ushio, J.; Yonezawa, T. *J. Organomet. Chem.* **1983**, *258*, C1–C4.

tion-metal ions with alkanes. This difference in reactivity is attributed to the thermodynamically less demanding process of generating silylene from the silanes compard to carbene formation from the corresponding alkanes. Metal–silylene bond dissociation energies, estimated by examining the reaction thermochemistry associated with metal silylene formation, are stronger for Co^+ and Ni^+ than for the other metal ions. The bonding between transition-metal ions and silylene is described by σ-donation of nonbonding lone-pair electrons from the ground-state silylene to the metal center, and π-back-donation of paired 3d electrons from the metal into the empty 3p orbital of Si is invoked to account for the strengthened Ni^+–SiH_2 and Co^+–SiH_2 bonds.

Acknowledgment. We gratefully acknowledge the support of the National Science Foundation under Grants CHE 8407857 (J.L.B.) and CHE 8512711 (M.T.B.). Graduate fellowship support by the Korean Government (H.K., 1980–1984) is gratefully acknowledged.

Registry No. Ni^+, 14903-34-5; Co^+, 16610-75-6; Fe^+, 14067-02-8; Cr^+, 14067-03-9; V^+, 14782-33-3; Ti^+, 14067-04-0; SiH_4, 7803-62-5; SiH_3Me, 992-94-9; SiH_2Me_2, 1111-74-6; $SiHMe_3$, 993-07-7; $SiMe_4$, 75-76-3; Si_2Me_6, 1450-14-2.

Appendix II

Photoionization Mass Spectrometric Studies of the Methylsilanes $Si(CH_3)_nH_{4-n}$ (n = 0–3).

Photoionization Mass Spectrometric Studies of the Methylsilanes $Si(CH_3)_nH_{4-n}(n = 0-3)$.

Reed R. Corderman[1], Seung Koo Shin, and J. L. Beauchamp*

Contribution No. 7713 from the

Arthur Amos Noyes Laboratory of Chemical Physics

California Institute of Technology, Pasadena, California 91125

Abstract

Photoionization efficiency curves for the low energy fragment ions $(P-H)^+$, $(P-H_2)^+$, and $(P-CH_4)^+$ for the series of methyl substituted silanes $Si(CH_3)_nH_{4-n}(n = 0-3)$ are reported. These data are interpreted in terms of the thermochemistry of the various ionic and neutral silicon species and afford accurate calculation of hydride affinities, $D(R_3Si^+-H^-)$, of 260.7, 245.7, 232.0, and 217.8 kcal/mol for the silicenium ions SiH_3^+, $SiMeH_2^+$, $SiMe_2H^+$, and $SiMe_3^+$, respectively. These values are $15-54$ kcal/mol lower than the analogous carbonium ions, which indicates that the silicenium ions are significantly more stable than the corresponding carbonium ions in the gas phase when H^- is used as a reference base. Within experimental error, the hydride affinities for the silylene cations ($RR'Si^+$; R,R' = H, CH_3) are slightly greater than or identical to those for silicenium ions substituted with the same number of methyl groups.

I. Introduction

Studies in our laboratory of the positive ion chemistry of methylsilanes utilizing ion cyclotron resonance techniques[2] have provided information regarding the relative stabilities of methyl substituted silicenium ions, $Si(CH_3)_nH_{3-n}^+(n = 0 - 3)$, in the absence of complicating solvation phenomena[3,4]. It was shown that methyl substituents effect variations in silicenium ion stabilities, $SiH_3^+ < SiMeH_2^+ < SiMe_2H^+ < SiMe_3^+$, for H^- as the reference base, paralleling trends previously observed in the analogous series of carbonium ions. The more complete ion stability order (with H^- as the reference base), $CH_3^+ < CMeH_2^+ < SiH_3^+ < CMe_2H^+ < SiMeH_2^+ < CMe_3^+ < SiMe_2H^+ < SiMe_3^+$, has been established from investigations of hydride and fluoride exchange reactions between substituted carbonium and silicenium ions.[4] Recently, part of this stability order has been confirmed in studies by Eyler et al.[5], in which $SiMe_3^+$ is found to be 15 ± 5 kcal/mol more stable than CMe_3^+ from chloride and hydride transfer reactions involving the trimethylsilyl cation. In contrast to the high gas phase stability of the silicenium ions compared with analogous carbonium ions with respect to the hydride reference base, numerous attempts to generate these ions in solution have been unsuccessful.[6] Only a little progress[7,8] has been achieved since the "siliconium ion[9] question"[6a] was debated to explain the exceedingly low stability of silicenium ions in solution under conditions where analogous carbonium ions are long-lived.

Accurate heats of formation for carbonium ions, obtained from the known heats of formation and ionization potentials of the corresponding radicals, in addition to the well-established homolytic C–H bond dissociation energies of the corresponding alkanes, have been used to calculate quantitative hydride affinities of carbonium ions.[10] These values serve to bracket the silicenium ion stabilities within known bounds. Although some thermochemical data describing methylsilyl cations are available from electron impact mass spectral studies,[11,12] the experimental uncertainties in these low resolution experiments make comparison with carbonium

ions somewhat unreliable. Photoionization mass spectrometry (PIMS) affords relatively accurate determination of appearance potentials for fragmentation processes, with threshold resolution greater than conventional electron impact techniques.[13] In the present report, photoionization efficiency curves are presented for the low energy silicenium ion fragments produced from photoionization of the methylsilanes, $Si(CH_3)_nH_{4-n}$ ($n = 0 - 3$). The yield of molecular ions from most of the methylsilanes are so low as to preclude accurate measurement of their ionization potentials in this study. He(I) photoelectron spectroscopic measurements of the adiabatic ionization potentials of these methylsilanes are used.[11b] Heats of formation and hydride affinities of silicenium ions and silylene cations derived from the present data permit a detailed quantitative evaluation of the effects of methyl-substitution α to silicon charge centers.

II. Experimental Section

The Caltech-Jet Propulsion Laboratory photoionization mass spectrometer used in this study has been described in detail elsewhere.[14] A MgF_2 coated grating blazed at 1200 Å ruled with 1200 lines/mm was used in first order in the present experiments. The sample pressure (typically 1×10^{-4} Torr) was measured with a MKS Baratron Model 90H1 capacitance manometer. Other pertinent operating conditions include: source temperature, ambient ($20 \sim 25°$ C); resolution, 2 Å FWHM; ion energy for mass analysis, 10.0 eV, and repeller field, 0.3 V/cm. In order to minimize ion-molecule reactions in the ion source region, measurements were also made at higher repeller fields ($1 \sim 2$ V/cm), resulting in shorter ion residence times of ~ 5 μsec. The many-lined molecular emission spectrum of hydrogen was utilized in the wavelength range examined ($900 \sim 1300$ Å). Ion intensities were corrected for ^{28}Si (92.2%), ^{29}Si (4.7%), and ^{30}Si (3.1%) isotope contributions.[15] Unless explicitly stated, all ion notations refer to the ^{28}Si isotope.

Samples of SiH_4, $SiMe_2H_2$, and $SiMe_3H$ were available from commercial sources. $SiMeD_3$ was graciously provided by Professors F. S. Rowland and M.

J. Molina. Before use each sample was degassed by repeated freeze-pump-thaw cycles.

III. Results

SiH_4. Photoionization efficiency curves for the molecular ion SiH_4^+ and the two low energy fragment ions SiH_3^+ and SiH_2^+ for wavelengths between 960 and 1140 Å are presented in Figure 1. These are the only ions observed in this wavelength range. Overall features for the photoionization of SiH_4 are similar to those observed by Berkowitz et al.[16]. The photoionization efficiency curve shape for SiH_4^+ ion (process 1) in the wavelengths below 1100 Å may be introduced by either autoionization or hot bands.

$$SiH_4 + h\nu \longrightarrow SiH_4^+ \quad (1)$$

$$\longrightarrow SiH_2^+ + H_2 \quad (2)$$

$$\longrightarrow SiH_3^+ + H \quad (3)$$

If we regard this as an autoionization feature, there is a very weak onset for molecular ion production at $\sim$ 1120 Å, corresponding to an appearance potential of 11.07 eV. The shape near threshold may be obscured by spectral features due to vibrational hot bands, since at 300°K about 6% of the molecules will be in the excited ν_2 (978 cm^{-1}, doubly degenerate) and ν_4 (910 cm^{-1}, triply degenerate) vibrational modes.[17] A definite increase in the photoionization efficiency occurs at 1102 Å, which would correspond to an appearance potential of 11.26 eV. The value of either 11.07 or 11.26 eV for the molecular ion appearance potential is significantly lower than the onset attributed to an adiabatic ionization potential of 11.67 eV measured by He(I) photoelectron spectroscopy for silane.[18] However, this result supports the observation of the molecular ion at energies below the appearance potential of the first fragment SiH_2^+ by Berkowitz et al.[16]. The production of molecular ion increases to peak at $\sim 1075 \pm 5$ Å and declines at shorter wavelength. This result strongly

suggests that the fragmentation process yielding SiH_2^+ occurs at the threshold of 1075 ± 5 Å.

The observed threshold at 1075 ± 5 Å, corresponding to an appearance potential of 11.53 ± 0.05 eV, for fragmentation producing SiH_2^+ by loss of H_2 from the molecular ion (process 2), is close to the reported AP of 11.54 eV (0°K) by Berkowitz et al.[16]. Similarly, the SiH_3^+ ion is produced by fragmentation of the molecular ion (process 3) with an onset at 1028 ± 3 Å, corresponding to an appearance potential of 12.06 ± 0.03 eV, which is in close agreement with the reported AP of ≤ 12.086 (0°K) by Berkowitz et al.[16]. The previously reported values of 11.67 and 12.23 eV for $SiH_2^+(SiH_4)$ and $SiH_3^+(SiH_4)$ photoionization thresholds by Lampe and coworkers[19] are slightly higher than our results. Table I summarizes the observed photoionization thresholds and ion heats of formation calculated therefrom at 298°K using a stationary electron convention[20]. Also included in Table I are heats of formation of parent neutrals utilized in these calculations, and the ionization potentials determined using He(I) photoelectron spectroscopy.[11b]

$SiMeD_3$. Photoionization efficiency curves for $SiMeD_2^+$, $SiMeD^+$, and SiD_2^+ produced by the photoionization of methylsilane-d_3 in the wavelength region between 1030 and 1160 Å are presented in Figure 2. The photoionization efficiency curve for ions of m/e 49 (not shown) is coincident with and approximately 3% of the abundance of the photoionization efficiency curve for $^{28}SiMeD_2^+$, and is attributed to $^{30}SiMeD_2^+$. This result indicates that the molecular ion, $SiMeD_3^+$, is not observed, most likely because of the low energy fragmentation threshold for production of $SiMeD^+$.[12] The lowest fragmentation process most likely invloves an ion-pair formation of $SiMeD_2^+$ and D^- (process 4), which exhibits a very weak onset at 1150 Å = 10.78 eV.

$$SiMeD_3 + h\nu \longrightarrow SiMeD_2^+ + D^- \quad (4)$$

$$\longrightarrow SiMeD^+ + D_2 \quad (5)$$

$$\longrightarrow SiD_2^+ + CH_3D \quad (6)$$

$$\longrightarrow \mathrm{SiMeD_2^+ + D} \qquad (7)$$

The D^- ion produced in this process 4 has not been observed due to experimental limitations. The formation of $SiMeD^+$ with loss of D_2 (process 5) exhibits an onset at 1111 ± 3 Å, corresponding to an appearance potential of 11.16 ± 0.03 eV. The coincidence of the $SiMeD^+$ and $SiMeD_2^+$ curves from 1110 to 1130 Å suggests that the rapid ion-molecule reaction 8 ($k = 5.3 \times 10^{-10}$ $cm^3 molecule^{-1} sec^{-1}$)[21] may be partially responsible for the production of $SiMeD_2^+$.

$$\mathrm{SiMeD^+ + SiMeD_3 \longrightarrow SiMeD_2^+ + SiMeD_2} \qquad (8)$$

The photoionization efficiency curve for the production of SiD_2^+ by loss of CH_3D from the molecular ion (process 6), exhibits a sharp onset at 1085 ± 3 Å, corresponding to an appearance potential of 11.42 ± 0.03 eV. The photoionization efficiency curve for $SiMeD_2^+$ ion produced by a simple Si–D bond rupture process 7 from the molecular ion is obscured by the ion-pair formation process 4, a rapid ion–molecule reaction 8, and a pronounced thermal tail near threshold region. Experiments at higher source repeller fields, however, where ion residence times are much reduced, did not appreciably change the appearance of this threshold. The thermochemical data presented in Table I for $SiMeD_2^+$ is calculated by choosing an onset at 1083 ± 10 Å, corresponding to an appearance potential of 11.44 ± 0.11 eV, from extrapolation of the linearly rising portion of the $SiMeD_2^+$ photoionization efficiency curve to zero photoionization efficiency.[22] For the formation of $SiMeD_2^+$, the difference of 0.66 ± 0.11 eV in thresholds between the ion-pair process 4 and the simple Si–D bond rupture process 7 is somewhat smaller than the electron affinity of the hydrogen atom (0.754 eV)[23] but the discrepancy is not ouside experimental error. Since either or both processes can have a significant kinetic shift, there is no reason to expect precise agreement in any case.[24] This kinetic shift could be especially large for the ion-pair process, which may have to compete with very fast processes such as dissociation to neutral fragments or autoionization.[24]

$SiMe_2H_2$. Figure 3 presents photoionization efficiency curves for the production of ions from $SiMe_2H_2$ at wavelengths between 1060 and 1240 Å. Three ions are observed in this energy range, $SiMe_2^+$, $SiMeH^+$, and $SiMe_2H^+$, corresponding to processes 9–11, respectively.

$$SiMe_2H_2 + h\nu \longrightarrow SiMe_2^+ + H_2 \quad (9)$$

$$\longrightarrow SiMeH^+ + CH_4 \quad (10)$$

$$\longrightarrow SiMe_2H^+ + H \quad (11)$$

There is no evidence for an ion-pair process. As for SiH_4, the lowest energy fragmentation process 9 involves loss of H_2 and production of $SiMe_2^+$, which has an onset at 1172 ± 4 Å, corresponding to an appearance potential of 10.58 ± 0.03 eV. At higher energies CH_4 is lost from the molecular ion (process 10), resulting in formation of $SiMeH^+$, which exhibits an onset at 1154 ± 3 Å, corresponding to an appearance potential of 10.74 ± 0.03 eV. The fragmentation process 11 yielding $SiMe_2H^+$, loss of H from the parent ion, exhibits an onset at 1135 ± 5 Å, corresponding to an appearance potential of 10.92 ± 0.05 eV. As in methylsilane-d_3, the molecular ion is not observed.[12]

$SiMe_3H$. Photoionization efficiency curves for $SiMe_2^+$, $SiMe_3^+$, and $SiMe_2H^+$ generated in trimethylsilane at wavelengths between 1080 and 1280 Å are shown in Figure 4. There is no indication of the occurrence of the ion-pair formation process. The lowest energy fragmentation involves production of $SiMe_2^+$ by loss of CH_4 from the molecular ion (process 12), and exhibits a sharp onset at 1230 ± 4 Å, corresponding to an appearance potential of 10.08 ± 0.03 eV.

$$SiMe_3H + h\nu \longrightarrow SiMe_2^+ + CH_4 \quad (12)$$

$$\longrightarrow SiMe_3^+ + H \quad (13)$$

$$\longrightarrow SiMe_2H^+ + CH_3 \quad (14)$$

The onset for formation of the $SiMe_3^+$ ion (process 13) also displays a sharp threshold at 1215 ± 3 Å, corresponding to an appearance potential of 10.20 ± 0.03 eV. The

threshold for production of $SiMe_2H^+$ (process 14) exhibits a larger thermal tail than either of the thresholds for formation of $SiMe_2^+$ or $SiMe_3^+$. The quoted appearance potential for this species in Table I (10.77 ± 0.10 eV) is obtained by extrapolation of the linearly rising portion of the $SiMe_2H^+$ photoionization efficiency curve to zero photoionization efficiency. The observed thresholds and derived ion heats of formation are presented in Table I.

IV. Discussion

The interpretation of observed photoionization thresholds requires consideration of the contribution of thermal internal energy[25] of the neutral to dissociation processes and the possibility of significant kinetic shifts.[26] These phenomena have been discussed in detail elsewhere.[25-27] The absence of the molecular ions in photoionization of $Si(CH_3)_nH_{4-n}$ ($n = 1 - 3$) may indicate that the parent ion equilibrium geometry is so different that the Franck-Condon transition does not reach a stable region of the ion potential surface.[13] For evaluations of thermochemical properties, we adopt the stationary electron convention[20] and use the observed appearance potentials at ambient temperature without any corrections. Ion heats of formation in Table I are calculated using the recommended heats of formation for the parent neutrals by Walsh.[28]

Choosing a value of 11.07eV for the appearance potential of SiH_4^+ parent ion, which is in close agreement with the reported value of 11.00 eV at 0°K by Berkowitz et. al.[16], leads to a value of 263.5 kcal/mol for $\Delta H^\circ_{f298}(SiH_4^+)$. The derived heat of formation of 274.1 kcal/mol for SiH_2^+ from the threshold feature of the photoionization efficiency curve for the silane molecular ion is identical to the value of 274.2 kcal/mol for SiD_2^+ fragment ion produced by loss of CH_3D from the methylsilane-d_3 molecular ion, within experimental error. This result suggests that the fragmentation process involving loss of methane from the parent molecular ion may not require any excess energy. A value of 234.2 kcal/mol for $\Delta H^\circ_{f298}(SiH_3^+)$ from the simple Si–H bond rupture process is in very good agreement with $\Delta H^\circ_{f298}(SiH_3^+)$

= 235.1 kcal/mol based on the $SiH_3^+(SiH_4)$ threshold by Berkowitz et al.[16]. A value of 250.4 kcal/mol for $\Delta H^\circ_{f298}(SiMeD^+)$ from the $SiMeD_3^+$ fragmentation process involving loss of D_2 is 7.8 kcal/mol (0.34 eV) greater than the value of 242.6 kcal/mol for $\Delta H^\circ_{f298}(SiMeH^+)$ from the $SiMe_2H_2^+$ fragmentation process involving loss of CH_4. Also, a value of 221.0 kcal/mol for $\Delta H^\circ_{f298}(SiMe_2^+)$ from the $SiMe_2H_2^+$ fragmentation process involving loss of H_2 is 9.7 kcal/mol (0.42 eV) greater than the value of 211.3 kcal/mol from the $SiMe_3H^+$ fragmentation process involving loss of CH_4. These discrepancies are well outside experimental error and indicate that the fragmentation process involving loss of H_2 from the molecular ion requires a more significant excess energy than that involving loss of CH_4 by 0.34 – 0.42 eV. This excess energy may be attributed to a small excess activation energy or to a kinetic shift or to both.[24] It is well known that the formation of $C_3H_6^+$ ion involving loss of H_2 or CH_4 from the photoionization of propane or *iso*–butane requires an excess energy of 0.72[24] or 0.42[29] eV, respectively. It is of particular interest to compare the formation of $SiC_2H_6^+$ from the $SiMe_2H_2^+$ or $SiMe_3H^+$ fragmentation process involving loss of H_2 or CH_4, respectively, with the formation of the $C_3H_6^+$ from the corresponding hydrocarbon analogue parent ion fragmentation processes. As shown in scheme I, methylsilane molecular ions undergo three-center geminal elimination of hydrogen or methane to give dimethylsilylene cation, but propane or *iso*-butane molecular ion undergoes four-center elimination involving vicinal loss of hydrogen or methane from two neighboring carbon centers to give propene molecular ion.

Scheme I

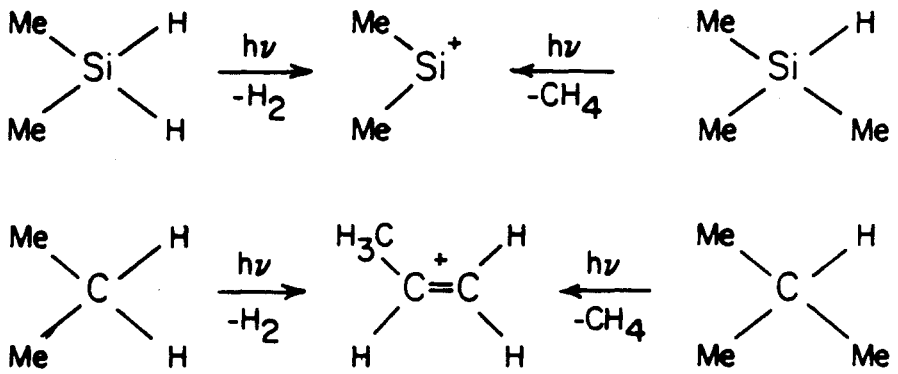

A value of 204 ± 3 kcal/mol for $\Delta H^{\circ}_{f298}(SiMeD_2^+)$ from the $SiMeD_2^+(SiMeD_3)$ threshold is identical to $\Delta H^{\circ}_{f298}(SiMeH_2^+) = 204 \pm 1$ kcal/mol derived from the hydride transfer equilibrium studies of methylsilane with cyclopentane using Fourier transform ion cyclotron resonance spectroscopy by Shin and Beauchamp.[30] The derived heat of formation for $SiMe_2H^+$ (176.7 ± 1.2 kcal/mol) from the simple bond rupture process such as loss of either H from $SiMe_2H_2^+$ or CH_3 from $SiMe_3H^+$ (174.3 ± 2.3 kcal/mol) is in close agreement within the combined experimental error. The $SiMe_3^+(SiMe_3H)$ threshold leads to $\Delta H^{\circ}_{f298}(SiMe_3^+) = 144.1$ kcal/mol which is slightly higher than the previously reported value of 140.8 kcal/mol from the $SiMe_3^+(SiMe_4)$ photoionization threshold[31], but significantly lower than the reported value of 150.5 kcal/mol estimated from the unimolecular decomposition of the $Si_2Me_6^+$ molecular ion using the photoelectron–photoion coincidence technique by Szepes and Baer.[32] We choose values of 174.3 and 144.1 kcal/mol for heats of formation for $SiMe_2H^+$ and $SiMe_3^+$, respectively, which are close to the derived values of 173 ± 2 and 146 ± 2 kcal/mol from the hydride transfer equilibrium studies of methylsilanes with various hydrocarbons in our laboratory[30].

For the evaluation of thermochemical properties, we used the lower values for heats of formation of ions from this work in Table I.

Hydride Affinities. Perhaps the most important results of the present study are the values for the hydride affinities presented in Table III, $D(M^+-H^-)$ (where M = SiR_3 or SiR_2, R = H, CH_3), of the four silicenium ions, $Si(CH_3)_nH^+_{3-n}$ ($n = 0-3$), and the three silylene cations, $Si(CH_3)_mH^+_{2-m}$ ($m = 0-2$), which are calculated using relationship 15 with thermochemical data in Table II.

$$D(M^+ - H^-) = \Delta H^{\circ}_{f298}(M^+) + \Delta H^{\circ}_{f298}(H^-) - \Delta H^{\circ}_{f298}(MH) \qquad (15)$$

The calculated hydride affinities for silicenium ions are 260.7, 245.7, 232.0, and 217.8 kcal/mol for SiH_3^+, $SiMeH_2^+$, $SiMe_2H^+$, and $SiMe_3^+$, respectively. These hydride affinities for the methyl substituted silicenium ions are in close agreement with the hydride affinities of 245.6, 230.5, and 219.7 kcal/mol for $SiMeH_2^+$, $SiMe_2H^+$, and

$SiMe_3^+$, respectively, derived from hydride transfer equilibrium studies of methylsilanes with various hydrocarbons in our laboratory.[30] The estimated hydride affinities for silylene cations are 261.1, 246.8, and 231.7 kcal/mol for SiH_2^+, $SiMeH^+$, and $SiMe_2^+$, respectively. Interestingly, within experimental error, the hydride affinities for the silylene cations are slightly greater than or identical to those for silicenium ions with the same number of methyl groups. The hydride transfer reactions 16 (where R, R', R'' = H, CH_3) observed in ICR experiments support this result.[21,30,33]

$$RR'Si^+ + RR'R''SiH \longrightarrow RR'R''Si^+ + RR'SiH \qquad (16)$$

For comparison with hydride affinities derived in this study for silicenium ions, literature data for the analogous carbonium ions are summarized in Table IV. The hydride affinities of silicenium ions exhibit a linear decrease of ~14 kcal/mol with increasing methyl substitution in place of hydrogen, compared with the nonlinear behaviour of the hydride affinities of the corresponding carbonium ions. From the calculated hydride affinities, an ion stability order (with H^- as the reference base), $CH_3^+ < CMeH_2^+ < SiH_3^+ \sim SiH_2^+ < CMe_2H^+ < SiMeH_2^+ \sim SiMeH^+ < CMe_3^+ < SiMe_2H^+ \sim SiMe_2^+ < SiMe_3^+$, is observed. This ordering is entirely consistent with the experimentally observed ordering as discussed in the introduction.

Related Thermochemical Properties. Included in Table III are estimates of the ionization potentials for silyl radicals and silylenes. The ionization potentials for silyl radicals are evaluated from equation 17, using the recommended heats of formation for silyl radicals by Walsh[28] except SiH_3.

$$IP(M) = \Delta H^\circ_{f298}(M^+) - \Delta H^\circ_{f298}(M)\ (M = SiR_2 \text{ or } SiR_3,\ R = H,\ CH_3) \qquad (17)$$

A value of 47.6 kcal/mol for $\Delta H^\circ_{f298}(SiH_3)$ is taken from the average value of 46.4 kcal/mol by Walsh[28], 47.9 kcal/mol estimated from the gas phase acidity of SiH_4 by Bartmess[34] and the electron affinity of SiH_3 by Reed and Brauman[35], and the recent recommendation of 48.5 kcal/mol by Boo and Armentrout[36]. This value yields 8.09 eV for $IP(SiH_3)$ which is in close agreement with other reported values,

8.01[16], 8.14[37], and 8.23[38] eV. The recent recommendation of heats of formation for silylenes from this laboratory[21,33] are used for the evaluation of the ionization potentials for silylenes. A value of 8.89 eV for IP(SiH_2) is slightly less than the reported value of 9.02 eV by Berkowitz and co-workers[16]. The estimated ionization potentials show a methyl substituent effect of 0.57 eV and 0.67 eV for silyl radicals and silylenes, respectively. Values for $D(M^+–H)$ and $D(M^+–CH_3)$ (where $M = SiR_2$ or SiR_3, $R = H$, CH_3) shown in Table III are calculated from equation 18, using the heats of formation given in Tables II, III, and IV.

$$D(M^+ - R) = \Delta H^\circ_{f298}(M^+) + \Delta H^\circ_{f298}(R) - \Delta H^\circ_{f298}(MR^+) \qquad (18)$$

Interestingly, values for $D(R_2Si^+–H)$ are identical to those for $D(R_3Si–H)$ within experimental error, but values for $D(R_2Si^+–CH_3)$ are ~15 kcal/mol greater than those for $D(R_3Si–CH_3)$. This extra stabilization of the silicenium ions by methyl substitution may be due to some hyperconjugative interactions as shown in scheme II through space of an incipient empty 3p orbital of a silicon charge center with the electrons in a neighboring $\sigma_{(C-H)}$ bond.[39]

Scheme II

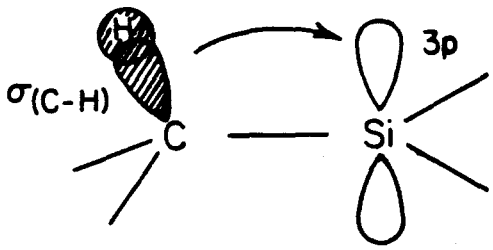

Similarly, the bond dissociation energy differences between $D(RSi^+–CH_3)$ (where $R = H$, CH_3) and $D(RHSi–CH_3)$ are ~14 kcal/mol greater than those between $D(RSi^+–H)$ and $D(RHSi–H)$.[40] This may indicate that the hyperconjugative interaction also stabilizes the methyl substituted silylene cations.

Consider the hydride affinity data for the carbonium ions in Table IV. In the series CH_3^+, $CMeH_2^+$, CMe_2H^+, and CMe_3^+, successive replacements of H in CH_3^+ by a methyl group decrease the hydride affinity by 44.2, 19.0, and 17.5 kcal/mol,

following in order. Since the incremental decrease in hydride affinity (ΔHA) directly reflects the difference between $D(R_2C^+-CH_3) - D(R_2HC-CH_3)$ (where R = H, CH_3) and $D(R_2C^+-H) - D(R_2HC-H)$,[41] this ΔHA is an index of an extra stabilization of the carbonium ions by methyl substitution. This extra stabilization effected by successive methyl substitution appears to be consistently smaller for silicenium ions than carbonium ions, presumably due to poorer spatial overlap of occupied substituent orbitals with an empty Si^+ 3p orbital relative to C^+ 2p orbital because of the greater size of Si 3p orbital and the longer Si–C bond. For example, the introduction of a first CH_3 on CH_3^+ in place of H decreases $D(C_2H_5^+-H^-)$ 44.2 kcal/mol below $D(CH_3^+-H^-)$ as compared with the 15 kcal/mol decrease in going from SiH_3^+ to $CH_3SiH_2^+$. This difference in methyl substituent effect between $C_2H_5^+$ and $CH_3SiH_2^+$ may indicate that $\sigma_{(C-H)}$ participation[39] in $C_2H_5^+$ is so extensive to form a fully delocalized, two-electron, three-center nonclassical hydrogen-bridged ion **1**, on the other hand, the C–H bonding electrons in $CH_3SiH_2^+$ are so less effectively available to the empty Si^+ 3p orbital to form a classical methyl-silicenium ion **2**.

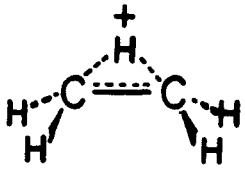

1

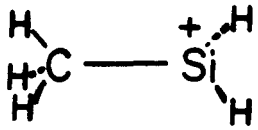

2

Both of the nonclassical hydrogen-bridged $C_2H_5^+$(**1**)[42] and the classical $CH_3SiH_2^+$(**2**)[43] are found to lie at a minimum on the potential energy surface from the theoretical calculations.

It is of particular interest to compare the effect of silyl-substitution α to silicon charge center with that of the methyl substitution. Further work is underway in our laboratory to elucidate the relative importance of these effects.

Acknowledgement. This research was supported in part by the Energy Research and Development Administration under Grant No. E(04–3) 767–8 and repre-

sents one phase of research carried out at the Jet Propulsion Laboratory, California Institute of Technology under Contract No. NAS7–100, sponsored by the National Aeronautics and Space Administration. The PIMS instrumentation was made possible by a grant from the President's Fund of the California Institute of Technology. We also thank the National Science Foundation (Grant No. CHE84-07857) for partial support of this work.

References and Notes

(1) Present Address: Brookhaven Natl. Lab., Upton, New York, 11973.

(2) For reviews of ion cyclotron resonance spectroscopy, see (a) Beauchamp, J. L. *Ann. Rev. Phys. Chem.* **1971**, *22*, 527. (b) Lehman, T. A.; Bursey, M. M. *Ion Cyclotron Resonance Spectrometry*; Wiley: New York, 1976. (c) Marshall, A. G. *Acc. Chem. Res.* **1985**, *18*, 316 and references contained therein.

(3) Murphy, M. K. Ph.D. Thesis, California Institute of Technology, Pasadena, Calif. 1977.

(4) Corderman, R. R.; Murphy, M. K.; Beauchamp, J. L. unpublished results: Corderman, R. R. Ph.D. Thesis, California Institute of Technology, Pasadena, Calif. 1977.

(5) Eyler, J. R.; Silverman, G.; Battiste, M. A. *Organometallics*, **1982**, *1*, 477.

(6) (a) Corriu, R. J. P.; Henner, M. *J. Organomet. Chem.* **1974**, *74*, 1. (b) Bickart, P.; Llort, F. M.; Mislow, K. *ibid.* **1976**, *116*, C1. (c) Cowley, A. H.; Cushner, M. C.; Riley, P. E. *J. Am. Chem. Soc.* **1980**, *102*, 624. and references therein.

(7) (a) Lambert, J. B.; Schulz, W. J., Jr., *J. Am. Chem. Soc.* **1983**, *105*, 1671. Lambert, J. B.; McConnell, J. A.; Schulz, W. J., Jr., *J. Am. Chem. Soc.* **1986**, *108*, 2482. (b) Robinson, L. R.; Burns, G. T.; Barton, T. J. *J. Am. Chem. Soc.* **1985**, *107*, 3935. (c) Eaborn, C.; Lickiss, P. D.; Najim, S. T.; Romanelli, M. N. *J. Chem. Soc., Chem. Commun.* **1985**, 1754 and earlier work referenced therein.

(8) Apeloig, Y.; Stanger, A. *J. Am. Chem. Soc.* **1987**, *109*, 272 and references therein.

(9) These species have been named silicenium, siliconium, silylenium, or silacenium ions.

(10) See Table IV.

(11) (a) Potzinger, P.; Lampe, F. W. *J. Phys. Chem.* **1970**, *74*, 587. (b) Potzinger,

P.; Ritter, A.; Krause, J. R. *Z. Naturforsh.* **1975**, *30a*, 347. (c) Krause, J. R.; Potzinger, P. *Int. J. Mass Spectrom. Ion Phys.* **1975**, *18*, 303.

(12) van der Kelen, G. P.; Volders, O.; van Onckelen, H.; Eeckhaut, Z. *Z. Anorg. Allg. Chem.* **1965**, *338*, 106.

(13) Rosenstock, H. M.; Draxl, K.; Steiner, B. W.; Herron, J. T. *J. Phys. Chem. Ref. Data* **1977**, *6*, Suppl 1.

(14) (a) Corderman, R. R.; Lebreton, P. R.; Buttrill, S. E.; Williamson, A. D.; Beauchamp, J. L. *J. Chem. Phys.* **1976**, *65*, 4929. (b) Lebreton, P. R.; Wiliamson, A. D.; Beauchamp, J. L.; Huntress, W. T. *J. Chem. Phys.* **1975**, *62*, 1623. (c) Williamson, A. D. Ph.D. Thesis, California Institute of Technology, Pasadena, Calif. 1975.

(15) Weast, R. C. Ed. *Handbook of Chemistry and Physics*, 60th ed.; Chemical Rubber Co: Cleveland, 1979; p. B-240.

(16) Berkowitz, J.; Greene, J. P.; Cho, H.; Ruščić, B. *J. Chem. Phys.* **1987**, *86*, 1235.

(17) Herzberg, G. *Infrared and Raman Spectra of Polyatomic Molecules*; Van Nostrand Reinhold: Princeton, 1955.

(18) (a) Potts, A. W.; Price, W. C. *Proc. R. Soc. London Ser. A* **1972**, *326*, 165. (b) Pullen, B. P.; Carlson, T. A.; Moddeman, W. E.; Schweitzer, G. K.; Bull, W. E.; Grimm, F. A. *J. Chem. Phys.* **1970**, *5*, 768.

(19) Ding, A.; Cassidy, R. A.; Cordis, L. S.; Lampe, F. W. *J. Chem. Phys.* **1985**, *83*, 3426.

(20) Lias, S. G.; Liebman, J. F.; Levin, R. D. *J. Phys. Chem. Ref. Data* **1984**, *13*, 695.

(21) Shin, S. K.; Irikura, K. K.; Beauchamp, J. L.; Goddard, W. A., III *J. Am. Chem. Soc.* **1988**, *110*, 24.

(22) Guyon, P. M.; Berkowitz, J. *J. Chem. Phys.* **1971**, *54*, 1814.

(23) (a) Branscomb, L. M. In *Atomic and Molecular Processes*; Bates, D. R. Ed.; Academic Press: New York, 1962; p. 136. (b) Mead, R. D.; Stevens, A. E.;

Lineberger, W. C. In *Gas Phase Ion Chemistry*; Bowers, M. T. Ed.; Academic Press: London, 1984; Vol. 3, Chapter 22.

(24) Chupka, W. A.; Berkowitz, J. *J. Chem. Phys.* **1967**, *47*, 2921.

(25) Chupka, W. A. *J. Chem. Phys.* **1971**, *54*, 1936.

(26) (a) Chupka, W. A. *J. Chem. Phys.* **1959**, *30*, 191. (b) Rosenstock, H. M.; Larkins, J. T.; Walker, J. A. *Int. J. Mass Spectrom. Ion Phys.* **1973**, *11*, 309.

(27) Walter, T.; Lifshitz, C.; Chupka, W. A.; Berkowitz, J. *J. Chem. Phys.* **1969**, *51*, 3531. (b) Vestal, M. L. In *Fundamental Processes in Radiation Chemistry*; Ausloos, P., Ed.; Wiley Interscience: New York, 1968.

(28) Walsh, R. *Acc. Chem. Res.* **1981**, *14*, 246.

(29) Steiner, B.; Giese, C. F.; Inghram, M. G. *J. Chem. Phys.* **1961**, *34*, 189.

(30) Shin. S. K.; Beauchamp, J. L. manuscript in preparation.

(31) Murphy, M. K.; Beauchamp, J. L. *J. Am. Chem. Soc.* **1977**, *99*, 2085.

(32) Szepes, L.; Baer, T. *J. Am. Chem. Soc.* **1984**, *106*, 273.

(33) Shin, S. K.; Beauchamp, J. L. *J. Phys. Chem.* **1986**, *90*, 1507.

(34) Bartmess, J. E. In *Structure/Reactivity and Thermochemistry of Ions* (NATO ASI Series); Ausloos, P., Lias, S. G. Eds; Reidel: Dordrect, 1987; pp 367-380.

(35) Reed, K. J.; Brauman, J. I. *J. Chem. Phys.* **1974**, *61*, 4380.

(36) Boo, B. H.; Armentrout, P. B. *J. Am. Chem. Soc.* **1987**, *109*, 3549.

(37) Dyke, J. M.; Jonathan, N.; Morris, A.; Ridha, A.; Winter, M. J. *Chem. Phys.* **1973**, *11*, 289.

(38) Nimlos, M. R.; Ellison, G. B. *J. Am. Chem. Soc.* **1986**, *108*, 6522.

(39) Lowry, T. H.; Richardson, K. S. *Mechanism and Theory in Organic Chemistry*; Harper & Row: New York, 1981.

(40) Since values for D(RHSi–H) are identical to those for D(RHSi–CH_3) within experimental error, the difference, Δ (= D(RSi^+–CH_3) – D(RHSi–CH_3) – D(RSi^+–H) + D(RHSi–H)), is approximately equal to the difference between D(RSi^+–CH_3) and D(RSi^+–H), which is equal to $\Delta H^\circ_{f298}(RSiH^+)$ –

$\Delta H^{\circ}_{f298}(RSiCH_3^+) + \Delta H^{\circ}_{f298}(CH_3) - \Delta H^{\circ}_{f298}(H)$. From values for heats of formation of silylene cations in Table III, CH_3 in Table IV and H in Table II(reference e), the difference Δ is estimated to be $\sim$ 14 kcal/mol.

(41) $D(R_2C^+-CH_3) - D(R_2HC-CH_3) - (D(R_2C^+-H) - D(R_2HC-H)) = \Delta H^{\circ}_{f298}(R_2HCCH_3) - \Delta H^{\circ}_{f298}(R_2CCH_3^+) - (\Delta H^{\circ}_{f298}(R_2HCH) - \Delta H^{\circ}_{f298}(R_2CH^+)) = D(R_2CH^+-H^-) - D(R_2CCH_3^+-H^-) = \Delta HA.$

(42) (a) Lischka, H.; Köhler, H. J. *J. Am. Chem. Soc.* **1978**, *100*, 5297. (b) Raghavachari, K.; Whiteside, R. A.; Pople, J. A.; Schleyer, P. v. R. *J. Am. Chem. Soc.* **1981**, *103*, 5649.

(43) Hopkinson, A. C.; Lien, M. H. *J. Org. Chem.* **1981**, *46*, 998.

Table I. Photoionization Data for Methylsilanes.

molecule	ΔH°_{f298}[a] (kcal/mol)	IP (eV)	observed ion + other product	AP (eV)	ΔH°_{f298}(ion)[b] (kcal/mol)
SiH_4	8.2	11.00(PI)[c]	SiH_4^+	11.07 or 11.26	263.5 or 267.9
		11.67(PE)[d]	$SiH_2^+ + H_2$	11.53 ± 0.05	274.1
			$SiH_3^+ + H$	12.06 ± 0.03	234.2
$Si(CH_3)D_3$	−7.0	10.7(PE)[e]			239.7
			$SiMeD_2^+ + D^-$	10.78	—
			$SiMeD^+ + D_2$	11.16 ± 0.03	250.4
			$SiD_2^+ + CH_3D$	11.42 ± 0.03	274.2
			$SiMeD_2^+ + D$	11.44 ± 0.11	204 ± 3[f]
$Si(CH_3)_2H_2$	−23.0	10.3(PE)[e]			214.5
			$SiMe_2^+ + H_2$	10.58 ± 0.03	221.0
			$SiMeH^+ + CH_4$	10.74 ± 0.03	242.6
			$SiMe_2H^+ + H$	10.92 ± 0.05	176.7
$Si(CH_3)_3H$	−39.0	9.9(PE)[e]			189.3
			$SiMe_3^+ + CH_4$	10.08 ± 0.03	211.3
			$SiMe_3^+ + H$	10.20 ± 0.03	144.1
			$SiMe_2H^+ + CH_3$	10.77 ± 0.10	174.3 ± 2.3
$Si(CH_3)_4$	−55.4	9.42(PE)[g]	$SiMe_4^+$	9.80[h]	161.8[i]
			$SiMe_3^+ + CH_3$	10.03[h]	140.8

a) Reference 28. *b*) For evaluations of ion heats of formation, we adopt the stationary electron convention (ref 20) and use the observed appearance potentials at ambient temperature without any corrections. *c*) Reference 16; PI stands for photoionisation mass spectrometric measurement. *d*) Reference 18; PE stands for photoelectron spectroscopic measurement. *e*) Reference 11b. *f*) Using $\Delta H^{\circ}_{f298}(D) = 52.981$ kcal/mol (ref 13). *g*) Evans, S.; Green, J. C.; Joachim, P. J.; Orchard, A. F.; Turner, D. W.; Maier, J. P. *J. Chem. Soc. Faraday Trans.II* **1972**, *68*, 905. *h*) Reference 31. *i*) Using $IP(SiMe_4) = 9.42$ eV.

Table II. Thermochemical Data used in Text.

molecule (MH)	ΔH°_{f298}(MH) (kcal/mol)	IP(MH) (eV)	$\Delta H^\circ_{f298}(MH^+)$[a] (kcal/mol)	D(M–H) (kcal/mol)	ΔH°_{f298}(M) (kcal/mol)	D(M–CH_3)[b] (kcal/mol)
SiH_4	8.2[c]	11.07(PI)[d]	263.5	91.5[e]	47.6[f]	89.7
$Si(CH_3)H_3$	−7.0[c]	10.7(PE)[g]	239.7	89.6[e]	30.5[c]	88.6
$Si(CH_3)_2H_2$	−23.0[c]	10.3(PE)[g]	214.5	89.4[e]	14.3[c]	88.4
$Si(CH_3)_3H$	−39.0[c]	9.9(PE)[g]	189.3	90.3[e]	−0.8[c]	89.7
$Si(CH_3)_4$	−55.4[c]	9.42(PE)[h]	161.8	99.2[e]	−8.3[c]	—
SiH_3	47.6[f]			73.5[e]	69 ± 3[i,j]	73.6
$Si(CH_3)H_2$	30.5[c]			74.6[e,h]	53 ± 4[j,h]	73.8
$Si(CH_3)_2H$	14.3[c]			74.8[e]	37 ± 6[j]	72.9

a) $\Delta H^\circ_{f298}(MH^+) = \Delta H^\circ_{f298}(MH)$ + IP(MH). *b*) D(M–CH_3) = ΔH°_{f298}(M) + $\Delta H^\circ_{f298}(CH_3)$ − $\Delta H^\circ_{f298}(MCH_3)$. *c*) Reference 28. *d*) This work. *e*) D(M–H) = ΔH°_{f298}(M) + ΔH°_{f298}(H) − ΔH°_{f298}(MH); ΔH°_{f298}(H) = 52.095 kcal/mol from Moore, C. E. *Natl. Stand. Ref. Data Ser., Natl. Bur. Stand.* **1970**, No. 34. *f*) See text and reference 21. *g*) Reference 11b. *h*) Evans, S.; Green, J. C.; Joachim, P. J.; Orchard, A. F.; Turner, D. W.; Maier, J. P. *J. Chem. Soc. Faraday Trans. II* **1972**, *68*, 905. *i*) Reference 33. *j*) Reference 21. *k*) Recently, Strauss and coworkers derived D(CH_3HSi–H) = 73.5 kcal/mol and $\Delta H^\circ_{f298}(CH_3SiH)$ = 51.9 kcal/mol from the gas-phase thermolysis of monomethylsilane, which are in excellent agreement with our results (Neudorfl, P. S.; Lown, E. M.; Safarik, I.; Jodhan, A.; Strauss, O. P. *J. Am. Chem. Soc.* **1987**, *109*, 5780).

Table III. Calculated Thermochemical Properties.

ion (M^+)	$\Delta H^\circ_{f298}(M^+)^a$ (kcal/mol)	$IP(M)^b$ (eV)	$D(M^+-H^-)^c$ (kcal/mol)	$D(M^+-H)^d$ (kcal/mol)	$D(M^+-CH_3)^e$ (kcal/mol)
SiH_3^+	234.2	8.09	260.7	22.8	29.6
$Si(CH_3)H_2^+$	204[f]	7.52	245.7	16.4	24.6
$Si(CH_3)_2H^+$	174.3	6.94	232.0	11.9	20.1
$Si(CH_3)_3^+$	144.1	6.28	217.8	6.9	17.4
SiH_2^+	274.1	8.89	261.2	92.0	105.2
$Si(CH_3)H^+$	242.6	8.22	246.8	90.7	103.4
$Si(CH_3)_2^+$	211.3	7.56	231.7	89.1	102.3

a) This work. *b*) $IP(M) = \Delta H^\circ_{f298}(M^+) - \Delta H^\circ_{f298}(M)$. *c*) $D(M^+-H^-) = \Delta H^\circ_{f298}(M^+) + \Delta H^\circ_{f298}(H^-) - \Delta H^\circ_{f298}(MH)$; $\Delta H^\circ_{f298}(H^-) = 34.7$ kcal/mol (ref 13 and 23). *d*) $D(M^+-H) = \Delta H^\circ_{f298}(M^+) + \Delta H^\circ_{f298}(H) - \Delta H^\circ_{f298}(MH^+)$. *e*) $D(M^+-CH_3) = \Delta H^\circ_{f298}(M^+) + \Delta H^\circ_{f298}(CH_3) - \Delta H^\circ_{f298}(MCH_3^+)$. *f*) Use the value for $\Delta H^\circ_{f298}(Si(CH_3)D_2^+)$ without any corrections.

Table IV. Thermochemical Data for Alkanes used in Text.

molecule (RH)	$\Delta H^\circ_{f298}(RH)^a$ (kcal/mol)	IP(RH) (eV)	$\Delta H^\circ_{f298}(RH^+)^b$ (kcal/mol)	$\Delta H^\circ_{f298}(R)$ (kcal/mol)	$D(R-H)^c$ (kcal/mol)	IP(R) (eV)	$\Delta H^\circ_{f298}(R^+)^d$ (kcal/mol)	$D(R^+-H^-)^e$ (kcal/mol)
CH_4	−17.89	12.615(PI)[f]	273.0	35.1[g]	105.1	9.842(S)[h]	262.1	314.7
$C(CH_3)H_3$	−20.24	11.51(PE)[i]	245.2	28.4[j]	100.6	8.12[k]	215.6[l]	270.5
$C(CH_3)_2H_2$	−24.83	10.95(PI)[m]	227.7	22.3[n]	99.2	7.36(PE)[o]	192.0	251.5
$C(CH_3)_3H$	−32.41	10.5(PI)[p]	209.7	12.4[n]	96.9	6.70(PE)[o]	166.9	234.0
$C(CH_3)_4$	−40.27	10.21(PE)[q]	195.2	8.7[r]	101.1	—	—	—

a) Cox, J. D.; Pilcher, G. ***Thermochemistry of Organic and Organometallic Compounds***; Academic Press: New York, 1970. *b*) $\Delta H^\circ_{f298}(RH^+) = \Delta H^\circ_{f298}(RH) + IP(RH)$. *c*) $D(R-H) = \Delta H^\circ_{f298}(R) + \Delta H^\circ_{f298}(H) - \Delta H^\circ_{f298}(RH)$. *d*) $\Delta H^\circ_{f298}(R^+) = \Delta H^\circ_{f298}(R) + IP(R)$. *e*) $D(R^+-H^-) = \Delta H^\circ_{f298}(R^+) + \Delta H^\circ_{f298}(H^-) - \Delta H^\circ_{f298}(RH)$. *f*) Chupka, W. A.; Berkowitz, J. *J. Chem. Phys.* **1971**. *54*, 4256. *g*) Wagman, D. D.; Evans, W. H.; Parker, V. B.; Schumm, R. H.; Halow, I.; Bailey, S. M.; Churney, K. L.; Nuttall, R. L. *J. Phys. Chem. Ref. Data* **1982**, *11*, suppl. 2. *h*) Herzberg, G.; Shoosmith, J. *Can. J. Phys.* **1956**, *34*, 523; S stands for spectrocsopic measurement. *i*) Dewar, M. J. S.; Worley, S. D. *J. Chem. Phys.* **1969**, *50*, 654. *j*) Brouard, M.; Lightfoot, P. D.; Pilling, M. J. *J. Phys. Chem.* **1986**, *90*, 445. *k*) $IP(C_2H_5) = \Delta H^\circ_{f298}(C_2H_5^+) - \Delta H^\circ_{f298}(C_2H_5)$. The previously reported values for $IP(C_2H_5)$ are 8.39 eV determined from Ne(I) photoelectron spectrum of ethyl radical generated by the pyrolysis of *n*-propyl nitrite (Houle, F. A.; Beauchamp, J. L. *J. Am. Chem.. Soc.* **1979**, *101*, 4067) and 8.26 eV measured from He(I) photoelectron spectrum of ethyl radical produced by the reaction of fluorine atoms with ethane (Dyke, J. M.; Ellis, A. R.; Keddar, N.; Morris, A. *J. Phys. Chem.* **1984**, *88*, 2565). *l*) Reference 20. *m*) References 13 and 24; may not be adiabatic. *n*) Tsang, W. *J. Am. Chem. Soc.* **1985**, *107*, 2872. *o*) Houle, F. A.; Beauchamp, J. L. *J. Am. Chem. Soc.* **1979**, *101*, 4067. *p*) References 13 and 29; may not be adiabatic. *q*) Jonas, A. E.; Schweitzer, G. K.; Grimm, F. A.; Carlson, T. A. *J. Electron spectrosc. Relat. Phenom.* **1972/73**, *1*, 29. *r*) McMillen, D. F.; Golden. D. M. *Ann. Rev. Phys. Chem.* **1982**, *33*, 493.

Figure Captions

Figure 1: Photoionization efficiency curves for SiH_4^+, SiH_2^+, and SiH_3^+ generated from SiH_4 in the photon wavelength range 960 – 1140 Å.

Figure 2: Photoionization efficiency curves for $SiMeD^+$, $SiMeD_2^+$, and SiD_2^+ generated from $SiMeD_3$ in the photon wavelength range 1030 – 1160 Å.

Figure 3: Photoionization efficiency curves for $SiMe_2^+$, $SiMeH^+$, and $SiMe_2H^+$ generated from $SiMe_2H_2$ in the photon wavelength range 1060 – 1240 Å.

Figure 4: Photoionization efficiency curves for $SiMe_2^+$, $SiMe_3^+$, and $SiMe_2H^+$ generated from $SiMe_3H$ in the photon wavelength range 1080 – 1280 Å.

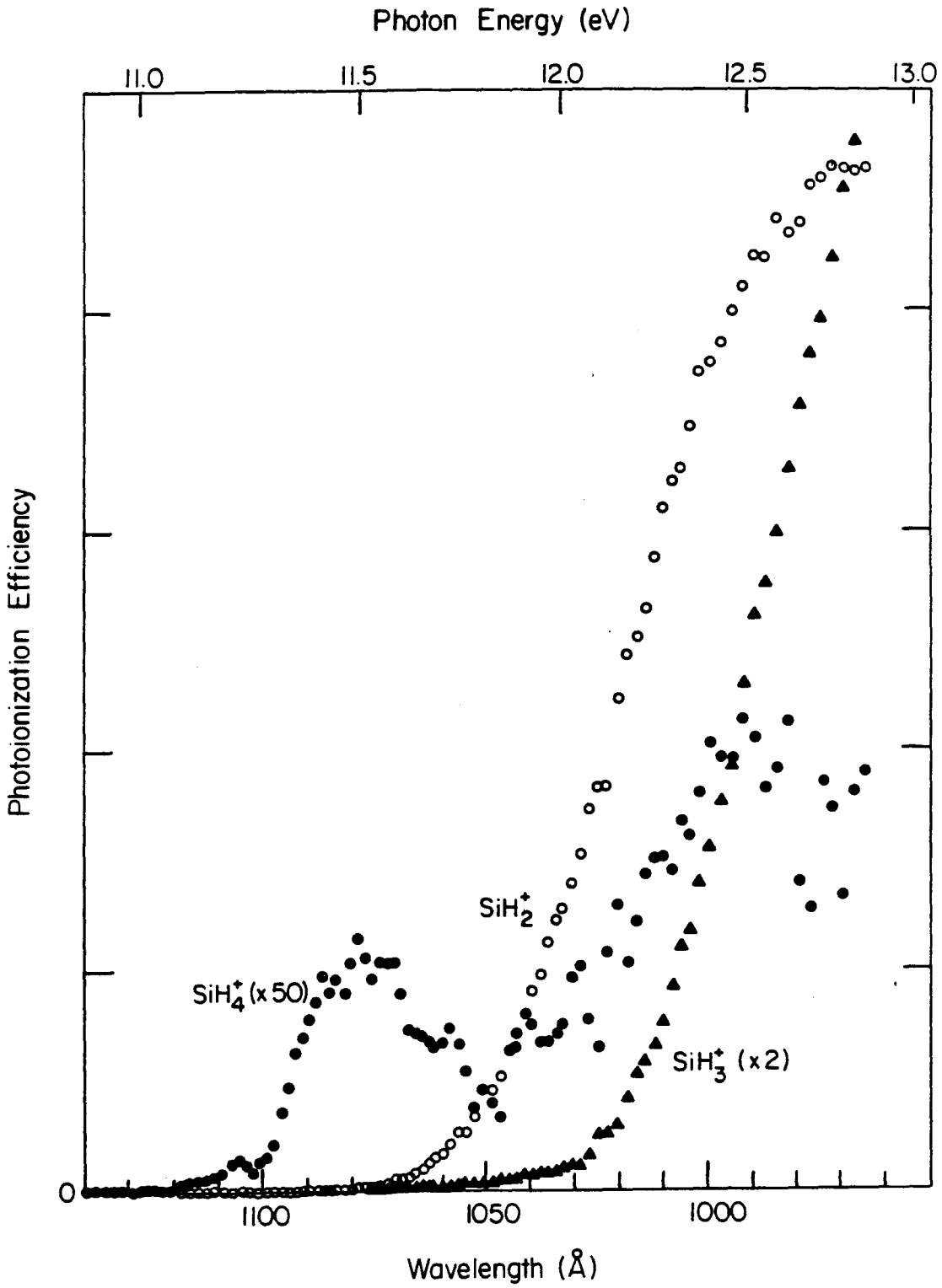
Photon Energy (eV)
11.0
11.5
12.0
12.5
13.0
Photoionization Efficiency
0
SiH_4^+ (x 50)
SiH_2^+
SiH_3^+ (x 2)
1100
1050
1000
Wavelength (Å)

Figure 1

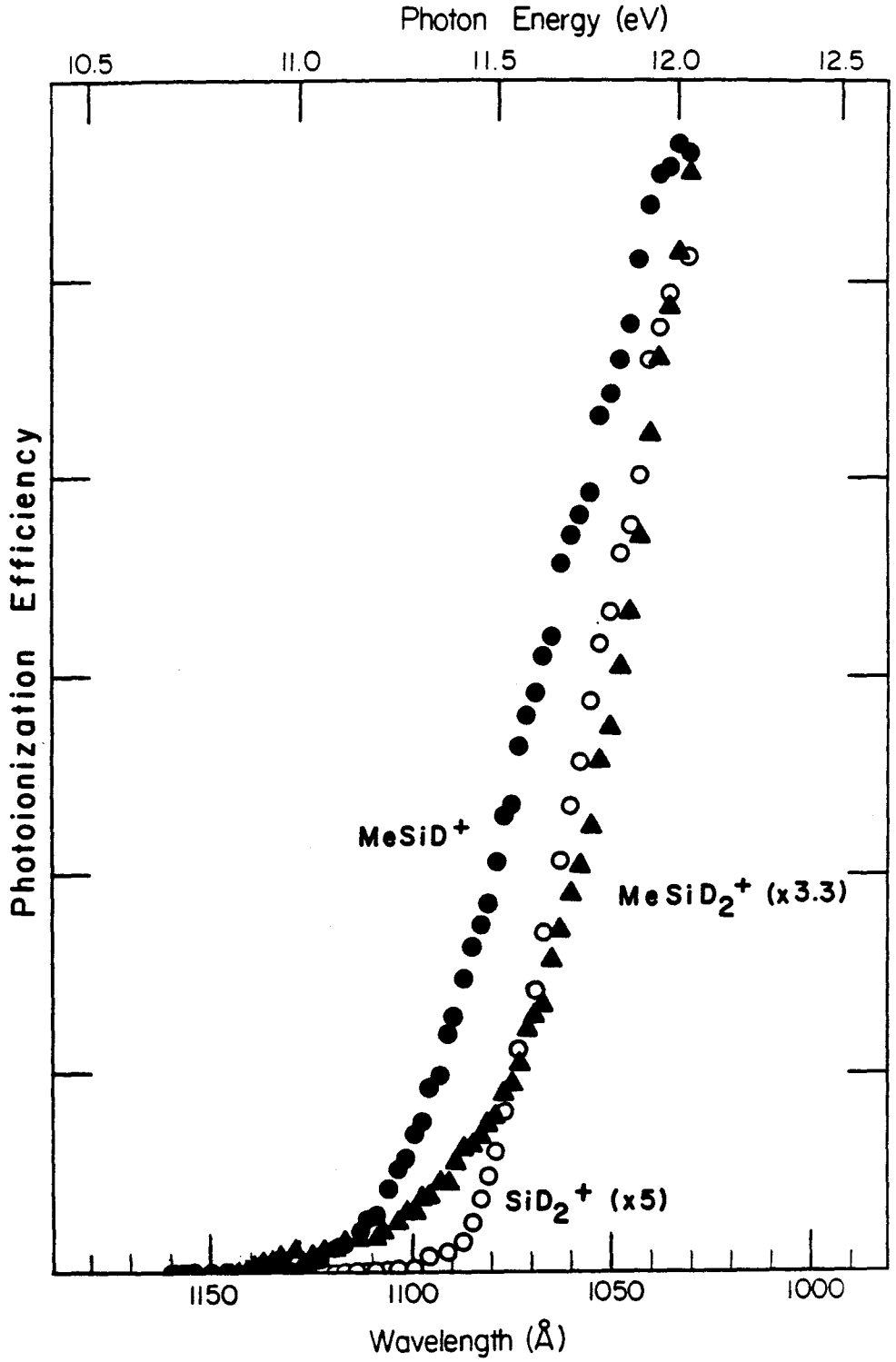
Photon Energy (eV)
10.5
11.0
11.5
12.0
12.5
Photoionization Efficiency
MeSiD+
MeSiD2+ (x3.3)
SiD2+ (x5)
1150
1100
1050
1000
Wavelength (Å)

Figure 2

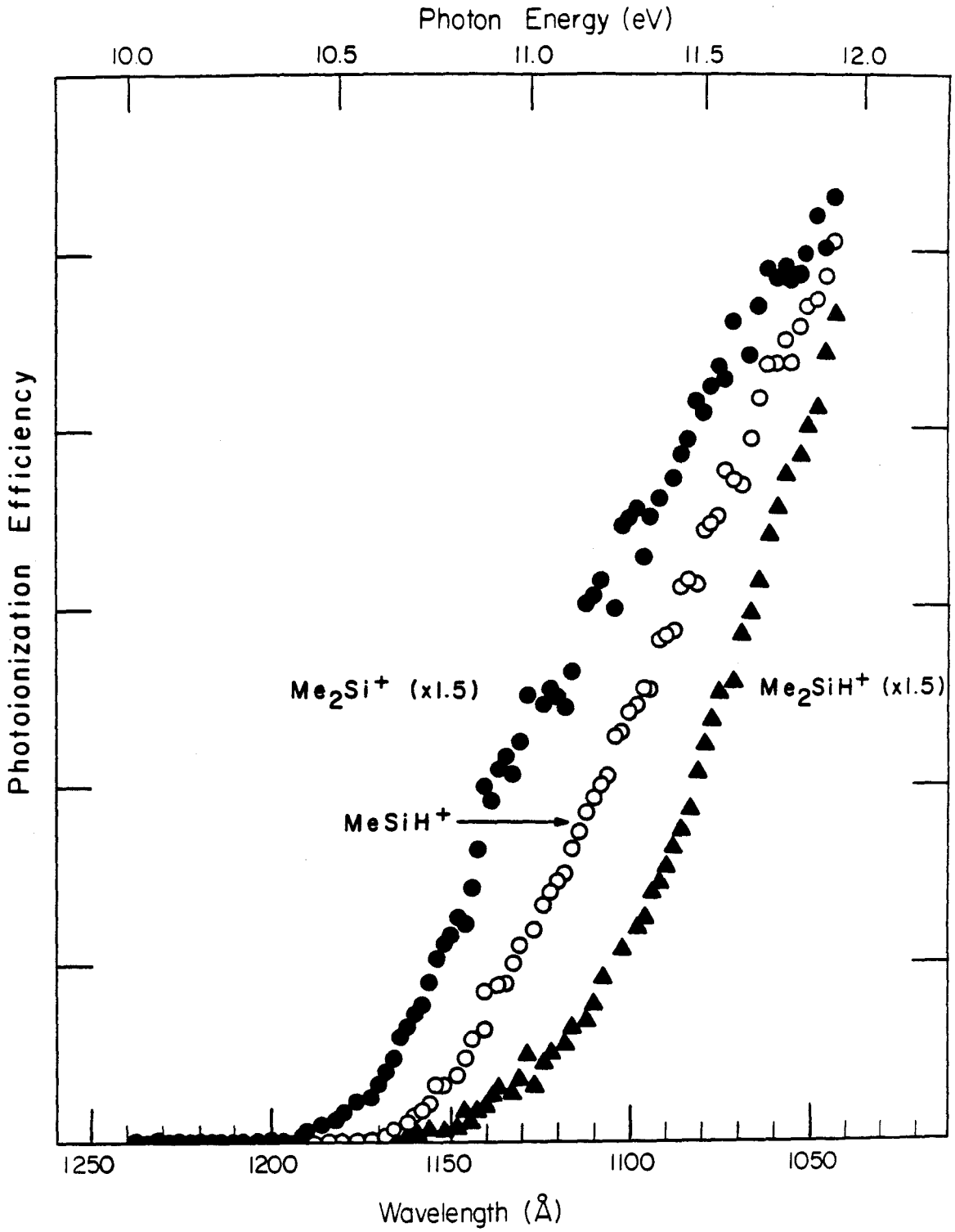
Photon Energy (eV)
10.0
10.5
11.0
11.5
12.0
Photoionization Efficiency
Me_2Si^+ (x1.5)
Me_2SiH^+ (x1.5)
$MeSiH^+$
1250
1200
1150
1100
1050
Wavelength (Å)

Figure 3

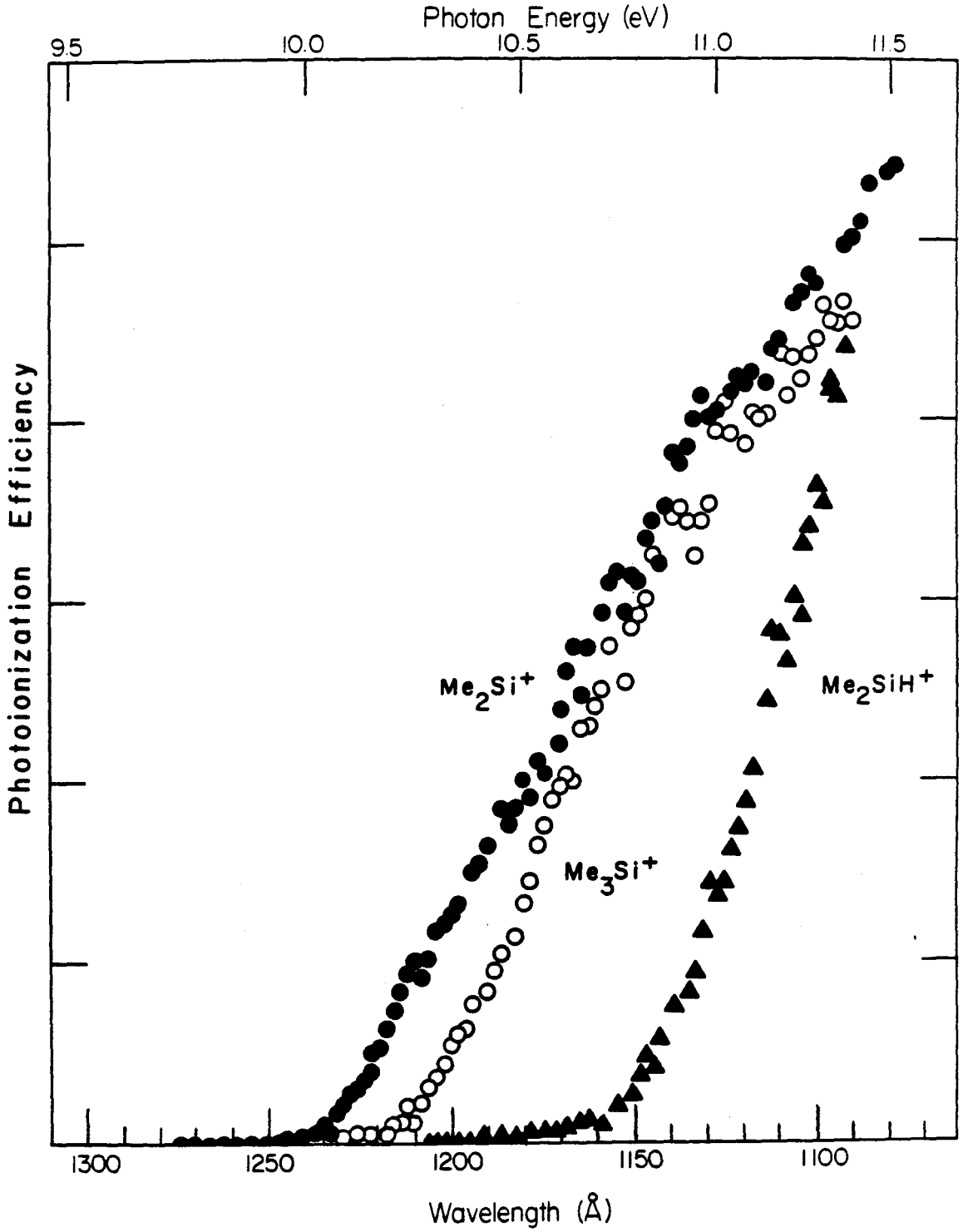
Photon Energy (eV)
9.5
10.0
10.5
11.0
11.5
Photoionization Efficiency
Me2Si+
Me2SiH+
Me3Si+
1300
1250
1200
1150
1100
Wavelength (Å)

Figure 4